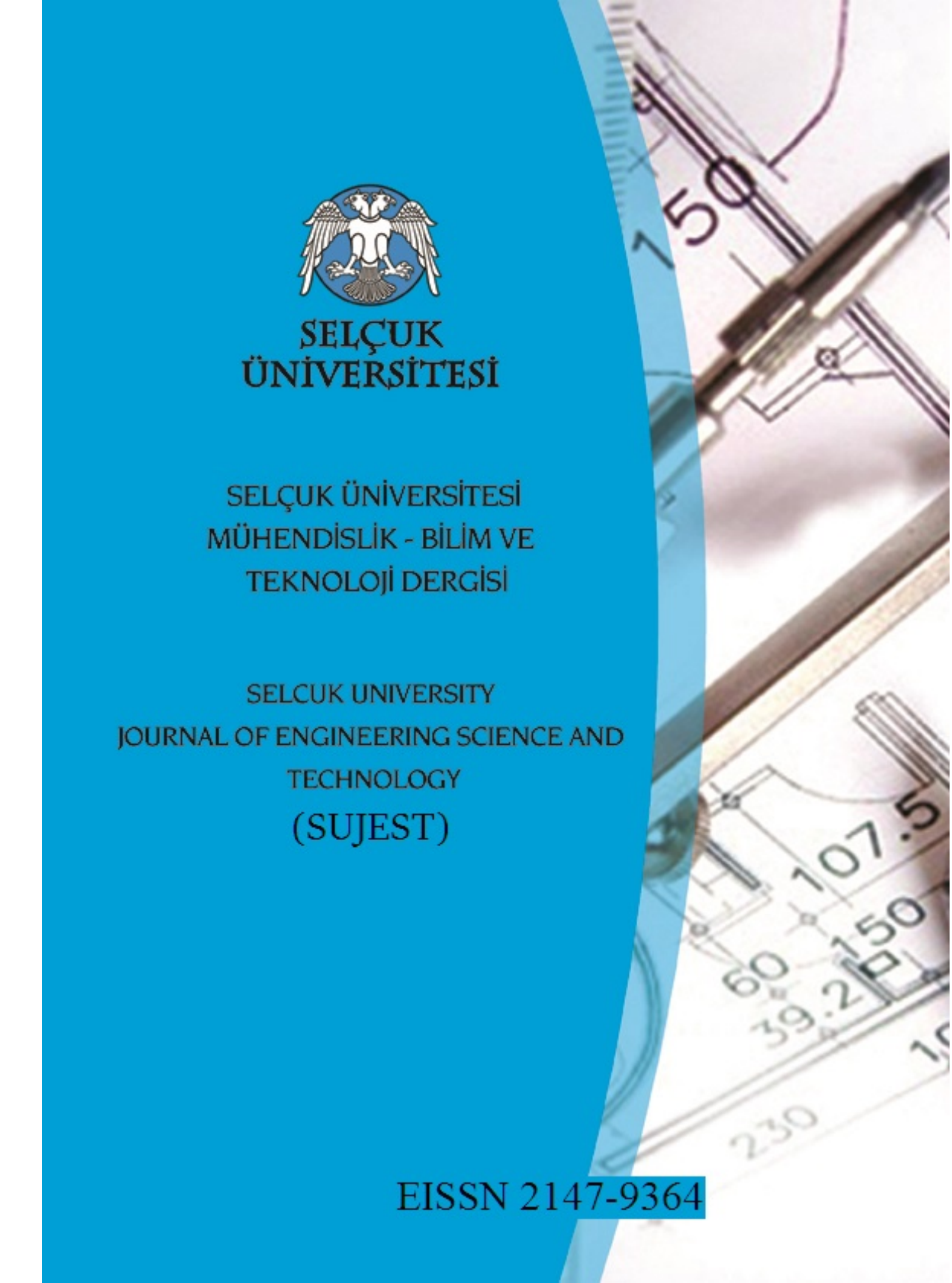

SELÇUK
ÜNİVERSİTESİ

SELÇUK ÜNİVERSİTESİ MÜHENDİSLİK - BİLİM VE TEKNOLOJİ DERGİSİ

SELCUK UNIVERSITY JOURNAL OF ENGINEERING SCIENCE AND TECHNOLOGY (SUJEST)

EISSN 2147-9364

SELCUK UNIVERSITY JOURNAL OF ENGINEERING, SCIENCE AND TECHNOLOGY (SUJEST)
SELÇUK ÜNİVERSİTESİ MÜHENDİSLİK, BİLİM VE TEKNOLOJİ DERGİSİ

HAKEMLİ DERGİDİR

OWNER/SAHİBİ
Owner on Behalf of Engeenering Faculty of Selcuk University **Prof. Dr. Ferruh YILDIZ**
Selçuk Üniversitesi Mühendislik Fakültesi Adına Dekan **Prof. Dr. Ferruh YILDIZ**

Chief Editor/Şef Editör
Assoc. Prof. Dr. Murat YAKAR

Editors/Editörler
Assoc. Prof. Dr. Mustafa TABAKCI
Assist. Prof. Dr. Ömer Kaan BAYKAN

Advisory Board/Danışma Kurulu

Prof. Dr. Cengiz ALYILMAZ, Ataturk University
Prof. Dr. Ercan AKSOY, Bitlis Eren University
Prof. Dr. Lena HALOUNOVA, Czech Technical University
Prof. Dr. Petros PATIAS, The Aristotle University
Prof. Dr. Sitki KULUR, Istanbul Technical University
Prof. Dr. Dervis KARABOGA, Erciyes University
Prof. Dr. Ibaraki SOICHI, Kyoto University
Prof. Dr. Matchavariani LIA, Tbilisi State University
Prof. Dr. Seref SAGIROGLU, Gazi University
Prof. Dr. Vijay P. SINGH, Texas A and M University

Language Editing/Yabancı Dil Editörü
Prof. Dr. Ali BERKTAY

Composition and Printing/Baskı ve Dizgi
Dr. Lutfiye Karasaka
Res. Assist. Ismail KOC

Correspondance Address/ Yazışma Adresi
Selçuk Üniversitesi Muhendislik Fakültesi Dekanlığı
42075-Kampüs, Selçuklu, Konya-TURKEY

Tel : 0 332 241 0 634
Fax : 0 332 241 0 635
E-mail : sujest@selcuk.edu.tr
Web : http://sujest.selcuk.edu.tr

Editorial Board (Yayın Kurulu)

SELÇUK ÜNİVERSİTESİ MÜHENDİSLİK, BİLİM VE TEKNOLOJİ DERGİSİ
Selcuk University Journal of Engineering, Science and Technology
(SUJEST)

ISSN 2147 – 9364 (Elektronik)

Cilt	5	Eylül	2017	Sayı	3
Volume	5	September	2017	Number	3

İÇİNDEKİLER (CONTENTS)

Araştırma Makalesi (Research Article)

SELÇUK ÜNİVERSİTESİ
MÜHENDİSLİK FAKÜLTESİ

SUJEST, c.5, s.3, 2017
SUJEST, v.5, n.3, 2017
ISSN: 2147-9364 (Electronic)

IMPROVING OF RENEWABLE ENERGY SUPPORT POLICY AND A PERFORMANCE ANALYSIS OF A GRID-CONNECTED 1 MWP PV POWER PLANT IN KONYA

[1]Nurettin ÇETİNKAYA

[1]Selcuk University, Department of Electrical-Electronics Engineering, Campus, Selcuklu, Konya, TURKEY
[1]ncetinkaya@selcuk.edu.tr

(Geliş/Received: 30.11.2016; Kabul/Accepted in Revised Form: 13.03.2017)

ABSTRACT: Ever increasing energy needs in today's world no longer corresponds to the continuous production of new solutions are required. Supporting renewable energy sources has been required to remedy this need. Renewable energy support for the world-wide accepted feed-in tariff (FiT) policy is being used effectively. FiT support policies, structure and application vary between countries. In this study a new support model is proposed. The most important aim of this model is to obtain highest benefit for both the government and the investors. The proposed flexible pricing model is depending on a country's economic status, the energy market and energy production plants technical data. Efficiency increasing of the photovoltaic (PV) systems and reduction of the costs has increased the choice of renewable energy. Thanks to the spread of environmentally friendly solutions and production, load flow problems in electric power systems can be solved and losses can be reduced. There are many areas in Konya to establish solar power plant. In this study a performance analysis of the 1 MW grid-connected PV power plants which was founded in Konya was conducted. In addition, proposals have been made for investors and legislators for more efficient and less costly energy production.

Key Words: *Cost analysis, Energy market, Renewable energy support, Solar energy.*

Yenilenebilir Enerji Destek Politikası Geliştirilmesi ve Konya'da Bulunan Şebekeye Bağlı 1 MWp Güneş Enerjisi Santralinin Performans Analizi

ÖZ: Dünya'da hızla artan enerji ihtiyacının karşılanması için sürekli üretim yapabilen yeni çözümlerin bulunması gereklidir. Bu ihtiyacı karşılamanın yollarından biri de yenilenebilir enerji kaynaklarının desteklenmesidir. Dünya genelinde uygulanan yenilenebilir enerji desteği, tarife destekleme politikası olarak etkin ve yaygın bir şekilde kullanılmaktadır. Tarife destekleme politikalarının yapıları ülkeden ülkeye değişiklik göstermektedir. Bu çalışmada yeni bir destek modeli önerilmektedir. Önerilen yeni modelin en önemli amacı hem yatırımcıların hem de devletin kazancını arttırmaktır. Önerilen değişken fiyatlandırma modeli ülkenin ekonomik durumuna, enerji piyasasının durumuna ve yeni kurulan yenilenebilir santralin teknik verilerine bağlıdır. Güneş enerji sistemlerindeki verimliliğin artması ve kurulum maliyetlerinin aşağı düşmesi yenilenebilir enerjiye yönelimi arttırmıştır. Çevre dostu çözümlerin ve üretimlerin yaygınlaşması sayesinde elektrik sistemlerinde yaşanan yük akışı problemleri çözülebilir ve güç kayıpları azaltılabilir. Konya'da güneş enerjisi santrali kurulabilecek birçok alan bulunmaktadır. Bu çalışmada şebekeye bağlı olan 1MWp gücündeki bir güneş enerjisi santralinin performans analizi de yapılmıştır. Buna ilaveten daha verimli ve daha düşük maliyetli enerji üretebilmek için yatırımcılar ve yeni çıkacak yönetmelikler için önemli önerilerde bulunulmuştur.

Anahtar Kelimeler: *Maliyet analizi, Enerji piyasası, Yenilenebilir enerji desteği, Güneş enerjisi.*

DOI: 10.15317/Scitech.2017.86

INTRODUCTION

Today, energy is the number one problem on the world and also will be in the future. That's why it's very important that economic energy production and use. One of the latest methods applied by governments in order to obtain electrical energy economically is to support of energy production. One of the most effective support models is Feed-in tariff (FiT). FiT was applied in US and Germany in 1978 and 1990, respectively (CEER, 2012). FiT for most of the world's countries rapidly increased is a renewable energy support model. This support policy needs to improve the applicability for cleaner world (Palmer et al., 2005; Stokes, 2013). In the last decade, the generation of electricity from solar energy, thanks to the support policy has become quite common. The FiT policy has proven to be one of the most effective mechanisms that encourage the deployment of solar power. In this way renewable energy production and research and development activities in the field is supported. Until today, continuous increase in the inverter and the panel efficiency is thanks to this supports.

Many countries and scientists conduct many researches for a cleaner and more economic energy sources (Oğuz et al., 2014; Gokgoz and Atmaca, 2012; Ding et al., 2010). Scientists also research costs of renewable energy sources and support policies for greener world (Haasa et al., 2004; Dincer, 2011; Benli, 2013).

The main principle of FiT policies is to offer guaranteed prices for fixed periods of time for electricity produced from renewable energy sources (RES) (Couture et al., 2010). FiTs can significantly reduce the risks of investing in renewable energy technologies and thus create conditions conductive to rapid market growth (Lipp, 2007; IEA, 2008). However, installation costs will not go down as quickly. A number of different FiT designs expose investors to uncertain market prices (Pablo, 2012). These structures, and potential augmentations, may allow for apportionment of market uncertainty. A guaranteed price floor may be enforced to reduce investors' exposure to low market prices, with potential investors receiving the benefit should the market price exceed the guaranteed floor. The Irish Renewable Energy Feed-in Tariff (REFIT) is designed in this way (Ireland, 2006). Globally, more than 40 countries have adopted some type of FiT system in order to take advantage of their solar potential. The installed renewable power capacity has increased considerably in many of the countries after the introduction of FiT policy (EPIA, 2011).

The FiTs are guaranteed for a reasonably long period of time in order to ensure security of the investment for investors and operators (Mendonca, 2007). The FiT term is commonly determined such that income is guaranteed over the lifetime of the system, i.e. at least 10-15 years. Different support price and electrical market researches have also been studied before (Topkaya, 2012; Somasekhar et al., 2014; Chang et al., 2013; Gozen, 2014).

Support policies, primarily evaluated in three different situations: FiT, Feed-in Premiums (FiP) and Tradable Green Certificates (TGC). FiT provide a defined payment to investors for the Amount of kWh generated over a certain number of years (10 up to 30 years). This tariff system, rather than technical requirements are regulated by many political future plans. FiP provide a fixed or variable premium payment above the wholesale electricity market price. Operators and investors have encourages to adjust their production to price changes, but this also implies higher risk premiums. TGC Quota system that obliges suppliers to source an increasing amount of their electricity from RES. Investors now also face the TGC market risk (Leonardo, 2012).

In market-independent FiT policies, the first and most basic option is to determine a fixed, minimum price at which the electricity generated from RES will be bought for a contracted period of time. The electricity market regulator, keep up the prices fixed for the duration of the contract, irrespective of the retail price of electricity. This support method should be applied only to the small renewable systems.

The alternative FiT policy option is the fixed price model with full or partial inflation adjustment. Inflation adjustments guard renewable energy investors against a decline in the real value of project revenues by tracking changes in the broader economy. Partial FiT policy is more risky than the fixed FiT policy. Partial FiT should be applied to medium-sized renewable systems.

Another policy model considered is the spot market gap model. In this model, the actual FiT payment is occurred of the gap between the spot market price and the required FiT price. As a result, the total payment is a fixed price consisting of the sum of the spot market price and the variable FiT premium, when combined, create the total FiT payment. Mostly hourly pricing policies are applied when purchasing energy. If the support price is higher than the hourly rate, the subsidy will be made.

RENEWABLE SUPPORT POLICY APPLIED IN TURKEY

Turkey is one of the fastest growing economies on the world with economic recovery. Turkey's annual primary energy consumption has increased by about 7% in last decade. Turkey has an annual electricity consumption of 264 TWh with a nearly 78,7 million people in 2015. It is estimated that the energy consumption in 2023 and in 2035, 400 TWh and 500 TWh, respectively (TETC, 2016). Rapidly increasing energy needs requires making efforts to reduce production costs down. Another way to ensure the energy needs is also supported in different ways in which renewable plant investment. Depending on the type and amount of support to the future of the electricity market are directed. Renewable resources should be correct guidance and should be supported for the correct use of the existing capacity. Moreover, the wind power plants provide the largest contribution to renewable sources more than the solar power plants. Most of the resources used to generate electricity are hydraulic, coal and natural gas. The share of renewable energy sources is quite low.

Turkey faces large barriers to grid connectivity and electricity transmission from renewable energy sources such as wind and solar power. This will likely be the major constraint to large-scale solar PV development as well as the domestic market expands. Turkey's distribution grid capacity currently lags behind the peak-hour supply of electricity generated by renewable. Because renewable sources have accounted for only about 6% of total electricity generation, there has been little incentive for grid companies to invest in innovation.

There are some failures in policy enforcement. For example, the Renewable Energy Law stipulates that distribution utilities have to buy all of the electricity generated from renewable sources. However in some cases wind power producers have faced significant difficulties in connecting to the grid and obtaining a government-approved price.

The challenges facing Turkey's solar PV industry are even bigger than those facing the wind industry, because they originate largely from the demand side. Turkey has yet to establish an official national renewable energy industry association to effectively coordinate industry development and to bridge the industry and policy-making process in a formal way. The true potential of renewable energy should be provided with the right support and the right technology.

The potential of renewable energy sources in Turkey was estimated by the General Directorate of Renewable Energy managed by Republic of Turkey Ministry of Energy and Natural Resources (MENR). Turkey has six different renewable and usable economic sources, namely hydro, wind, geothermal, solar, biomass and biogas, respectively. While the wind energy potential is 48 GW, geothermal energy potential is around 32 GW. Until 2023, Turkey aims to achieve at least 30% of electricity production obtained from renewable energy sources (Caynak, 2012). At the end of 2023, 3000 MW installed capacity of solar power plants are planned to be obtained.

Turkey has a high potential for solar energy due to its advantageous geographical position. Many studies for the map of the solar energy potential in Turkey have been made. Solar Potential: It was determined that Turkey's average period of sunlight is 2.640 hours per year (7,2 hours per day). The average annual radiation force amounts to 1.311 kWh/m^2-year (3,6 kWh/m^2-per day). The solar energy potential is calculated as 380 billion kWh/year (EIE, 2016).

Turkey supports that the renewable energy power plants to meet the electricity needs. Therefore The law on Electricity Production from Renewable Energy Sources (No. 6094, Official Newspaper: 8 January 2011, No.27809) was put into effect (Resmî Gazete, 2011). Turkish renewable FiT is guaranteed for 10 years at the same price while European renewable FiTs are generally guaranteed for a longer period, i.e.

20 years or more. Turkish solar industry calculates the return period as ten years if solar FiT is about 18$cent/kWh. Therefore, 10 years duration seems to be insufficient to pay back solar investments with a FiT of 13,3 $cent/kWh. But now, it can be said that; payback times are down for unit costs are also reduced (Cetinkaya, 2015).

The fixed ten-year guarantee of purchase price prevent the rapid fall. The decreasing amounts of the price support for the ten-year period allow electricity market balancing. Especially after the fifth year, the price must be reduced on a regular basis. In this way, the investor deal with the installation and the operation for the payback time is below five years. Renewable energy support prices applied in Turkey is given in Table 1 (Resmî Gazete, 2011) below.

Table 1. Renewable energy support prices.

Type of Renewable Energy	Support Prices USD cent/kWh
Hydroelectric	7,3
Wind	7,3
Geothermal	10,5
Biomass	13,3
Solar	13,3

A new regulation came into force for the determination of the contribution of domestic production in the installation of solar plants (Regulation no: 29752 date: June 24, 2016) (Resmî Gazete, 2016). According to this regulation in order to calculate the amount of additional local contribution the formula (1) should be used.

$$DCEP = [\sum_{i=1}^{n}(MCR_i)] * DCFP \quad (1)$$

Where *DCEP* is domestic contribution extra price (USDcent/kWh); *MCR* is material contribution ratio; *DCFP* is domestic contribution full price (USDcent/kWh); *n* is number of pieces in material.

If some parts of renewable energy plants are domestic manufacturing, support prices will increase. Domestic production support is available for the first five years. In fact, all kinds of support can be limited as five years to force the investors to be more conscious. In this way, the costs of renewable energy investments can be pull down. Technically all the parts are important for a power plant. But the first, PV panels and the inverters play the most important role for solar power plants.

Average sales prices in the daytime hours for Solar PV, and 24-hour average sales prices for wind can be used to calculate support prices. The hourly price application can be used for the other types of power plants because of amount of the power production can be adjusted. If the hourly price application for the renewable power plants is made the priority guarantee of purchase should be applied. The average hourly prices should pay to operators who accept the support prices. In this way, the balance of the price in all over the grid will be preserved.

Investments directed by the government by the showing the place or location are more accurate, efficient, and equitable. Recycle time; not included in the cost of land and included in the cost of land is about 7 and 10 years, respectively. In this study the land fee: $35/m^2 has been recognized. This price may be more variable by location.

The aim of this study is to ensure that different FiT/kWh supports are given to the different plants. Because all economic benefits and environmental impacts of renewable power plants are not the same.

The Potential of Solar Power in Konya

Konya province is one of the most suitable solar PV fields in Turkey with the appropriate temperature and low humidity. The most important problem of land suitable for agriculture in Konya

is used for PV power plants. Firstly, a macro plan must be done by the government to solve this problem. Secondly, the declaration of eligible land can be more articulate in detail. Location, capacity and name of the power transformers that can be linked to renewable power plants are advertised in the present application.

Konya is an very important area with a monthly average radiation of 130,45 kWh/m^2 and an average temperature of 12,25 °C along with an annual average sunshine duration of 2876 h. Climate data are used in the forecasting of the total annual energy that can be produced. Especially PvGiS (JRC, 2016) use of this data is one of the most effective examples. The efficiency of the systems except the solar panels is taken as 0,9249. The angle of the panels is selected as 30° which are most appropriate for Konya province. The highest electricity that can be produced in one year is forecasted as 1650 MWh. The real value of energy produced at the PV power plant is 1567 MWh. It is clear that the actual values are very close to forecasted values. The difference between actual data and forecasted data is determined as %5. One of the biggest factors in the occurrence of this difference, especially this year is sudden changes in the weather conditions.

1 MW Solar PV System Design for Konya

A Supervisory Control and Data Acquisition (SCADA) center is established in the Konya organized industrial region for the monitoring of the electrical power grid. At the same time, remote control like opening and closing operations can be performed in this SCADA center. Also SCADA center is used for monitoring of the solar power plant.

The general structure of the solar power plant in Konya is shown in Figure 1. 4200 pcs total power 1008 kW solar panel is used. AC inverters total output power is designed as 850 kW. Connection to the power grid is made through a Star/Delta transformer. The overall efficiency of solar power plant is about 84%.

The important characteristics of 1 MW solar PV power plant are shown in Table 2. The most important values of the feasibility study are panel efficiency, efficiency drop and many unspoken inverter prices. Inverter prices constitute approximately 18% of the total power plant cost.

Table 2. Characteristics of PV power plant

panel power	240 W
panel efficiency	14,75%
efficiency drop	10 years 90%, 25 years 80%
operating temperatures	-25/+60
inverter power	17 kW AC
inverter max input voltage	1000 VDC
inverter efficiency	98%
total PV plant power	1008 kWp
grounding, lightning protection	Yes
data recording, remote monitoring	Yes

The data received from solar radiation measuring device and energy analyzer of the power plant as shown in Figure 2 is saved hourly basis. Actually this curve shows how well the system is working in the winter months. In this way, the power system production curve can be evaluated together with the solar radiation. If the energy production cannot be done, the sources of failure should be reviewed.

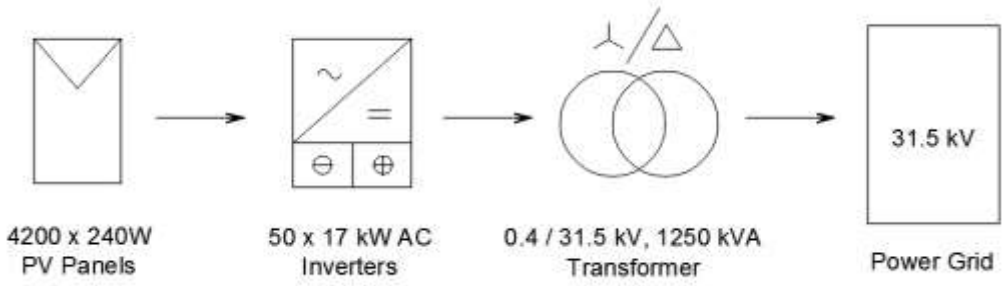

Figure 1. General structure of the solar power plant

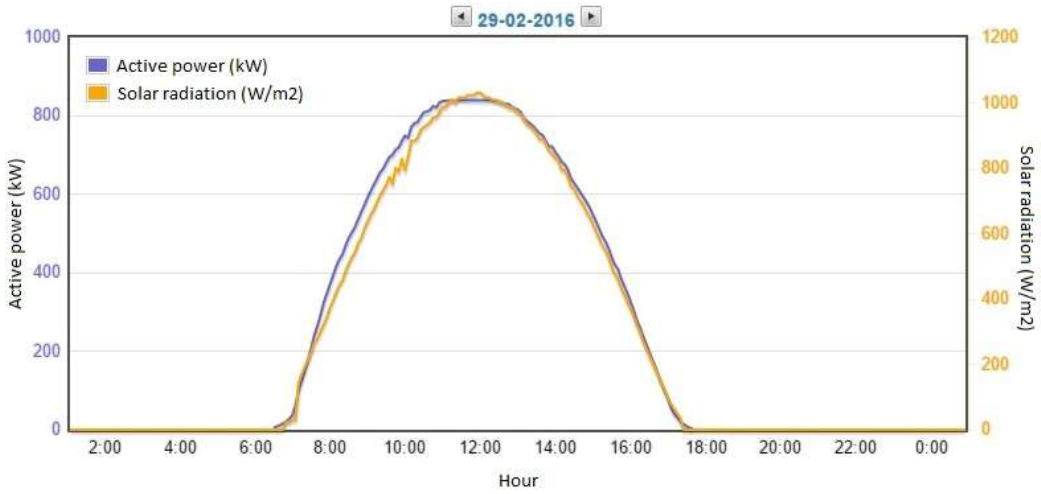

Figure 2. Active power and solar radiations curves

Daily energy production and solar irradiance for January 2016 are shown together in Figure 3. Approximately 82000 kWh was produced in a month (January 2016). The system performance ratio is calculated as 81,5%. The average daily solar irradiance is determined as 3135,13 Wh/m². Thus, it is proven that the solar system is capable of producing acceptable amounts in cold weather.

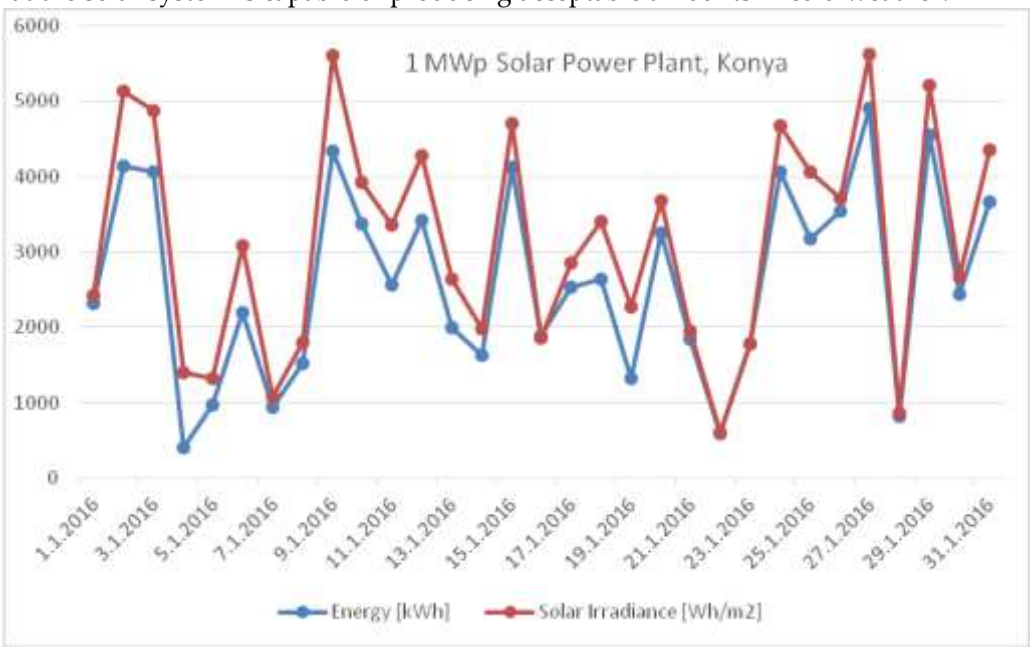

Figure 3. Energy and solar irradiance for January 2016

PROPOSED RENEWABLE ENERGY SUPPORT ALGORITHM

The main objective of the proposed model; according to the benefits of different renewable energy sources in the power system is to provide support price different amount. This allows all investors to design the plants in an optimum way to get more support; they follow better the operation of the plant. Thus, the efficiency of the power system is increased. A novel FiT support price algorithm is proposed in this study. The information about technical data of the power plant and the production/consumption balance of the power grid is taken at the start of the algorithm. According to the power plant's technical data benefit/cost ratio is calculated. Support type, fixed or flexible, is decided. The support mechanism now provides a flexible FiT which is calculated according to an algorithm based on economic situation and technical data of the RES. The flowchart of the proposed model is shown in Figure 4.

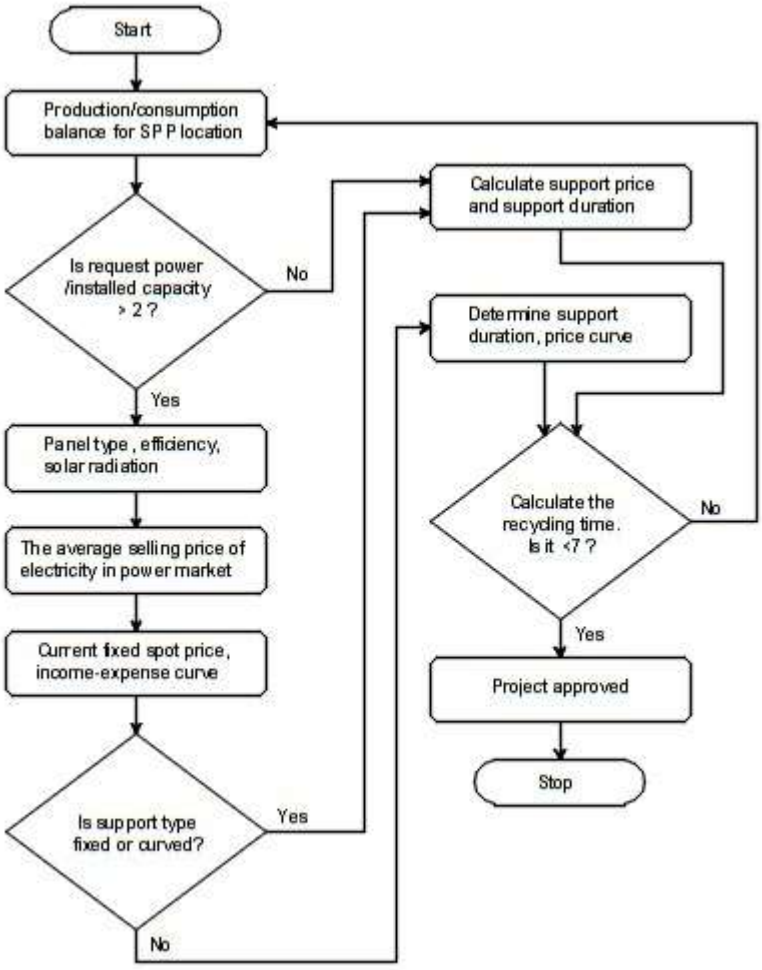

Figure 4. Flowchart of the proposed model

According to the proposed algorithm, the evaluation of the solar system is performed as follows. The power system production/consumption balance in place of power plant must be known especially for directing investment to areas where production is minimal. If this ratio is below 0,5, the support coefficient is regarded as 1. If this ratio is above 1, the support coefficient is taken as 0,5. In this way if production is greater than consumption in the region where the plant will be built, the system reduces the support rate by half. If production/consumption ratio is between 0,5 and 1 for to find support ratio, inverse ratio is applied. Thus priority in the areas where energy production is less will be recognized. Another goal of this model is aimed to provide investors primarily to produce for their own needs.

If power demand/capacity ratio is smaller than 2, the support coefficient is taken as 1, and then support duration and price are determined. If this ratio is greater than 2, panel efficiency, type, solar radiation, selling price of electricity, current fixed price and income-expense curve are evaluated to determine support coefficient and duration. The coefficient of the usefulness of the power plant is determined using this data. According to the coefficient of usefulness, the support type and duration are determined. If recycling time calculated is less than 7 years the project will be supported. Otherwise, algorithm is directed to 2. step for the new project entry. As a result, according to the proposed algorithm price support for power plants as 100% is determined for power plants capacity not exceeding need twice in an area that production less than consumption. If the proposed algorithm is presented to users in real terms in a web page, investors can evaluate before the actual application. In this way, the proposed algorithm can be used more effectively for energy efficiency, economical operation, power system security and right investment.

FEASIBILITY ANALYSIS

The economic feasibility study summarizing the four different cases is shown in Table 3. Comparisons have been made in the financial structure of all plants considered the same. In this paper, the feasibility studies were performed for Konya province. The investors are interested in this province due to sunshine durations and vastness of the land. RES power increases installation costs are reduced. The energy production of the RES is proportional to plants powers. Annual energy production is calculated using PVGIS (JRC, 2016). Annual energy production varies between 1500-1650 MWh depending on the angle of placement of the solar panel. It has been considered to be the same efficiency and operate under the same conditions. The average support prices are calculated by the proposed algorithm. This study proposed a new FiT model that can be applied to the support policy. This model has been named as semi fixed semi flexible FiT (SFFiT) that can be apply for all of RES. Full flexible FiT (FFiT) support policies should apply only to high power RES (≥10MW). Standard FiT (SFiT) should be apply for low power RES (≤ 1MW). Partial FiT (PFiT) should be apply for middle power RES (1MW< RES < 10MW). The proposed SFFiT model includes SFiT, PFiT and FFiT models. Even though the less support price is given, payback time is shorter for SFFiT support model. Thus, both the state as well as the investors would have won more. PFiT support can be considered as the worst case. In this case, the payback time is the maximum. Support price is higher than FFiT and SFFiT cases even though it is not the lowest risk. According to Table 3 it is seen that the proposed SFFiT model can be used for all plant power. The carbon support has been taken into consideration for all cases. In the calculations, the carbon emission for Turkey is assumed as 0,535 [kg/kWh] and the profit obtained from a ton of carbon is 20 €. €/$ parity is taken as 1,12. Annual income/expense chart for 1 MW solar power plant may vary according to the investors overall income/expense plan. Investors usually targets own plants to pay their debt with their income. Payment balance is varying according to the size of the investors' financial status.

Table 3. Comparison of the case studies

Proposed models	**SFiT**	**PFiT**	**FFiT**	**SFFiT**
installed power [kWp]	1,000	5,000	10,000	10,000
unit cost [€/kWp]	1,100	1,050	1,000	1,000
total investment cost [K€]	1,100	5,250	10,000	10,000
ann. energy prod. [MWh]	1,550	7,750	15,500	15,500
ann. energy profit [K€/year]	184.06	864.90	1,660.67	1,702.21
carbon emissions [tone/year]	829.25	4,146.25	8,292.50	8,292.50
ann. carbon profit [K€/year]	16.58	82.92	165.85	165.85
average support price [€cent/kWh]	11.87	11.16	10.71	10.98
payback time [year]	**5.48**	**5.54**	**5.47**	**5.35**

CONCLUSION

It is clear that the support time for renewable energy for Turkey is sufficient. In this study, the proposed model seems to be more appropriate because the economic feasibility time is less than the other support models. FiT support time in all countries definitely should not exceed 10 years. Fixed price support policies for the installed capacity over 1 MW power plants should be abandoned definitely. Large investors should develop appropriate management and investment policies to market requirements. Especially in very large renewable energy power plants (>10 MW) like other power plants can be operated with day-ahead pricing. Part-time flexible and part-time fixed structured support policies should be developed and implemented. In this study, a support model (SFFiT) proposed to improve the electrical market conditions. Turkey should continue the renewable energy support policies for to reach year 2023 or year 2030 targets. The renewable energy support should not only be done in time and cost, but also the renewable power production system efficiency must also be added into the support policies. That will accelerate the transition to more efficient and more economic renewable power systems. In this way, more informed investors and operators will earn more.

Turkey's transmission system is mostly regional in functionality, and could benefit from improved connectivity across region if renewable resources in remote areas are to be more fully harnessed. The cost of developing the transmission system will be great. But surely the power system should be strengthened and the voltage level should be increased. The new regulations are required for building integration of solar renewable energy systems. The types of constraints, principles of using and installation requirements necessarily must be defined. Feed-in tariffs, quotas, priority dispatch, technical standards, mandatory connection and purchase should be decided at the beginning of the renewable project. However the government also faces a few challenges such as the integration problem of renewable power into the grid, and low operation efficiency during implementation.

The following recommendations are suggested for the regulation which will be removed in the future for renewable energy production, sales and distribution.

Over the next five to ten years, Turkey plans to construct several giga watts wind power plants and generate a large amount of grid-connected solar PV. It will be very difficult to connect large amount of this renewable power to the electricity distribution grid, particularly at peak hours without smart-grid technology. The Turkish Government should begin planning how to deploy smart-grid technology to maximize renewable energy connection to the distribution grid.

A road-map should establish for renewable energy investors. A detailed feasibility study and income expense report for renewable project application should be requested necessarily.

Fixed price supports should not to exceed seven years. If the renewable energy support duration is determined as ten years, price support should be reduced gradually necessarily.

The researcher, investors, operators, the power system management and the legislators should work together for cleaner and more economical RES.

ACKNOWLEDGE

The author is grateful for the technical support provided by Konya Organized Industrial Zone Directorate.

REFERENCES

Benli, H., 2013, "Potential of Renewable Energy in Electrical Energy Production and Sustainable Energy Development of Turkey: Performance and Policies", Renewable Energy, Vol. 50, pp. 33-46.

Caynak, S., "Renewable Energy Strategy of Turkey", ICCI 2012 18. International Energy & Environment Fair and Conf., Istanbul, 25-27 April 2012.

CEER, "Implications of Non-harmonised Renewable Support Schemes", Council of European Energy Regulators, 18 June 2012.

Cetinkaya, N., 2015, "A New Financial Model and Economic Feasibility of Grid-Connected Power Plants for the Future of Renewable Energy in Turkey", International Journal of Electrical Energy, Vol. 3(2), pp. 110-114.

Chang, M.C., Hu, J.L., Han, T.F., 2013, "An Analysis of a Feed-in Tariff in Taiwans Electricity Market", International Journal of Electrical Power & Energy Systems, Vol. 44(1), pp. 916-920.

Couture, T., Gagnon, Y., 2010, "An Analysis of Feed-In Tariff Remuneration Models: Implications for Renewable Energy Investment", Energy Policy, Vol. 38(2), pp. 955-965.

Dincer, F., 2011, "The analysis on Photovoltaic Electricity Generation Status, Potential and Policies Of The Leading Countries in Solar Energy", Renewable and Sustainable Energy Reviews, Vol. 15, pp. 713-720.

Ding, J., Somani, A., "A Long-term Investment Planning Model for mixed Energy Infrastructure Integrated with Renewable Energy", Green Technologies Conf. IEEE, Grapevine, TX, USA, pp. 1-10, 15-16 April 2010.

EIE, 2016, http://www.eie.gov.tr/MyCalculator/Default.aspx [15.03.2016]

EPIA (European Photovoltaic Industry Association), Greenpeace, 2011, "Solar Photovoltaic Electricity Empowering The World", Solar generation 6 full report.

Gokgoz, F., Atmaca, M.E., 2012, "Financial Optimization in The Turkish Electricity Market: Markowitz's Mean-variance Approach", Renewable and Sustainable Energy Reviews, Vol. 16, pp. 357-368.

Gözen, M., 2014, "Renewable Energy Support Mechanism in Turkey: Financial Analysis and Recommendations to Policymakers", International Journal of Energy Economics and Policy, Vol. 4(2), pp. 274-287.

Haasa, R., Eichhammer, W., Huber, C., Langniss, O., Lorenzoni, A., Madlener, R., Menanteau, P., Morthorst, P.E., Martins, A., Oniszk, A., Schleich, J., Smith, A., Vass, Z., Verbruggen, A., 2004, "How to Promote Renewable Energy Systems Successfully and Effectively", Energy Policy, Vol. 32, pp. 833-839.

IEA (International Energy Agency), 2008, Deploying Renewables: Principles for Effective Policies, Paris, 978-92-64-04220-9.

Ireland (Department of Communications, Energy and Natural Resources), 2006, Renewable Energy Feed-in Tariff: Terms and Conditions, May1, 2006. http://www.dcenr.gov.ie/NR/rdonlyres/E260E316-B65A-4FDC-92F0-9F623BA18B55/0/REFITtermsandconditionsV2.doc [01.02.2016]

JRC (Joint Research Centre), IET (Institute for Energy and Transport), 2016, http://re.jrc.ec. europa.eu/pvgis/apps4/pvest.php [15.03.2016]

Leonardo, M., "Renewable Energy: Support Mechanisms Analysis", FSR Summer School on Regulation of Energy Utilities, Florence, 28 June 2012.

Lipp, J., 2007, "Lessons for Effective Renewable Electricity Policy from Denmark, Germany and the United Kingdom", Energy Policy, Vol. 35(11), pp. 5481-5495.

Mendonca, M., 2007, Feed-in-tariffs: Accelerating the Deployment of Renewable Energy, Routledge, UK, ISBN: 9781844074662.

Oğuz, F., Akkemik, K.A., Göksal, K., 2014, "Can Law Impose Competition? A Critical Discussion and Evidence from The Turkish Electricity Generation Market", Renewable and Sustainable Energy Reviews, Vol. 30, pp. 381-387.

Pablo, D.R., 2012, "The Dynamic Efficiency of Feed-in Tariffs: The Impact of Different Design Elements", Energy Policy, Vol. 41, pp. 139-151.

Palmer, K., Burtraw, D., 2005, "Cost-effectiveness of Renewable Electricity Policies", Energy Economics, Vol. 27, pp. 873-894.

Resmî Gazete, 2011, http://www.resmigazete.gov.tr/eskiler/2011/01/20110108-3.htm [15.03.2016]

Resmî Gazete, 2016, http://www.resmigazete.gov.tr/eskiler/2016/06/20160624-1.htm [30.07.2016]

Somasekhar, G., Bharathi, G., GirijaEureka, M., 2014, "Marketing Methodology of Solar PV Power Packs", Journal of Economics and Finance, Special Issue Vol.1, pp. 38-43.

Stokes, L.C., 2013, "The Politics of Renewable Energy Policies: The Case of Feed-in Tariffs in Ontario, Canada", Energy Policy, Vol. 56, pp. 490-500.

TETC, Turkish Electricity Transmission Company, 2016, http://www.teias.gov.tr/YukTevziRaporlari.aspx [15.03.2016]

Topkaya, S.O., 2012, "A Discussion on Recent Developments in Turkey's Emerging Solar Power Market", Renewable and Sustainable Energy Reviews, Vol. 16, pp. 3754-3765.

SELÇUK ÜNİVERSİTESİ MÜHENDİSLİK FAKÜLTESİ

SUJEST, c.5, s.3 2017
SUJEST, v.5, n.3, 2017
ISSN: 2147-9364 (Electronic)

BER OF ANNULAR BEAMS IN WEAK OCEANIC TURBULENCE

[1]Hamza GERÇEKCİOĞLU

[1]Republic of Turkey, Ministry of Transport, Maritime Affairs and Communications, Directorate General of Aeronautics and Space Technologies, Gazi Mustafa Kemal Blv. No.128, 06100 Maltepe, Ankara, Turkey
[1]hgercekcioglu@hotmail.com

(Geliş/Received: 01.04.2017; Kabul/Accepted in Revised Form: 14.04.2017)

ABSTRACT: Based on Rytov method, on-axis scintillation index of laser communication link in a weak oceanic medium is formulated for collimated annular beam. Employing these obtained scintillation values, average bit error rate (<BER>) is evaluated where the intensity has log-normal distribution. Scintillation indices of collimated annular beams are found for fixed primary source size α_{s_1}, varying annular beam thickness, propagation distance L, source size α_s, the rate of dissipation of the mean squared temperature χ_T, non-dimensional parameter representing the relative strength of temperature and salinity fluctuation w. <BER> versus the source size and the average signal to noise <SNR> found for the collimated annular beams are exhibited for various rate of dissipation of turbulent kinetic energy per unit mass of fluid ε and source sizes α_s. At the stated link lengths, as secondary source size of annular beam equals to zero, that is, for Gaussian beam, <BER> will offer more advantages.

Key Words : *Oceanic turbulence, Ocean optics, Optical communication, Scintillation, BER*

Halkasal Hüzmenin Zayıf Okyanussal Türbülansta Bit Hata Oranı

ÖZ: Rytov yöntemine dayalı olarak zayıf bir okyanussal ortamdaki lazer iletişim bağlantısının eksen üzerine ıpıldama indeksi, paralelleştirilmiş halka hüzmesi için formüle edilmiştir. Elde edilen bu değerler kullanılarak, ortalama bit hata oranı (<BER>), log-normal dağılımlı olarak değerlendirilmiştir. Paralelleştirilmiş halkalı hüzmelerin ıpldama indeksleri; sabit birincil kaynak boyutu α_{s_1}, değişen dairesel hüzme kalınlığı, yayılma mesafesi L, kaynak boyutu α_s, ortalama karesel sıcaklığın dağılma oranı χ_T, sıcaklık ve tuzluluk dalgalanmasının göreli kuvvetini temsil eden boyutsuz parametresi w için bulunur. Paralelleştirilmiş halka hüzmesi için kayanak büyüklüğü ve ortalama sinyal gürültü oranı (<SNR>)' na göre <BER>, birim kütle akışkanı ve kaynak boyutları için türbülans kinetik enerjinin çeşitli dağılım oranı için sergilenmektedir. Belirtilen iletişim bağlantısında, halkasal hüzmelerin ikincil kaynak boyutu sıfıra eşit olduğunda, yani Gaussian hüzmesi olduğunda, <BER> daha fazla avantaj sağlayacaktır.

Anahtar Kelimeler : *Okyanussal türbülans, Okyanus optiği, Optiksel haberleşme, ıpıldama, BER*

INTRODUCTION

Optical communications in underwater channels have fluctuations in the intensity measured by the scintillation index. This affects the behaviour of the <BER> which is one of the most important performance criteria in the link design. Some studies concerning the scintillation index of laser beams

DOI: 10.15317/Scitech.2017.87

show how much the fluctuations in the intensity, measured by the scintillation index, impress the optical communication in not only weak turbulence but also in strong turbulence. Also the types of beam model effect the scintillations, hence the <BER> at the receiver (Tatarski, 1961; Ishimaru, 1978; Andrews *et al.*, 2001; Andrews *et al*., 2005; Arpalı and Baykal, 2009; Arpalı *et al.,2008;* Vetelino *et al.*, 2007; Sandalidis *et al.*, 2008; Tyson *et al.*, 2005; Namazi *et al.*, 2007; Gerçekcioglu *et al.*, 2010; Gerçekcioglu and Baykal, 2013; Gerçekcioglu and Baykal, 2013; Gerçekcioglu *et al.*, 2010; Gerçekcioglu and Baykal, 2011; Gerçekcioglu *et al.*, 2010). Studies involving scintillation index of annular beams have revealed important results at the atmospheric channel (Gerçekcioglu *et al.*, 2010; Gerçekcioglu and Baykal., 2013; Gerçekcioglu and Baykal, 2013; Gerçekcioglu *et al.*, 2010; Gerçekcioglu and Baykal, 2011; Gerçekcioglu *et al.*, 2010).

The propagation of various kind of laser beams used in wireless optical links in underwater channels will cause intensity fluctuations, also affect the performance of optical communication link (Kumar *et al.*, 2011; Lu *et al.*, 2006; Korotkova *et al.*, 2012; Baykal, 2015; Yousefi *et al.*, 2015; Yi *et al.*, 2015; Gökçe *et al.*, 2016; Baykal, 2016; Cheng *et al.*, 2016; Peng *et al.*, 2017; Nikishov and Nikishov, 2000; Gerçekcioglu, 2014; Ata and Baykal, 2014). Especially, the scintillation indices of optical plane and spherical and Gaussian beams propagating in underwater turbulent media are researched by using the Rytov method (Gerçekcioglu, 2014; Ata and Baykal, 2014).

In this study, thanks to utilizing the spatial power spectrum of the refractive index of atmospheric media and developed on-axis scintillations in the weak atmospheric optical horizontal links, with the spatial power spectrum of the refractive index of homogeneous and isotropic oceanic water, collimated annular beams propagating in underwater turbulent media are analyzed and the scintillations and <BER> are evaluated in horizontal oceanic optics links by using the Rytov method. Scintillation index of collimated annular beams at changing features for propagation distance and source size is shown. Furthermore, scintillation index and <BER> versus <SNR> are found by using the log-normal distributed intensity for the collimated annular beams versus the for non-dimensional ratio of the relative strength of temperature and salinity fluctuations w, various source sizes α_s, the rate of dissipation of the mean squared temperature χ_T and the rate of dissipation of turbulent kinetic energy per unit mass of fluid ε.

FORMULATION

The on-axis scintillation index m^2 of annular beams in ocean turbulence (Gercekcioğlu and Baykal, 2011) with the spatial power spectrum of the refractive index of homogeneous and isotropic oceanic water represented by $\Phi_n(\kappa)$ for $\kappa > 0$ is represented as (Lu *et al.*, 2006; Nikishov and Nikishov, 2000),

$$m^2 = 4\pi \,\mathrm{Re}\left\{ \int_0^L d\eta \int_0^\infty \kappa d\kappa \int_0^{2\pi} d\phi \left[T_{A_1}(\eta,\kappa,\phi) + T_{A_2}(\eta,\kappa,\phi) \right] \Phi_n(\kappa) \right\} \tag{1}$$

where Re(.) is to the real part of the argument, η is the variable showing the length along the propagation axis, L is the propagation distance of the link, $\kappa \exp(i\phi)$ is the two dimensional spatial frequency in polar coordinates, κ is the magnitude, $\Gamma(.)$ is the Gamma function,

$$\Phi_n(\kappa)=(4\pi)^{-1}\beta\chi_n\varepsilon^{-1/3}\kappa^{-11/3}\left[1+Q(\kappa\eta_s)^{2/3}\right]\left[w^2\theta+1-w(1+\theta)\right]^{-1}$$
$$\times\left(w^2\theta\exp\left\{-\beta Pr_T^{-1}\left[\frac{2}{3}(\kappa\eta_s)^{4/3}+Q(\kappa\eta_s)^2\right]\right\}+\exp\left\{-\beta Pr_S^{-1}\left[\frac{2}{3}(\kappa\eta_s)^{4/3}+Q(\kappa\eta_s)^2\right]\right\}\right.$$
$$\left.-w(1+\theta)\exp\left\{-0.5\beta\frac{(Pr_T+Pr_S)}{Pr_TPr_S}\left[\frac{2}{3}(\kappa\eta_s)^{4/3}+Q(\kappa\eta_s)^2\right]\right\}\right) \quad (2)$$

where, the rate of the dissipation of the mean squared refractive index fluctuation is $\chi_n=A^2\chi_T(w-1)^2/w^2$, χ_T is the rate of dissipation of the mean squared temperature taking values for smaller ε close in the range from 10^{-2} K²/s to 10^{-10} K²/s, β is the Obukhov–Corrsin constant whose value is taken as 0.72, ε is the rate of dissipation of turbulent kinetic energy per unit mass of fluid, the non-dimensional constant Q is a free parameter to be determined by comparison with experiment where its value is taken as 2.35, and $\eta_s=(\nu^3/\varepsilon)^{1/4}$ is the Kolmogorov microscale, ν being the kinematic viscosity, w is non-dimensional representing the relative strength of temperature and salinity fluctuations, which in the ocean waters can vary between -5 and 0, $\theta=1$ when the quantity of eddy thermal diffusivity equals to the quantity of diffusion of the salt, Pr_T and Pr_S represent the Prandtl numbers for temperature and salinity respectively, where Pr_T=7 and Pr_S=700, and the refractive index is expressed as a function of temperature and salinity fluctuation, $A=2.6\times10^{-4}$ 1/deg is a constant.

The expressions in the integrand of Eq. (1) are

$$T_{A_1}(\eta,\kappa,\phi)=-k^2D(L)^{-2}A^2(1+i\alpha L)^{-2}\exp\left[-i(L-\eta)k^{-1}(1+i\alpha\eta)(1+i\alpha L)^{-1}\kappa^2\right] \quad (3)$$

$$T_{A_2}(\eta,\kappa,\phi)=k^2|D(L)|^{-2}AA^*(1+i\alpha L)^{-1}(1-i\alpha^*L)^{-1}$$
$$\times\exp\left\{-0.5i(L-\eta)k^{-1}\left[(1+i\alpha\eta)(1+i\alpha L)^{-1}-(1-i\alpha^*\eta)(1-i\alpha^*L)^{-1}\right]\kappa^2\right\} \quad (4)$$

where $D(L)=A(1+i\alpha L)^{-1}$ and the annular beam incident field at the source plane is given as $u_s(\mathbf{s})=u_s(s_x,s_y)=\sum_{l=1}^{2}A_l\exp\left[-0.5k\alpha_l s_x^2-0.5k\alpha_l s_y^2\right]$, these examples of annular beam expressed by $\mathbf{s}=(s_x,s_y)$ is the transverse coordinate at the source plane, s_x,s_y representing the x and y components, A_l is in general the complex amplitude of the source field, $A_1=-A_2=1$, $*$ is the complex conjugate, $i=(-1)^{0.5}$, $k=2\pi/\lambda$ is the wave number, λ is the wavelength, $\alpha_1=1/k\alpha_{s1}^2+j/F_1$, α_{s1} and F_1 are the Gaussian source size and focusing parameter of the symmetrical primary beam. Likewise, $\alpha_2=1/k\alpha_{s2}^2+j/F_2$, α_{s2} and F_2 are the Gaussian source size and focusing parameter of the symmetrical secondary beam, thickness is defined as difference between primary and secondary source (Gerçekcioğlu *et al.*, 2010).

Substituting Eqs. (3), (4) and the spatial power spectrum of refractive index fluctuation given in Eq. (2) into Eq. (1), performing the integration over κ and ψ, the on-axis scintillation index of annular beams in weak oceanic turbulence is found which is expressed as,

$$m^2 = 8\pi^2 k^2 \,\mathrm{Re}\left\{ \left|D(L)\right|^{-2} AA^* \left(1+i\alpha L\right)^{-1} \left(1-i\alpha^* L\right)^{-1} \int_0^L d\eta \left(E_{A_1} + F_{B_1}\right) - D(L)^{-2} A^2 \left(1+i\alpha L\right)^{-2} \int_0^L d\eta \left(E_{A_2} + F_{B_2}\right) \right\} \tag{5}$$

where

$$E_{A_1} = (8\pi)^{-1} K_{k_1} \left\{ w^2\theta \sum_{k=0}^{\infty} \frac{(-1)^k A_{T_1}^k \Gamma(2k/3-5/6)}{k!} \left[A_{T_2} + \frac{i(L-\eta)}{2k} \left(\frac{1+i\alpha\eta}{1+i\alpha L} - \frac{1-i\alpha^*\eta}{1-i\alpha^* L} \right) \right]^{-2k/3+5/6} - w(1+\theta) \sum_{k=0}^{\infty} \frac{(-1)^k A_{TS_1}^k \Gamma(2k/3-5/6)}{k!} \left[A_{TS_2} + \frac{i(L-\eta)}{2k} \left(\frac{1+i\alpha\eta}{1+i\alpha L} - \frac{1-i\alpha^*\eta}{1-i\alpha^* L} \right) \right]^{-2k/3+5/6} + \sum_{k=0}^{\infty} \frac{(-1)^k A_{S_1}^k \Gamma(2k/3-5/6)}{k!} \left[A_{S_2} + \frac{i(L-\eta)}{2k} \left(\frac{1+i\alpha\eta}{1+i\alpha L} - \frac{1-i\alpha^*\eta}{1-i\alpha^* L} \right) \right]^{-2k/3+5/6} \right\} \tag{6}$$

$$F_{B_1} = (8\pi)^{-1} K_{k_2} \left\{ w^2\theta \sum_{k=0}^{\infty} \frac{(-1)^k A_{T_1}^k \Gamma(2k/3-1/2)}{k!} \left[A_{T_2} + \frac{i(L-\eta)}{2k} \left(\frac{1+i\alpha\eta}{1+i\alpha L} - \frac{1-i\alpha^*\eta}{1-i\alpha^* L} \right) \right]^{-2k/3+1/2} - w(1+\theta) \sum_{k=0}^{\infty} \frac{(-1)^k A_{TS_1}^k \Gamma(2k/3-1/2)}{k!} \left[A_{TS_2} + \frac{i(L-\eta)}{2k} \left(\frac{1+i\alpha\eta}{1+i\alpha L} - \frac{1-i\alpha^*\eta}{1-i\alpha^* L} \right) \right]^{-2k/3+1/2} + \sum_{k=0}^{\infty} \frac{(-1)^k A_{S_1}^k \Gamma(2k/3-1/2)}{k!} \left[A_{S_2} + \frac{i(L-\eta)}{2k} \left(\frac{1+i\alpha\eta}{1+i\alpha L} - \frac{1-i\alpha^*\eta}{1-i\alpha^* L} \right) \right]^{-2k/3+1/2} \right\} \tag{7}$$

$$E_{A_2} = (8\pi)^{-1} K_{k_1} \left\{ w^2\theta \sum_{k=0}^{\infty} \frac{(-1)^k A_{T_1}^k \Gamma(2k/3-5/6)}{k!} \left[A_{T_2} + \frac{i(L-\eta)}{k} \frac{1+i\alpha\eta}{1+i\alpha L} \right]^{-2k/3+5/6} + \sum_{k=0}^{\infty} \frac{(-1)^k \Gamma(2k/3-5/6)}{k!} A_{S_1}^k \left[A_{S_2} + \frac{i(L-\eta)}{k} \frac{1+i\alpha\eta}{1+i\alpha L} \right]^{-2k/3+5/6} - w(1+\theta) \sum_{k=0}^{\infty} \frac{(-1)^k A_{TS_1}^k \Gamma(2k/3-5/6)}{k!} \left[A_{TS_2} + \frac{i(L-\eta)}{k} \frac{1+i\alpha\eta}{1+i\alpha L} \right]^{-2k/3+5/6} \right\} \tag{8}$$

$$F_{B_2}=(8\pi)^{-1}K_{k_2}\left\{w^2\theta\sum_{k=0}^{\infty}\frac{(-1)^k}{k!}A_{T_1}^k\Gamma(2k/3-1/2)\left[A_{T_2}+\frac{i(L-\eta)}{k}\frac{1+i\alpha\eta}{1+i\alpha L}\right]^{-2k/3+1/2}\right.$$
$$+\sum_{k=0}^{\infty}\frac{(-1)^k A_{S_1}^k\Gamma(2k/3-1/2)}{k!}\left[A_{S_2}+\frac{i(L-\eta)}{k}\frac{1+i\alpha\eta}{1+i\alpha L}\right]^{-2k/3+1/2}$$
$$\left.-w(1+\theta)\sum_{k=0}^{\infty}\frac{(-1)^k A_{TS_1\Gamma(2k/3-1/2)}^k}{k!}\left[A_{TS_2}+\frac{i(L-\eta)}{k}\frac{1+i\alpha\eta}{1+i\alpha L}\right]^{-2k/3+1/2}\right\},\qquad(9)$$

$K_{k_1}=\beta\chi_n\varepsilon^{-1/3}\left[w^2\theta+1-w(1+\theta)\right]^{-1}$, $K_{k_2}=\beta\chi_n\varepsilon^{-1/3}Q\eta_s^{2/3}\left[w^2\theta+1-w(1+\theta)\right]^{-1}$, ! denotes the factorial, $A_{S_1}=\frac{2}{3}\eta_s^{4/3}\beta P_{r_S}^{-1}$, $A_{S_2}=\beta P_{r_S}^{-1}Q\eta_s^2$, $A_{T_1}=\frac{2}{3}\eta_s^{4/3}\beta P_{r_T}^{-1}$, $A_{T_2}=\beta P_{r_T}^{-1}Q\eta_s^2$, $A_{TS_1}=\frac{1}{3}\eta_s^{4/3}\beta\left(P_{r_T}+P_{r_S}\right)P_{r_T}^{-1}P_{r_S}^{-1}$, $A_{TS_2}=\frac{1}{2}Q\eta_s^2\beta\left(P_{r_T}+P_{r_S}\right)P_{r_T}^{-1}P_{r_S}^{-1}$.

The <BER> is given by Eq. (3) of [4] as,

$$<\text{BER}>=0.5\int_0^{\infty}p_I(u)erfc\left(<\text{SNR}>2^{-3/2}u\right)du\qquad(10)$$

where $erfc(.)$ is the complementary error function, $p_I(u)$ is identified in weak oceanic turbulence as the probability density function of the intensity with $u>0$ as [4],

$$p_I(u)=\frac{1}{m\sqrt{2\pi}u}\exp\left\{-0.5m^{-2}\left[\ln(u)+0.5m^2\right]^2\right\}.\qquad(11)$$

For the collimated annular beams at the origin of the receiver in a weakly turbulent ocean., the <BER> is found by using m^2 given in Eq. (5) inserted into $p_I(u)$ given in Eq. (11) which in turn is substituted into Eq. (10).

RESULTS AND DISCUSSIONS

In this section, the results are obtained by utilizing the derived formulations in section 2 which are valid in oceanic weak turbulence. As taken in my article published in 2014, it is noted that $\lambda=1.55\ \mu$m and $\chi_t=10^{-8}\ \text{K}^2s^{-1}$ are chosen. While Figs.1, 2, 3, 4 and 5 indicate the scintillation indices versus the propagation distance L, source size α_s, rate of dissipation of the mean squared temperature χ_T and the ratio of temperature and salinity fluctuations w, respectively, Figs. 6, 7 and 8 indicate the variations of <BER> versus the primary source size α_{s_1} at various thickness, versus <SNR> for fixed primary source size $\alpha_{s_1}=1$ cm and $\alpha_{s_1}=2$ cm , respectively.

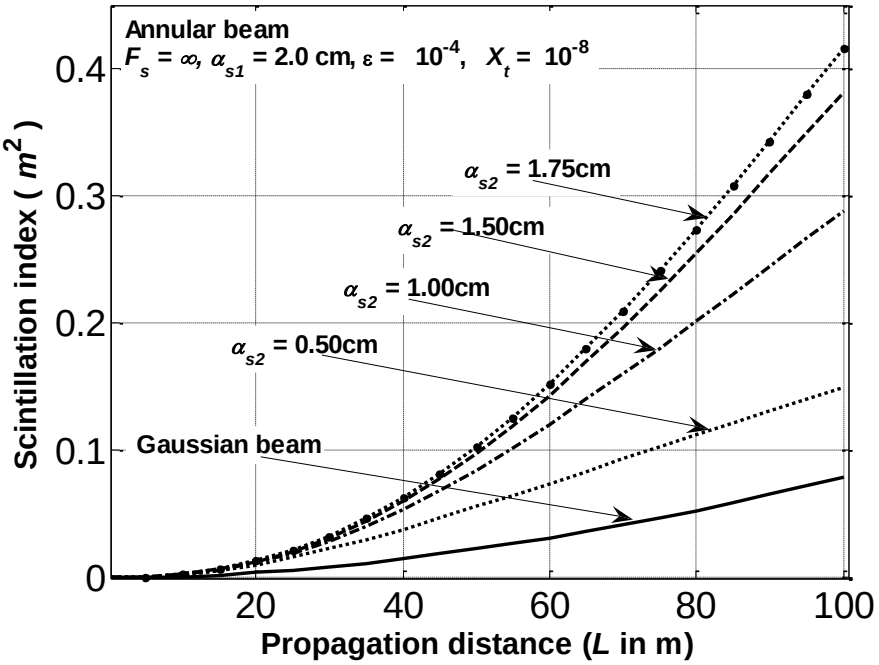

Figure 1. Scintillation index versus propagation distance L for collimated annular beams at fixed primary source size (α_{s1}= 1 cm) and various thickness.

.

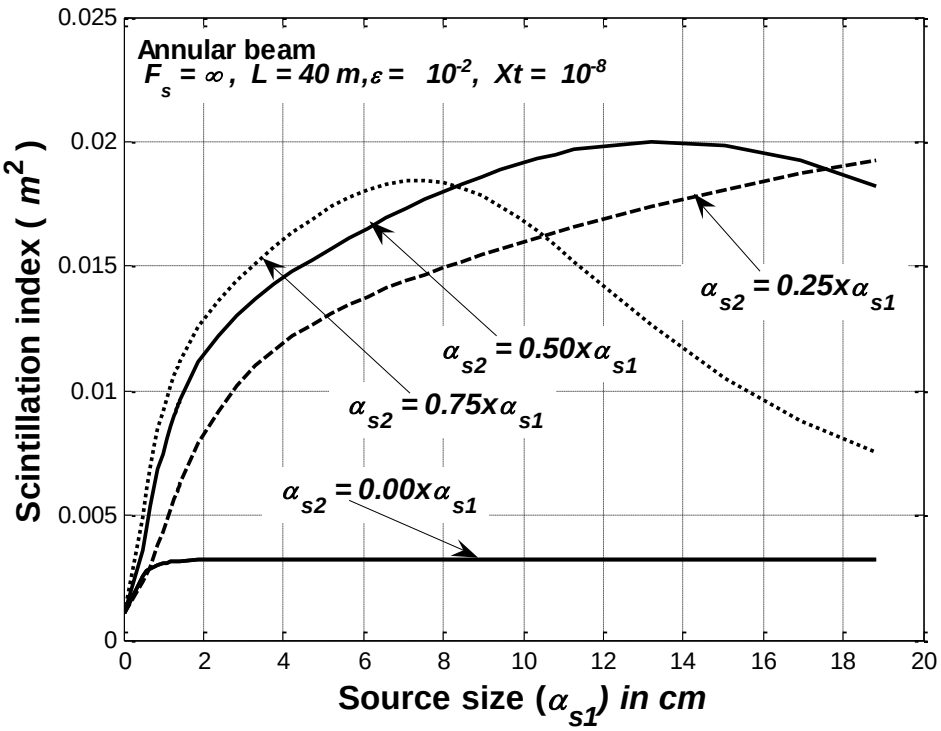

Figure 2. Scintillation index versus primary source size α_{s1} for collimated annular beams at various thickness.

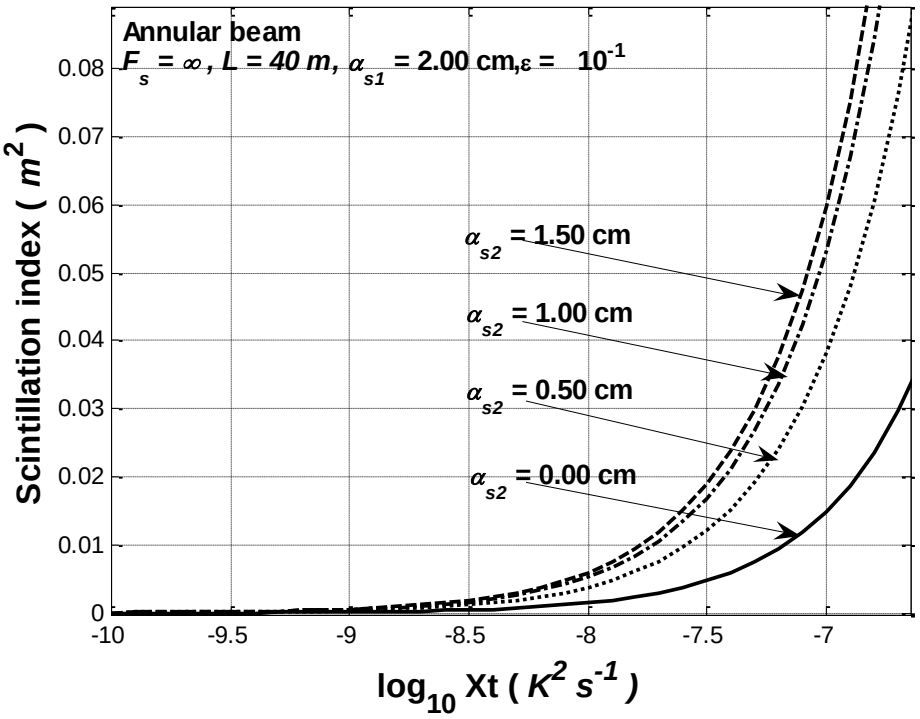

Figure 3. Scintillation index versus the rate of dissipation of the mean squared temperature χ_T for collimated annular beams at fixed primary source size ($\alpha_{s1} = 2$ cm) and various thickness.

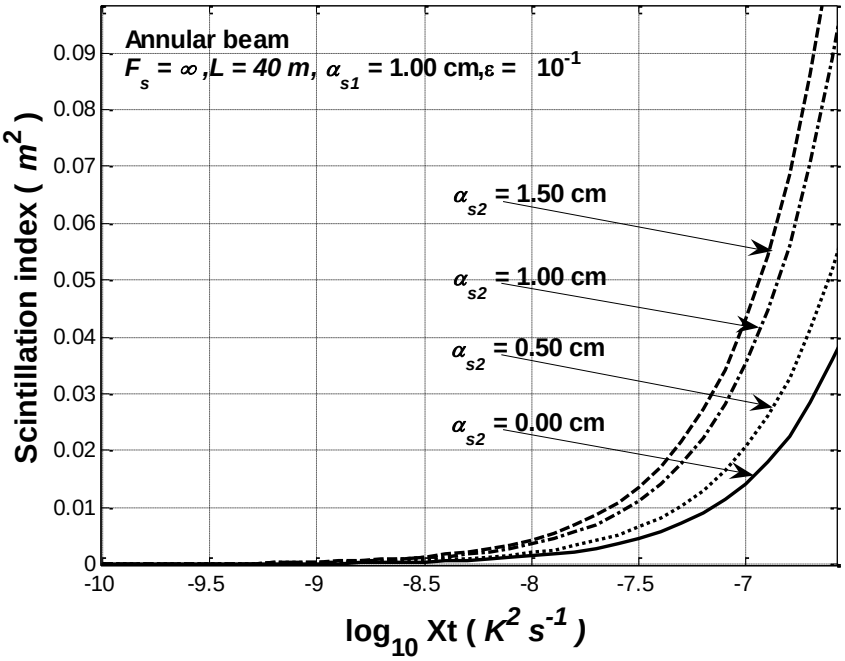

Figure 4. Scintillation index versus the rate of dissipation of the mean squared temperature χ_T for collimated annular beams at fixed primary source size ($\alpha_{s1} = 1$ cm) and various thickness.

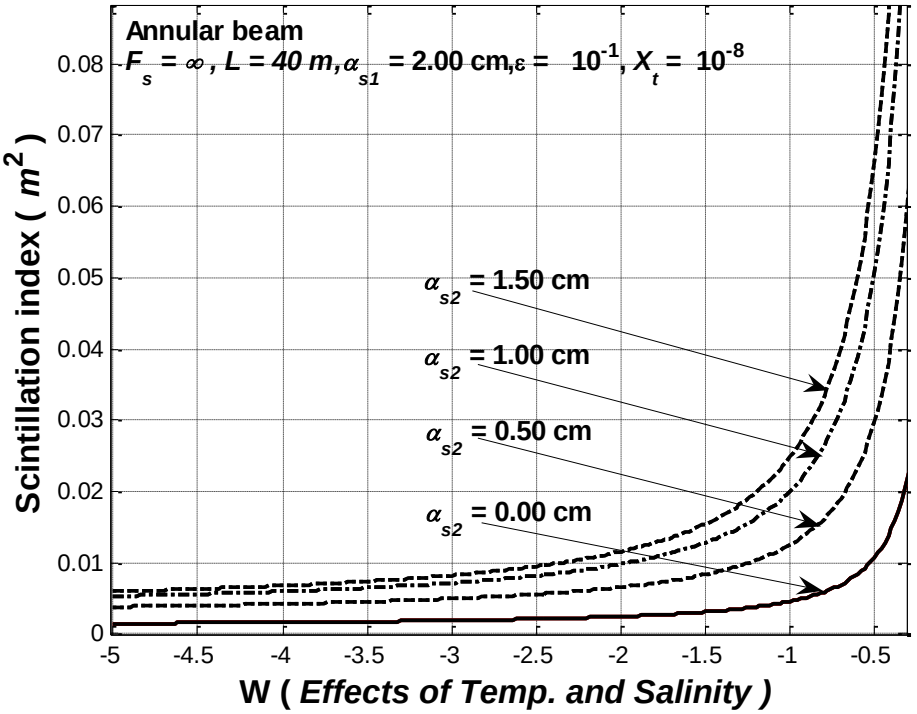

Figure 5. Scintillation index versus effects of temperature and salinity fluctuations *w* for collimated annular beams at fixed primary source size ($\alpha_{s1} = 2$ cm) and various thickness.

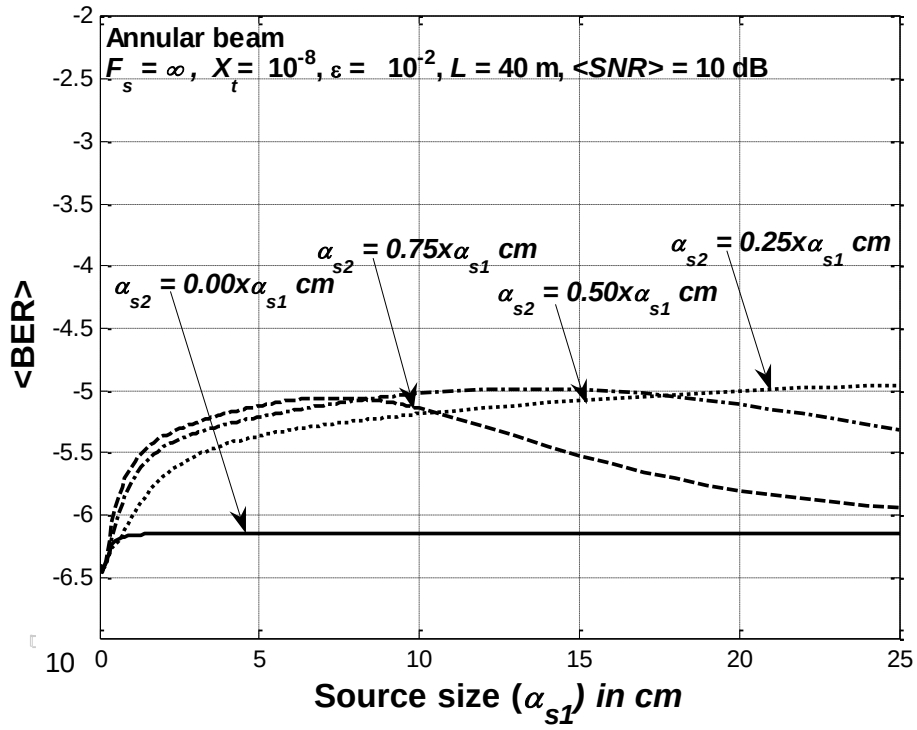

Figure 6. <*BER*> versus scintillation index versus primary source size α_{s1} for collimated annular beams at various thickness.

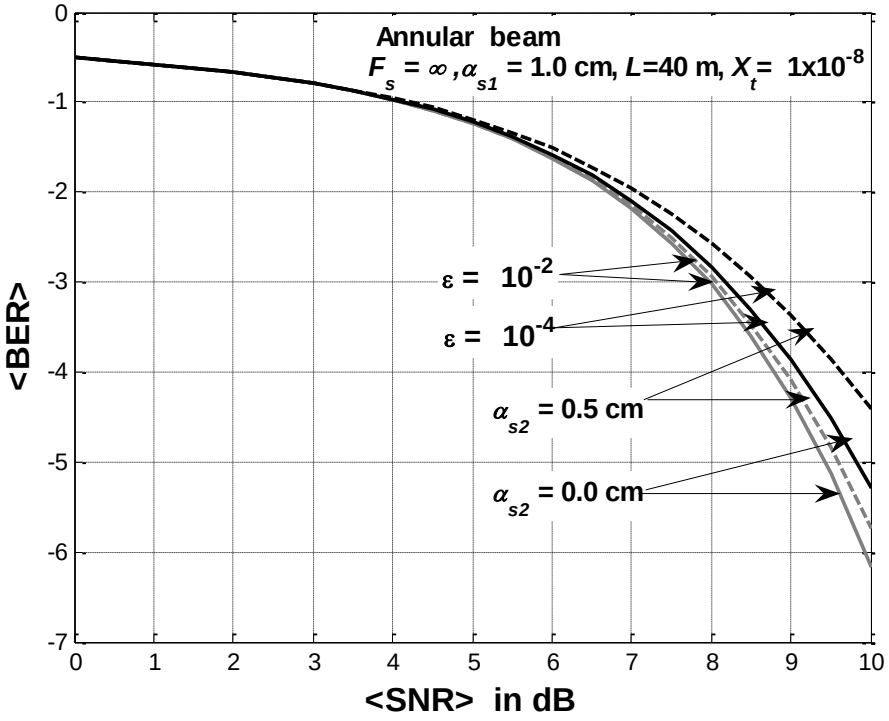

Figure 7. <*BER*> versus <*SNR*> for collimated annular beams at fixed primary source size ($\alpha_{s1} = 1$ cm), various thickness, and various rate of dissipation of turbulent kinetic energy per unit mass of fluid ε .

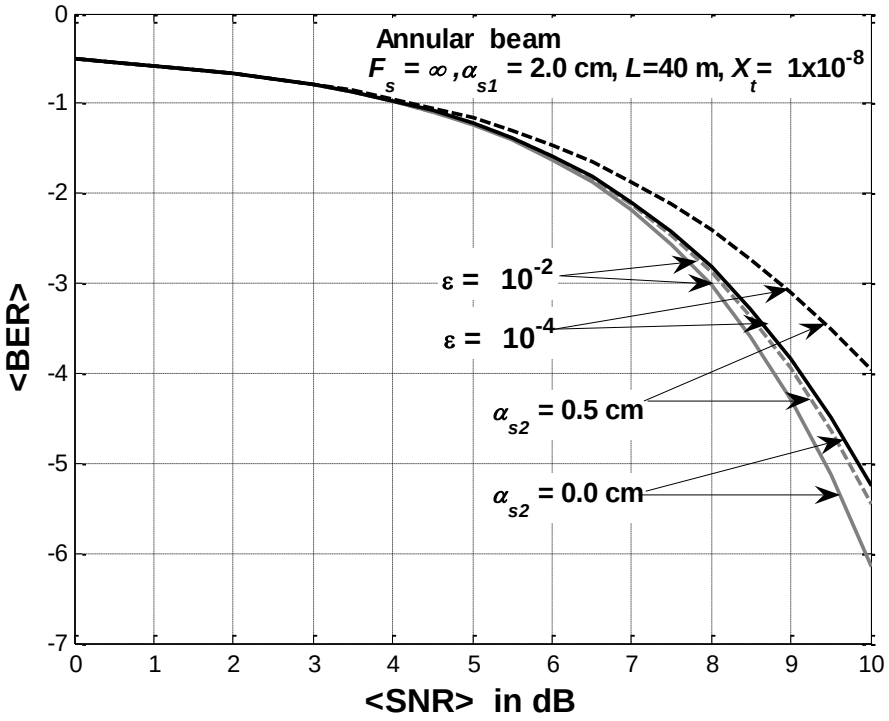

Figure 8. <*BER*> versus <*SNR*> for collimated annular beams at fixed primary source size ($\alpha_{s1} = 2$ cm), various thickness, and various rate of dissipation of turbulent kinetic energy per unit mass of fluid ε .

Scintillation index versus propagation distance L for collimated annular beams at $\alpha_{s_1} = 2$ cm, $\chi_t = 10^{-8}$ $K^2 s^{-1}$, $\varepsilon = 10^{-4}$ and various thickness is depicted in Fig.1. As thickness increases, scintillation indices decreases until α_{s_2} equals to zero, i.e, Gaussian beam case. In Fig. 2, scintillation index versus the primary source size α_{s_1} for collimated annular beams at various thickness is drawn for propagation distance $L = 40$ m, $\chi_t = 10^{-8}$ $K^2 s^{-1}$ and $\varepsilon = 10^{-2}$ and is seen that the lowest scintillation indices are at $\alpha_{s_2} = 0$ cm. Fig. 3 and 4 show the scintillation index versus the rate of dissipation of the mean squared temperature χ_T for collimated annular beams at fixed primary source sizes of $\alpha_{s_1} = 2$ cm and $\alpha_{s_1} = 1$ cm, respectively. Figs. 3 and 4 are drawn at various thickness at the propagation distance $L = 40$ m, $\chi_t = 10^{-8}$ $K^2 s^{-1}$ and $\varepsilon = 10^{-1}$. As the thickness decreases, scintillation indices increase. When Figs.3 and 4 are compared in terms of the scintillation indices at two different source size, smaller source size value has better scintillation indices values.

Scintillation indices are plotted in Fig. 5 versus the ratio of temperature and salinity fluctuations, w for collimated annular beams at $\alpha_{s1} = 2$ cm for fixed primary source size and various thicknesses. The propagation distance is $L = 40$ m, $\chi_t = 10^{-8}$ $K^2 s^{-1}$ and $\varepsilon = 10^{-1}$. Increasing values w cause a rise in scintillations. In Fig. 6, <BER> is depicted versus the primary source size α_{s1} at various thickness values at propagation distance $L = 40$ m, $\chi_t = 10^{-8}$ $K^2 s^{-1}$, $\varepsilon = 10^{-2}$ and <SNR>=10 dB. <BER> is found to have much smaller values when annular beam approaches the Gaussian beam. Figs. 7 and 8 indicate <BER> versus <SNR> for various thickness and ε values for fixed primary source sizes of $\alpha_{s_1} = 1$ cm and $\alpha_{s_1} = 2$ cm, respectively. For the Gaussian beam, <BER> is found not to change at various ε. However, for the annular beam, small source size yields much lower <BER>. It is also observed that when ε is larger,<BER> increases.

CONCLUSION

In this study, based on the temperature and salinity spatial power spectrum of underwater fluctuations, on-axis scintillation index of annular beam is derived analytically for horizontal optics communication links in a weak oceanic turbulence by utilizing Rytov solution, and <BER> with log-normal intensity distribution is examined. The results of the on-axis scintillation index of annular beam for horizontal optics communication link in weak oceanic turbulence are found to be similar to the previously obtained results for horizontal optics communication links in weak atmospheric turbulence. Our results show that as compared to collimated annular beam, annular beam yields much bigger scintillations at short distances, unlike long distances as in other articles (Namazi *et al.*, 2007; Gerçekcioglu *et al.*, 2010; Gerçekcioglu and Baykal, 2013; Gerçekcioglu and Baykal, 2013; Gerçekcioglu *et al.*, 2010; Gerçekcioglu and Baykal, 2011). Propagation distance is taken shorter than the distances in atmospheric links because strong oceanic turbulence can occur at short distances (Lu *et al.*, 2006). As the annular beam thickness decreases, the scintillation index, and naturally <BER> as well increase. Gaussian beams are found to be favorable when compared to annular beams at the stated distances.

For collimated annular beam in a weak oceanic medium, the figure, including scintillation indices versus propagation distance, shows that as secondary source size increases, scintillation index increases at constant, primary source size, rate of dissipation of turbulent kinetic energy per unit mass of fluid, and rate of dissipation of the mean squared temperature. Again, at constant, stated propagation

distance, rate of dissipation of turbulent kinetic energy per unit mass of fluid, and rate of dissipation of the mean squared temperature, when scintillation index and <BER> at fixed <SNR> versus source size is depicted, as secondary source size increases in proportional to the primary source size, scintillation index grows up. But, thinner annular beam has more advantages after a certain value without zero secondary source size. Just as the growth in the rate of dissipation of the mean squared temperature increases scintillation index at fixed, the stated propagation distance, primary source size, and the rate of dissipation of turbulent kinetic energy per unit mass of fluid, the growth in the ratio of temperature and salinity fluctuations increases scintillation index, and the growth in the rate of dissipation of the mean squared temperature increases scintillation index at fixed, the stated propagation distance, primary source size, the rate of dissipation of turbulent kinetic energy per unit mass of fluid. At certain values for the propagation distance, primary source size, and the rate of dissipation of the mean squared temperature, for the smaller value of the rate of dissipation of turbulent kinetic energy per unit mass of fluid and chancing <SNR>, annular beam has more disadvantage than Gaussian beam. However, derived formulation analytically is more important for horizontal optics communication link. The results yielded in this paper can be used in the analysis of wireless optical communication links employed in ocean.

ACKNOWLEDGMENTS

The author would like to thank Hacettepe University and Gazi University for their scientific contributions.

REFERENCES

Andrews, L. C., Phillips, R. L., Hopen, C. Y., 2001, Laser Beam Scintillation with Applications, SPIE, Bellingham, Washington.

Andrews, L. C., Phillips, R. L., 2005, Laser Beam Propagation through Random Media, SPIE, Bellingham, Washington.

Arpalı, S. A., Baykal, Y., 2009, "Bit Error Rates for Focused General-Type Beams", in Progress in Electromagnetics Research Symposium, Moscow, Russia, Vol. 5, No. 7, pp. 633-636.

Arpalı, S. A., Eyyuboğlu, H. T., Baykal, Y., 2008, "Bit Error Rates for General Beams", Applied Optics, Vol. 47, No. 32, pp. 5971-5975.

Ata, Y., Baykal, Y., 2014, "Scintillations Of Optical Plane And Spherical Waves In Underwater Turbulence", J. Opt. Soc. Am. A, Vol. 31, No. 7, pp. 1552-1556.

Baykal, Y., 2015, "Intensity Fluctuations of Multimode Laser Beams in Underwater Medium", J. Opt. Soc. Am. A, Vol.32, No. 4, pp. 593-598.

Baykal, Y., 2016, "Fourth-order Mutual Coherence Function in oceanic Turbulence", Applied Optics, Vol. 55, No. 11, pp. 2976-2979.

Cheng, M., Guo, L., Li, J., Huang, Q., Cheng, Q., Zhang, D., 2016, "Propagation of An Optical Vortex Carried by a Partially Coherent Laguerre-Gaussian Beam in Turbulent Ocean", Applied Optics, Vol. 55, No. 17, pp. 4642-4648.

Gerçekcioğlu, H., 2014, "Bit Error Focused Gaussian Beams in Weak Oceanic Turbulence", J. Opt. Soc. Am. A, Vol. 31, No. 9, 1963-1968.

Gerçekcioglu, H., Baykal, Y., 2011, ''Annular Beam Scintillations in Non-Kolmogorov Weak Turbulence", Applied Physics B - Lasers and Optics, Vol. 106, No. 4, pp. 933-937.

Gerçekcioglu, H., Baykal, Y., 2013, "BER of Annular and Flat-topped Beams in Strong Turbulence", Optics Communication, Vol. 298-299, pp. 18-21.

Gerçekcioglu, H., Baykal, Y., 2013, "BER of Annular and Flat-topped Beams in non-Kolmogorov Weak Turbulence", Optics Communications, Vol. 286, pp. 30-33.

Gerçekcioglu, H., and Baykal, Y., Nakiboğlu, C., 2010, "Annular Beam Scintillations in Strong Turbulence", J. Opt. Soc. Am. A, Vol. 27, No. 8, pp. 1834-1839.

Gerçekcioglu, H., Baykal, Y., Eyyuboğlu, H. T., 2010, "BER of Annular Beams in Strong Turbulence", Applications of Lasers for Sensing and Free Space Communications (LS&C) Topical Meeting, OSA / ASSP/LACSEA/LS&C, LSTuA4, 3 pp.

Gökçe, M. C., Baykal, Y., 2016, "Scintillation Analysis of Multiple-input Single-output Underwater Optical Links", Applied Optics, Vol. 55, No. 22, pp. 6130-6136.

Ishimaru, A., 1978, Wave Propagation and Scattering In Random Media, Vol.2, Academic Press, New York.

Korotkova, O., Farwell, N., Shchepakina, E., 2012, "Light Scintillation in Oceanic Turbulence", Waves Random Complex, Vol. 22, No. 2, pp. 260-266.

Kumar, P. V., Praneeth, S. S. K., and Narender, R. B., 2011, "Analysis of Optical Wireless Communication for Underwater Wireless Communication", International Journal of Scientific & Engineering Research, Vol. 2, No. 6, pp.194-202.

Lu, W., Liu, L., Sun, J., 2006, "Influence of Temperature and Salinity Fluctuations on Propagation Behaviour of Partially Coherent Beams in Oceanic Turbulence", Journal of Optics A, Vol. 8, pp. 1052–1058.

Namazi, N., Burris, R. J., Gilbreath, G. C., 2007, "Analytical Approach to The Calculation of Probability of Bit Error and Optimum Thresholds in Free-Space Optical Communication", Optical Engineering, Vol. 46, 025007-1-025007-7.

Nikishov, V. V., and Nikishov, V. I., 2000, "Spectrum of Turbulent Fluctuation of Sea-Water Refractive Index", International Journal of Fluid Mechanics Research, Vol. 27, pp.82-98.

Peng, X., Liu, L., Cai, Y., Baykal,Y., 2017, "Statistical Properties of a Radially Polarized Twisted Gaussian Schell-model Beam in an Underwater Turbulent Medium", J. Opt. Soc. Am. A, Vol. 34, No. 1, pp. 133-139.

Sandalidis, H. G., Tsiftsis, T. A., Karagiannidis, G. K., Uysal, M., 2008, "BER Performance of FSO Links Over Strong Atmospheric Turbulence Channels with Pointing Errors", IEEE Communications Letters, Vol. 12, No. 1, pp. 44-46.

Tatarski,V. I., 1961, Wave Propagation in a Turbulent Medium, McGraw-Hill, New York.

Tyson, R. K., Canning, D. E., Tharp, J. S., 2005, "Measurement of The Bit-error Rate of an Adaptive Optics, Free-space Laser Communications System, part 1: Tip-tilt Configuration, Diagnostics, and Closed-Loop Results", Optical Engineering, Vol. 44, 096002-1-096002-6.

Vetelino, F. S., Young,C., Andrews,L., 2007, "Fade Statistics and Aperture Averaging for Gaussian Beam Waves in Moderate-To Strong Turbulence", Applied Optics, Vol. 46, No. 18, pp. 3780–3789.

Yi, X., Li, Z., and Liu, Z., 2015, "Underwater Optical Communication Performance for laser Beam Propagation Through weak Oceanic Turbulence", Applied Optics, Vol. 54, No. 6, pp. 1273-1278.

Yousefi, M., Golmohammady, S., Mashal, A., Kashani, F. D., 2015, "Analyzing the Propagation Behavior of Scintillation Index and Bit Error Rate of a partially Coherent Flat-Topped Laser Beam in Oceanic Turbulence," J. Opt. Soc. Am. A, Vol. 32, No. 11, pp. 1982-1992.

SELÇUK ÜNİVERSİTESİ
MÜHENDİSLİK FAKÜLTESİ

S.Ü. Müh. Bilim ve Tekn. Derg., c.5, s.3, 2017
Selcuk Univ. J. Eng. Sci. Tech., v.5, n.3, 2017
ISSN: 2147-9364 (Electronic)

EFFECT OF HEIGHT ON THE STATIC STABILITY OF HETEROGENEOUS EMBANKMENT DAMS

[1]Mohsen YAZDANIAN[,*], [2]Hamid Reza AFSHOON, [3]Sadegh GHASEMI, [4]Vahid AFSHOON, [5]Farhad FAHIM

[1, 2, 3, 5] Young Researchers and Elite Club, Ahvaz Branch, Islamic Azad University, Ahvaz, Iran
[4]M.Sc student, Department of Civil Engineering, Yasooj Branch, Islamic Azad University, Yasooj, Iran
[1]m.yazdanian@iauahvaz.ac.ir, [2]hr.afshoo@yahoo.com, [3]s.ghasemi@iauahvaz.ac.ir,
[4]vahid.afshoon@yahoo.com, [5]farhad_fahim90@yahoo.com

(Geliş/Received: 23.03.2016; Kabul/Accepted in Revised Form: 03.05.2016)

ABSTRACT: The main objective in designing an embankment dam is to achieve a structure that keeps water and in addition prevents seepage in downstream that has piping and rupture. Therefore, the present study examined the effect of height on upstream and downstream slope stability of heterogeneous embankment dams with the same characteristics but with different heights at the end of construction and Steady-State Seepage and Rapid Drawdown. To investigate the effects of height, two dams with a height of 62 meters and 133 meters and 6 meters crest width were modeled in Geostudio software. The embankment dam is composed of 14 different areas with different characteristics. To analyze the dam stability, SLOP/W and to model the movement of water in dam due to presence of water behind the dam in a Rapid Drawdown and Steady-State, seepage SEEP/W in Geostudio was used. Finally, the obtained safety factors in two dams with different height are compared with each other and the obtained safety factor was compared with USBR safety factor. This research showed that the safety factor is safer for 62 meters dam. The safety factor in shorter dam is safer than long dam.

Key Words: *Embankment dam, Height, Geostudio, Slope/w, Stability analysis,*

Hetorojen Embankment Barajların Statik Stabilisezi Üzerinde Yüksekliğin Etkisi

ÖZ: Bir dolgu baraj tasarımında temel amaç suyu tutan bir yapı elde etmektir ve buna ek olarak b oru ve yırtılması olduğu mansabında sızıntı önler. Bu nedenle, bu çalışmada inşaat ve-Kararlı Hal Sızma ve hızlı Drawdown sonunda aynı özelliklere sahip heterojen dolgu barajların memba ve mansap şev stabilitesi üzerine ancak farklı yükseklikleri ile yüksekliğinin etkisi incelenmiştir. yüksekliği etkilerini araştırmak amacıyla, 62 metre ve 133 metre 6 metre kret genişliği yüksekliğinde iki baraj Geostudio yazılımında modellenmiştir. su bendi, farklı özelliklere sahip 14 farklı alanlardan oluşmaktadır. Yansımalar SLOP/W , baraj kararlılığını analiz etmek ve nedeniyle hızlı Drawdown ve Sabit-Devlet baraj arkasında suyun varlığına baraj su hareketini model, Geostudio içinde sızıntı SEEP / W kullanıldı. Son olarak, farklı yüksekliğe sahip iki baraj elde edilen güvenlik faktörleri birbirleriyle karşılaştırılmış ve elde edilen güvenlik faktörü USBR emniyet faktörü ile karşılaştırıldı. Bu araştırma emniyet faktörü 62 metre baraj için daha güvenli olduğunu göstermiştir. kısa baraj emniyet faktörü uzun baraj daha güvenlidir.

Anahtar Kelimeler: *Su bendi, Yükseklik, Geostudio, Slope/w, Stabilite analizi,*

DOI: 10.15317/Scitech.2017.88

INTRODUCTION

Embankments are made up of unsaturated compacted soils and their behaviour is strongly affected by the climatic or environmental perturbations (Cui et al., 2010; and Maharjan and Takahashi, 2014) Understanding of the structural deformation performance can be causes to design structures in a safety situation. Design and construction of structures must be including the environmental protection, the preservation of structures during natural accidents and also construction costs (Gikas and Sakellariou, 2008).

Dams are type of structures constructed against stream, river, or waterway for the purpose of restrict and controlling the move of water. A dam is constructed for particular duty such as water storage; irrigation; flood controlling and also dams are used for yield hydroelectric power (Ismail et al., 2012; Novak et al., 2001). There are two types of modern dam namely embankment dam and concrete dam.

One of the most important subjects of concern in Geotechnical and structural engineering for embankment dam is Slope stability. Slope stability analysis of earthen dam is dependent to many parameters which must consider in design and construction. Stability of these structures is composed of many ambiguities relevant to lack of precise geotechnical parameters. Because of the importance of dam construction and its related expenses, determination of dam behavior has an important result for makers. By considering the uncertainties of geotechnical parameters, applying risk analysis is unavoidable in dam construction (Manafi Ghorabaei et al., 2012).

Investigating of slope stability of earthen dam slopes is an advanced procedure which has been shown to lead to a more economical design by many researchers like (Banaki et al., 2013) which states that the cases that computed safety factor without modeling uncertainties is more than reality value. These methods do not consider many uncertainties in their computations. Also, many conservative factor of safety are using to cover some uncertainties which in most cases are more than required, and in some cases less than amount that is necessary. Actually, it is not possible to recognize the accurate effect of these factors of safety on safety level (Manafi Ghorabaei and Noorzad, 2011).

Numerical simulation methods is a good method that usually lead to make easier the real behavior of structure and widely applied in last decades. The numerical analysis is also able to simulate the behavior and any possible damage pattern of a dam (Sakamoto et al., 2002). Dams should be designed and constructed from available materials in any place that possible usually dams are constructed from material which are near to location of work due to Dams required many materials and this will not be economical to carry this material from places which are far from the location. The dams should stay stable and showed suitable and useful performance under all conditions, during construction, and ultimately in operation, both at the normal reservoir operating level and under all flood and dry conditions. Also, the dam and foundation should be having suitable behavior across to manage seepage and manage the suitable reservoir level (Ratnayaka et al., 2009). Considering the items mentioned above and knowing that dams are structures which disruption and deterioration can cause irreparable financial and physical damages, analysis of stability of embankment dams are of utmost importance. In this study, dam static stability was examined using Geostudio (Geostudio, 2007) in different modes and safety factor obtained for both cases.

MATERIALS AND METHODS

In this research, the stability of the upstream and downstream slopes of the dam embankment is performed for the most critical or severe loading conditions that may take place along the life of the dam as follow (USSD, 2007).

1) End of Construction — when significant pore pressure development is expected either in the embankment or foundation during construction of the embankment.

2) Steady-State Seepage — when the long-term phreatic surface within the embankment has been established.

3) Rapid (or Sudden) Drawdown — when the reservoir is drawn down faster than the pore pressures can dissipate within the embankment after the establishment of steady-state seepage conditions.

In this paper, Geostudio (Geostudio, 2007) is used to model two embankment dams. To study the effects of height, two dams with a height of 62 and 133 meters and 6 meters crest width were modeled in Geostudio. To analyze the dam stability, SLOP/W (2007) and to model the movement of water in the dam to analyze steady-state seepage condition, SEEP/W (2007) were used. One of the capabilities of SEEP/W is to plot the balance passing the soil and velocity vectors and drawing the flow lines and potential as well as calculating the discharge for a certain level of water. Also in Rapid Drawdown, it is assumed that the balance of the reservoir water has dropped by 60 percent, for this purpose, the 60 percent is multiplied in the height of the reservoir water in the Steady-State seepage mode to obtain the water drop then by subtracting the amount of the total height of the reservoir, the water height after drop is achieved. In this case, the materials are assumed to be consolidated and undrained (CU). In modeling, both embankment dams are modeled with the same materials. Also both embankment dams are composed of 14 different areas with different characteristics. In table 1 the properties of material is expressed. Mohr-Coulomb method, the most common way of defining the shear strength of geotechnical materials is used in current research.

Table 1. Characteristics of materials

Material		$\gamma(\frac{t}{m^3})$	$\gamma_{sat}(\frac{t}{m^3})$	ϕ	$c\ (\frac{t}{m^2})$
Clay core	Zone1(UU)	2	2.06	10	10
	Zone1(CU)	2	2.06	20	5
	Zone1(CD)	2	2.06	28	0
Upstream section	Zone 2	2.1	2.2	43	0
	Zone 3	2.1	2.2	41	0
	Zone 4	2.1	2.2	39	0
	Zone 5	2.1	2.2	38	0
	Zone 6	2.1	2.2	37	0
	Zone 7	2.1	2.2	41	0
	Zone 8	2.1	2.2	39	0
Downstream section	Zone 9	2.1	2.2	37	0
	Zone 10	2.1	2.2	36	0
Depth 0-20 m Zone 11	Depth 0-20 m Zone 11	2.6	2.65	35	30
	Depth 20-100 m zone 12	2.6	2.65	55	35
Mudstone	Zone 13	2	2.1	25	10
Conglomerate, mud stone	Zone 14	2	2.1	24	20

FACTOR OF SAFETY

Conventional analysis methods characterize the stability of a slope by computing a safety factor. The safety factor is clarified with respect to the shear strength of the soil as the ratio of the available shear strength (s) to the shear strength required for equilibrium τ as follow (US Army Corps of Engineers, 2003).

$$F = \frac{Avaliable\ shear\ strength}{Equilibrium\ shear\ stress} = \frac{s}{\tau} \quad (1)$$

If the shear strength is defined in terms of effective stresses, the safety factor is indicated as follow (US Army Corps of Engineers, 2003).

$$F = \frac{c' + (\sigma - u)\tan\phi'}{\tau} \quad (2)$$

where c' , ϕ' are Mohr-Coulomb cohesion and friction angle, respectively, expressed in terms of effective stresses; σ is total normal stress on the failure plane; u is pore water pressure; $(\sigma - u)$ is the effective normal stress on the failure plane. If the failure envelope is curved, the safety factor can be stated as follow follow (US Army Corps of Engineers, 2003).

$$F = \frac{s(\sigma')}{\tau} \quad (3)$$

Where $s(\sigma')$ characterizes the shear strength determined from the effective stress failure envelope for the particular effective normal stress, σ'. Eq 2 can be utilized with a curved failure envelope by letting c' and ϕ' characterize the intercept and slope of an equivalent linear Mohr-Coulomb envelope that is tangent to the curved failure envelope at the proper amount of normal stress, σ'. For total stresses, the safety factor is stated using the shear strength parameters in terms of total stresses, as follow (Spencer, 1967 and USBR, 2011).

$$F = \frac{c + \sigma\tan\phi'}{\tau} \quad (4)$$

Where c , ϕ are the Mohr-Coulomb cohesion and friction angle, respectively, are expressed in terms of total stresses. For analysis of Embankment dams, Morgenstern-Price (Morgenstern and Price, 1965) method is used. Morgenstern and Price (1965) developed a method similar to the Spencer (Spencer, 1967) Method, but they allowed for various user-specified interslice force functions. This method Considers both shear and normal interslice forces, Satisfies both moment and force equilibrium, and also allows for a variety of user-selected interslice force function.

RESULT AND DISCUSSION

Embankment dams during construction and operation are exposed to a variety of stresses that should be designed and implemented safe to withstand these stresses. Different researchers and engineers have already introduced various methods to analyze the stability of the slope of the embankment or rock-fill dam that can be divided into two general methods: limiting equilibrium and stress-strain. The basis of limiting equilibrium methods is on determining the imposed stress and mobilized resistance in a hypothetical fractured surface in embankment slope and then determining the safety factor given the ratio of these two quantities. In stress – deformation method, stresses and strains caused by dam in different parts of the body and foundation of embankment dam are analyzed and according to it, while preparing a picture of the behavior of the dam, safety factor on the most potential rupture surface is determined by comparing the mobilized shear strength in the surface. In examining the stability of embankment dams, forces that cause slope instability include: gravity and leakage. Given that the basic calculations are based on effective stress need to know the pore pressure, therefore, to design three critical steps should be considered: 1) the end of construction, which is affected by the compression due to the increased height of the embankment. 2) Steady-State seepage which occurs after filling the dam reservoir and passing enough time. 3) Rapid Drawdown of the reservoir, which occurs during or after the lowering of the water level in the reservoir after establishment of Steady-State seepage condition.

End of Construction Loading Condition

End of Construction phase has always higher safety factor than other phases, prior to the start of catchment, due to the reduction of pore water pressure distribution. In this case, the stability of the dam should be examined in the case of effective stress and total stress. For effective stress analyses, pore water pressures must be defined and their values must be specified. For total stress analyses using computer program, hand calculation, or slope stability charts, pore water pressures are defined as zero, actually, the pore pressures are not equal zero. This is essential because of all computer programs for slope stability analyses subtract pore pressure from the total normal stress at the base of the slice [12]. In end of the construction condition, both downstream and upstream slope of the embankment dam is in critical condition. In this case, the materials used in the clay core are undrained and unconsolidated (UU). In the effective stress space, pore water pressure is dedicated for the core. The core is also divided into some parts. To allocate these coefficients to the core, 8 identical materials are defined for the core. For these materials, according to the figure 1 values of Ru are defined and Ru related to each part is assigned to the appropriate section. Also in the total stress, the core is considered without pore water pressure. According to the obtained values, it was observed that in both dams, resulting safety factors in upstream are safer than safety factors in downstream.

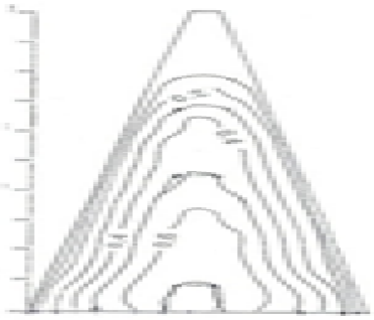

Figure 1. The values of pore water pressure Ru at the end of construction

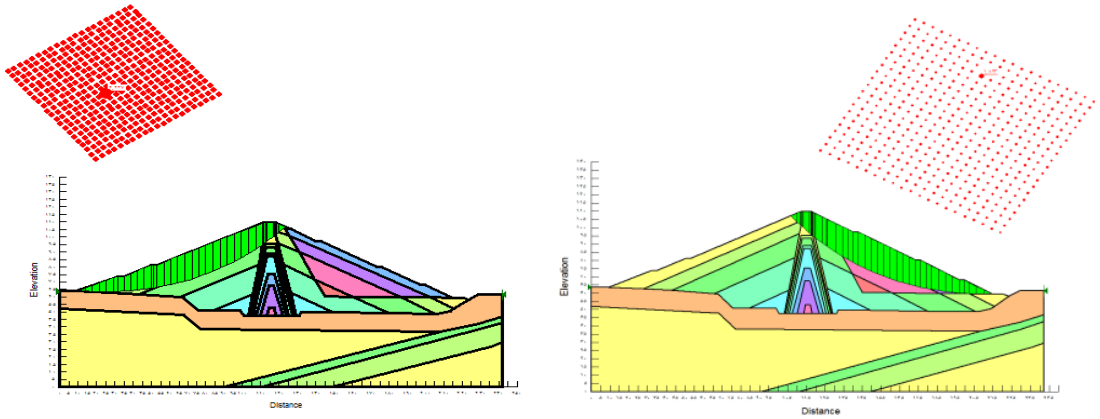

Figure 2. Analysis in effective stress space for upstream and downstream of the dam with a height of 62 meters.

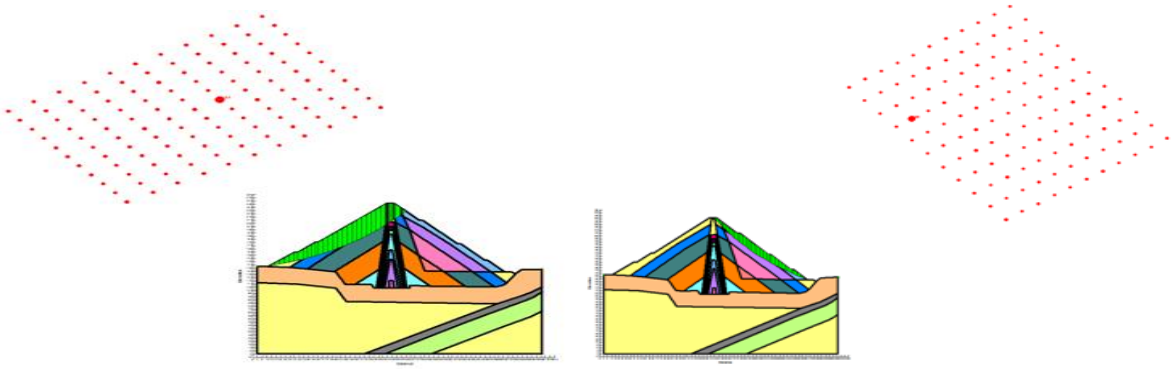

Figure 3. Analysis in effective stress space for upstream and downstream of the dam with a height of 133 meters.

Steady-State Seepage Loading Condition

After the construction of the dam and passage of the time required, Steady-State seepage condition will be established in dam body and foundation and over time the consolidation will take place in dam body. So the stability of upstream and downstream slope should be analyzed based on effective stress analysis. The basic equation of groundwater motion is obtained as two-dimensional under conditions of saturated and unsaturated flow by combining the Darcy's law and continuity equation. In Steady-State seepage condition, the upstream and downstream of dam is analyzed after the dam catchment and the stability safety factor will be controlled. Steady-state seepage loading condition should be performed using effective stress shear strength parameters joined with measured or estimated embankment and foundation pore pressures. The use of the CD triaxial shear test is appropriate for this phase (USBR, 2011). In Steady-state seepage conditions, first it should be determined the reservoir level that controls development of the steady-state phreatic surface .Since the embankment dam in most of its lifetime is in Steady-State seepage, and then it needed high safety factor. In this part, pore water pressure condition is not defined by Ru. In this case, it needed to draw phreatic line for the dam and to this end; it is performed by using SEEP/W of the software. One of the special features of this software is the possibility of modeling the condition of half-saturated soil that affect the permeability. The materials used in clay core are examined in consolidation and drained (CD) mode to let the materials to be fully consolidated and also to have the opportunity for drainage. In this analysis, after the points are extracted from SEEP/W, the extracted points are drawn in SLOP/W. in figure 4 the phreatic line obtained from SEEP/W is displayed for a dam with a height of 62 meters. Figure 5 is shown the Steady-State seepage analysis in upstream and downstream for a dam with a height of 133 meters.

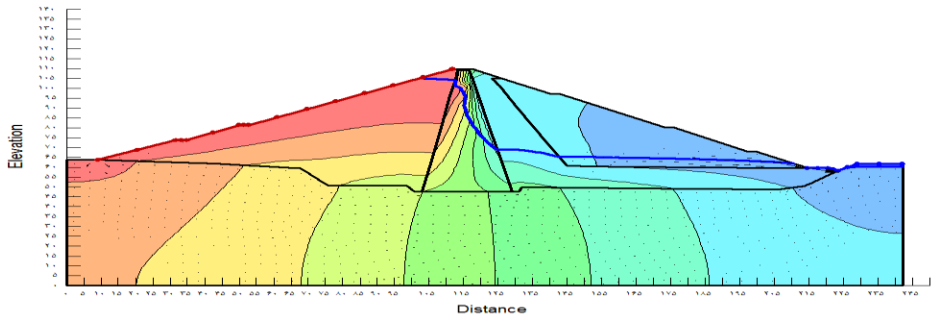

Figure 4. The movement of water in the dam using SEEP/W for a dam with a height of 62 meters.

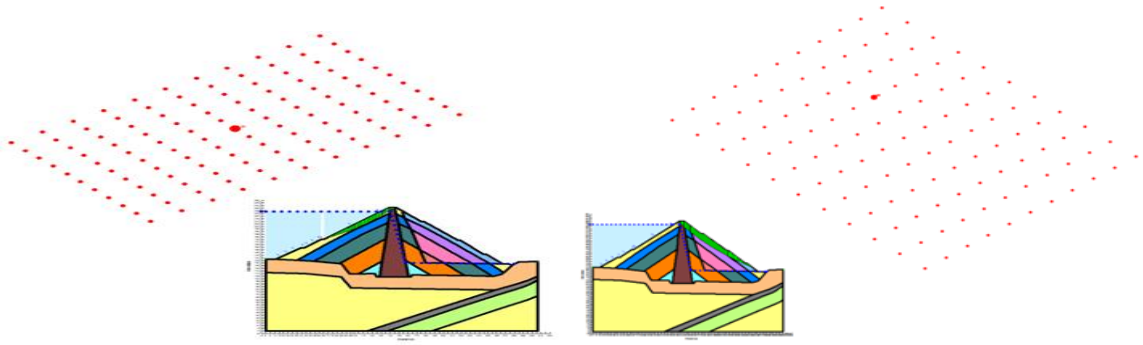

Figure 5. Steady-State seepage analysis in upstream and downstream for a dam with a height of 133 meters.

Rapid Drawdown Loading Condition

If the water level behind the dam can be lowered, the seepage in the dam body will change and seepage line will be reversed. That's why the study of upstream slope against rapid Drawdown is important. The reservoir rapid Drawdown can cause instability and incidence slip in the upstream slope which results is remaining the dam materials in saturation and starting the leakage flow towards upstream slope. If the reservoir discharge is done at a rate that in time of drop in water level, the pore water pressure inside the body is not changed and phreatic line remains in its previous position, this process is called reservoir rapid Drawdown. In the rapid Drawdown of reservoirs, sharp reduction of the pore water pressure will be created and with sharp and abrupt decrease in pore pressure, the pressure imposed to the on the dam body will increase and cause rupture in the dam body. The use of the CU triaxial shear test is appropriate for rapid drawdown condition (USBR, 2011). Tran (2004) by studying the phenomenon of rapid Drawdown in the dam reservoir concluded that with water level drops to one-third of the height of dam, confidence level decreases to a considerable amount. His studies showed that safety factor of upstream slope stability is reduced to 34% for the water level to drop for a third of the height of the dam, and the amount for the complete discharge of the reservoir is 43 percent. In rapid Drawdown , it is assumed that the reservoir level has dropped 60 percent, to this end, 60 percent is multiplied in the height of the water reservoir to obtain the water depression, then by subtracting the amount of the total height of the reservoir, the water level after loss will be obtained. In this case, materials are assumed as undrained and consolidated (CU). In Table 2 the overall results obtained for the safety factors in different states are presented, these values are obtained by performing a lot of analysis on dams.

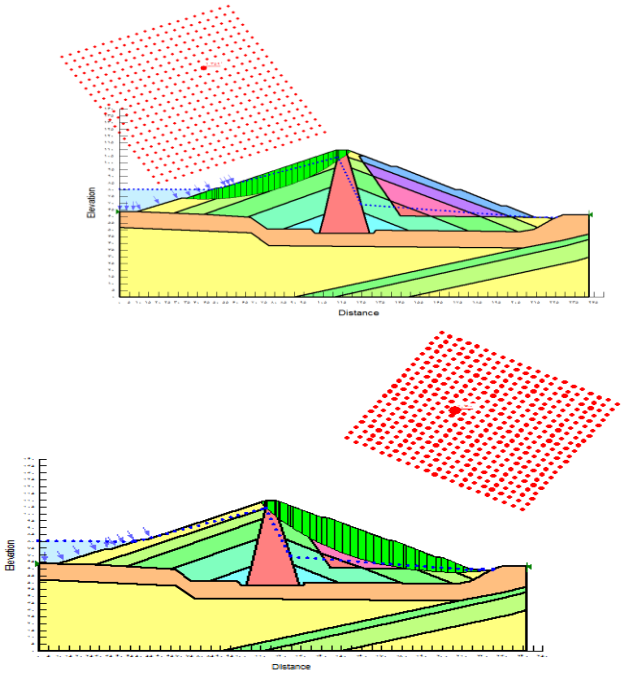

Figure 6. Rapid Drawdown analysis in upstream and downstream of dam with a height of 62 meters.

Table 2. safety factors presented in different modes

Loading condition	62(m)		133(m)	
	downstream	upstream	downstream	upstream
End of Construction (σ)	1.823	2.227	0.986	1.264
End of Construction (σ')	1.825	2.189	0.998	1.247
Steady-State Seepage	1.801	2.125	0.994	1.166
Rapid Drawdown	1.78	1.359	0.979	0.967

CONCLUSION

In this study, two dams with the completely identical characteristics and different heights were modelled using software and the effects of height on the obtained safety factor were studied. In the state of end of construction, for dams with different heights, the effective stress and the total stress of the upstream slope is more stable than downstream slope. Comparing the safety factor, it is clearly seen that the safety factor in shorter dam is safer than the higher dam. Also the value of safety factor obtained from the minimum value of USBR, which is 1.3, is more for shorter dam, which is concluded that the shorter dam is stable in this case. In case of steady-state seepage of the dam upstream slope is more stable than the downstream slope and by comparing with the value of USBR which is 1.5, it is determined that the safety factor is safer for 62-meters dam. In this case, the safety factor in shorter dam is safer than long dam. In the case of the rapid Drawdown due to change for upstream phreatic surface, and inversing the direction of seepage, pore water pressure distribution changes and seepage force may cause instability of the slope and threatens the upstream slope and it should be used proper filter and drainage for the dam. In this case, the safety factor in shorter dam is safer than the higher one. In this case, the minimum USBR value is 1.3, and then the safety factor value should be higher than the amount that for 62-meters dam it is the same, although the use of filters and drainage for upstream dam for reassuring is necessary. With an overall review of the study, it was determined that by increasing the height, dam stability and safety factors will be reduced for stability.

REFERENCES

Banaki, R., Ahmad, F., Tabarroki M., Yahaya A.S., 2013, "Probabilistic Analyses of Slopes: A State of the Art", International Journal of Current Engineering and Technology, Vol. 3(1), pp. 58-63.

Cui, Y. J., Gao, Y. B., Ferber, V., 2010, "Simulating the Water Content and Temperature Changes in an Experimental Embankment Using Meteorological Data", Engineering Geology, Vol. 114(3), pp. 456-471.

Gikas, V., Sakellariou M., 2008. "Settlement Analysis of The Mornos Earth Dam (Greece): Evidence from Numerical Modeling and Geodetic Monitoring", Engineering Structures, Vol. 30(11), pp. 3074–3081.

Ismail, M.A.M, Ng, S. M, Gey, E.K., 2012, "Stability Analysis of Kelau Earth-Fill Dam Design under Main Critical Conditions", The Electronic Journal of Geotechnical Engineering, Vol. 17

Maharjan, M., Takahashi, A., 2014, "Liquefaction-Induced Deformation of Earthen Embankments on Non-Homogeneous Soil Deposits Under Sequential Ground Motions", Soil Dynamics and Earthquake Engineering, Vol. 66, pp. 113-124.

Manafi Ghorabaei S.M, Noorzad, A., Mahdavifar, M., Soleimannejad, A., 2012, "Risk Analysis of the Slope Stability of Embankment Dam Using Three Different Approaches", 6th International Symposium on Advances In Science and Technology, Kuala Lumpur, Malaysia, 24-25 March, 2012.

Manafi Ghorabaei, S M, Noorzad, A, 2011. "Role of Risk Assessment in Repair and Rehabilitation of Earth Dams", Proceedings of the National Workshop on Operation, Maintenance and Rehabilitation of Dams and Hydropower Plants, Tehran, Iran: Iranian National Committee on Large Dams (IRCOLD).

Morgenstern, N.R., Price, V.E., 1965, "The Analysis of the Stability of General Slip Surface" Geotechnique, Vol. 15, pp. 79-93.

Novak, P., Moffat, A.I.B., Nalluri, C., Narayanan, R., 2001, Hydraulic Structures Fourth Edition, Taylor & Francis Group, London.

Ratnayaka, D.D., Brandt, M.J., Johnson, M., 2009, Twort's Water Supply 6th Edition, Butterworth-Heinemann: Elsevier.

Sakamoto, T., Yoshida, H., Yamaguchi, Y., Satoh, H., Tomoya, I., 2002, "Numerical Simulation of Sliding of An Earth Dam During The 1995 Kobe Earthquake" in Proceedings of the 22nd USSD Annual Meeting and Conference, Pre-conference Workshop, 3rd U.S.Japan Workshop on Advanced Research on Earthquake Engineering for Dams, San Diego, California, 26-31 March 2001.

Seepage Modeling with SEEP/W, 2007, An Engineering Methodology Third Edition, March 2008, GEO-SLOPE International Ltd., Canada.

Spencer E, 1967, "A Method of Analysis of The Stability of Embankments assuming Parallel Interslice Forces", Geotechnique, Vol 17 (1), pp. 11-26.

Stability Modeling with SLOPE/W, 2007, An Engineering Methodology Third Edition, March 2008, GEO-SLOPE International Ltd

Tran, T.X., 2004, Stability problems of An Earth Fill Dam in Rapid Drawdown Condition, Doctoral dissertation Slovak University of Technology, Bratislava, Slovak Republic.

United States Society on Dams, 2007, Strength of Materials for Embankment Dams, Denver, USA: US Society on Dams.

US Army Corps of Engineers, 2003, Engineering and Design - Slope Stability, Washington DC, USA: US Army Corps of Engineers.

USBR, 2011, Design standard No. 13, Embankment Dams, Chapter 4: Static Stability Analysis, U.S, Department of the Interior, Bureau of Reclamation.

SELÇUK ÜNİVERSİTESİ
MÜHENDİSLİK FAKÜLTESİ

S.Ü. Müh. Bilim ve Tekn. Derg., c.5, s.3, 2017
Selcuk Univ. J. Eng. Sci. Tech., v.5, n.3, 2017
ISSN: 2147-9364 (Electronic)

LANDSLIDE SUSCEPTIBILITY MAPPING OF CANIK (SAMSUN) DISTRICT USING BAYESIAN PROBABILITY AND FREQUENCY RATIO MODELS

[1]Halil AKINCI, [2]Sedat DOĞAN, [3]Cem KILIÇOĞLU

[1]Artvin Çoruh University, Department of Geomatics Engineering, Seyitler, Artvin, TURKEY
[2]Ondokuz Mayıs University, Department of Geomatics Engineering, Kurupelit, Samsun, TURKEY
[3]Ondokuz Mayıs University, Kavak Vocational School, Kavak, Samsun, TURKEY
[1]hakinci@artvin.edu.tr, [2]sedatdo@omu.edu.tr, [3]cemk@omu.edu.tr

(Geliş/Received: 14.11.2016; Kabul/Accepted in Revised Form: 10.02.2017)

ABSTRACT: Landslides cause serious damage to infrastructure and property in many cities of Turkey, as well as the loss of life. Samsun is one of the cities where landslides are most frequently seen in Turkey. Most of the landslides occurred throughout the province, especially within the Atakum, Canik and İlkadım districts, have been described as natural disaster. In this study, the aim was to produce landslide susceptibility maps for one of these highly sensitive districts, Canik. For this purpose, the parameters of slope, aspect, altitude, topographic wetness index, profile and plan curvature, lithology, distance to drainage network and roads have been used in the landslide susceptibility analysis. Bayesian Probability (BP) and frequency ratio (FR) models have been used in the study. The areas in the produced susceptibility maps have been classified into five groups as "very low, low, moderate, high and very high susceptible". The verification and control results revealed that the landslide susceptibility map generated using the BP model is more accurate than the FR model. At the same time, the very high and high susceptible areas in the landslide susceptibility map produced by BP model were compatible with the control landslides with a rate of 83.5%. These results indicated that the landslide susceptibility map generated using the BP model can be used for land use planning and landslide risk reduction studies.

Key Words: *GIS, Landslide susceptibility, Bayesian probability model, Frequency ratio model, Canik, Samsun.*

Bayes Olasılık ve Frekans Oranı Modelleri Kullanılarak Canik (Samsun) İlçesinin Heyelan Duyarlılığının Haritalanması

ÖZ: Heyelanlar, Türkiye'nin birçok şehrinde altyapı ve mülkiyete ciddi zarar vermenin yanı sıra can kaybına da neden olmaktadır. Samsun, Türkiye'de heyelanların en sık görüldüğü şehirlerden birisidir. İl genelinde doğal afet olarak nitelendirilen çok sayıda heyelan meydana gelmiştir. Bu çalışmada, Samsun ili Canik ilçesinin heyelan duyarlılık haritaları üretilmiştir. Heyelan duyarlılık analizinde eğim, bakı, yükseklik, topoğrafik nemlilik indeksi, profil ve plan eğriliği, litoloji, drenaj ağlarına ve yola uzaklık parametreleri kullanılmıştır. Çalışmada, bayes olasılık (BO) ve frekans oranı (FO) modelleri kullanılmıştır. Üretilen duyarlılık haritaları, "çok düşük, düşük, orta, yüksek ve çok yüksek derecede duyarlı" alanlar olmak üzere 5 grup altında sınıflandırılmıştır. Doğrulama ve kontrol sonuçları, BO modeli kullanılarak üretilen heyelan duyarlılık haritasının FO modelinden daha doğru olduğunu ortaya koymuştur. Aynı zamanda, BO modeli kullanılarak üretilen heyelan duyarlılık haritasındaki çok yüksek ve yüksek derecede heyelana duyarlı alanların kontrol heyelanları ile %83,5 oranında uyumlu olduğu

Note: This paper has been presented at the Selcuk International Scientific Conference on Applied Sciences (ISCAS 2016) held in Antalya (Turkey), September 27-30, 2016.

DOI: 10.15317/Scitech.2017.89

tespit edilmiştir. Bu sonuçlar, BO modeli kullanılarak üretilen heyelan duyarlılık haritasının, arazi kullanım planlaması ve heyelan risk azaltma çalışmalarında kullanılabileceğini göstermiştir.

Anahtar Kelimeler: *CBS, heyelan duyarlılığı, Bayes olasılık modeli, Frekans oranı modeli, Canik, Samsun.*

INTRODUCTION

Disasters are the events that cause social, cultural and economic devastation. Vos et al. (2010) defines disaster as "a situation or an event which overwhelms local capacity, necessitating a request at a national or international level for external assistance; an unforeseen and often sudden event that causes great damage, destruction, and human suffering". In 2015, 376 natural disasters were reported at a global level, resulting in death of 22,765 people, affecting more than 110.3 million victims, and causing an economic loss of more than US$ 70.3 billion (Guha-Sapir et al., 2016).

In 1988, the Centre for Research on the Epidemiology of Disasters (CRED) launched the "Emergency Events Database (EM-DAT) that contains essential core data on the occurrence and impact of over 13,800 natural and 8,200 technological disasters across the globe, dating from 1900 to the present day" (Guha-Sapir et al., 2016). EM-DAT handles disasters in two categories such as technological and natural disasters. The category of natural disasters is divided into six subgroups including 17 disaster types. On the basis of this classification, natural disasters can be defined as the "results of biological, meteorological, hydrological, climatological, and geophysical based events, which are unpredictable and cannot be prevented".

Landslide is one of the most common natural hazards in the world. Varnes (1958) defines the landslide as "the downward and outward movement of the slopes composed of natural rock, soils, artificial fills, or combinations of these materials". As in other natural disasters, landslides cause injuries, deaths, economic losses, and loss of natural and cultural heritage. For example, in April 2017, because of the massive landslide, 11 houses were devastated and 24 people were killed in the Uzgen district of southern Kyrgyzstan.

Landslides are known as the most dangerous and widespread natural hazards in Turkey. When natural hazards between 1950–2000 were examined in Turkey, it is seen that they are most common natural hazard with a rate of 45% (Gokce et al., 2008). In Turkey, the devastating effect of the landslides has been lastly seen in the Borçka district of the Artvin Province on 11 November 2015. 11 people were injured and 2 people lost their lives in this landslide, which was caused by heavy rains. In Turkey, Samsun is one of the foremost provinces, wherein landslides occur at a higher frequency. In the damage distribution and microzonation study performed by Doyuran et al. (1985) in Samsun, the city center including Atakum, İlkadım and Canik districts was divided into three regions; (a) inconvenient areas for construction (existing buildings must be evacuated), (b) areas where new construction is objectionable (existing structures will be freezed), and (c) the areas where new construction will be allowed under certain circumstances. However, urbanization rate is higher in the mentioned districts where landslides occur more frequently. Considering the fact that the landslides are the most important natural hazards that cause property and life losses in Turkey, there is a need for producing landslide susceptibility maps especially for cities with high landslide potential such as Samsun to prevent the possible loss of life and property.

The economic, cultural and social losses caused by landslides can be reduced by effective planning and management. For this purpose, different kinds of maps are prepared with different information by making land and laboratory studies for geological and geotechnical purposes in the selection of settlement areas, infrastructure works and other engineering works. One of the most important geological based maps prepared in this framework is landslide susceptibility maps (Yalçın, 2007). These maps provide information about susceptive areas for landslides in the future and the inclination of an area towards possible landslides (Dağdelenler, 2013; Chalkias et al., 2014; Petschko et al., 2014). In the studies evaluating the methods and parameters used to prepare the such maps (Gökçeoğlu and

Ercanoğlu, 2001; Dağ et al., 2011; Jebur et al., 2014; Kayastha 2015; Kavzoglu et al., 2015), it has been stated that the lithology, slope, land cover and aspect are frequently used parameters, although the researchers have been using different parameters in landslide susceptibility analysis due to regional characteristics. However, in parameter selection, it is also important whether or not the data related to any parameter can be obtained easily. Moreover, the literature shows that there is not yet consensus among researchers about the parameters and methods used in the production of landslide susceptibility maps, leading a large number of methods and parameters to be used (Chen et al., 2017; Sezer et al., 2017; Colkesen et al., 2016; Barrile et al., 2016; Hong et al., 2016) because each researcher take into consideration the parameters related to field that they work (Gökçeoğlu and Ercanoğlu, 2001; Dağ et al., 2011). Dağ *et al.* (2011) stated that in the preparation of landslide susceptibility maps, statistical methods are used in rate of 64%.

The main objective of this research was to produce landslide susceptibility maps for Canik, one of the districts of Samsun province, known as highly sensitive to landslide occurrence. In this study, the parameters of altitude, aspect, slope, topographic wetness index (TWI), profile curvature, plan curvature, lithology, and distance to drainage network and roads were used. Bayesian probability and frequency ratio models were chosen for this study since they are widely used in the literature, consist of understandable and simple statistical models, provide accurate results, and can easily be applied.

MATERIAL AND METHOD

Study Area

Canik district is located in Samsun Metropolitan Municipality boundaries. It neighbors Tekkeköy district on the east, İlkadım district and Mert River on the west, Black Sea on the north, Kavak and Asarcık district on the south (Figure 1).

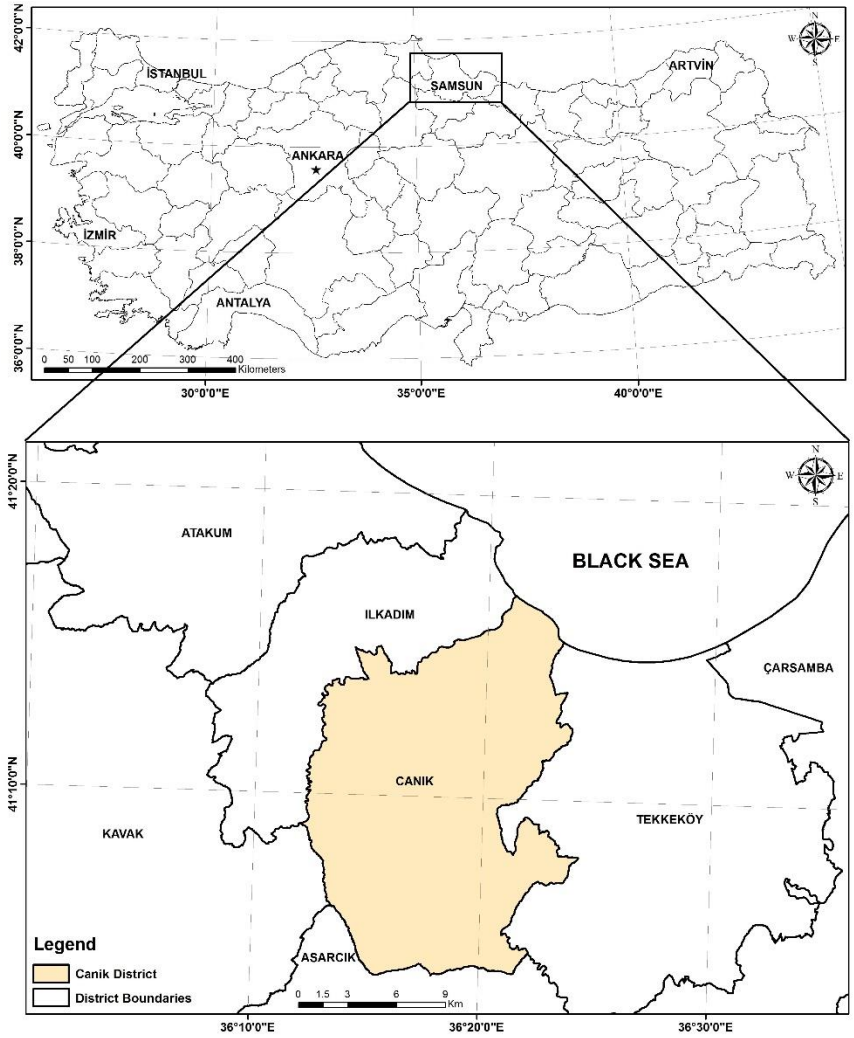

Figure 1. Location map of the study area

According to the Address Based Population Registration System, population of Canik was 96.541 in 2015. The district is between 41° 4′ 4.59″ – 41° 16′ 44.64″ north latitude and 36° 12′ 2.89″ – 36° 24′ 13.35″ east longitude and has an area of 262 km².

The slope ranges from 0° to 79.32° in the district. The average slope is about 18°. Approximately 19% of the study area, the slope is below 10°. The areas where the slope is between 10° and 20° cover 34% of the study area and the areas with the slope above 20° are about 47%. According to CORINE 2012 land cover data, 58% of the study area is composed of agricultural and 35% is forest area. In Samsun, the climate of the Black Sea is seen. This kind of climate is rainy every season, hot in summers and warm in winters. The long-term average annual rainfall in Samsun is 694mm. According to the average of 40 years between 1970 and 2010, the average annual temperature in Samsun is 14.4°C. The hottest months are July (23.3°C) and August (23.5°C), while the coldest months are January (7.0°C) and February (6.9°C) (Bahadır, 2013).

Lithology of the Study Area

As shown in Figure 2, seven different formations are seen from older to younger in the Canik district (Öztekeşin, 2008; Keskin, 2011; Temizel et al., 2014).

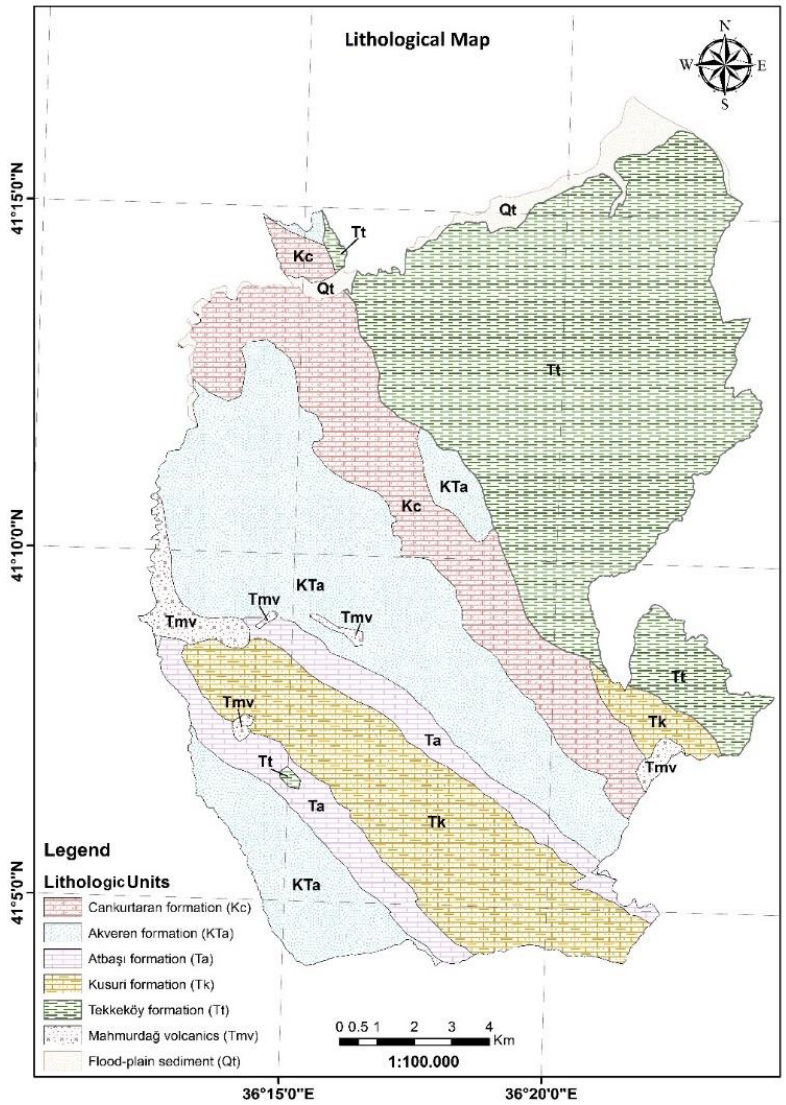

Figure 2. Lithological map of the study area

Cankurtaran formation (Kc): Cankurtaran formation consists of tuff-tuffite, sandy limestone, and marl intercalated with sandstone and shale alternations (Temizel et al., 2014).

Akveren formation (Kta): Akveren formation consists of sandstone, sandy limestone, limestone, and marl with siltstone and shale intercalations (Temizel et al., 2014).

Atbaşı formation (Ta): Atbaşı formation consists of limestone, sandy limestone, sandstone, and marl intercalations (Temizel et al., 2014).

Kusuri formation (Tk): Kusuri formation consist of marl, sandstone, siltstone, limestone and calcareous sandstone alternations (Keskin, 2011).

Tekkeköy formation (Tt): Tekkeköy formation consist of sandstone, marl and tuffite alternations, basalt and anglomera (Keskin, 2011).

Mahmurdağ volcanics (Tmv): Mahmurdağ volcanics consist of basaltic lava, dike and sills (Keskin, 2011).

Current flood-plain deposits (Qt): These deposits consist of silt, clay and very fine sand and their thickness range from 10 to 15 m (Keskin, 2011).

Data Handling and Data Preparation

In this study, the parameters, such as altitude, aspect, slope, profile and plan curvatures, TWI, lithology, proximity to the drainage networks and roads were used. Descriptive statistical data of the environmental parameters used in the study was presented in Table 1. The basic data required to produce the landslide susceptibility maps of the study area were obtained from 1/25.000 scale Standard Topographic Maps. At first, the digital elevation model (DEM) of the study area was created by using contour lines in the topographic maps in ArcGIS 10.2. The DEM was converted into 10×10 m cell size raster format and then altitude, aspect, slope, TWI, profile and plan curvature maps of the study area were produced. 1/25.000 scale digital geology and landslide inventory maps of the study area were procured from the MREI (General Directorate of Mineral Research and Exploration Institute). These maps were also converted into 10×10 m cell size raster format. In order to produce the landslide susceptibility map, the produced parameters maps were compared one by one with the landslide inventory map, and thus the relations of each layer to landslides were found.

Table 1. Descriptive statistical data of the environmental parameters used in the study

Parameter	Min.	Max.	Mean	Std. Deviation	Data Type	Scale
Elevation (m)	0	1000	535.01	212.26	GRID	10x10 m
Slope (°)	0	79.32	18.30	9.58	GRID	10x10 m
Plan curvature	-16.55	13.63	-0.06	0.82	GRID	10x10 m
Profile curvature	-49.34	58.23	-0.20	1.08	GRID	10x10 m
TWI	2.51	28.24	7.04	2.13	GRID	10x10 m
Proximity to road	0	1933.42	298.41	264.38	GRID	10x10 m
Proximity to drainage	0	819.39	151.77	105.01	GRID	10x10 m

The first step in assessing landslide susceptibility is to learn about the past landslides occurred within the research area. This is based on the assumption that future landslides can occur under similar conditions, wherein the past landslides occurred (Lee and Talip, 2005; Kumtepe et al., 2009; Erener and Düzgün, 2010; Kavzoglu et al., 2015). Therefore, one of the most important datasets required for studying landslide susceptibility is "landslide inventory maps", as these maps show the existing landslide areas on land (Çevik and Topal, 2003; Yalçın 2007). In this study, 1/25000 scale digital landslide inventory maps produced by MREI were used. There are 20 landslides (6 active and 14 inactive) with a total area of 232.52 ha on the landslide inventory map. In the 1/25.000 scale landslide inventory maps produced by the MREI, classification of landslides was based on Varnes (1978) classification (Çan et al., 2013). However, in the digital landslide inventory map provided from MREI within the scope of the study, landslides were classified as active and inactive according to their activities only. 46.8% of the landslides were in the Cankurtaran formation and 29.11% were in the Akveren formation. Approximately 77% of the landslide areas were analyzed and 23% were used as validation data sets.

Lithology is one of the most important parameters affecting the formation of landslides (Kumtepe et al., 2009) and is an important parameter considered in the susceptibility studies, owing to the fact that different lithological units have different levels of sensitivity to active geomorphological processes including landslides. Geomorphological processes are partly based on the lithology and the dissociation properties of the basic materials constituting to the lithology (Dai et al., 2001, Çevik and Topal, 2003). Lithological units in the study area were obtained from the 1/25.000 scale geological maps produced by MREI (Figure 2).

Slope angle is considered as the most important parameter of the landslide susceptibility analysis (Lee and Min, 2001; Dai et al., 2001). In several studies, this parameter was given the first priority for producing landslide susceptibility maps (Yalçın, 2008; Yılmaz, 2009; Erener and Düzgün, 2010). Previous studies and field observations have indicated that susceptibility to landslide increases with the rising slope (Yalçın, 2007). Therefore, the DEM of the study area was produced by using the contour lines in

ArcGIS 10.2 GIS software. Generated DEM was converted into 10 m × 10 m cell size ESRI GRID format and the slope of the study area map was determined. The produced slope map was reclassified with 5^0 increments and the distribution of the landslides corresponding to each slope group was identified by comparing it to the landslide inventory maps (Table 2). The maximum slope in the study area was found to be 79^0 and the most of the landslides according to the slope map were in $15–20^0$ slope group with 21.97% occurrence.

Like slope, aspect is also used as an important parameter in the generation of landslide susceptibility maps (Çevik and Topal, 2003; Ercanoğlu *et al*., 2004). An increase in the frequency of landslides in certain aspects can generally be associated with both the morphology of the study area and the meteorological conditions such as general rainfall direction or solar radiation intake. The soil infiltration capacity depends on many factors such as soil type, slope, permeability, porosity, soil moisture, organic matter contents, vegetation cover, and the season of precipitation. The slopes receiving more rainfall will reach saturation more quickly than the other slopes. Accordingly, this leads to the development of pore water pressure in such slopes (Gökçeoğlu and Ercanoğlu, 2001). In order to reveal the relationship between the aspect and landslides, aspect map of the study area was produced with DEM. The aspect map was divided into nine classes and the percentage presence of landslides in each group was calculated (Tables 2). The aspect map revealed that 21.65% of the landslides in the study area occur on the slopes with south aspect, and 20.33% on the slopes with southwest aspect.

The altitude map of the area was produced using DEM to determine the landslide-altitude relations in the study area. The altitude of the study area varies between 20 and 1000 m. The values of elevation were divided into ten categories with 100 m increments, and landslide-altitude relationship was identified. Using this map, it was identified that the most of the landslides with 36.31% frequency occurred in areas at altitudes ranging from 300 to 400 m in the study area (Tables 2).

Curvature shows the morphological structure of topography (Lee and Min, 2001; Erener and Düzgün, 2010). Curvature maps are obtained as second derivative of DEM, thus they show changes in the slope (Erener and Düzgün, 2010). A positive curvature indicates an upward convex surface, while a negative curvature is indicative of an upward concave surface, and zero represents a flat surface. Plan curvature refers to the tendency of the surface for the water flow to converge (where the flow is collected) or diverge (where the flow is dispersed). The plan curvature with negative value indicates that the flow is collected, and a positive value indicates that the flow is dispersed. Streams and ridges can be removed from these values. Profile curvature indicates flow speed of the water on the surface and convection of sediments along the slope of the curvature and erosion by expressing the slope change. Negative profile component shows concave (hollow) and positive values show convex (top) structure (Kılıç and Gökaşan, 2009). The plan and profile curvature maps of the study area were produced from DEM.

Table 2. Spatial relationship between elevation, slope, aspect, plan and profile curvature with landslides

Factor	Category	No. of cells in category	No. of landslide cells	PoL	PoC	FR	W^+	W^-	C
Elevation (m)	20-100	112506	510	2.19	4.29	0.5102	-0.6773	0.0219	-0.6992
	100-200	136814	2469	10.61	5.22	2.0312	0.7179	-0.0590	0.7769
	200-300	177784	3182	13.67	6.79	2.0146	0.7095	-0.0774	0.7869
	300-400	247729	8452	36.31	9.46	3.8402	1.3713	-0.3545	1.7258
	400-500	300688	5889	25.30	11.48	2.2044	0.8013	-0.1712	0.9725
	500-600	426588	1860	7.99	16.28	0.4908	-0.7163	0.0953	-0.8117
	600-700	615338	620	2.66	23.49	0.1134	-2.1847	0.2432	-2.4278
	700-800	423978	293	1.26	16.18	0.0778	-2.5620	0.1655	-2.7275
	800-900	152730	0	0.00	5.83	0.0000	-6.3771	0.0606	-6.4377
	900-1000	25606	0	0.00	0.98	0.0000	-4.5913	0.0099	-4.6012

Slope (°)	0-5°	317804	1579	6.78	12.13	0.5592	-0.5851	0.0596	-0.6447
	5-10°	172537	2284	9.81	6.59	1.4900	0.4032	-0.0355	0.4386
	10-15°	364151	4454	19.14	13.90	1.3767	0.3231	-0.0633	0.3864
	15-20°	518619	5113	21.97	19.80	1.1097	0.1051	-0.0277	0.1327
	20-25°	568313	4927	21.17	21.69	0.9758	-0.0247	0.0067	-0.0314
	25-30°	416583	3047	13.09	15.90	0.8233	-0.1961	0.0332	-0.2292
	30-35°	188781	1230	5.28	7.21	0.7334	-0.3125	0.0207	-0.3332
	35-40°	58196	521	2.24	2.22	1.0077	0.0077	-0.0002	0.0079
	40-45°	12833	106	0.46	0.49	0.9297	-0.0735	0.0003	-0.0739
	> 45°	1944	14	0.06	0.07	0.8106	-0.2117	0.0001	-0.2118
Aspect	Flat	212888	740	3.18	8.13	0.3912	-0.9439	0.0529	-0.9968
	North	325497	2367	10.17	12.42	0.8185	-0.2019	0.0257	-0.2276
	Northeast	283137	2883	12.39	10.81	1.1461	0.1377	-0.0180	0.1557
	East	319733	1901	8.17	12.20	0.6692	-0.4046	0.0454	-0.4500
	Southeast	301823	1567	6.73	11.52	0.5844	-0.5409	0.0532	-0.5941
	South	251493	5038	21.65	9.60	2.2548	0.8244	-0.1442	0.9686
	Southwest	229258	4732	20.33	8.75	2.3232	0.8549	-0.1368	0.9917
	West	285199	2442	10.49	10.89	0.9638	-0.0372	0.0045	-0.0417
	Northwest	410733	1605	6.90	15.68	0.4398	-0.8264	0.1000	-0.9264
Plan Curvature	Concave	1041698	10053	43.19	39.76	1.0862	0.0835	-0.0591	0.1426
	Flat	352312	1716	7.37	13.45	0.5482	-0.6051	0.0685	-0.6736
	Convex	1225751	11506	49.44	46.79	1.0566	0.0555	-0.0515	0.1070
Profile Curvature	Concave	1211429	11365	48.83	46.24	1.0560	0.0549	-0.0498	0.1047
	Flat	285623	1232	5.29	10.90	0.4855	-0.7272	0.0616	-0.7888
	Convex	1122709	10678	45.88	42.86	1.0705	0.0688	-0.0548	0.1236

PoL: percentage of landslide occurrence in each subcategory, PoC: percentage of each subcategory, FR: Frequency Ratio, W^+: positive weight, W^-: negative weight, C: weights contrast

Another important variable controlling the stability of the slope is the degree of saturation of the material on the slopes. The proximity of slopes to drainage network is another important factor in terms of stability. Running waters such as rivers or creeks disrupt the stability by eroding the filling and toe of slopes or by saturating the material constituting the slope to the level of the stream or in both ways (Yalçın, 2008). The drainage network in the study area was produced from DEM and the proximity map of the drainage using related GIS analysis routines. The relationship between distance to drainage networks and landslides is shown in Table 3. Approximately 90% of the landslides in the study area were in the first 300 m distance to drainage networks.

Table 3. Spatial relationship between lithology, TWI, distance to roads and drainage with landslides

Factor	Category	No. of cells in category	No. of landslide cells	PoL	PoC	FR	W^+	W^-	C
Distance to drainage	0-100	991780	7103	30.52	37.86	0.8061	-0.2173	0.1127	-0.3300
	100-200	788517	8282	35.58	30.10	1.1822	0.1690	-0.0824	0.2514
	200-300	567426	5557	23.88	21.66	1.1023	0.0983	-0.0289	0.1273
	300-400	235527	2201	9.46	8.99	1.0518	0.0510	-0.0052	0.0562
	400-500	33698	132	0.57	1.29	0.4409	-0.8239	0.0073	-0.8313
	500-600	2248	0	0.00	0.09	0.0000	-4.4611	0.0009	-4.4619
	600-700	373	0	0.00	0.01	0.0000	-2.6648	0.0001	-2.6650
	700-819	192	0	0.00	0.01	0.0000	-2.0008	0.0001	-2.0008
Distance to roads	0-100	691487	7208	30.97	26.40	1.1733	0.1614	-0.0647	0.2261
	100-200	496860	5287	22.72	18.97	1.1977	0.1822	-0.0478	0.2300
	200-300	380317	4666	20.05	14.52	1.3809	0.3262	-0.0675	0.3936
	300-400	295019	2538	10.90	11.26	0.9683	-0.0325	0.0040	-0.0365
	400-500	228447	1548	6.65	8.72	0.7627	-0.2730	0.0226	-0.2956
	500-600	167421	955	4.10	6.39	0.6420	-0.4463	0.0244	-0.4707
	600-700	117792	452	1.94	4.50	0.4319	-0.8446	0.0266	-0.8712
	700-1100	212091	621	2.67	8.10	0.3296	-1.1160	0.0579	-1.1739
	1100-1500	28059	0	0.00	1.07	0.0000	-4.6827	0.0109	-4.6936
	1500-1933	2268	0	0.00	0.09	0.0000	-2.1673	0.0009	-2.1682
TWI	2.51-6.04	854329	8784	37.74	32.61	1.1573	0.1475	-0.0798	0.2273
	6.04-7.86	1176947	9712	41.73	44.93	0.9288	-0.0745	0.0570	-0.1315
	7.86-10.38	383989	3598	15.46	14.66	1.0547	0.0537	-0.0095	0.0632
	10.38-14.12	171865	1088	4.67	6.56	0.7125	-0.3415	0.0202	-0.3616
	14.12-28.24	32631	93	0.40	1.25	0.3208	-1.1430	0.0086	-1.1516
Lithology	Ta	185202	0	0.00	7.07	0.0000	-4.2673	0.0740	-4.3413
	Tk	382681	0	0.00	14.60	0.0000	-4.9930	0.1594	-5.1525
	Tmv	46912	0	0.00	1.79	0.0000	-2.8941	0.0182	-2.9123
	Tt	916458	5228	22.47	34.98	0.6423	-0.4462	0.1778	-0.6241
	Kc	340041	10890	46.80	12.98	3.6061	-4.8424	-0.4953	-4.3470
	Kta	689789	6775	29.11	26.32	1.1059	0.1013	-0.0388	0.1400
	Qt	59223	378	1.62	2.26	0.7187	-0.3332	0.0066	-0.3398

PoL: percentage of landslide occurrence in each subcategory, PoC: percentage of each subcategory, FR: Frequency Ratio, W^+: positive weight, W^-: negative weight, C: weights contrast

The stability problems can also be seen in slopes that are affected by the construction of roads (Yalçın, 2008). The roads opened on the slopes cause load reduction both at the toe of slopes and in the topography, leading to an increase in the tension behind the slope and the development of tension cracks. Instability might be caused as the negative effects of road constructions, as water entering the roads from outside may disturb the equilibrium on slope. The road network in the study area was obtained digitally from Başarsoft Company. The map showing the proximity of the road was produced using the corresponding GIS analysis routines. In order to determine the relationship between the proximity to roads and the landslides, the road map and the landslide map were overlaid and it was found that 30.97% of the landslides in the study area were occurred within 100 m of the roads (Table 3).

One of the indicators used while evaluating the saturation of geological material in a field is topographic wetness index (TWI). This index provides information about the aerial dimension of the

study area in respect to its water saturation. The infiltration of water into the material increases pore water pressure in the material as well as reduces the strength of the material (Gökçeoğlu et al., 2005). Therefore, the direction and density of flow in the study area were calculated using the DEM; and the relative TWI map of the area was prepared. The relationship between landslides with TWI is shown in Table 3.

METHODS USED IN THE STUDY

Bayesian Probability Model

Bayesian probability model is a probability theorem, which can be used to obtain posteriori probability by updating the premise of probability expectations related to an event with new information obtained in case of the realization of the event (Akıncı et al., 2015). Accordingly, when an estimation of the risk of landslides in a region is desired, some of the possible situations must be determined. In such a case, there might be following conditions of landslide events. The selected area can be really a landslide area having two possibilities: there will be or will not be a landslide in the future. If the selected area is not actually a landslide area, even in this case, there would be the same two possibilities in the future about the prediction of a landslide. These instances can be expressed in the form of probability propositions.

What is the probability of future landslides P(A|L) for the selected area in case of being a landslide area according to the past experiences? What is probability of future landslides P (A|notL) for the selected area in case of not being a landslide area according to the experience? In case of the selected area being a landslide area, according to the past experience, it is clear that the probability of no landslide in the future P(notA|L) and similarly P(notA|notL) should be effective on the final decision. The posteriori probability values can be calculated with bayesian probability model by evaluating these possibilities together in accordance with probability axioms. The forecasts predicting that the selected area will face a landslide in the future are assigned positive weights, otherwise negative weights. This approach is also called "weights of evidence (WoE)" model (Doğan et al., 2012).

WoE model was mathematically expressed by van Westen et al. (2003) and Regmi et al. (2010). The equations, used in this study, were proposed by Regmi et al. (2010) and employed by Özdemir and Altural (2013) to calculate the weight of the sub-categories of factors affecting landslides:

$$W^{+} = ln\left[\frac{\frac{A1}{A1+A2}}{\frac{A3}{A3+A4}}\right] \quad (1)$$

$$W^{-} = ln\left[\frac{\frac{A2}{A1+A2}}{\frac{A4}{A3+A4}}\right] \quad (2)$$

$$C = W^{+} - W^{-} \quad (3)$$

In these equations, *A1* represents the number of cells of landslide in a selected subcategory, *A2* represents the total number of landslide cells outside the selected category, *A3* represents number of cells with no landslide in the selected category, and *A4* represents the total number of cells with no landslide outside the selected category. Thus, *(A1 + A2)* represents the total number of cells in landslide work area and *(A3 + A4)* represents the total number of cells with no landslide in the studied area.

As stated by van Westen (2002) and Vijith et al. (2014), "the positive weight (W^{+}) is used to indicate the importance of the presence of the factor for the occurrence of landslides. If W^{+} is positive the presence of the factor is favorable for the occurrence of landslides, and if W^{+} is negative it is not

favorable. Negative weight (W^-) is used to evaluate the importance of the absence of the factor for the occurrence of landslides. When W^- is positive the absence of the factor is favorable for the occurrence of landslides, and when it is negative, the factor is non-favorable". The difference between the W^+ and W^- weights is called "weights contrast (C)", and it reflects the overall spatial association of the predictor variable with the landslide. A contrast value equal to zero indicates that the sub-categories of the factors causing landslides are not significant for the analysis. Positive contrast refers to a positive spatial correlation, and negative contrast refers to the opposite (Özdemir and Altural, 2013). W^+ and W^- weights of the sub-category of the factors affecting landslide in study areas and C contrasts were calculated using the above formula (Tables 2 and Table 3) and the landslide susceptibility map shown on Figure 3 was generated using these weights.

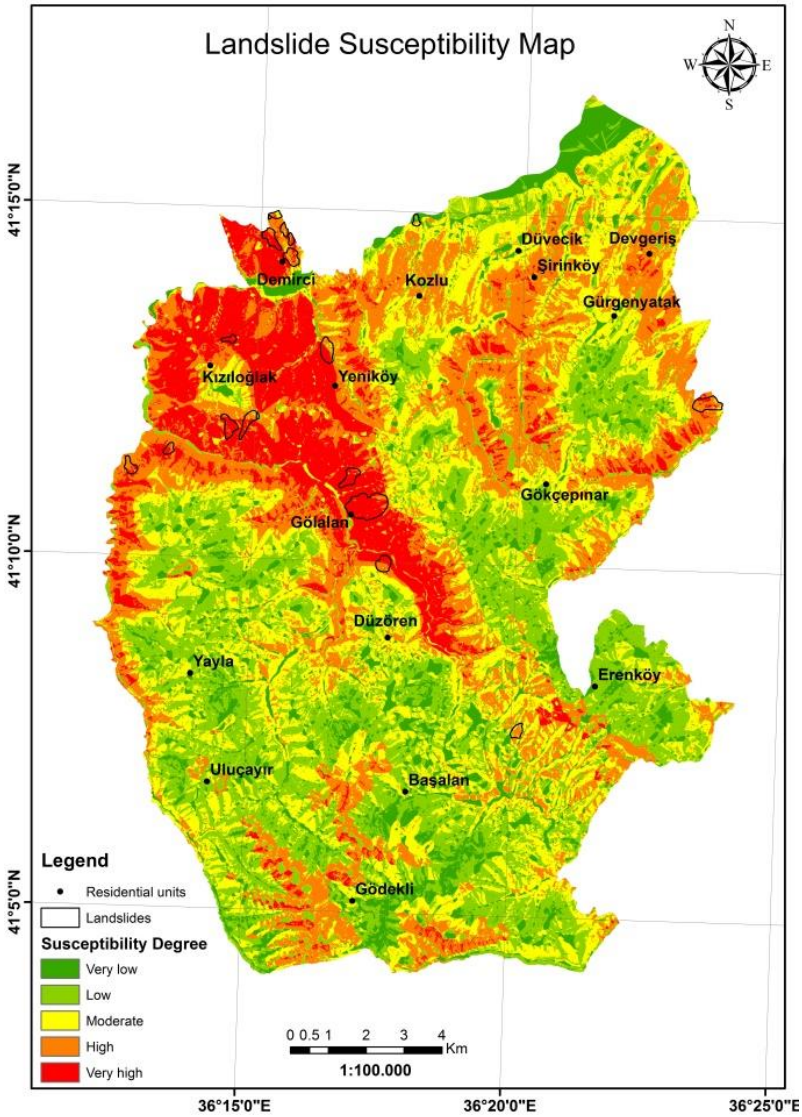

Figure 3. Landslide susceptibility map produced by bayesian probability model

Frequency Ratio Model

The frequency ratio model was used to determine the correlation between past landslide locations and each factor affecting landslides (Lee and Min, 2001; Lee et al., 2004; Erener and Düzgün, 2010). As defined by the Lee and Talib (2005), the frequency ratio is the "ratio of the area where landslides occurred in the total study area, and also, is the ratio of the probabilities of a landslide occurrence to a

non-occurrence for a given attribute". In order to find the frequency ratio of each factor that affects landslides in the study area, each factor was assigned to a subcategory and the number of cells where a landslide has occurred in each subcategory of each factor was determined. The following equation was used to calculate the frequency ratio.

$$FR = \frac{PoL}{PoC} \tag{4}$$

Here, *PoL* is the percentage of landslide occurrence in each subcategory of a factor that affects landslide and *PoC* is the percentage of each subcategory of a factor that affects landslide. *PoL* is determined as *A*/*B* and *PoC* as *C*/*D*, where *A* refers to the number of landslide cells in each subcategory, *B* refers to the total number of landslide cells, *C* refers to the number of cells in each subcategory and *D* refers to the total number of cells in the study area (Erener and Lacasse, 2007).

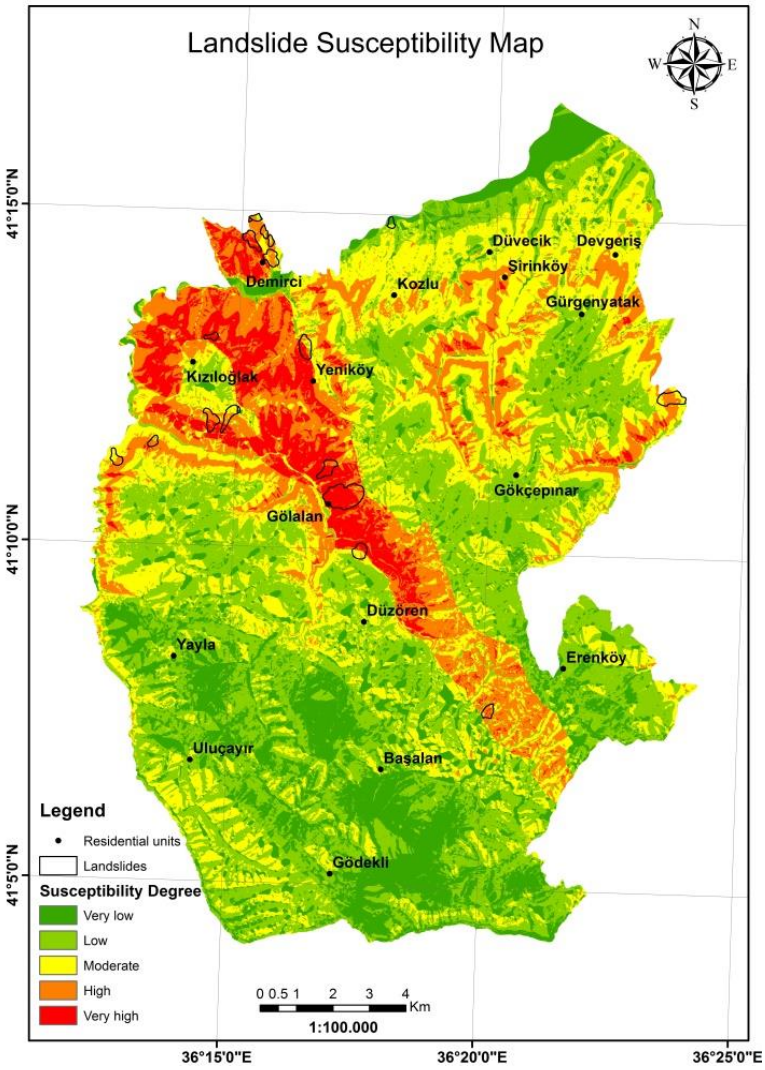

Figure 4. Landslide susceptibility map produced by frequency ratio model

The frequency ratios greater than 1 indicate high correlations with the landslides, while smaller than 1 indicate low correlations (Lee and Pradhan, 2007). The frequency ratios computed for each category were assigned to the relevant layer in the ArcGIS 10.2 software and afterwards the Landslide

Susceptibility Index (LSI) were calculated by overlapping all layers over each other. The frequency ratios of each subcategory were summed to calculate the LSI, as shown in equation 5.

$$LSI = \Sigma Fr \quad (5)$$

The LSI value varied between 3.18 and 17.13 in our case study. If the LSI value is high, it means a higher susceptibility to landslide; a lower value means a lower susceptibility to landslides (Lee and Evangelista, 2005). Subsequently, the LSI was divided into five classes with natural break classification, each representing "very low, low, moderate, high and very high susceptible" areas. The final susceptibility map with the five risk areas is shown in Figure 4.

RESULTS

In this study, we focused on two issues according to the findings. The first one is the prediction (estimation) capabilities of models used in the production of landslide susceptibility maps, and the second one is the determination of the principal factors causing landslides in the study area.

In the present study, two models were used in the production of landslide susceptibility maps. Correct classification approach was primarily used to test the reliability of the landslide susceptibility maps. The correct classification approach showed the estimated accuracy of the landslide area in the control dataset in landslide susceptibility maps. For this purpose, the landslides in the landslide inventory maps were not included in the analysis for controlling purpose; and the landslide susceptibility maps were compared and distribution of landslide areas was determined according to the susceptibility class.

For the evaluation of the landslide susceptibility map produced by the frequency ratio model, as seen in Table 4, it was identified that 27% of the control landslides occurred in an area with a very high degree of susceptibility, 39% in an area with a high degree of susceptibility, 24% in an area with a moderate degree of susceptibility (90% in total).

On the other side, for the evaluation of the susceptibility map produced by the bayesian probability model, as seen in Table 4, it was identified that 42.5% of the control landslides occurred in an area with a very high degree of susceptibility, 41% in an area with a high degree of susceptibility, 9% in an area with a moderate degree of susceptibility (92.5% in total).

Table 4. Distribution of susceptibility degree and density of control landslides

Susceptibility degree	Bayesian Probability (WoE) Model		Frequency Ratio (FR) Model		Distribution of control landslides			
					WoE Model		FR Model	
	ha	%	ha	%	ha	%	ha	%
Very low	2434.36	9.29	4608.75	17.59	1.62	3.00	3.52	6.50
Low	7008.98	26.75	9426.01	35.98	2.43	4.50	1.89	3.50
Moderate	7443.91	28.41	6958.48	26.56	4.87	9.00	12.98	24.00
High	6413.96	24.48	3668.89	14.00	22.18	41.00	21.10	39.00
Very high	2900.04	11.09	1539.11	5.87	22.99	42.50	14.60	27.00
TOTAL	**26201.24**	**100**	**26201.24**	**100**	**54.09**	**100**	**54.09**	**100**

By all accounts, it was concluded that the produced landslide susceptibility maps offer an acceptable level of accurate performance, whereas the best performance was obtained by bayesian probability model.

The factors that make up the mass movement are divided into four groups in general: ground conditions, geomorphological processes, physical processes, and the human effects. In the evaluations, it was determined that the mass movements in Canik district were caused by ground conditions. When the relationship between the factors used in landslide susceptibility analysis (and sub-categories) and the landslide areas found in the landslide inventory maps was considered, it is observed that landslides

occur at a frequency of 46.79% in the fields with Cankurtaran formation, 29.13% in the fields with Akveren formation, and 22.46% in the fields with Tekkeköy formation as per the characteristics of lithological unit (Table 2). The landslides in these three formations account a total of 98.38% of the landslides occurring in the study area.

CONCLUSION

In this study, the landslide susceptibility maps of the area of the Canik district of Samsun province were produced using bayesian probability and frequency ratio models. Nine different factors affecting landslides were used in the susceptibility analysis. The landslide susceptibility maps produced were classified into five types as "very low, low, moderate, high and very high susceptible" areas. In order to test the reliability of the landslide susceptibility maps, control landslides found in the landslide inventory maps, which were not included in the analysis for control purpose, were analyzed; and landslides susceptibility maps were compared and distribution of landslide areas was determined according to the susceptibility class. The verification results showed that the landslide susceptibility mapping using bayesian probability model is more accurate than frequency ratio model. Accordingly, it was identified that 42.5% of the control landslides occurred in an area with a very high degree of susceptibility and 41% in an area with a high degree of susceptibility, 9% in an area with a moderate degree of susceptibility. As a result, it can be ascertained that the landslide susceptibility map produced by using bayesian probability model is consistent with the control landslides occurring in very high and high susceptible areas with 83.5% frequency. This landslide susceptibility map can be used for preliminary land use planning and hazard mitigation purpose.

REFERENCES

Akıncı, H., Özalp, A. Y., Özalp, M., Kılıçer, S. T., Kılıçoğlu, C., Everan, E., 2015, "Production of Landslide Susceptibility Map using Bayesian Probability Model", International Journal of 3-D Information Modeling, Vol. 4(2), pp. 16-33.

Bahadır, M., 2013, "Samsun İli İklim Özelliklerinin Enterpolasyon Teknikleri ile Analizi", Anadolu Doğa Bilimleri Dergisi, Vol. 4(1), pp. 28-46.

Hong, V., Cirianni, F., Leonardi, G., Palamara, R., 2016, "A Fuzzy-based Methodology for Landslide Susceptibility Mapping", Procedia - Social and Behavioral Sciences, Vol. 223, pp. 896-902.

Chalkias, C., Ferentinou, M., Polykretis, C., 2014, "GIS-Based Landslide Susceptibility Mapping on the Peloponnese Peninsula, Greece", Geosciences, Vol. 4, pp. 176-190.

Chen, W., Xie, X., Wang, J., Pradhan, B., Hong, H., Bui, D.T., Duan, Z., Ma, J., 2017, "A Comparative Study of Logistic Model Tree, Random Forest and Classification and Regression Tree Models for Spatial Prediction of Landslide Susceptibility", Catena, Vol. 151, pp. 147-160.

Colkesen, I., Sahin, E.K., Kavzoglu, T., 2016, "Susceptibility Mapping of Shallow Landslides Using Kernel-Based Gaussian Process, Support Vector Machines and Logistic Regression", Journal of African Earth Sciences, Vol. 118, pp. 53-64.

Çan, T., Duman, T.Y., Olgun, Ş., Çörekçioğlu, Ş., Gülmez, F.K., Elmacı, H., Hamzaçebi, S., Emre, Ö., 2013, "Türkiye Heyelan Veri Tabanı", TMMOB Coğrafi Bilgi Sistemleri Kongresi 2013, Ankara, 11-13 Kasım 2013.

Çevik, E., Topal, T., 2003, "GIS-Based Landslide Susceptibility Mapping for a Problematic Segment of the Natural Gas Pipeline, Hendek (Turkey)", *Environmental Geology*, Vol. 44, pp. 949–962.

Dağ, S., Bulut, F., Alemdağ, S., Kaya, A., 2011, "Heyelan Duyarlılık Haritalarının Üretilmesinde Kullanılan Yöntem ve Parametrelere İlişkin Genel Bir Değerlendirme", *Gümüşhane Üniversitesi Fen Bilimleri Enstitüsü Dergisi*, Vol. 1(2), pp. 151–176.

Dağdelenler, G., 2013, *Heyelan Duyarlılık Haritalarının Üretilmesinde Örneklem ve Doğrulama Stratejilerinin Değerlendirilmesi (Gelibolu Yarımadası'nın Doğu Kesimi)*, Doktora Tezi, Hacettepe Üniversitesi, Ankara.

Dai, F.C., Lee, C.F., Li, J., Xu, Z.W., 2001, "Assessment of Landslide Susceptibility on The Natural Terrain of Lantau Island, Hong Kong", *Environmental Geology*, Vol. 40(3), pp. 381–391.

Doğan, S., Akıncı, H., Kılıçoğlu, C., 2012, "Bayes Olasılık Teoremi Kullanılarak Samsun İl Merkezinin Heyelan Duyarlılık Haritasının Üretilmesi", *65. Türkiye Jeoloji Kurultayı*, Ankara, 2-6 Nisan 2012.

Doyuran, V., Lünel, T., Altıner, D., Koçyiğit, A., 1985, "Samsun Yerleşim Sahası Mikrobölgelendirme Çalışmaları", Türkiye Jeoloji Kurumu Bülteni, Vol.28, pp. 93-103.

Ercanoğlu, M., Gökçeoğlu, C., Van Asch, Th. W.J., 2004, "Landslide Susceptibility Zoning North of Yenice (NW Turkey) by Multivariate Statistical Techniques", *Natural Hazards*, Vol. 32(1), pp. 1–23.

Erener, A., Lacasse, S., 2007, "Landslide Susceptibility Mapping Using GIS", The Union of Chambers of Turkish Engineers and Architects (UCTEA) Geographical Information Systems Congress, Trabzon, KTU, October 30 – November 02.

Erener, A., Düzgün, H.S.B., 2010, "Improvement of Statistical Landslide Susceptibility Mapping by Using Spatial and Global Regression Methods in the case of More and Romsdal (Norway)", *Landslides*, Vol. 7(1), pp. 55–68.

Gokce, O., Ozden, S., Demir, A., 2008, "Türkiye'de Afetlerin Mekânsal ve İstatistiksel Dağılımı Afet Bilgileri Envanteri", *Bayındırlık ve İskân Bakanlığı Afet İşleri Genel Müdürlüğü, Afet Etüt ve Hasar Tespit Daire Başkanlığı*, Ankara.

Gökçeoğlu, C., Duman, T. Y., Sönmez, H., Nefeslioğlu, H.A., 2005, "17 Mart 2005 Kuzulu (Koyulhisar, Sivas) Heyelanı", *Mühendislik Jeolojisi Bülteni*, Vol. 20, pp. 17–28.

Gökçeoğlu, C., Ercanoğlu, M., 2001, "Heyelan Duyarlılık Haritalarının Hazırlanmasında Kullanılan Parametrelere Ilişkin Belirsizlikler", *Hacettepe Üniversitesi Yerbilimleri Uygulama ve Araştırma Merkezi Bülteni*, Vol. 23, pp. 189–206.

Guha-Sapir, D., Hoyois, Ph., Below, R., 2016, "Annual Disaster Statistical Review 2015: The Numbers and Trends", Centre for Research on the Epidemiology of Disasters (CRED), Université catholique de Louvain, Brussels, Belgium.

Hong, H., Pourghasemi, H.R., Pourtaghi, Z.S., 2016, "Landslide Susceptibility Assessment in Lianhua County (China): A Comparison between a Random Forest Data Mining Technique and Bivariate and Multivariate Statistical Models", Geomorphology, Vol. 259, pp. 105-118.

Jebur, M.N., Pradhan, B., Tehrany, M.S., 2014, "Optimization of Landslide Conditioning Factors Using Very High-Resolution Airborne Laser Scanning (Lidar) Data at Catchment Scale", Remote Sensing of Environment, Vol. 152 (2014), pp. 150-165.

Kavzoglu, T., Sahin, E.K., Colkesen, I., 2015, "Selecting Optimal Conditioning Factors in Shallow Translational Landslide Susceptibility Mapping Using Genetic Algorithm", Engineering Geology, Vol. 192 (2015), pp. 101-112.

Kayastha, P., 2015, "Landslide Susceptibility Mapping and Factor Effect Analysis Using Frequency Ratio in a Catchment Scale: A case study from Garuwa sub-basin, East Nepal", Arabian Journal of Geosciences, Vol. 8(10), pp. 8601-8613.

Keskin, İ., 2011, "1:100.000 Ölçekli Türkiye Jeoloji Haritaları, SAMSUN E-36 ve F-36 Paftaları", Maden Tetkik ve Arama Genel Müdürlüğü, No:149, Ankara.

Kılıç, F., Gökaşan, E., 2009, "Yeryüzü Şekillerinin SYM ile CBS Ortamında Değerlendirilmesi (Ders Notu)", YTÜ Fen Bilimleri Enstitüsü, http://www.yildiz.edu.tr/~fkilic/CBSYeryuzuV4.pdf, visit date: August 6, 2014.

Kumtepe, P., Nurlu, Y., Cengiz, T., Sütçü, E., 2009, "Bolu Çevresinin Heyelan Duyarlılık Analizi", TMMOB Coğrafi Bilgi Sistemleri Kongresi, 02-06 Kasım İzmir.

Lee, S., Min, K., 2001, "Statistical Analyses of Landslide Susceptibility at Yongin, Korea", *Environmental Geology*, Vol. 40(9), pp. 1095–1113.

Lee, S., Choi, J., Min, K., 2004, "Probabilistic Landslide Hazard Mapping Using GIS and Remote Sensing Data at Boun, Korea", Int. J. Remote Sensing, Vol. 25(11), pp. 2037-2052.

Lee, S., Evangelista, D.G., 2005, "Landslide Susceptibility Mapping using Probability and Statistics Models in Baguio City, Philippines", ISPRS 31st International Symposium on Remote Sensing of Environment, Saint Petersburg, Russia, 20-24 May 2005.

Lee, S., Talip, J.A., 2005, "Probabilistic Landslide Susceptibility and Factor Effect Analysis", Environmental Geology, Vol. 47(7), pp. 982-990.

Lee, S., Pradhan, B., 2007, "Landslide hazard mapping at Selangor, Malaysia using frequency ratio and logistic regression models", Landslides, Vol. 4, pp. 33-41.

Özdemir, A., Altural, T., 2013, "A Comparative Study of Frequency Ratio, Weights of Evidence and Logistic Regression Methods for Landslide Susceptibility Mapping: Sultan Mountains, SW Turkey", *Journal of Asian Earth Sciences*, Vol. 64, pp. 180–197.

Öztekeşin, K., 2008, "Samsun Kenti (Büyükşehir Belediyesi) İçmesuyu Potansiyeli", TMMOB Samsun Kent Sempozyumu, Samsun, 27-29 Kasım 2008.

Petschko, H., Brenning, A., Bell, R., Goetz, J., Glade, T., 2014, "Assessing The Quality of Landslide Susceptibility Maps – Case Study Lower Austria", Nat. Hazards Earth Syst. Sci., Vol. 14, pp. 95–118.

Regmi, N.R., Giardino, J.R., Vitek, J.D., 2010, "Modeling Susceptibility to Landslides Using The Weight of Evidence Approach: Western Colorado, USA", *Geomorphology*, Vol. 115(1-2), pp. 172–187.

Sezer, E.A., Nefeslioglu, H.A., Osna, T., 2017, "An Expert-based Landslide Susceptibility Mapping (LSM) Module Developed for Netcad Architect Software", Computers & Geosciences, Vol. 98, pp. 26-37.

Temizel, İ., Arslan, M., Abdioğlu, E., Yücel, C., 2014, "Mineral Chemistry and Thermobarometry of Eocene Monzogabbroic Stocks from the Bafra (Samsun) area in Turkey: Implications for Disequilibrium Crystallization and Emplacement Conditions", International Geology Review, Vol. 56 (10), pp. 1226-1245.

van Westen, C.J., 2002, "Use of Weights of Evidence Modeling for Landslide Susceptibility Mapping", http://www.adpc.net/casita/Case_studies/Landslide hazard assessment/Statistical landslide susceptibility assessment Weights of evidence modeling CS C Colombia/Weights_of_evidence_modelling_for_landslide_susceptibility_mapping.pdf, visit date: 15 July 2016.

van Westen, C.J., Rengers, N., Soeters, R., 2003, "Use of Geomorphological Information in Indirect Landslide Assessment", *Natural Hazards*, Vol. 30(3), pp. 399–419.

Varnes, D.J., 1958, *Landslide Types and Processes,* in Eckel E.B., ed., Landslides and Engineering Practice, Highway Research Board Special Report 29 (pp.20-47). NAS-NRC Publication 544, Washington, D.C.

Varnes, D.J., 1978, Slope Movement Types and Processes, in Schuster, R.L., and Krizek, R.J., eds., Landslides—Analysis and control: National Research Council, Washington, D.C., Transportation Research Board, Special Report 176, p. 11–33.

Vijith, H., Krishnakumar, K.N., Pradeep, G.S., Ninu Krishnan, M.V., Madhu, G., 2014, "Shallow Landslide İnitiation Susceptibility Mapping by GIS-based Weights-of-Evidence Analysis of Multi-Class Spatial Data-Sets: A Case Study From The Natural Sloping Terrain of Western Ghats, India", Georisk: Assessment and Management of Risk for Engineered Systems and Geohazards, Vol. 8(1), pp. 48-62.

Vos, F., Rodriguez, J., Below, R., Guha-Sapir D., 2010, "Annual Disaster Statistical Review 2009: The Numbers and Trends", Centre for Research on the Epidemiology of Disasters (CRED), Université catholique de Louvain, Brussels, Belgium.

Yalçın, A., 2007, "Heyelan Duyarlılık Haritalarının Üretilmesinde Analitik Hiyerarşi Yönteminin ve CBS'nin Kullanımı", *Selçuk Üniversitesi Mühendislik-Mimarlık Fakültesi Dergisi*, Vol. 22(3), pp. 1–14.

Yalçın, A., 2008, "GIS-based Landslide Susceptibility Mapping Using Analytical Hierarchy Process and Bivariate Statistics in Ardesen (Turkey): Comparisons of Results and Confirmations", *Catena*, Vol. 72(1), pp. 1–12.

Yılmaz, I., 2009, "Landslide Susceptibility Mapping Using Frequency Ratio, Logistic Regression, Artificial Neural Networks and Their Comparison: A Case Study from Kat landslides (Tokat-Turkey)", *Computers & Geosciences*, Vol. 35(6), pp. 1125–1138.

SELÇUK ÜNİVERSİTESİ
MÜHENDİSLİK FAKÜLTESİ

S.Ü. Müh. Bilim ve Tekn. Derg., c.5, s.3, 2017
Selcuk Univ. J. Eng. Sci. Tech., v.5, n.3, 2017
ISSN: 2147-9364 (Elektronik)

THE DYNAMIC FACILITY LAYOUT PROBLEMS WITH CLOSENESS RATE: A FUZZY DECISION SUPPORT SYSTEM APPROACH

[1]Betül TURANOĞLU, [2]Gökay AKKAYA

[1]Ataturk University, Department of Industrial Engineering, Yakutiye, Erzurum, Turkey
[2]Ataturk University, Department of Industrial Engineering, Yakutiye, Erzurum, Turkey
[1]b.turanoglu@atauni.edu.tr, [2]gakkaya@atauni.edu.tr

(Geliş/Received: 08.02.2017 ; Kabul/Accepted in Revised Form: 30.03.2017)

ABSTRACT: One of the most important characteristics of modern manufacturing is the continuous variability of the demand. Today's business world should be able to respond to sudden changes in order to survive the competitive environment. The dynamic layout planning that take into account the variability of demand in certain time periods is an example of these studies. The dynamic facility layout problems (DFLP) attempt to balance the handling and transportation costs. In this study, closeness rates between the departments are used as a parameter in DFLP model. In addition, a fuzzy decision system which integrates multiple input types is proposed to determine the closeness rates and an DFLP instance consisting of six departments and five periods is solved. Results obtained for conventional closeness rates and the rates obtained by the offered method are reported. The results indicate the superiority of the offered model over the conventional one.

Keywords: Fuzzy decision support system, Fuzzy rule base, Closeness rates, Dynamic facility layout problem

Yakınlık Oranlı Dinamik Yerleşim Düzeni Problemleri: Bir Bulanık Karar Destek Sistemi Yaklaşımı

ÖZ: Modern imalatın en önemli özelliklerinden biri, talebin sürekli değişkenlik göstermesidir. Günümüzün iş dünyası, rekabet ortamında hayatta kalabilmek için ani değişikliklere cevap verebilmelidir. Belli zaman aralıklarında talebin değişkenliğini ele alan dinamik yerleşim planlaması, bu çalışmaların bir örneğidir. Dinamik tesis düzeni problemleri (DYDP) taşıma ve taşıma maliyetlerini dengelemeye çalışmaktadır. Bu çalışmada DYDP modelinde, departmanlar arasındaki yakınlık oranları bir parametre olarak kullanılmıştır. Buna ek olarak, yakınlık oranlarını belirlemek için birkaç girdi türünü entegre eden bulanık bir karar sistemi önerilmiş ve altı bölüm ve beş periyottan oluşan bir DYDP örneği çözülmüştür. Geleneksel yakınlık oranları ve önerilen yöntemle elde edilen oranlar için elde edilen sonuçlar raporlanmıştır. Sonuçlar, önerilen modelin geleneksel model üzerindeki üstünlüğünü göstermektedir.

***Anahtar Kelimeler*:** Bulanık karar destek sistemi, Bulanık kural tabanı, Yakınlık oranları, Dinamik tesis düzeni problemi

INTRODUCTION

Facility layout problem is one of the complex problems that have been widely studied in the literature. It is about the physical organization of the departments within a facility. The facility can be

DOI: 10.15317/Scitech.2017.90

described as a machine, a manufacturing cell or an office. A well-designed placement of the facility contributes to the effectiveness of the processes and reduces the total operating expenditures, work-in-process, idle times, manufacturing lead times, etc. In the other words, facility layout design plays an important role for the productivity of a manufacturing system. The objective of the facility layout problem is to minimize the total cost by placement of the departments (Nourelfath et al., 2007). The effectiveness of layout problems conventionally has been attributed to flow of materials. The material handling cost is commonly used to evaluate alternative layout designs. Hence, the location of facilities in a production system is determined under the criterion of material handling cost minimization (Baykasoğlu and Gindy, 2001). These costs are based on the quantity of material flow and the distance between the facilities (Ulutaş and Islier, 2009).

If the characteristic of the material flows does not change from time to time, the layout problem is said to posses a static nature. In such cases, a single period facility layout problem is solved to minimize total material handling cost. However, in application, companies generally produce in dynamic environments. Due to demand variability, minor changes in the locations of departments or machines may provide some advantages. Dynamic facility layout problems are based on the arrangement of facilities to minimize the sum of material handling and re-layout costs by considering multi periods. Dynamic approach provides more effective layouts to meet the requirements of the changing environments compared to the static layout problems (Ulutaş and Islier, 2009).

If a facility is configured without considering the demand variability, a new facility layout should be determined. The re-layout of the departments may cause some production losses and some indirect costs such as production control, loss of time and training costs. However, if the potential gain after changes is large enough, the re-layout is considered as economical and reasonable. In such cases, the planner may be willing to play a game against the nature. In this game, there are chance and decision points. The customer changes his/her preferences, and a new structure of demand occur at the change points. Then, the planner decides whether or not he will change the facility layout in the decision point. This decision should balance the material handling and the re-layout costs. If the re-layout costs are lower than the material handling costs, a new layout can be made (Ulutaş and Islier, 2009).

The assumptions for the DFLP are clarified as follows (Pourvaziri and Naderi, 2014):

- Planning horizon is splited to T period.
- The distances between locations and the material flow between each pair of facilities are known.
- In each time period, each facility should be assigned only one location and one facility can be placed to only one location.
- The objective is to achieved the layout plan which minimizes the sum of the material handling and re-layout costs for all periods.

The static approach may be used in the dynamic environment though there are disadvantages. For instance, a short planning horizon can be used so that the flows are fairly constant during the horizon or a long planning horizon can be used and ignored the changes in flow. The total flow over the planning horizon can be determined by adding the material flows in each period to get the total flow. There will be no re-layout costs, but this may cause in the layout being uneffective throughout the horizon. The dynamic approach corrects these imperfections by striking a balance between the material handling and rearrangement costs and planning future layout rearrangements (Balakrishnan and Cheng, 1998).

One of the assumptions of the classical linear programming is the certainty of the parameters. The data often possess a stochastic nature in practice. Therefore, real-life problems can be modeled by using fuzzy numbers representing indefinite numerical data. In this study, the closeness rates between departments have been added to the model of DFLP as a new parameter. Besides, the fuzzy system approach has been proposed to calculate the closeness rates. The conventional closeness rates and the closeness rates which are obtained by the proposed approach have been tested on a DFLP instance with 6 departments and 5 periods. It has been shown that the proposed method produce better results.

The paper is structured as follows: Quadratic Assignment Problem (QAP) and Dynamic Facility Layout Problem (DFLP) are mentioned in Section 2. Then, the structure of fuzzy decision making system is discussed in Section 3. Section 4 proposes the fuzzy decision making system to calculate the closeness rates and tests the proposed method on an illustrative example. The last section comprises conclusions.

QUADRATIC ASSIGNMENT PROBLEM AND DYNAMIC FACILITY LAYOUT PROBLEM

The Quadratic Assignment Problem (QAP) is commonly seen in facility location studies. The basic difference between the QAP and the classic assignment problem is that there is interaction between the assignment pairs in the QAP, leading to a non-linear objective function. The QAP is NP-hard as shown implying that finding a polynomial time heuristic solution method is unlikely by Sahni and Gonzales (Sahni and Gonzales, 1976). Indeed, the computational complexity of QAP is such that even instances of size $20 \leq n \leq 30$ represent a real challenge for the current exact approaches (Benlic and Hao, 2013).

The QAP is initially introduced by Koopmans and Beckman (1957), where the cost of assigning facility i to location j and of facility k to location l is $f_{ik}.d_{jl}$ with f_{ik} denoting the material flow per unit time between facilities i and k and d_{jl} denoting the distance between locations j and l. Let x_{ij} to be 1 if facility i is assigned to location j, and 0 otherwise. The formulation of the QAP is as follows:

$$Minimize = \sum_{i,j,k,l=1}^{n} f_{ik} d_{jl} x_{ij} x_{kl} \tag{1}$$

$$\sum_{i=1}^{n} x_{ij} = 1, \qquad \forall j \in \{1,...,n\} \tag{2}$$

$$\sum_{j=1}^{n} x_{ij} = 1, \qquad \forall i \in \{1,...,n\} \tag{3}$$

$$x_{ij} \in \{0,1\}$$

DFLP extends the QAP by minimizing the sum of material handling and re-layout costs by arranging the layout for each production period. The mathematical model introduced by Balakrishnan and Cheng is as follows:

$$Min \sum_{t=2}^{T}\sum_{i=1}^{N}\sum_{j=1}^{N}\sum_{l=1}^{N} A_{tijl} x_{(t-1)ij} x_{til} + \sum_{t=1}^{T}\sum_{i=1}^{N}\sum_{j=1}^{N}\sum_{k=1}^{N}\sum_{l=1}^{N} f_{tik} d_{jl} x_{tij} x_{tkl} \tag{4}$$

$$\sum_{j=1}^{N} x_{tij} = 1, \quad i = 1,2,\ldots,N, \qquad t = 1,2,\ldots,T \tag{5}$$

$$\sum_{i=1}^{N} x_{tij} = 1, \quad j = 1,2,\ldots,N, \qquad t = 1,2,\ldots,T \tag{6}$$

$$x_{tij} \in \{0,1\}, \forall i, j, t$$

where N is the number of locations and departments; T denotes the number of periods; f_{tik} indicates material flow between departments i and k at period t; d_{jl} stands for the distance between locations j and l; and finally A_{tijl} is the re-layout cost of department i from location j to l at period t.

Rosenblatt (1986) makes the first attempt to model the DFLP. He proposes a dynamic programming model for solution of the DFLP. Heuristic methods are also used for the DFLP. For instance, Conway and Venkataramanan (1994), Ulutaş and Islier (2009), Mazinani *et al.* (2013), Pourvaziri and Naderi

(2014) use genetic algorithm while Kaku and Mazzola (1997) present a tabu search algorithm to solve the DFLP. Balakrishnan *et al.* (1992) presents solutions for constrained DFLP. Lacksonen and Enscore (1993) examine different mathematical programming approaches. Hirabayashi *et al.* (1999) propose evolutionary methods for flexible manufacturing systems. Balakrishnan and Cheng (2000) enhance the genetic algorithm presented in the study of Conway and Venkataramanan (1994), Baykasoglu and Gindy (2001) also present a simulated annealing application. Balakrishnan *et al.* (2003) develop two heuristics that improve Urban's steepest-drop pairwise interchange heuristic. The first one uses Urban's heuristic to generate solutions of the DFLP. The solutions generated for each forecast window is improved by using a backward-pass pairwise exchange heuristic and the best solution is selected. The second one combines Urban's heuristic with dynamic programming. Besides, Erel *et al.* (2003) propose a three-phase method to solve the DFLP. In the first phase, a set of "good" layouts are produced by integrating the flow data using a weighting scheme and solving the static facility layout problem for each period. In the second phase, the set of solutions generated in the first stage and dynamic programming is used to produce solutions for the DFLP. In the third phase, the solutions obtained in the second stage are improved using a random drop pairwise swap approach. Baykasoglu *et al.* (2006) made the first attempt for DFLP with budget constraints. McKendall and Shang (2006) present hybrid ant systems for the DFLP. Moslemipour *et al.* (2012) review the intelligent approaches for dynamic and robust layout problems. El-Rayes and Said (2009) study a dynamic programming approach for a dynamic site layout. Zouein and Tommelein (1999) solve a dynamic layout planning using a hybrid method. McKendall and Liu (2012) propose new tabu search heuristics for the problem while Sahin *et al.* (2010) study the DFLP with a budget constraint. Finally, Hosseini *et al.* (2014) propose a hybrid meta-heuristic to solve the DFLP.

Fortenberry and Cox (1985) use the material handling cost as $A_{ijkl} = f_{ik}d_{jl}r_{ik}$ in their study on the static facility layout problem. Here, f_{ik} shows the material flow between departments i and k while d_{jl} shows the distance between locations j and l, and r_{ik} is the closeness rate between departments i and k. We make use of the closeness rate idea but extend it to multiple periods. Parameter r_{tik} represent the closeness rate between departments i and k in period t. As a result, the model is regulated as follows:

$$Min \sum_{t=2}^{T}\sum_{i=1}^{N}\sum_{j=1}^{N}\sum_{l=1}^{N} A_{tijl}\, x_{(t-1)ij}\, x_{til} + \sum_{t=1}^{T}\sum_{i=1}^{N}\sum_{j=1}^{N}\sum_{k=1}^{N}\sum_{l=1}^{N} f_{tik}\, d_{jl}\, r_{tik}\, x_{tij}\, x_{tkl} \tag{7}$$

$$\sum_{j=1}^{N} x_{tij} = 1, \quad i = 1,2,\ldots,N, \qquad t = 1,2,\ldots,T \tag{8}$$

$$\sum_{i=1}^{N} x_{tij} = 1, \quad j = 1,2,\ldots,N, \qquad t = 1,2,\ldots,T \tag{9}$$

$$x_{tij} \in \{0,1\}, \forall i, j, t$$

THE STRUCTURE OF FUZZY DECISION MAKING SYSTEM

The word "fuzzy" describe all the information that is vague and deficient about an issue. In a fuzzy environment, researchers cannot directly use the equations derived by conventional methods. Fortunately, the problem at hand can be modeled by the fuzzy approach instead of deterministic programming models. Since the events of the real world is too complex, it is unlikely controlling and modeling of the events. In this case, the methods that can be solved are prefered. The fuzzy decision making system approach can be shown as one of the methods.

Fuzzy set theory is introduced by Zadeh (1965). Accordingly, fuzzy set is defined which permits partial membership. Consequently, the membership of an element is indicated by a number within [0,1] interval. The fuzzy set theory is developed to solve problems having uncertain boundaries. It models

uncertainties of the real life and has a wide range of the application. The fuzzy set theory is used in many fields such as operations research, management science, artificial intelligence and expert systems.

The first application of fuzzy set theory for the facility layout problems is by Wilhelm *et al.* (1987). Instead of the traditional closeness rates, proximity significance between each department pair is calculated by an approach what they call as "similarity index". Grobelny (1987a, 1987b, 1988) and Raoott and Rakshit (1991, 1993) also use the fuzzy method for layout problems. Dweiri (1999)'s the fuzzy approach incorparates Analytic Hierarchy Process (AHP) for determinig the closeness rates. Deb and Bhattacharyya (2005) develop a fuzzy decision support system for the development of facility layout with fixed pickup/drop-off points.

The four main components of a fuzzy decision making system are given below (Altaş, 1999; Deb and Bhattacharyya, 2005; Dweiri, 1999; Şen, 2001):

- **Fuzzification:** The values of the input and output variables are measured, the range of these values is determined, and converted into natural language (low, very low, high, etc.).
- **Knowledge base:** The membership functions are described by the experts of the system.
- **Fuzzy rule base:** "IF-THEN" type of rules logically connecting the input and output variables are created. The structure of the rules should be as "If Ax and Bx, then Cz". The connective 'and' can be considered as the intersection operation in set operations. When the membership functions of fuzzy sets are considered, conjunction function "and" determines the minimum value of the input variables' membership values. Therefore, the membership value of output variable 'z' for each rule is determined as follows:

$$\mu(z) = \min[\mu(x), \mu(y)] \tag{10}$$

This expression represents the relationship between X and Y spaces and is shown as $Z = X \times Y$ Cartesian product.

All fuzzy set connections between the input and output data should be considered while creating the fuzzy rules. The rule base is a result of these fuzzy rules and so the implied connections. Fuzzy relations are usually illustrated by tables, relationship diagrams and matrix.

- **Defuzzification:** All the rules created in the fuzzy rule base are converted to a crisp value using a defuzzification method. The structure of the fuzzy decision support system is summarized in Figure 1.

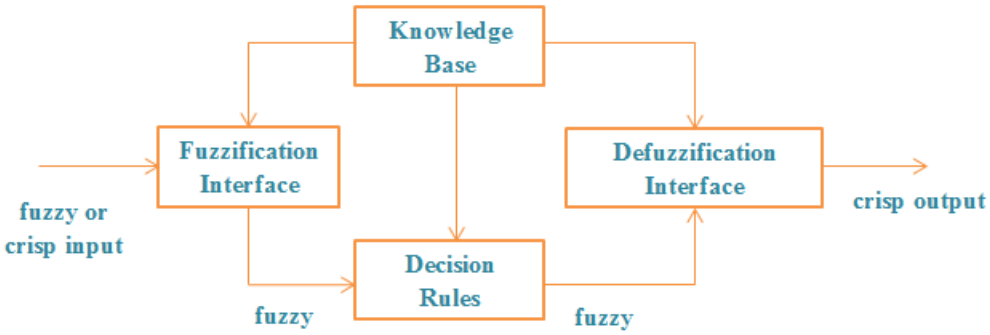

Figure 1. Fuzzy decision making system (Dweiri, 1999)

AN APPLICATION ON AN ILLUSTRATIVE EXAMPLE

The relationship between departments in a facility is an important factor while designing the facility layout. Some of the most common relationships considered in literature for facility layout problems are (Dweiri, 1999):

- Flow relationships such as material flow, equipment, people, information and money.
- Environmental relationships such as safety, noise and temperature.
- Organizational relationships such as reporting.

- Control relationships such as control of materials, inventory and shop floor.

Quantitative or qualitative data can be used in facility layout problems. For instance; from-to chart includes quantitative data while activity relationship diagram works for qualitative data. The data used in activity relationship diagram can be considered as the closeness degree. The relationships have 6 categories listed as A (Absolutely essential), E (Especially necessary), I (Important), O (Ordinary), U (Unimportant) and X (Not desirable).

We summarize the steps of the calculation of the r_{ik} closeness rates for DFLP as follows:

Step 1- Determination of input variables and fuzzification: Material flow, information flow and environmental condition are considered as input variables. The levels of material and information flow are determined as "very low, low, medium, high and very high". Alternatively, the levels are set as "very dangerless, dangerless, medium dangerous, dangerous and very dangerous" for environmental condition. On the other hand, the levels of the closeness rate which is output variables are expressed as A, E, I, O, U and X.

Step 2 - Determination of membership functions: In this step, the membership functions of the input variables are decided. The membership functions of material flow, information flow and the environmental condition are given respectively, in Figure 2, Figure 3 and Figure 4 depending on the sample data in the implementation of the study. The trapezoidal membership functions are preferred and the range of the closeness rate (A, E, I, O, U, X) is considered as [0, 6]. Figure 5 shows the membership function of the closeness rating.

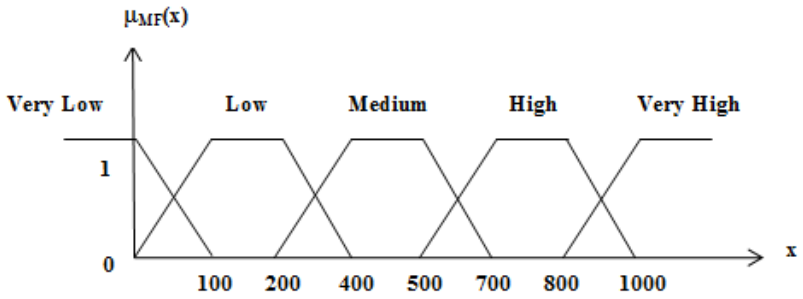

Figure 2. Membership function of material flow

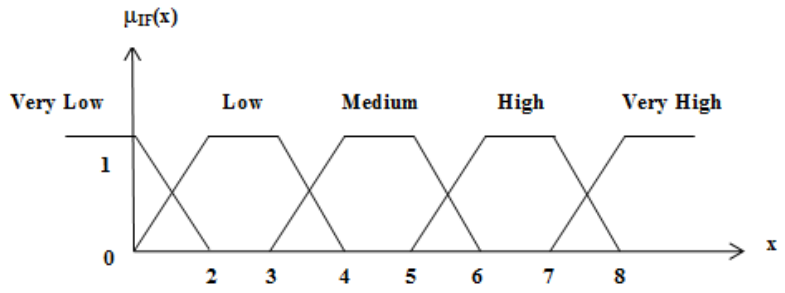

Figure 3. Membership function of information flow

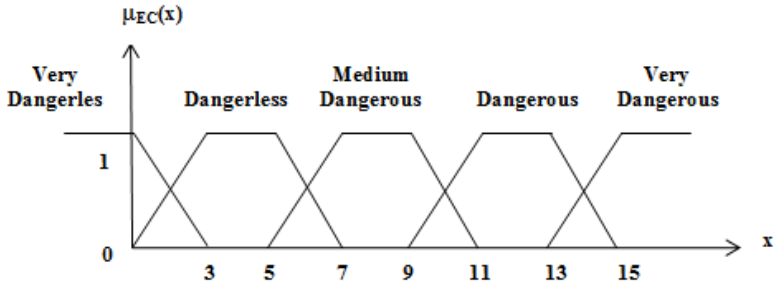

Figure 4. Membership function of environmental condition

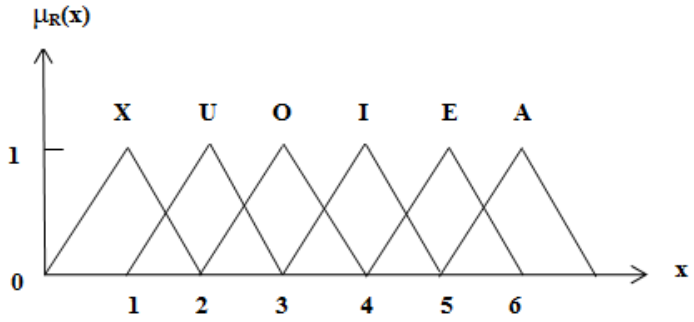

Figure 5. Membership function of closeness rating

Step 3 - The creation of fuzzy rules: In this step, Table 1, Table 2 and Table 3 are prepared to create "IF-THEN" rules between the input variables. According to these tables, a sample rule can be created as "***If*** the material flow is medium ***and*** information flow between two departments is high, ***then*** closeness rate between these departments is E (Especially)". Tables are prepared by the experts or the decision makers who know the system well. These tables may vary depending on the type of the facility layout. The number of the rules is calculated by the following formula (Deb and Bhattacharyya, 2005):

$$N = \sum_{j=1}^{m} \left(\prod_{i=1}^{n} L_i \right) \tag{11}$$

m: number of set of rules (j = 1,2,…,m)
n: number of input variables used in each set of rules (i = 1,2,..,n)
L: number of membership functions or levels
According to the above formula, the total number of rules is N=5x5x5=125 in this study.

Table 1. If-then rules of material flow and information flow

Material Flow (MF)	**Information Flow (IF)**				
	Very Low	**Low**	**Medium**	**High**	**Very High**
Very Low	U	U	O	O	I
Low	U	O	O	I	E
Medium	O	O	I	E	E
High	O	I	E	E	A
Very High	I	E	E	A	A

Table 2. If-then rules of material flow and environmental condition

Material Flow (MF)	Environmental Condition (EC)				
	Very Dangerless	Dangerless	Medium Dangerous	Dangerous	Very Dangerous
Very Low	U	U	U	U	U
Low	O	O	U	U	X
Medium	I	O	U	U	X
High	E	E	O	U	X
Very High	A	A	I	O	X

Table 3. If-then rules of information flow and environmental condition

Information Flow (IF)	Environmental Condition (EC)				
	Very Dangerless	Dangerless	Medium Dangerous	Dangerous	Very Dangerous
Very Low	U	U	U	U	U
Low	O	O	U	U	X
Medium	I	O	U	U	X
High	E	I	U	U	X
Very High	A	E	O	U	X

Step 4 - Defuzzification process: In this step, the defuzzification is performed to calculate the closeness rates (*r*) between all department pairs for each period. The center of area (COA) method is chosen for the defuzzification since it is the most commonly used defuzzification method in the literature. Accordingly, the closeness rates are obtained as follows (Altaş, 1999):

$$r = \frac{\sum_{i=1}^{N} \mu_i(r_i) \times \mathrm{r}_i}{\sum_{i=1}^{N} \mu_i(r_i)} \tag{12}$$

where *i* denotes the rule number and *N* is the total number of rules. $\mu_i(r_i)$ is set to zero for inactive rules. For instance, consider that MF = 232 (Low), IF = 1 (Low) and EF = 1 (Very dangerless) for any department pair. The active rules are created by:

- **Rule 1:** If the MF is low and IF is low, then the closeness rate is O (Ordinary).
- **Rule 2:** If the MF is low and EF is very dangerless, then the closeness rate is O (Ordinary).
- **Rule 3:** If the IF is low and EF is very dangerless, then the closeness rate is O (Ordinary).

The value of $\mu_1(r_1)$ for Rule 1 equal to minimum of the membership values of MF=232 and IF=1. In this case, it is determined as $\mu_1(r_1)$ = min[0.68, 0.5] = 0.5. Here, the membership value of the MF is 0.68 while the membership value of the IF is 0.5. In the same way, it is found as $\mu_2(r_2)$ = 0.66 and $\mu_3(r_3)$ = 0.5. The closeness rate for this department pair is calculated as follows:

$$r = \left[\mu(r_1) \times r_1 + \mu(r_2) \times r_2 + \mu(r_3) \times r_3\right] / \left[\mu(r_1) + \mu(r_2) + \mu(r_3)\right] \tag{13}$$
$$r = (0.5 \times 3 + 0.66 \times 3 + 0.5 \times 3) / (0.5 + 0.66 + 0.5) = 3$$

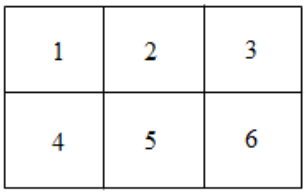

Figure 6. Representation of the facility area

In the case study, the best layout for a dynamic layout problem with 6 departments and 5 periods is found. The material flows and relocation costs of the problem are taken from (Rosenblatt, 1986). The information flows and environmental condition data of the problem are randomly generated. The closeness rates used in the model are calculated by MATLAB. The data of the problem are given in Appendix A. GAMS mathematical modeling language is used to solve the resulting DFLP formulation. The total facility area that the departments assigned is shown in Figure 6. If the conventional closeness rates are used, the total cost turns out to be 330,727 and the layouts for each period are as given in Figure 7. On the other hand, the fuzzy system approach for the offered study is used to compute the closeness rates, the total cost is reduced to 281,901.54 and the resulting layouts for each period are illustrated in Figure 8. Therefore, it is seen that a 14.76% reduction in the total cost is achieved by the fuzzy system approach.

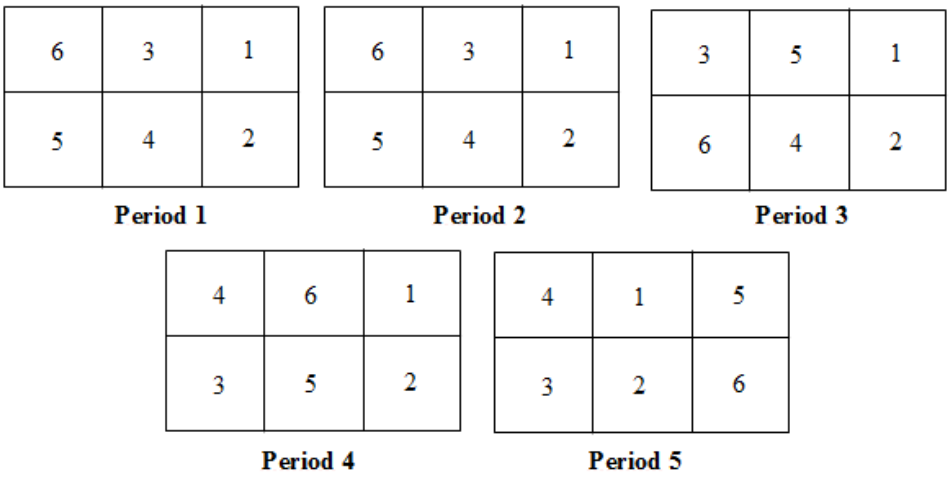

Figure 7. Layouts based on the traditional closeness rates

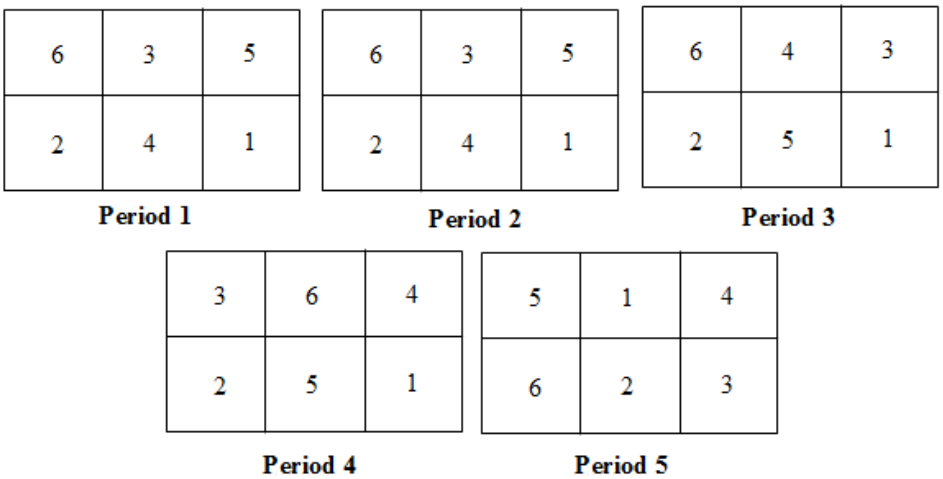

Figure 8. Layouts based on the closeness rates obtained by the fuzzy system approach

CONCLUSION

FLP is considered to be static if the material flows don't change. However, production quantities can be periodically changed in today's market. This variability may be caused by the reasons such as the entry into production of new products, replacement of materials and equipment used in production, changes in the quantity demanded. As results of these, the plant layout becomes a dynamic structure. Each layout is associated with a period in the problems identified as DFLP in literature. Therefore, the total cost of a dynamic facility layout plan is the sum of material handling and reorganization costs in all periods. The reorganization costs occur when the departments are replaced to minimize the material handling costs in the transition from period to the period.

In this study, the closeness rates between departments are added to the model of DFLP as new parameters. The fuzzy system method is proposed to determine the rates. Thus, a final closeness rate is obtained by integrating several types of input variables. Also, ignored factors can be used to determine the conventional closeness rates. For an experiment, a DFLP with 6 departments and 5 periods is considered. The conventional closeness rates and the rates obtained by the fuzzy system approach in the DFLP formulation are separately used. In comparison of the results, it is seen that a 14.76% reduction in the total cost, and the different layouts are obtained.

The most important innovation of this study is to consider the environmental condition as an ergonomic factor in estimating the closeness rates with the fuzzy system approach. In the next studies, the input variable type can be increased to determine the rates, and heuristic methods can be improved to solve problems of larger size.

REFERENCES

Altaş, İ.H., 1999, "Bulanık Mantık: Bulanık denetim", *Enerji, Elektrik, Elektromekanik-3e*, Vol. 64, pp. 76-81.

Balakrishnan, J., Jacobs, F.R.,Venkataramanan, M.A., 1992, "Solutions for The Constrained Dynamic Facility Layout Problem", *European Journal of Operational Research*, Vol. 15, pp. 280-286.

Balakrishnan, J., Cheng, C.H., 1998, "Dynamic Layout Algorithms: A State-of-The-Art Survey", *Omega*, Vol. 26(4), pp. 507-521.

Balakrishnan, J., Cheng, C.H., 2000, "Genetic Search and The Dynamic Layout Problem", *Computers and Operations Research*, Vol. 27(6), pp. 587-593.

Balakrishnan, J., Cheng, C.H., Conway, D.G., Lau, C.M., 2003, "A Hybrid Genetic Algorithm For The Dynamic Plant Layout Problem", *International Journal of Production Economics*, Vol. 86, pp. 107–120.

Baykasoğlu, A., Gindy, N.N.Z., 2001, "A Simulated Annealing Algorithm for Dynamic Layout Problem", *Computers and Operations Research*, Vol. 28, pp. 1403-1426.

Baykasoglu, A., Dereli, T., Sabuncu, I., 2006, "An Ant Colony Algorithm for Solving Budget Constrained and Unconstrained Dynamic Facility Layout Problems", *Omega-International Journal of Management Science*, Vol. 34(4), pp. 385–396.

Benlic, U., Hao, J-K., 2013, "Break Local Search for The Quadratic Assignment Problem", *Applied Mathematics and Computation*, Vol. 219(9), pp. 4800-4815.

Conway, D.G., Venkataramanan, M.A., 1994, "Genetic Search and The Dynamic Facility Layout Problem", *Computers and Operations Research*, Vol. 21(8), pp. 955-960.

Deb, S.K., Bhattacharyya, B., 2005, "Fuzzy Decision Support System for Manufacturing Facilities Layout Planning", *Decision Support Systems*, Vol. 40, pp. 305– 314.

Dweiri, F., 1999, "Fuzzy Development of Crisp Activity Relationship Charts for Facilities Layout", *Computers & Industrial Engineering*, Vol. 36, pp. 1-16.

El-Rayes, K., Said, H., 2009, Dynamic Site Layout Planning Using Approximate Dynamic Programming, *Journal of Computing in Civil Engineering*, Vol. 23(2), pp. 119–127.

Erel, E., Ghosh, J.B., Simon, J.T., 2003, "New Heuristic for The Dynamic Layout Problem", *Journal of the Operational Research Society*, Vol. 54, pp. 1275–1282.

Fortenberry, J.F., Cox, J.S., 1985, "Multiple Criteria Approach to The Facilities Layout Problem", *International Journal of Production Research*, Vol. 23(4), pp. 773-782.

GrobeIny, J., 1987a, "The Fuzzy Approach to Facility Layout Problems", *Fuzzy Sets and Systems*, Vol. 23, pp. 175-190.

GrobeIny, J., 1987b, "On One Possible Fuzzy Approach to Facility Layout Problems", *International Journal of Production Research*, Vol. 25, pp. 1123-1141.

Grobelny, J., 1988, "The `Linguistic Pattern' Method for A Work Station Layout Analysis", *International Journal of Production Research*, Vol. 26, pp. 1779-1798.

Hirabayashi, N., Kita, H., Nagasawa, H., 1999, "Dynamic Facility Layout Using Evolution Strategies", *Proceedings of the Second World Manufacturing Congress*, 154–159.

Hosseini, S., Al Khaled, A., Vadlamani, S., 2014, "Hybrid Imperialist Competitive Algorithm,Variable Neighborhood Search, and Simulated Annealing for Dynamic Facilitylayout Problem", *Neural Computing and Applications*, Vol. 25, pp. 1871–1885.

Kaku, B.K., Mazzola, J.B., 1997, "A Tabu-Search Heuristic for The Dynamic Plant Layout Problem", *INFORMS Journal on Computing*, Vol. 9(4), pp. 374–384.

Koopmans, T.C., Beckmann, M.J., 1957, "Assignment Problems and The Location of Economic Activities", *Econometrica*, Vol. 25, pp. 53-76.

Lacksonen, T.A., Enscore, E.E., 1993, "Quadratic Assignment Algorithms for The Dynamic Layout Problem", *International Journal of Production Research*, Vol. 31(3), pp. 503–517.

Mazinani, M., Abedzadeh, M., Mohebali, N., 2013, "Dynamic Facility Layout Problem Basedon Flexible Bay Structure and Solving by Genetic Algorithm", *International Journal of Advanced Manufacturing Technology*, Vol. 65, pp. 929–943.

McKendall, A.R., Shang, J., 2006, "Hybrid Ant Systems for The Dynamic Facility Layout Problem", *Computers & Operations Research*, Vol. 33(3), pp. 790-803.

McKendall, A.R., Liu, W.H., 2012, "New Tabu Search Heuristics for The Dynamic Facility Layout Problem", *International Journal of Production Research.*, Vol. 50(3), pp.867–78.

Moslemipour, G., Lee, T.S., Rilling, D., 2012, "A Review of Intelligent Approaches for Design-Ing Dynamic and Robust Layouts in Flexible Manufacturing Systems", *International Journal of Advanced Manufacturing Technology*, Vol. 60, pp. 11–27.

Nourelfath, M., Nahas, N. Montreuil, B., 2007, "Coupling Ant Colony Optimization and The Extended Great Deluge Algortihm for The Discrete Facility Layout Problem", *Engineering Optimization*, Vol. 39(8), pp. 953-998.

Pourvaziri, H., Naderi, B., 2014, "A Hybrid Multi-Population Genetic Algorithm for The Dynamic Facilitylayout Problem", *Applied Soft Computing*, Vol. 24, pp. 457–469.

Rosenblatt, M.J., 1986, "The Dynamics of Plant Layout", *Management Science*, Vol. 32(1), pp. 76-86.

Raoot, A.D., Rakshit, A., 1991, "A Fuzzy Approach to Facilities Layout Planning", *International Journal of Production Research*, Vol. 29, pp. 835-857.

Raoot, A.D., Rakshit, A., 1993, "A `Linguistic Pattern' Approach for Multiple Criteria Facility Layout Problems", *International Journal of Production Research*, Vol. 31, pp. 203-222.

Sahin, R., Ertogral, K., Turkbey, O., 2010, "A Simulated Annealing Heuristic for The Dynamic Layout Problem with Budget Constraint", *Computers & Industrial Engineering, Vol.* 59, pp. 308–13.

Sahni, S., Gonzales, T., 1976, "P-Complete Approximation Problems", *Journal of the Association for Computing Machinery*, Vol. 23, pp. 555-565.

Şen, Z. 2001, *Bulanık Mantık ve Modelleme İlkeleri*, Bilge Yayıncılık, İstanbul.

Ulutaş, H.B., Islier, A.A., 2009, "A Clonal Selection Algorithm for Dynamic Facility Layout Problems", *Journal of Manufacturing Systems*, Vol. 28(4), pp. 123-131.

Ulutaş, B., Islier, A.A., 2015, "Dynamic Facility Layout Problem in Footwear Industry", *Journal of Manufacturing Systems*, Vol. 36, pp. 55-61.

Wilhelm, M.R., Karwowski, W., Evans G.W., 1987, "A Fuzzy Set Approach to Layout Analysis", *International Journal of Production Research*, Vol. 25, pp. 1431-1450.

Zadeh, L.A. , 1965, "Fuzzy Sets", *Information and Control*, Vol. 8, pp. 338-353.

Zouein, P.P., Tommelein, I.D., 1999, "Dynamic Layout Planning Using A Hybrid Incremental Solution Method", *Journal of Construction Engineering and Management*, Vol. 125(6), pp. 400–408.

SELÇUK ÜNİVERSİTESİ
MÜHENDİSLİK FAKÜLTESİ

S.Ü. Müh. Bilim ve Tekn. Derg., c.5, s.3, 2017
Selcuk Univ. J. Eng. Sci. Tech., v.5, n.3, 2017
ISSN: 2147-9364 (Elektronik)

Appendix A. The data of the problem

		Material flow						Information flow						Environmental condition						Traditional closeness rates						Closeness rates obtained by the proposed method					
		1	**2**	**3**	**1**	**5**	**6**	**1**	**2**	**3**	**4**	**5**	**6**	**1**	**2**	**3**	**4**	**5**	**6**	**1**	**2**	**3**	**4**	**5**	**6**	**1**	**2**	**3**	**4**	**5**	**6**
Period 1	**1**	0	63	605	551	116	136	0	1	4	4	3	2	0	1	2	2	1	3	0	3	5	5	3	3	0	3	4.33	4.27	3	3
	2	63	0	635	941	50	191	1	0	3	7	1	1	1	0	5	7	2	2	3	0	5	6	3	3	3	0	4	4	3	3
	3	104	71	0	569	136	55	4	3	0	8	5	4	2	5	0	4	1	1	5	5	0	6	5	5	4.43	4	0	6	4.72	4.72
	4	65	193	622	0	77	90	4	7	8	0	2	4	2	7	4	0	11	6	5	6	6	0	5	5	4.27	4	6	0	2.62	3.75
	5	162	174	607	591	0	179	3	1	5	2	0	2	1	2	1	11	0	1	3	3	5	5	0	4	3	3	4.72	2.62	0	3.32
	6	156	13	667	611	175	0	2	1	4	4	2	0	3	2	1	6	1	0	3	3	5	5	4	0	3	3	4.72	3.75	3.32	0
Period 2	**1**	0	175	804	904	56	176	0	5	3	3	1	2	0	2	2	3	1	3	0	3	6	6	3	3	0	3	4.7	4.52	3	3
	2	63	0	743	936	45	177	5	0	4	4	3	3	2	0	4	8	3	2	3	0	5	6	3	3	3	0	5	5	3	3
	3	168	85	0	918	138	134	3	4	0	8	5	6	2	4	0	3	2	3	6	5	0	6	5	6	4.7	5	0	5.67	4.33	5.33
	4	51	94	962	0	173	39	3	4	8	0	4	3	3	8	3	0	9	7	6	6	6	0	5	5	4.52	5	5.67	0	3.32	2.86
	5	97	104	730	634	0	144	1	3	5	4	0	4	1	3	2	9	0	2	3	3	5	5	0	3	3	3	4.33	3.32	0	3
	6	95	115	983	597	24	0	2	3	6	3	4	0	3	2	3	7	2	0	3	3	6	5	3	0	3	3	5.33	2.86	3	0
Period 3	**1**	0	90	77	553	769	139	0	5	1	3	6	2	0	13	2	1	3	1	0	3	3	4	6	3	0	2.29	3	3.32	5.24	3
	2	168	0	114	653	525	185	5	0	3	5	6	2	13	0	4	7	3	2	3	0	3	5	4	4	2.29	0	3	3.29	4	3
	3	32	35	0	664	898	87	1	3	0	6	5	4	2	4	0	1	2	1	3	3	0	5	6	3	3	3	0	5	4.67	3.33
	4	27	166	42	0	960	179	3	5	6	0	5	3	1	7	1	0	7	5	4	5	5	0	6	5	3.32	3.29	5	0	3.67	3.98
	5	185	56	44	926	0	104	6	6	5	5	0	5	3	3	2	7	0	1	6	4	6	6	0	5	5.54	4	4.67	3.67	0	4.72
	6	72	128	173	634	687	0	2	2	4	3	5	0	1	2	1	5	1	0	3	4	3	5	5	0	3	3	3.33	3.98	4.72	0
Period 4	**1**	0	112	15	199	665	649	0	4	1	3	6	5	0	2	1	2	1	3	0	3	2	3	5	5	0	3	2.3	3	5	4.33
	2	153	0	116	173	912	671	4	0	2	3	7	5	2	0	3	6	2	2	3	0	3	3	6	5	3	0	3	2.44	5.4	4.43
	3	10	28	0	182	855	542	1	2	0	1	2	4	1	3	0	4	1	2	2	3	0	3	4	5	2.3	3	0	3	3.91	4.43
	4	29	69	15	0	552	751	3	3	1	0	5	6	2	6	4	0	7	6	3	3	3	0	4	5	3	2.44	3	0	2.55	3.6
	5	198	71	42	24	0	758	6	7	2	5	0	7	1	2	1	7	0	3	5	6	4	4	0	6	5	5.4	3.91	2.55	0	5.33
	6	62	109	170	90	973	0	5	5	4	6	7	0	3	2	2	6	3	0	5	5	5	5	6	0	4.33	4.43	4.43	3.6	5.33	0
Period 5	**1**	0	663	23	128	119	50	0	7	6	4	8	4	0	11	3	3	2	1	0	6	5	6	6	5	0	3.67	4.6	4.52	5.72	4.69
	2	820	0	5	98	141	66	7	0	3	3	4	4	11	0	5	8	4	1	6	0	5	5	5	5	3.67	0	3.91	4	5	4.72
	3	822	650	0	137	78	91	6	3	0	5	4	3	3	5	0	3	2	2	5	5	0	3	3	3	4.6	3.91	0	3	3	3
	4	826	570	149	0	93	151	4	3	5	0	2	1	3	8	3	0	9	3	6	5	3	0	3	3	4.52	4	3	0	2.33	3
	5	915	515	53	35	0	177	8	4	4	2	0	1	2	4	2	9	0	1	6	5	3	3	0	3	5.72	5	3	2.33	0	3
	6	614	729	178	10	99	0	4	4	3	1	1	0	1	1	2	3	1	0	5	5	3	3	3	0	4.69	4.72	3	3	3	0
Re-layout costs		887	964	213	367	289	477																								

SELÇUK ÜNİVERSİTESİ
MÜHENDİSLİK FAKÜLTESİ

S.Ü. Müh. Bilim ve Tekn. Derg., c.5, s.3, 2017
Selcuk Univ. J. Eng. Sci. Tech., v.5, n.3, 2017
ISSN: 2147-9364 (Elektronik)

REMOVAL OF REACTIVE BLUE 19 FROM AQUEOUS SOLUTION BY PEANUT SHELL: OPTIMIZATION BY RESPONSE SURFACE METHODOLOGY

[1]Elçin DEMİRHAN

[1]Yıldız Technical University, Chemical Engineering Department, Davutpasa Campus Esenler Istanbul, Turkey, TR 34220
[1]demirhan@yildiz.edu.tr

(Geliş/Received: 26.01.2017; Kabul/Accepted in Revised Form: 20.03.2017)

ABSTRACT: In the present study, it was aimed to optimize the removal of reactive blue 19 dye by using peanut shells as a low-cost adsorbent. The influence of various process parameters namely pH (2,3 and 4), temperature (25, 35 and 45°C) and adsorbent amount (0.5, 1 and 1.5 g/100 mL) were studied using Box-Behnken design. According to the ANOVA results, the quadratic model with coefficient of determination (R^2) value of 0.9984 and model F value of 487.80 was showed good fit of the experimental data to. Experimental conditions for optimum dye removal of 93.45% were determined as pH 2, 35°C and 1.5 g/100 mL adsorbent amount. Langmuir fitted better to the obtained equilibrium data for removal of reactive blue 19 than Freundlich and Temkin models. In addition, the adsorption kinetics was also studied for the reactive blue 19 removal onto peanut shell. The kinetic studies showed that the removal of reactive blue 19 fitted to pseudo-second-order model.

Keywords: *Adsorption, Experimental design, Reactive blue 19, Peanut shell*

Sulu Çözeltilerden Yer Fıstığı Kabukları ile Reaktif Mavi 19 Giderimi: Cevap Yüzey Yöntemi ile Optimizasyonu

ÖZ: Bu çalışmada, reaktif mavi 19 boyarmaddesinin düşük maliyetli adsorban olarak yerfıstığı kabukları kullanılarak gideriminin optimizasyonu amaçlanmıştır. Box-Behnken tasarım yöntemi kullanılarak pH, sıcaklık ve adsorban miktarı parametrelerinin etkileri incelenmiştir. ANOVA sonuçlarına göre, regresyon analizi regrasyon katsayısı 0.9984 ve model F değeri 487.80 ile deneysel verilerin quadratik modele uygun olduğunu göstermektedir. Optimum boyarmadde giderimi (%93.45) için deneysel koşullar pH 2, 35°C ve 1.5 g/100 mL adsorban miktarı olarak belirlenmiştir. Reaktif mavi 19 giderimi için denge verilerinden Langmuir izoterminin Freundlich ve Temkin izotermlerinden daha uygun olduğu bulunmuştur. Ayrıca, yerfıstığı kabuğu ile reaktif mavi 19 giderimi için adsorpsiyon kinetiği incelenmiştir. Kinetik çalışmalar yalancı ikinci derece kinetiğe uyduğunu göstermiştir.

Anahtar Kelimeler: *Adsorpsiyon, Deneysel tasarım, Yerfıstığı kabuğu, Reaktif mavi 19*

INTRODUCTION

The dyes in effluents can have serious harm to the aquatic life and also to humans and animals. They can disturbe the food chain organisms and lead to ecological disbalance (Cheng *et al*., 2015; Dutta, 2013). Dyes are synthetic, organic, and aromatic compounds and they contain of some heavy metals in their structure. The sources for dye effluents can be the industries such as textile, leather, paper, plastics, etc.

DOI: 10.15317/Scitech.2017.91

Dyes can accumulate into the soil and water. Due to this accumulation and environmental regulations, colour removal from textile effluent has become an imprtant research area. Nowadays, different methods are available for the treatment of dye wastewaters such as an reverse osmosis, ion exchange, chemical precipitation, ozonation and solvent extraction. However, high capital cost and operational costs or secondary sludge disposal problem are the disadvantages of the mentioned techniques (Daneshvara *et al*., 2015; Etorki and Massoudi, 2011; Ravikumara *et al*., 2005). The adsorption technique has significant adantages and it can be accepted as the best way to treat effluents. The highcost of activated carbon and its regeneration is limited the application of this process (Zaidi and Mohd Zulkhairi, 2014; Koushaa *et al*., 2012).

RSM is the combination of mathematical and statistical techniques for optimizing processes and can be used to investigate both the relative and complex interactions of several factors even (Ravikumara *et al*., 2005). The application of experimental design in adsorption process can improve product yields, reduce development time and overall costs and reduce process variability (Arunachalam and Annadurai, 2011; Liu *et al*., 2010).

In recent years, research on the production of low cost adsorbents alternative to commercially available activated carbon has increased. Therefore, in the present study, peanut shells was used as low cost adsorbent. It was aimed to optimize the adsorption of RB19 dye onto peanut shells. The effects of process parameters (pH, adsorbent amount and temperature) were investigated by applying Box–Behnken design. Moreover, modelling studies were performed to represent the adsorption isotherms and kinetics.

MATERIALS and METHODS

Materials

Reactive Blue 19 used in this work was obtained from Gülerçin Kimya A.Ş., Istanbul, Turkey. It was dissolved in the distilled water to form solutions of 300 mg/L. The pH of the solution was adjusted by diluted HCl or NaOH solution. The peanut shell samples were purchased from a local supplier in Istanbul. For experimental studies, the peanut shells were rinsed with tap water, then washed with distilled water dried at 80°C in a hot air oven for 24 h, ground and then sieved to uniform sizes of 100 mesh. The powder was preserved in airtight bottles for experimental use. Other chemicals of analytical grade were purchased from Sigma Aldrich.

Experimental Design

A three level Box-Behnken design was used to obtain the optimum process variables for the reactive blue 19 removal by using the individual and complex effects of these variables. The independent variables are temperature, pH and adsorbent amount and the dependent variable is the efficiency of adsorption. The range of independent variables and their levels were presented in Table 1. A second order polynomial model (Eq. 1) was fitted to the experimental data obtained from the Box–Behnken design:

$$Y = \beta_0 + \sum_{i=1}^{k} \beta_i x_i + \sum_{i=1}^{k} \beta_{ii} x_i^{\,2} + \sum_{i=1}^{k-1} \sum_{j=i+1}^{k} \beta_{ij} x_i x_j + \varepsilon \quad (1)$$

Where Y is the process response (dependent variable); x_i and x_j are the variables; β_0 is the intercept coefficient; β_i, β_{ii}, β_{ij} are the interaction coefficients of linear, quadratic and the second order terms, respectively; k is the number of independent parameters; ε is the random error. The data were subjected to analysis of variance to show the fitness of the model.

Table 1. Independent process variables, ranges and levels

Independent variable	Coded Levels		
	-1	**0**	**+1**
pH, x_1	2	3	4
Temperature, x_2	25	35	45
Adsorbent amount, x_3	0.5	1	1.5

Batch Experiments

Adsorption experiments were conducted by varying the process parameters obtained from Box–Behnken design. The experiment was initiated by the addition of adsorbent to 100 mL of RB19 solution at desired pH and adsorbent dose value. The mixture was shaken at 175 rpm agitation speed at room temperature on a translatory shaker for the obtained contact time. During the experiments, the samples were taken from the mixture at timed intervals and centrifuged to remove the adsorbent particles. After centrifuging, the concentration of RB19 was measured by using UV/vis spectrophotometer at a wavelength of 592 nm. The assay was carried out in triplicate for each sample and their averages were taken. In the study, all experiments were carried out at least in duplicate and the reproducibility between trials was within ±5%.

Adsorption capacities were calculated from Eq. 2:

$$q_e = \frac{(C_0 - C_e) \cdot V}{m} \tag{2}$$

where q_e is equilibrium adsorbed concentration (mg/g), C_0 and C_e are the initial and equilibrium dye concentrations (mg/L), respectively. V is the volume of the solutions and m is the weight of adsorbent (g).

Adsorption Isotherm Models

Langmuir, Freundlich and Temkin isotherm models were used to evaluate the data obtained from the reactive blue 19 adsorption experiments:

Langmuir model:
Langmuir model defines the monolayer adsorption on the surface of the adsorbent, and after that there is not further adsorption takes place (Dada *et al*., 2012).

$$\frac{1}{q_e} = \frac{1}{Q*b*C_e} + \frac{1}{Q} \tag{3}$$

where q_e is the equilibrium adsorbed concentration (mg g^{-1}), C_e is the equilibrium dye concentration (mg L^{-1}), Q is the maximum sorption capacity (mg g^{-1}) and b is the adsorption equilibrium constant.

Freundlich model:
The Freundlich model describes the multilayer adsorption and generally is used for heterogeneous systems (Piccin *et al*., 2011).

$$\ln q_e = \ln K_F + \frac{1}{n} \ln C_e \tag{4}$$

where K_F is the Freundlich affinity coefficient, n is the Freundlich exponential coefficient.

Temkin model:

Temkin isotherm can be derived from Langmuir isotherm. In this model, it is assumed that the heat of adsorption is decreased linearly due to sorbate/sorbent interactions. According to Temkin isotherm model, adsorption is a spontaneous process (Sampranpiboon *et al*., 2014; Khan, 2012).

$$q_e = \frac{RT}{b_T}\ln A_T + \frac{RT}{b_T}\ln C_e \quad (5)$$

where A_T is the Temkin isotherm constant and b_T is a constant related to heat of sorption.

Adsorption Kinetics of Removal of Reactive Blue 19

Several methods are available to study the adsorption mechanism. In this study, in order to determine the adsorption kinetics, the data obtained from the RB19 removal process were analysed with four different kinetic models as follows:

Pseudo first order model:

$$\log\frac{q_e - q_t}{q_e} = \frac{k_1 t}{2.303} \quad (6)$$

where; q_e is the adsorbed amount at equilibrium (mg g^{-1}); q_t is the adsorbed amount at time t (mg/g); k_1 is the pseudo first order adsorption kinetic parameter (min^{-1})

Pseudo second order model:

$$\frac{t}{q_t} = \frac{1}{k_2 q_e^{\,2}} + \frac{t}{q_e} \quad (7)$$

where, k_2 is the pseudo second order adsorption kinetic parameter (g mg^{-1} min^{-1}).

Elovich model:

The Elovich equation is valid for chemisorptions kinetics and systems in which the surface is heterogenous.

$$q_t = \frac{1}{\beta}\ln(\alpha\beta) + \frac{1}{\beta}\ln t \quad (8)$$

where; α is the initial adsorption rate (mg g^{-1} min); β is the constant related to extent of surface coverage and activation energy consumption (g mg^{-1}).

Intra particle diffusion model:

$$q_t = k_i t^{0.5} + C_i \quad (9)$$

where; k_i is the intra particle diffusion kinetic parameter (mg g^{-1} min^{-2}); C_i is the constant related to layer thickness (mg g^{-1}).

RESULTS AND DISCUSSION

Optimization of Reactive Blue 19 Adsorption Process Variables

Box–Behnken design and regression model

In order to obtain the optimum operational variables for the reactive blue 19 removal, a three level Box-Behnken design was employed. According to the Box–Behnken design, a series of experiments was

conducted for exploring different combined parameters and for evaluating the combined effects of these factors. The coefficients of the response function (Y) for different dependent variables were determined by using Design Expert 10.0 trial software. Table 2 shows the predicted, and an experimental data related to percentage removals of RB19 obtained. Using the experimental results from Table 2, the full quadratic second order polynomial equation (Eq. 10) was fitted to the data appropriately and the equation was presented as follows:

$$Removal\ (\%) = 45.94 - 18.46X_1 + 1.53X_2 + 13.42X_3 - 0.67X_1X_2 - 4.86X_1X_3 + 0.010\,X_2X_3 + 15.10{X_1}^2 + 1.60{X_2}^2 - 5.43{X_3}^2 \quad (10)$$

On the basis of the coefficients in this equation, it can be said that the removal % of reactive blue 19 increases with decreasing pH and increasing adsorbent amount. The pH and adsorbent amount have a more profound effect on the removal of dye. In order to determine the adequacy of model to represent percentage of removal of reactive blue, the adequacy of the model test were carried out and it was shown that the p-value for the quadratic model was lower than 0.05 and the R^2 for the quadratic model was highest as compared with other model. Therefore, the quadratic model was chosen to illustrate the relationship between independent variable and the response values. Comparison of the observed versus predicted values was shown in Fig.1. This figure showed the correlation between the experimental and predicted values and the cluster points around the diagonal line indicates the good fit of model (Zaidi and Mohd Zulkhairi, 2014).

Table 2. Box-Behnken design matrix and comparison of observed predicted values of dye removal (%)

Run	X_1	X_2	X_3	% Removal (Experimental)	% Removal (Predicted)
1	0	0	0	45.68	45.94
2	0	-1	+1	53.47	53.90
3	0	0	0	45.11	45.94
4	+1	0	+1	46.22	45.71
5	-1	+1	0	83.38	83.30
6	0	+1	-1	30.55	30.12
7	+1	-1	0	43.23	43.32
8	+1	+1	0	45.71	45.04
9	0	-1	-1	28.44	27.26
10	-1	0	+1	93.45	92.35
11	0	+1	+1	55.98	57.16
12	0	0	0	46.76	45.94
13	-1	0	-1	55.27	55.79
14	+1	0	-1	27.47	28.59
15	-1	-1	0	78.24	78.90
16	0	0	0	46.18	45.94
17	0	0	0	45.98	45.94

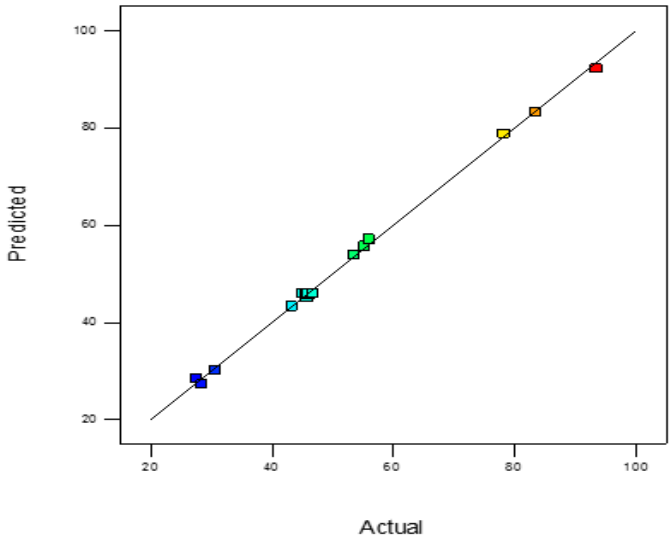

Figure 1. Scatter diagram of predicted response versus actual response of RB19 removal

The results of ANOVA studies for removal of RB19 were given in Table 3. As can be seen from the Table 3, the F value of the model is 487.80 and the p-value is <0.05 and it can be concluded that the model terms are significant. The coefficient of determination (R^2) and adjusted R^2 of this model were 0.9984 and 0.9964, respectively. The differences between these two values are small; therefore, it shows the adequacy of the model to the response. The lack of fit F-value of 6.32 implied that the lack of fit was not significant relative to the pure error. A non-significant lack of fit was considered good and was desired for the model to fit.

Table 3. Analysis of variance (ANOVA) of the fitted quadratic polynomial model

Source	Sum of Squares	df	Mean Square	F-value	P-value	
Model	5353.51	9	594.83	487.80	<0.0001	significant
A-pH	2727.28	1	2727.28	2236.52	<0.0001	
B- Temp.	18.73	1	18.73	15.36	0.0058	
C-Ads. Amount	1441.58	1	441.58	1182.17	<0.0001	
AB	1.77	1	1.77	1.45	0.2676	
AC	94.38	1	94.38	77.40	<0.0001	
BC	0.040	1	0.040	0.033	0.8614	
A^2	959.44	1	959.44	786.79	<0.0001	
B^2	10.82	1	10.82	8.87	0.0206	
C^2	124.36	1	124.36	101.99	<0.0001	
Residual	8.54	7	1.22			
Lack of Fit	7.05	3	2.35	6.32	0.0536	not significant
Pure Error	1.49	4	0.37			
Cor Total	5362.05	16				

Effects of process variables

In order to determine the effects of variables and their interactions, 3D response surface plots for the reactive blue 19 removal were shown in Fig. 2a–c. As can be seen from this figure, the decrease in the pH resulted an enhancement in the adsorption rate of the dye within the experimental range. It can be concluded that adsorption rate increases with increasing adsorbent amount due to the availability of more surface area of the adsorbent for adsorption. The pH and adsorbent amount are considered to be most effective in influencing the dye removal process as mentioned before. Moreoever, in the studied range, the temperature has little effect on the reactive blue 19 removal. A maximum dye removal (93.5 %) was observed at pH 2, adsorbent amount of 1.5 g and 35°C.

Adsorption Isotherms for Reactive Blue 19

In order to determine the adsorption isotherm of the RB19 onto peanut shells, three classic adsorption models (Langmuir, Freundlich and Temkin) were used. The estimated parameters of these models and statistical values were presented in Table 4. Among these isotherm models, Langmuir isotherm model was determined as the most appropriate one for the RB19 adsorption data with the high values of correlation coefficient (R^2). This result indicates that RB19 adsorption occurs as monolayer onto the homogenous adsorbent surface.

Table 4. The estimated parameters and statistical values of isotherm models for RB19 adsorption onto peanut shells

Langmuir İzotermi			
Q_{max}	**b**	R^2	**σ**
39.53	0.037	0.9827	0.2881
Freundlich İzotermi			
K_F	**n**	R^2	**σ**
5.165	2.597	0.8791	0.2647
Temkin İzotermi			
A_T	b_T	R^2	**σ**
0.4694	323.85	0.9436	3.5171

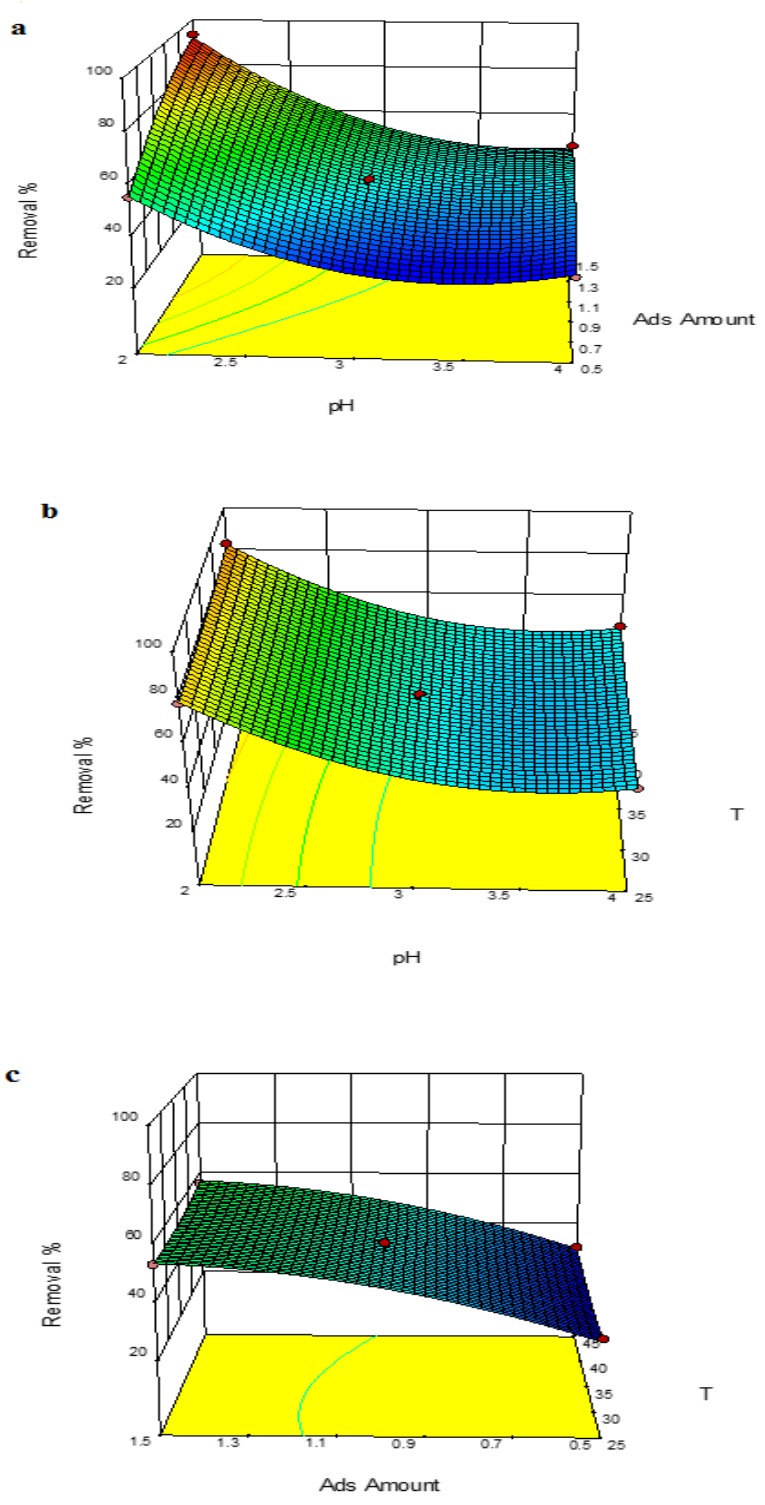

Figure 2. Response surface plots for the combined effects on the reactive blue 19 removal (a) Adsorbent amount and pH (b) T and pH (c) Adsorbent amount and T

Adsorption Kinetics of Reactive Blue 19

Evaluation of the adsorption kinetic as well as adsorption equilibrium is very important to plan and control the adsorption process. In order to describe the adsorption kinetic of RB19 onto peanut shell, the four different kinetic pseudo first order, the pseudo second order, Elovich and the intra particle diffusion models were used. The estimated parameters and statistical data of these models were presented in Table 5. As can be seen from this table, among these models, pseudo second order kinetic model was observed as the most appropriate one for all the experimental data with the high values for the coefficient of determination and low the standard error values. The result obtained was in agreement with the studies for RB19 removal onto rice straw fly ash (El-Bindary et al., 2016), citrus waste biomass (Asgher and Bhatti, 2012) and jujube stems powder (Ghaneian et al., 2014).

Table 5. The estimated parameters and statistical values of kinetic models for RB19 adsorption onto peanut shells

Pseudo First Order Kinetic Model			
k_1 (1/dak)		**R^2**	**σ**
0.0388		0.8833	0.7892
Pseudo Second Order Kinetic Model			
k_2 (g/mg.dak)		**R^2**	**σ**
0.0565		0.9999	0.0368
Elovich Kinetic Model			
α (mg g^{-1}dak)	**β (g mg^{-1})**	**R^2**	**σ**
4.14E+10	2.0530	0.9668	0.1421
Intra Particle Diffusion Model			
k_i (mg g^{-1} dak^{-2})	**C_i (mg g^{-1})**	**R^2**	**σ**
0.1609	12.925	0.9165	0.2225

CONCLUSION

In the present study, the removal of RB19 from aqueous solution using peanut shell as low-cost adsorbent was investigated. The effect of three parameters as pH, tempearute and adsorbent amount were studied. Results showed that a decrease in the pH resulted an enhancement in the adsorption rate of the dye within the experimental range. The pH and adsorbent amount are considered to be most effective in influencing the dye removal process as mentioned before. Moreoever, in the studied range, the temperature has little effect. A maximum dye removal (93.5 %) was observed at pH 2, adsorbent amount of 1.5 g and 35°C. The isotherm data for RB19 removal using peanut shell fitted well to the Langmuir isotherm model. Furthermore, kinetic data were fitted to the pseudo-second-order kinetic model. As a result, it can be concluded that peanut shell can be employed as an effective adsorbents for removal of RB19.

REFERENCES

Arunachalam, R., Annadurai, G., 2011, "Optimized Response Surface Methodology for Adsorption of Dyestuff from Aqueous Solution", Journal of Environmental Science and Technology, Vol. 4, pp. 65-72.

Asgher, M., Bhatti, H.N., 2012, "Removal of Reactive Blue 19 and Reactive Blue 49 Textile Dyes by Citrus Waste Biomass from Aqueous Solutıon: Equilibrium and Kinetic Study", The Canadian Journal of Chemical Engineering, Vol. 90, p.412-419.

Cheng, Z., Zhang, L., Guo, X., Jiang, X., Li, T., 2015, "Adsorption Behavior of Direct Red 80 and Congo Red onto Activated Carbon/Surfactant: Process Optimization, Kinetics and Equilibrium", Spectrochimica Acta Part A: Molecular and Biomolecular Spectroscopy, Vol. 137, pp.1126–1143.

Dada, A.O., Olalekan, A.P., Olatunya, A.M., Dada, O., 2012, "Langmuir, Freundlich, Temkin and Dubinin–Radushkevich Isotherms Studies of Equilibrium Sorption of Zn2+ Unto Phosphoric Acid Modified Rice Husk", IOSR Journal of Applied Chemistry, Vol. 3, No. 1, pp. 38-45.

Daneshvara, E., Koushaa, M., Sohrabia, M.S., Panahbehaghb, B., Bhatnagarc, A., Younesid, H., Sternberg, S.P.K., 2015, "Application of Response Surface Methodology for The Biosorption of Acid Blue 25 Dye Using Raw and HCl-Treated Macroalgae", Desalination and Water Treatment, Vol. 53, pp.1710–1723.

Dutta, S., 2013, "Optimization of Reactive Black 5 Removal by Adsorption Process Using Box–Behnken Design, Desalination and Water Treatment, Vol. 51, pp.7631–7638.

El-Bindary, A.A., Abd El-Kawi, M.A., Hafez, A.M., Rashed, I.G.A., Aboelnaga, E.E., 2016, Removal of Reactive Blue 19 from Aqueous Solution Using Rice Straw Fly Ash, Journal of Materials and Environmental Sciences, Vol. 7, No. 3, pp.1023-1036.

Etorki, A.M., Massoudi, F.M.N., 2011, "The Use of Peanut Hull for the Adsorption of Colour from Aqueous Dye Solutions and Dye Textile Effluent", Oriental Journal of Chemistry, Vol. 27, No. 3, pp.875-884.

Ghaneian, M.T., Ehrampoush, M.H., Sahlabadi, F., Mootab, M., Rezapour, I., Jasemizad, T., 2014, "Reactive Blue 19 Dye Adsorption Behavior on Jujube Stems Powder from Syntetic Textile Wastewater: Isotherm and Kinetic Adsorption Studies", Journal of Community Health Research, Vol. 3, No. 1, pp.67-78.

Khan, A.S.A., 2012, "Evaluation of Thermodynamic Parameters of Cadmium Adsorption on Sand from Temkin Adsorption Isotherm", Turkish Journal of Chemistry, Vol. 36, pp. 437 – 443

Koushaa, M., Daneshvara, E., Dopeikara, H., Taghavia, D., Bhatnagarb, A., 2012, "Box–Behnken Design Optimization of Acid Black 1 Dye Biosorption by Different Brown Macroalgae", Chemical Engineering Journal, Vol. 179, pp.158– 168.

Liu, Y., Zheng, Y., Wang, A., 2010, "Response Surface Methodology for Optimizing Adsorption Process Parameters for Methylene Blue Removal by a Hydrogel Composite", Adsorption Science & Technology, Vol. 28, No. 10, pp.913-922.

Piccin, J.S., Dotto, G.L., Pinto, L.A.A., 2011, "Adsorption Isotherms and Thermochemical Data of FD&C Red n° 40 Binding by Chitosan", Brazilian Journal of Chemical Engineering, Vol. 28, No. 02, pp. 295 – 304.

Ravikumara, K., Pakshirajanb, K., Swaminathanc, T., Balua, K., 2005, "Optimization of Batch Process Parameters Using Response Surface Methodology for Dye Removal by A Novel Adsorbent", Chemical Engineering Journal, Vol. 105, pp.131–138.

Sampranpiboon, P., Charnkeitkong, P., Feng, X., 2014, "Equilibrium Isotherm Models for Adsorption of Zinc (II) ion from Aqueous Solution on Pulp Waste", Wseas Transactions on Environment and Development, Vol. 10, pp. 35-47.

Zaidi, Y.R., Mohd Zulkhairi, A.R., 2014, "Removal of Methyl Red From Aqueous Solution by Adsorption on Treated Banana Pseudostem Fibers Using Response Surface Method (RSM)", The Malaysian Journal of Analytical Sciences, Vol. 18, No. 3, pp.592 – 603.

SELÇUK ÜNİVERSİTESİ
MÜHENDİSLİK FAKÜLTESİ

S.Ü. Müh. Bilim ve Tekn. Derg., c.5, s.3, 2017
Selcuk Univ. J. Eng. Sci. Tech., v.5, n.3, 2017
ISSN: 2147-9364 (Electronic)

Pd/C CATALYSTS SYNTHESIZED BY MICROWAVE ASSISTED POLYOL METHOD FOR FORMIC ACID ELECTRO-OXIDATION

[1]Özlem GÖKDOĞAN ŞAHİN

[1]Selcuk University, Faculty of Engineering, Chemical Engineering Department, Campus, Konya, TURKEY
[1]ozlem@selcuk.edu.tr

(Geliş/Received: 30.01.2017; Kabul/Accepted in Revised Form: 03.03.2017)

ABSTRACT: Synthesis of carbon supported palladium particles based on a polyol process was investigated. The activity of Pd catalysts, synthesized by microwave assisted polyol method on carbon support, has been examined for formic acid electro-oxidation reaction. The catalysts were characterized with XRD to identify their nanostructure properties. The effect of catalyst preparation parameters on electrocatalytic performance of catalysts was examined. The electrocatalytic properties of Pd/C catalysts for the oxidation of formic acid were investigated by cyclic voltammetry (CV). The electrocatalytic activity of Pd/C synthesized at 30 s and 130 °C are higher than the other Pd/C catalysts synthesized at different temperature and reaction time. It is proposed that the longer reaction time and higher temperature increased the particle size.

***Key Words**: Formic acid electro-oxidation, Palladium catalysts, Polyol method, Preparation conditions, Fuel cells*

Mikrodalga Destekli Poliol Yöntemiyle Sentezlenen Pd/C Katalizörler için Formik Asit Elektro-Oksidasyonu

ÖZ: Karbon destekli paladyum parçacıklarının sentezi poliol prosesi ile gerçekleştirildi. Mikrodalga destekli poliol yöntemi ile sentezlene Pd katalizörlerin formik asit elektrooksidasyon reaksiyonu için aktivitesi araştırıldı. Katalizör yapıları XRD ile karakterize edildi. Katalizör hazırlama parametrelerinin katalizörlerin elektrokatalitik performansına etkisi incelendi. Formik asitin oksidasyonu için Pd/C katalizörlerin elektrokatalitik özellikleri dönüşümlü voltametri (CV) ile incelendi. 30 s ve 130 °C'de sentezlenen Pd/C katalizörünün elektrokatalitik aktivitesinin, farklı sıcaklık ve reaksiyon zamanlarında sentezlenen diğer Pd /C katalizörlerinden daha yüksek olduğu bulundu. Artan reaksiyon süresinin ve sıcaklığın parçacık boyutunu arttırdığı düşünülmektedir.

***Anahtar Kelimeler:** Formik asit elektrooksidasyonu, Paladyum katalizörler, Hazırlama şartları, Poliol metodu Yakıt hücreleri.*

INTRODUCTION

The over-consumption of fossil fuels leads to environmental problems. Therefore, it is necessary to develop new power sources. As a high-efficiency energy conversion device, fuel cells have significant role in the energy utilization sector.

Hydrogen is often seen as an ideal fuel for fuel cells due to its ease of oxidation. However, the generation and storage of hydrogen is very difficult. Therefore, the use of liquid fuels such as methanol, ethanol or formic acid is an attractive way for the direct fuel cells.

DOI: 10.15317/Scitech.2017.92

Direct formic acid fuel cells (DFAFCs) have been investigated as potential power sources owing to their high theoretical energy density, fast oxidation kinetics, easy storage and low crossover effect through the nafion membrane (Zhu et al., 2004). Pt catalysts have been studied extensively for formic acid electro-oxidation. However the electro-oxidation of formic acid at the Pt catalyst is generally through the indirect pathway and Pt is easily poisoned by CO at lower potential. Therefore researches have been made to overcome the CO poisoning and improve the electrocatalytic activity of Pt (Mazumder et al., 2010). The use of bimetallic catalysts by alloying Pt with other metals is an effective way to solve the catalyst poisoning problem on formic acid electro-oxidation (Nethravathi et al., 2011). However CO could accumulate during long time operation and reduce the cell efficiency. In recent years, much attention has been focused on Pd based catalysts for formic acid oxidation. Pd-based catalysts are considered better catalysts for formic acid oxidation due to their high catalytic activity compared with Pt-based catalysts. The electro-oxidation of formic acid at the Pd catalysts is mainly through the direct pathway that means no formation of poising intermediates (Antolini, 2009). Moreover, Pd is more abundant and less expensive than Pt (Zhang et al., 2011).

The preparation method has great influence on the catalytic activities and properties of catalysts. At present palladium nanoparticles were synthesized using various methods such as polyol (Wang et al., 2015), electrochemical deposition (Sarto et al., 2014), chemical reduction (Shao et al., 2006) and hydrothermal (Guo et al., 2012) method. Among these methods, polyol synthesis is known very promising method for the preparation of metal catalysts. However, the polyol method with conventional heating needs a long preparation time. It has been known that using microwave heating provides selective, time and energy consuming synthesis (Harish et al., 2012; Husin et al., 2014).

In this study, the microwave assisted polyol method was used to synthesize the Pd nonoparticles supported on carbon black (Pd/C) catalysts for formic acid oxidation. A series of catalysts were synthesized to optimize the preparation conditions such as microwave heating time and temperature. The catalytic activities of prepared catalysts for formic acid oxidation were investigated by cyclic voltammetry.

EXPERIMENTAL

Preparation of catalysts

Pd/C catalysts were prepared by microwave- assisted polyol process in ethylene glycol 99.9%, J.T.Baker) with $PdCl_2$ (98%, Sigma-Aldrich). Carbon powder and 4.0 M HNO_3 (98% Sigma-Aldrich) was impregnated with aqueous solutions of Pd. 4 mL of 0.12 M KBr (99% Sigma-Aldrich) and appropriate amount of NaOH (Merck) was put into the above mixture to obtain a solution with a pH of 11 and then heated in a domestic microwave oven (Electrolux Ems model 21400W, 2450 MHz, 800 W). The temperature was measured by using an Infrared Thermometer Cole Palmer 800-323-4340.

Finally, the samples were filtered, washed and dried in a vacuum oven for 2 hours. The preparation conditions of different catalysts were shown in Table 1.

Table 1. Catalyst preparation conditions

No	Catalysts	Catalyst preparation conditions	
		Temperature (°C)	Time (s)
1	Pd/C	30	30
2	Pd/C	50	30
3	Pd/C	75	30
4	Pd/C	100	30
5	Pd/C	130	30
6	Pd/C	190	30
7	Pd/C	200	30
8	Pd/C	130	10
9	Pd/C	130	30
10	Pd/C	130	60

Preparation of catalyst modified electrodes

The bare glassy carbon electrode was polished carefully with alumina slurry and then washed with water. For the modification of electrode, 5 mg of catalyst was added into 1 mL of 0.5% Nafion solution to get catalyst mixture. Then, 3 mL of the mixture was pipetted onto the cleaned GCE. Finally, the modified electrode was dried under room temperature to evaporate the solvent.

Electrochemical measurements

Electrochemical measurements were carried out in a standard three-electrode cell using a CHI 6043d electrochemical workstation at room temperature. A Pt wire was used as the counter electrode and a saturated calomel electrode (SCE) was used as the reference electrode. The working electrode was a glassy carbon disk with a diameter of 3.0 mm. Cyclic voltammograms were recorded in 0.5 M H_2SO_4 solution on Pd/C catalysts at different preparation conditions. The formic acid oxidation reactions on the Pd/C catalysts were performed in 0.5 M H_2SO_4 + 1 M HCOOH. In all experiments, the electrolyte was previously saturated by nitrogen. To measure the activity of formic acid electrooxidation reaction, cyclic voltammograms were recorded between -0.25 V and 1.0 V vs. Ag/AgCl with a scan rate of 50 mV s^{-1}.

RESULTS and DISCUSSION

In this study, catalyst preparation is done by microwave assisted polyol synthesis method in microwave oven at different preparing conditions. The influence of heating temperature (30-200 °C) and time (10-60 s) on the particle size and the activity of the catalyst have been evaluated. The temperature and microwave heating time in oven has great influence on the catalysts structure and consequently on formic acid electro-oxidation activity.

The effect of heating temperature

First, the carbon supported Pd catalysts were kept in the microwave oven at different temperatures, keeping the heating time constant (30 s). This process was carried out to investigate the effect of the temperature on catalyst activity for formic acid electro-oxidation. For this aim Pd catalysts were synthesized in the microwave oven at seven different temperatures ranging from 30 to 200 °C.

The electrochemical characterization of Pd/C electrocatalysts prepared at different temperatures was evaluated by cyclic voltammetry in the 0.5 M H_2SO_4 solution. The cyclic voltammograms for formic acid electro-oxidation was recorded at a scan rate of 50 mV/s (Fig. 1a). Highest current value of hydrogen adsorption-desorption peaks was obtained for the Pd/C catalyst synthesized at 130 °C.

The cyclic voltammograms for formic acid electro-oxidation was also evaluated on Pd/C catalysts prepared with different temperatures in 0.5 M H_2SO_4+ 1.0 M HCOOH solution. As shown in Fig. 1b, the electro-oxidation peak currents increase with the temperature up to 130 °C. This result was attributed to the increase in the size of Pd nanoparticles with temperature. However, further increase in temperature resulted in the formation of particle aggregation.

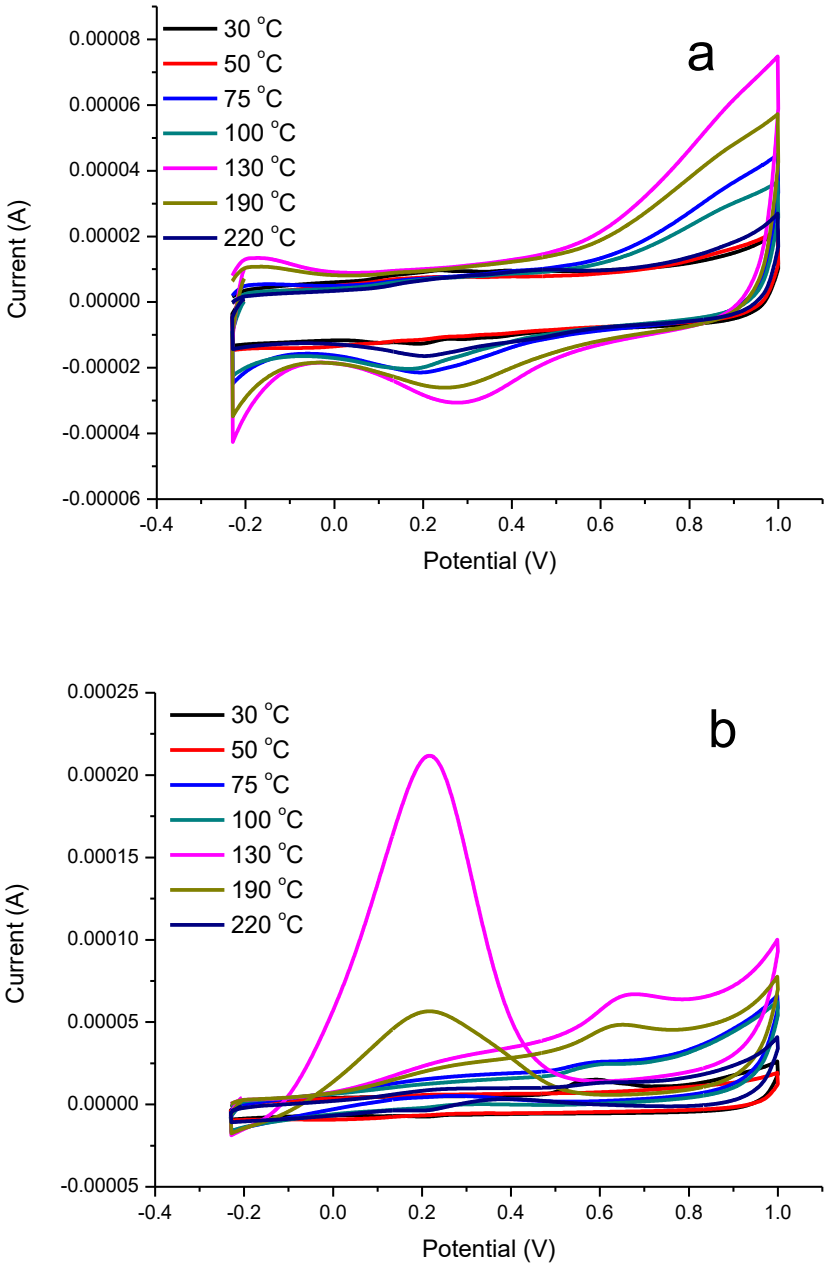

Figure 1. Cyclic voltammograms on Pd/C with different microwave heating temperature in an N_2-saturated solution of 0.5 M H_2SO_4 (a), 0.5 M H_2SO_4+1.0 M HCOOH (b). Scanning rate: 50 mV/s

The effect of heating time

Another important parameter affect the catalyst preparation is microwave heating time. After the optimum catalyst preparation temperature was determined, carbon supported Pd catalysts were

prepared at different heating times. Thus, three different catalysts were synthesized at a temperature of 130 ° C for 10, 30 and 60 s.

XRD pattern of these catalysts were shown in Fig. 2. XRD pattern of these catalysts exhibits a diffraction peak at around 20° value, related to the (002) reflection of the structure of hexagonal carbon (JCPDS card no 75-1621). Furthermore, XRD pattern of these catalysts have (111), (200), (220), and (311) planes, revealing that this catalyst Pd face-centered cubic (fcc) structure (JCPDS card no 46-1043). According to the XRD data, the catalysts prepared with the increasing time has been getting narrower that is attributed to the increase in the size of the particles with time.

The cyclic voltammograms (Fig. 3) for formic acid electro-oxidation was also recorded for Pd/C catalysts prepared with different heating time. The highest formic acid electrooxidation current has been obtained for 30 s heating time.

The above results indicated that the size of the palladium particles increases with time .Further increase in microwave heating time resulted agglomeration of palladium particles. When the particles are too small, crystallinity is not suitable for adsorption of formic acid on the Pd surface. If the particles are large, electrochemical active surface will decrease. The Pd/C catalysts synthesized at 30 s heating time has better catalytic performance for formic acid oxidation than the other synthesized palladium catalysts.

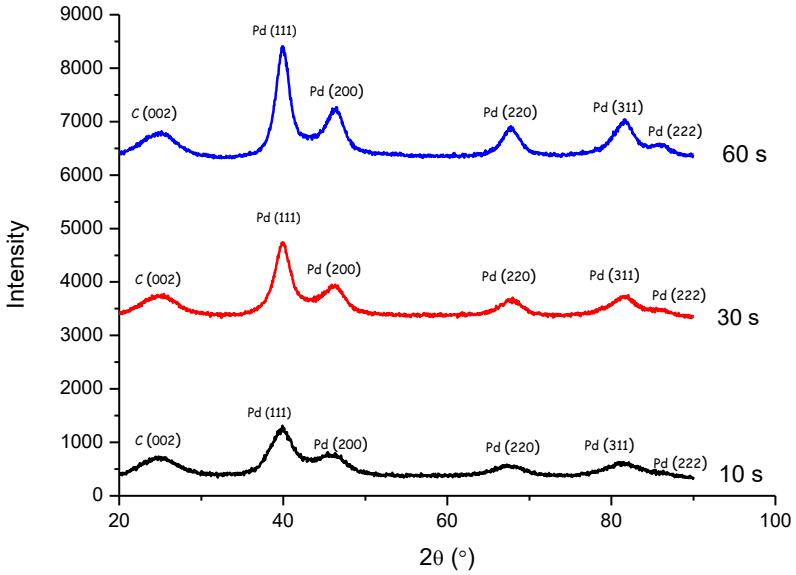

Figure 2. XRD patterns of catalysts prepared different heating time.

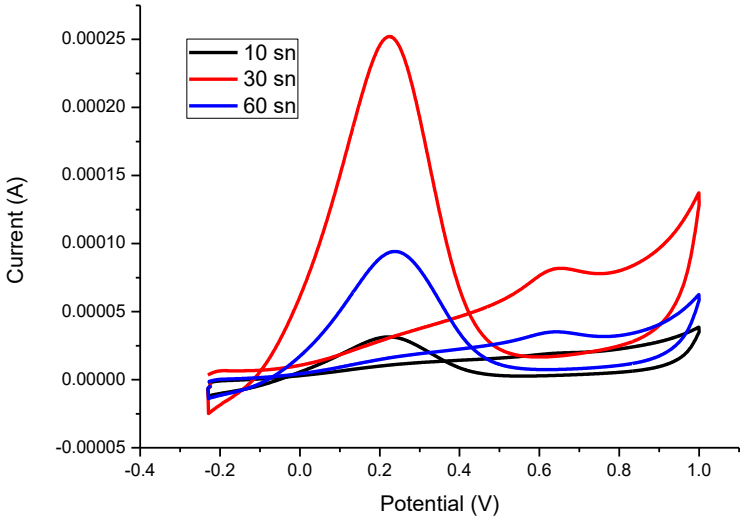

Figure 3. Cyclic voltammograms on Pd/C with different microwave heating time in an N_2-saturated solution of 0.5 M H_2SO_4+1.0 M HCOOH. Scanning rate: 50 mV/s

CONCLUSION

In summary different size of carbon supported Pd catalysts were prepared by microwave assisted polyol method and characterized by XRD technique. The electrocatalytic properties of the synthesized materials were investigated with cyclic voltammetric technique. Study on the electro-oxidation of formic acid on the catalysts showed that Pd/C catalysts prepared with 30 s microwave heating time at 130 °C temperature has much higher catalytic activity than the other Pd/C catalysts prepared at different preparation conditions. The longer microwave heating time and higher reaction temperature increased the size of palladium nanoparticles.

REFERENCES

Antolini E., 2009, "Palladium in Fuel Cell Catalysis", Energy & Environmental Science, Vol. 2 (9), pp. 915-931.

Guo, P., Wei, Z., Ye, W., Qin, W., Wang, Q., Guo, X., Lu, C., Zhao, X.S., 2012, "Preparation and Characterization of Nanostructured Pd with High Electrocatalytic Activity", Colloids and Surfaces A: Physicochemical and Engineering Aspects, Vol. 395, pp. 75–81.

Harish S., Baranton S., Coutanceau C., Joseph J., 2012, "Microwave Assisted Polyol Method for The Preparation of Pt/C, Ru/C and PtRu/C Nanoparticles and Its Application in Electrooxidation of Methanol" Journal of Power Sources, Vol. 214, pp. 33-39.

Husin M.H.M., Nordin M.R., Mohamad I.S., Yong L.K., 2014, "Pt–Cu Bimetallic Nanoparticles Synthesized by Polyol Method Under Different Reduction Conditions", Journal of Mechanical Engineering and Technology, Vol. 6 (1), pp. 77-86.

Mazumder V., Lee Y.M., Sun S.H., 2010, "Recent Development of Active Nanoparticle Catalysts for Fuel Cell Reactions", Advanced Functional Materials, Vol. 20, pp.1224-1231.

Nethravathi C., Anumol E.A., Rajamathi M., Ravishankar N., 2011, "Highly Dispersed Ultrafine Pt and PtRu Nanoparticles on Graphene: Formation Mechanism and Electrocatalytic Activity", Nanoscale, Vol. 3, pp. 569–571.

Sarto, F., Castagna, E., De Francesco, M., Dikonimos, T. M., Giorgi, L., Lecci, S., Sansovini, M., Violante, V., 2014, "Morphology and Electrochemical Properties of Pd-Based Catalysts Deposited by

Different Thin-Film Techniques", International Journal of Hydrogen Energy, Vol. 39, pp. 14701−14711.

Shao, M.H., Huang, T., Liu, P., Zhang, J., Sasaki, K., Vukmirovic, M.B., Adzic, R.R., 2006, "Palladium Monolayer and Palladium Alloy Electrocatalysts for Oxygen Reduction", Langmuir, Vol. 22(25), pp. 10409−10415.

Wang, Y., Peng, H.-C., Liu, J., Huang, C. Z., Xia, Y., 2015, "Use of Reduction Rate as a Quantitative Knob for Controlling the Twin Structure and Shape of Palladium Nanocrystals", Nano Lett., Vol. 15, pp. 1445−1450.

Zhang Z.Y., Xin L., Sun K., Li W.Z., 2011, "Pd–Ni Electrocatalysts for Efficient Ethanol Oxidation Reaction in Alkaline Electrolyte", International Journal of Hydrogen Energy, Vol. 36, pp. 12686-97.

Zhu Y., Ha S.Y., Masel R.I., 2004, "High Power Density Direct Formic Acid Fuel Cells", Journal of Power Sources, Vol. 130(1), pp. 8-14.

SELÇUK
ÜNİVERSİTESİ
MÜHENDİSLİK FAKÜLTESİ

S.Ü. Müh. Bilim ve Tekn. Derg., c.5, s.3, 2017
Selcuk Univ. J. Eng. Sci. Tech., v.5, n.3, 2017
ISSN: 2147-9364 (Elektronik)

YATAĞAN ESKİHİSAR LİNYİT AÇIK OCAĞI BATI ŞEVLERİNDE OLUŞAN DEFORMASYONLARIN JEODEZİK YÖNTEMLE İZLENMESİ VE MATEMATİKSEL MODELLENMESİ

[1]Hakan ÖZŞEN

Selçuk Üniversitesi, Mühendislik Fakültesi, Maden Mühendisliği Bölümü, KONYA
[1]hozsen@selcuk.edu.tr

(Geliş/Received: 31.01.2017; Kabul/Accepted in Revised Form: 10.03.2017)

ÖZ: Açık ocak basamaklarında şev duraysızlığı oluşması sonucu meydana gelen kaymalar yaşam kaybı yanında ekonomik kayıplara ve ocak geometrisinin bozulması gibi sonuçlara neden olabilmektedir. Bu tür olayların önüne geçilmesi için alınması gereken tedbirlerin başında emniyetli jeoteknik tasarımlar, desteklemeler, kaya düşme önleme sistemleri ve şevlerde oluşan deformasyonların değişiminin izlenmesi gelmektedir. Bu çalışma, günümüzde halen Yatağan Termik AŞ bünyesine olan ancak ölçümlerin yapıldığı yıl olan 2011'de Türkiye Kömür İşletmeleri Güney Ege Linyitleri İşletmesi'ne (TKİ-GELİ) bağlı olan Yatağan–Eskihisar linyit açık ocağında gerçekleştirilmiştir. Ocakta yapılan incelemeler ve ön değerlendirmeler neticesinde ocağın batı tarafındaki şevlerde şev duraysızlığı olasılığı bulunan alanlar tespit edilmiştir. Bu alanlarda karşılaşılan ve tehlike yaratacağından kuşkulanılan şevdeki hareketi izlemek amacıyla tespit edilen çekme çatlağındaki deformasyon değişimlerinin izlenmesine karar verilmiştir. Bu kapsamda sahada belirlenen bu sorunlu bölgelerde izleme çalışmaları yapılmasına karar verilmiştir. Ocakta dekapaj ve kömür üretimi sonrası batı şevlerinde oluşan gerilim çatlakları ve buna bağlı gelişen şev duraysızlığı olasılığı nedeniyle ölçüm istasyonları kurularak, jeodezik ölçüm yöntemleriyle 216 günlük bir süreçte belirli aralıklarla şev hareketliliği izlenmiştir. Elde edilen veriler sonucunda şevdeki deformasyon hareketliliği değerlendirilmiş ve hareketin orta hızlı bir eğilimde devam ettiği belirlenmiştir. Bu hareketliliğe bağlı bir matematiksel eşitlik geliştirilmiştir. Geliştirilen model sonuçları ile gerçek veriler arasında yüksek korelasyon mevcuttur. Bu model ile şevde gelecekte oluşabilecek deformasyon miktarları ve hızlarını tahmin etme ihtimali oluşabilecektir.

Anahtar Kelimeler: *Açık işletme, Şev, Duraylılık analizleri, Deformasyon*

Monitoring the Deformations in an Open Pit Lignite Mine Slopes by Geodetic Methods and Mathematical Analyses

ABSTRACT: Slope sliding and landslides occurring on the open pit benches can lead to consequences such as the loss of life as well as the economic loss and deterioration of the stove geometry. Safe geotechnical designs, supports, rock fall prevention systems and monitoring the deformations occurring on the slopes are among the most familiar precautions which must be taken to prevent these consequences. This study is performed in Muğla Province Yatağan District Eskihisar lignite open pit mine which was in the management of TKİ-GELİ (Turkish Coal Enterprises-South Aegean Lignite Management) in 2011. As a result of investigations and preliminary assessments at the mine regions which have instability problems were identified at the western side of the mine. Then, it is decided to monitor these regions which could have instability problems. Measurement stations were set up on the tension cracks which are the signs of a probable instability problem at the western slopes and slope movements were monitored periodically for 216 days by geodetic measurement methods. As a result of

DOI: 10.15317/Scitech.2017.93

the obtained data deformation movements were evaluated and it was determined that the movement was continuing in a moderate velocity trend. A mathematical model was developed related to these movements. It was seen that there is a good correlation between the results of the model and the in-situ data. It will be possible to predict future deformation rates and velocities on the slopes of this location with this model.

Key Words: *Open pit mining, Slope, Stability analyses, Deformation*

GİRİŞ (INTRODUCTION)

Açık ocak madenciliğinde oluşturulan şev basamaklarının duraylılığının korunması madencilik faaliyetinin sağlıklı yürütülebilmesi açısından büyük öneme sahiptir. Açık ocak maden işletmelerinde şev kaymalarına sebebiyet vermemek için ocağın kalıcı ve üretim basamaklarındaki şevlerin duraylılığının sağlanması gerekmektedir. Oluşabilecek herhangi bir şev kayması can ve mal kayıplarına yol açabilecektir. Bu anlamda, uygun şev açısının belirlenip bu değere uygun olarak madencilik faaliyetlerinin yürütülmesi esastır. Ancak uygulanan kazı tekniği, jeolojik yapısal özellikler, şevin geometrisi, yeraltı su durumu, malzeme özellikleri gibi faktörler şev duraylılığını etkileyen faktörlerdir (Özgenoğlu, 2005). Bu faktörler göz önünde bulundurularak şevlerin sürekli izlenmesi ve kontrol altında tutulması, şev duraylılığının bozulmasına yönelik belirtilerin önceden fark edilmesi açısından önemlidir. Bu izleme ve kontrol etme işlemleri için farklı teknikler geliştirilmiştir. Bunlardan bazıları, jeodezik ölçümler, elektronik mesafe ölçerlerin kullanılması, fotogrametrik yöntem, gerilim çatlağı ve eklemlerde açılma miktarlarının sürekli ölçülmesi, bir sondaj borusu içerisinden yüzeyin altında oluşabilecek deformasyonların izlenmesine olanak sağlayan inklinometrik yöntem ve yüzeye yerleştirilen ekstansometrelerdir (Kulaksız, 2012).

Bu yöntemlerden olan jeodezik yöntemle izlemede, heyelan bölgesinin hareket beklenen, hareket olasılığı olmayan ve hareket edeceğinden kuşku duyulan karakteristik yerlerinde seçilen noktalardan oluşan kontrol ağının uygun zaman aralıklarında tekrarlanan ölçülerinden, elde edilen nokta koordinatlarındaki değişimin matematik ve istatistik test yöntemleriyle kanıtlanması esasına dayanan yöntem, heyelan bölgesinde istinat duvarı, drenaj vb. önlemlerden sonra da uygulanarak alınan bu önlemlerin etkinliğinin kontrol edilmesinde de uygulanabilir (Altan ve diğ., 1991). Son yıllarda bu konuyla ilgilenen birçok araştırmacı araziden elde edilen verinin modellenmesi için farklı çalışmalar ortaya koymuşlardır. Arazideki deformasyon verilerinin toplanması için inklinometre, radar izlemesi, jeodezik izleme gibi birçok farklı metot kullanarak ardından da bu verileri laboratuvar test sonuçları ile birleştirmiş ve elde ettikleri veri tabanını çeşitli yöntemler ile modellemeye ve duraysızlık mekanizmasını çözümlemeye çalışmışlardır. Örneğin Frastia ve diğ. (2014), jeodezik yöntem kullanarak bir taş ocağında 2013 yılında oluşan şev kaymasının ardından yeni şev kaymalarının gelişiminin belirlenmesi ve önlenmesi amacıyla şev izleme çalışması gerçekleştirmişlerdir. Sonuç olarak deformasyon oluşum yönlerini ve büyüklüklerini yüksek hassasiyetle belirlemiş ve ocaktaki madencilik çalışmalarını bu sonuçlara bağlı olarak yönlendirmişlerdir. Kaizong ve diğ. (2016), çalışmalarında Chencko demir madeninde 8 yıl boyunca GPS ile ölçümler alarak yatay ve düşey deformasyonları belirlemeye çalışmışlardır. Zhao ve diğ. (2015), GB-InSAR metodu ile Fushun açık ocak kömür madeninde şev kayması mekanizmaları üzerine çalışmışlardır. Osasan ve Stacey (2014), radar izleme ile bir bakır açık ocağında kayma zamanını tahmin etme çalışmaları yapmışlardır. Dongming ve Da (2016) ve Shengwen ve diğ. (2006) uzun yıllar süren gözlemler ile Çin'in Gongjiafang ve Macoping bölgelerinde meydana gelen heyelanlarının oluşum mekanizmalarını anlamaya yönelik çalışmalar yapmışlardır.

Bu çalışmada TKİ-GELİ Müessesesi Yatağan–Eskihisar linyit sahası batı şevlerinde oluşan olası kayma alanları üzerinde oluşan deformasyonlar jeodezik ölçüm yöntemi ile izlenmiştir. Kaymanın önceden tespiti için, öncelikle kontrol ağları kurulmuş ve belirli aralıklarla ölçmeler yapılarak heyelanlı bölgedeki test noktalarının üç boyutlu koordinatlarının değişip değişmediği araştırılmıştır. Değişme

miktarları izlenerek kaydedilmiş ve elde edilen zamana bağlı deformasyon verilerinden matematiksel bir eşitlik geliştirilmiştir. Ardından bu eşitlikten elde edilen veriler gerçek verilerle karşılaştırılarak gerçek veriler ile tahmini veriler arasında oluşan bağıntılar ve bu bağıntıların istatistiksel doğrulukları belirlenmiştir.

ÇALIŞMA SAHASI (FIELD STUDY)

Eskihisar linyit ocağı, Güneybatı Anadolu'da Muğla iline bağlı Yatağan ilçesinin kuzey batısında yer almaktadır. Ocağın Yatağan ilçesine olan uzaklığı 8 km'dir. Sahanın uydu görüntüsü ile 2011 yılında TKİ-GELİ'ye bağlı işletmeler ve bu işletmelere ait ulaşım haritası Şekil 1'de verilmiştir.

Eskihisar havzasında değişik araştırmacılar tarafından jeolojik çalışmalar yapılmış olup, Ulusay ve Yoleri'ye göre hazırlanan havzadaki formasyonların stratigrafisi alttan üste doğru Paleozoik yaşlı şistler, Mezozoik yaşlı mermerler, Turgut Formasyonu (Kil, kum, silt), Sekköy Formasyonu ve Yatağan Formasyonu şeklinde dizilmiştir (Ulusay ve Yoleri, 1990). Bunlardan yola çıkarak, Yatağan bölgesindeki Eskihisar kömür havzasında temel kayaçları, Paleozoik yaşlı şistler ve Mezozoik yaşlı mermerler oluşturmaktadır. Turgut, Sekköy ve Yatağan Formasyonlarının Neojen dönemi çökeller olduğu görülmektedir.

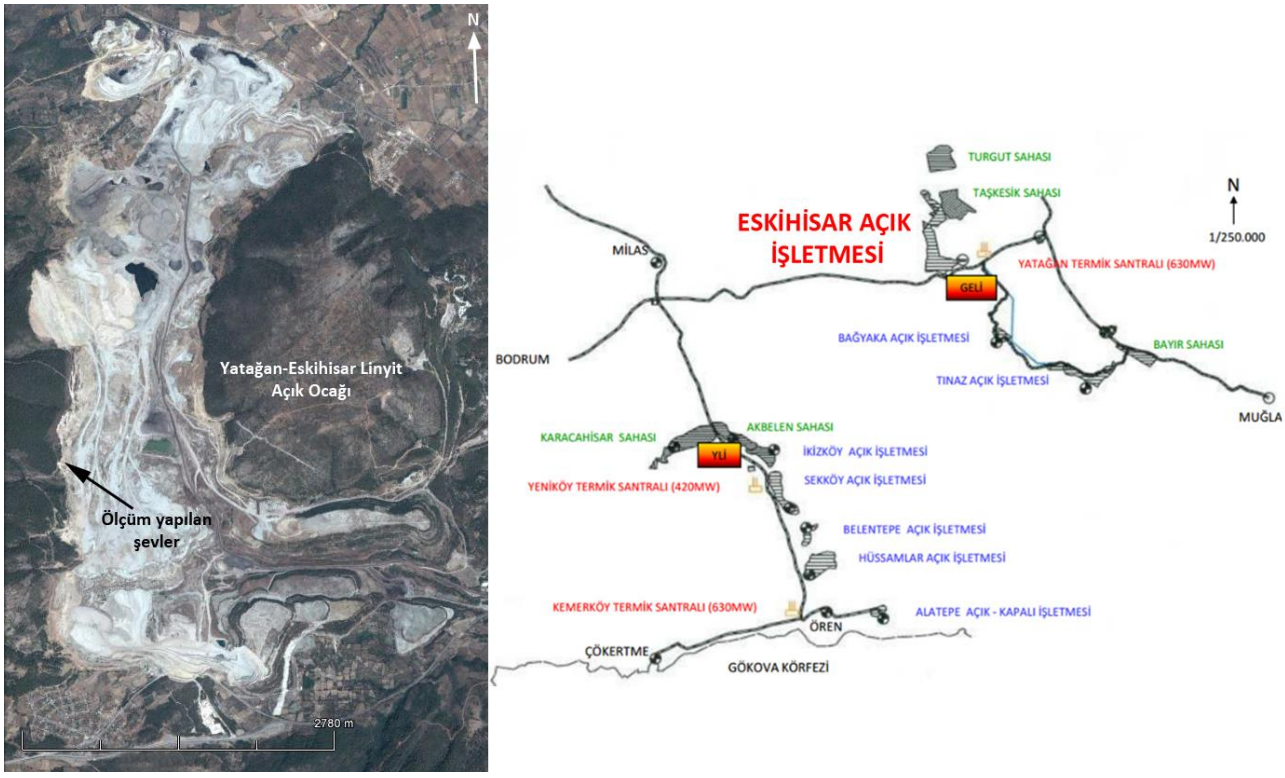

Şekil 1. TKİ-GELİ Yatağan Eskihisar Ocağının uydudan görüntüsü ve ocağa ulaşım haritası
Figure 1. *Appearance and site location of TKİ-GELİ Yatağan Eskihisar lignite mine*

ŞEV HAREKETLERİNİN ANALİZİ (ANALYSES OF SLOPE MOVEMENTS)

Bu çalışmada, Şekil 2'de görüldüğü gibi bazı kısmi kaymaların ve şev üzeri gerilim çatlaklarının görüldüğü bölgeler tespit edilerek bu bölgelerde olası kayma miktarı ve yönünü tespit etmeye yönelik çalışmalar yapılmasına karar verilmiştir. Bu kapsamda olası kayma bölgesi üzerinde 11 adet jeodezik ölçüm istasyonu kurulmuş ve periyodik aralıklarla bu istasyonlardan yatay ve düşey deformasyonları tespit etmeye yönelik ölçümler alınmıştır. Çizelge 1'de ölçüm istasyonlarında yapılan ölçümlerin

tarihleri görülmektedir. Çizelge 1'den de görüldüğü üzere ölçümler 7 Eylül 2010 tarihinde başlamış ve son ölçüm 11 Mayıs 2011 tarihinde alınmıştır. Toplamda 11 adet yapılan ölçümler 216 gün sürmüştür.

Çizelge 1. Jeodezik ölçüm tarihleri
Table 1. *Geodetic measurement dates*

Ölçüm No	Ölçüm Tarihi	Ölçüm No	Ölçüm Tarihi
1	07.09.2010	**7**	07.01.2011
2	16.09.2010	**8**	18.02.2011
3	21.09.2010	**9**	25.03.2011
4	28.09.2010	**10**	26.04.2011
5	10.11.2010	**11**	11.05.2011
6	07.12.2010		

Şekil 2. Sahada görülen gerilim çatlakları ile kısmi kaymaların gözlendiği ve muhtemel duraysızlıkların oluşması beklenen şevler
Figure 2. *Tension cracks seen on the field and probable instable slopes*

Sahada yer yer şev kaymaları gözlenmiş ve buna bağlı olarak da yine bazı bölgelerde şev duraysızlığı oluşabileceği ihtimali göz önünde bulundurularak bu bölgelerin izlenmesine karar verilmiştir. Sahada madencilik çalışmaları devam etmektedir. Eskihisar ocağında, 65 yd3 kapasiteli bir adet dragline, 15 yd3'lük altı adet ve 10 yd3'lük iki adet olmak üzere toplam 8 adet ekskavatör ile yapılan örtü tabakası ve kömür kazısı, 85 ve 150 short ton kapasiteli kamyonlar yardımıyla taşınmaktadır. Ocakta çalışma, doğu-batı istikametinde hazırlanan 80 m genişliğindeki dragline panoları ile yapılmakta olup ocağın asıl ana ilerleme yönü güneyden kuzeye doğrudur. İşletme projesine göre ocağın kuzey istikametine doğru artarda dizilmiş 56 dragline panosu mevcuttur. Ocakta projeye göre genel şev açısı 34°, basamak yüksekliği 12 m ve basamak şev açısı ise 70°-75°'dir. Saha özellikle bahar ve kış aylarında yağış alan bir bölgede bulunmaktadır. Bu etkenlerin sahada duraysızlığa yol açabilecek

deformasyonlara neden olması ve oluşan bu deformasyonların ilerlemesi neticesinde bir şev kaymasına dönüşme ihtimali mevcuttur. Bu kapsamda jeodezik yöntem kullanılarak sahada deformasyon ölçümleri gerçekleştirilmiştir. Deformasyon ölçümleri 216 güne yayılan bir süreçte 11 adet istasyondan izlenmiş ve bu süreçte belirli aralıklarla 11 adet jeodezik ölçüm alınmıştır. Ölçümlerde, x, y ve z koordinatları alınarak t1 ve t2 zamanındaki deformasyon farklılıkları tespit edilmiştir. Toplam deformasyon bu üç yöndeki ayrı ayrı deformasyonların bileşkesi şeklinde oluşturulmuş ve bu toplam deformasyon üzerinden hesaplama ve matematiksel eşitlik geliştirme işlemleri gerçekleştirilmiştir. Elde edilen toplam deformasyon miktarlarından öncelikle hareket hızları belirlenerek bu hıza göre bir sınıflama yapılmış ardından tespit edilen deformasyon davranışı matematiksel olarak ifade edilmeye çalışılmıştır. Matematiksel eşitlik geliştirme çalışmasında amaç sınırlı bir zaman diliminde alınan gerçek deformasyon hareketinin daha ileriki bir zaman dilimindeki davranışını belirlemeye yönelik çalışmayı yapmaktır.

Öncelikle sınıflama çalışması kapsamında Cruden ve Varnes'in hareket hızına göre sınıflama esasları dikkate alınmıştır. Cruden ve Varnes'e göre kütle hareketleri yenilme modellerine göre sınıflandırıldığı gibi hareketin hızları dikkate alınarak da sınıflandırılabilir. Duraysızlıklar hızlarına göre Çizelge 2'de verildiği gibi sınıflandırılabilir.

Çizelge 2. Duraysızlık hızlarına bağlı olarak oluşan hareketin sınıflandırılması

Table 2. *Classification of the movement related to the velocity of instability*

Hareketin hızı	>5,0 m/sn	5,0 m/sn-3 m/dak	3 m/dak-1,8 m/saat	1,8 m/saat-1,3 m/ay	1,3 m/ay-1,6 m/yıl	1,6 m/yıl-16 mm/yıl	<1,6 mm/yıl
Sınıfı	Aşırı hızlı	Çok hızlı	Hızlı	Orta hızlı	Yavaş	Çok yavaş	Aşırı yavaş

Bu ölçeğin üst limitini kaya düşmesi ve hareket mesafesi büyük akma-kaymalar, alt sınırını ise ana kayada meydana gelen sünme oluşturmaktadır (Cruden ve Varnes, 1996). Bu değerler ışığında ocaktaki hareket, hızlarına göre Çizelge 3'de verildiği gibi sınıflandırılmıştır.

Çizelge 3. İstasyon numaralarına göre ortalama deformasyon hızları ve Crudden ve Varnes (1996)'ya göre sınıflandırmaları

Table 3. *Average deformation velocities and classifications according to station numbers*

İstasyon Numarası	**Ortalama Deformasyon Hızı (m/yıl)**		**İstasyon Numarası**	**Ortalama Deformasyon Hızı (m/yıl)**	
1	2,503	Orta Hızlı	**7**	2,765	Orta Hızlı
2	2,847	Orta Hızlı	**8**	1,467	Yavaş
3	2,672	Orta Hızlı	**9**	1,671	Orta Hızlı
4	2,758	Orta Hızlı	**10**	2,820	Orta Hızlı
5	2,815	Orta Hızlı	**11**	2,236	Orta Hızlı
6	2,700	Orta Hızlı			

Çizelge 3'den görüldüğü üzere 8 nolu istasyon haricindeki tüm istasyonlarda deformasyon hızı Cruden ve Varnes sınıflamasına göre "1,8 m/saat-1,3 m/ay" aralığında kalmış olup "orta hızlı" hareket olarak nitelendirilebilir. Sadece 8 no'lu istasyonda deformasyon hızı "1,5 m/ay-1,5 m/yıl" aralığında kalmış olup "yavaş" hareket sınıfındadır (Cruden ve Varnes, 1996). En hızlı hareket eden istasyon 2,847 m/yıl hızıyla İstasyon 2'de görülürken, en yavaş hareket 8 no'lu istasyonda 1,467 m/yıl hızında kaydedilmiştir (Şekil 3). Ayrıca tüm istasyonlara ait hız-zaman ve hız-ivme grafikleri de oluşturulmuştur. Buradan elde edilen bulgulara göre ölçümlerin 33.gününde hız en yüksek seviyeye çıkmış ve bu günün ardından düşme eğiliminde devam ederek 1,467-2-847 m/yıl arasında değişen seviyelerde sabitlenme eğilimine girmiştir. Ancak sabit hızla da olsa hareket devam etmektedir ve bu hareket "orta hızlı" şeklinde nitelendirilen bir hareket tarzındadır. Şekil 4'deki grafikten de görüldüğü

üzere ölçümün 216. gününün sonunda Çizelge 1'de görülen nihai hız değerlerine ulaşılmıştır. Bu noktada hareketin ivmesinin de incelenmesi yararlı olacaktır. Şekil 4'de görülen ivme-zaman grafiği incelendiğinde hareketin ilk başladığı tarihlerde çok yüksek bir ivmenin olduğu ve zaman içerisinde azalma eğilimine girdiği, ancak hız analizlerinde de görülen 33. günde yine artma eğiliminde olduğu ve 33. günden sonra azalma hatta sıfırlanma eğilimine girdiği görülmüştür. İvmenin sıfıra doğru yaklaşması hareketin de sabit bir karakterde devam etme eğiliminde olduğunun kanıtıdır. İvmelenme neredeyse sıfırlanmıştır ancak hareketlilik sabit hızla devam etmektedir. Bu durumda 216 günlük gerçek veriye dayanarak ileride oluşabilecek deformasyon miktarlarını, hızlarını ve ivmelerinin tahmin edilebilir olması büyük önem taşımaktadır.

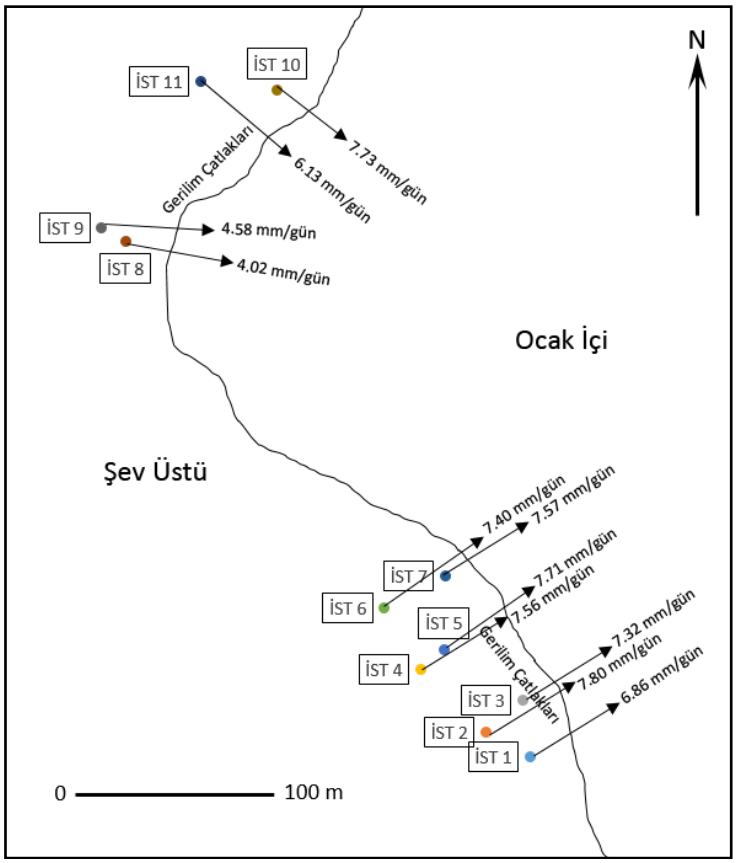

Şekil 3. İstasyonların yerleri ile hareket hızları ve deformasyon ilerleme yönleri

Figure 3. *Locations and the movement velocities of the stations and deformation dilatation directions*

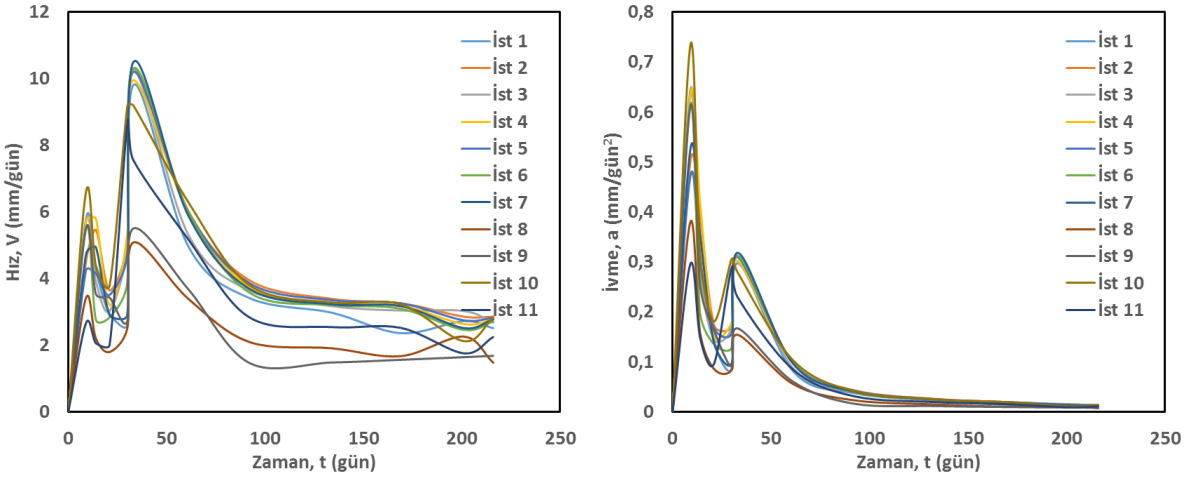

Şekil 4. Şevde oluşan deformasyon hareketlerinin hız ve ivme grafikleri

Figure 4.*Velocity and acceleration graphs of deformation movements occurred on the slopes*

MATEMATİKSEL EŞİTLİK (MATHEMATICAL EQUATION)

Bölüm 4'deki sınıflama sonucundan da görüleceği üzere ocakta "orta hızlı" şev hareketinin mevcut olduğu anlaşılmaktadır. Ciddi sonuçları olabilecek bu hareketliliğin ne tür bir eğilim içerisinde olduğunun belirlenmesi açısından her bir istasyondaki gerçek deformasyon verisi istatistiki olarak incelenmiş ve genel eğilim kapsamında her bir istasyon için bir matematiksel eşitlik geliştirilmiştir. Burada amaç eldeki verilerden yola çıkarak ileriki bir zamanda oluşabilecek deformasyon miktarı ve hızının belirlenmeye çalışılmasıdır.

Daha önce bu konuda yapılmış olan çalışmalarda deformasyon ile zaman arasında üstel bir ilişki olduğu tespit edilmiştir (Kennedy vd., 1970). Aynı üstel ilişki Kuzey Bohemia'da uluslararası bir yol kenarında kumtaşında meydana gelen bir heyelanın zamana bağlı izlenmesi sonucunda da görülmüş ve şev kayması 2 ay önceden tahmin edilmiştir (Zvelebil ve Moser, 2001). Yine bu çalışmaya konu olan TKİ-GELİ Yatağan ocağındakine benzer bir çalışma TKİ-GLİ Ilgın linyit açık ocağında gerçekleştirilmiş, oluşan gerilim çatlakları üzerinde deformasyon ölçümleri yapılarak bir matematiksel eşitlik geliştirilmeye çalışılmıştır. Söz konusu çalışmada deformasyon ile zaman arasında bir bağıntı oluşturularak Eşitlik-1'deki ilişki yüksek korelasyon ile belirlenmiş ve gerçek veri ile eşitlikten elde edilen veri karşılaştırılmıştır (Özşen ve Özkan, 2013).

$$\boldsymbol{U = \left(a + e^{bt}\right)t} \qquad (1)$$

Burada,
***U*:** Deformasyon miktarı (mm)
***t*:** Zaman (gün)
a ve ***b*:** Uygun istatistiksel parametrelerdir.

Aynı bağıntı bu çalışma kapsamında Yatağan'da elde edilen jeodezik ölçüm verileri ile de denenerek sonuçlar elde edilmiştir ve Çizelge 4'de sunulmuştur. Buna ek olarak Eşitlik 2'de verilen bağıntı ile de yüksek ilişki elde edilmiş ve çalışmaların bu yeni elde edilen eşitlik ile yapılmasına karar verilmiştir. Bu kapsamda elde edilen matematiksel eşitlikler ve korelasyonları yine Çizelge 4'de sunulmuştur. Çizelge 4'deki eşitlikler dikkate alınarak, örneğin İstasyon 2'deki model deformasyon verilerinin her iki eşitlik için zamana bağlı olarak değerlendirilmesi sonucunda Şekil 5'deki gibi bir eğilim içinde olduğu tespit edilmiştir.

$$U = (C_1 t)^{C_2} \quad (2)$$

Burada,
U: Deformasyon miktarı (mm)
t: Zaman (gün)
C_1 ve C_2: Uygun istatistiksel parametrelerdir.

Çizelge 4. Tüm istasyonlar için geliştirilen eşitlikler ve korelasyon katsayıları
Table 4. *Equations developed for all stations and correlation coefficients*

İstasyon No	$U=(a+e^{bt})t$	R^2	$U = (C_1 t)^{C_2}$	R^2
1	$U=(14,56+e^{-0,003763t})t$	0,89	$U=(578,3t)^{0,6217}$	0,89
2	$U=(18,35+e^{-0,004242t})t$	0,94	$U=(1240t)^{0,5952}$	0,93
3	$U=(16,35+e^{-0,003778t})t$	0,92	$U=(698,1t)^{0,6214}$	0,93
4	$U=(18,26+e^{-0,004468t})t$	0,93	$U=(1776t)^{0,5747}$	0,92
5	$U=(17,97+e^{-0,004223t})t$	0,93	$U=(1025t)^{0,6032}$	0,92
6	$U=(17,37+e^{-0,004380t})t$	0,90	$U=(1068t)^{0,5961}$	0,89
7	$U=(17,10+e^{-0,004180t})t$	0,90	$U=(873,2t)^{0,6077}$	0,89
8	$U=(8,76+e^{-0,003005t})t$	0,89	$U=(113,7t)^{0,6862}$	0,89
9	$U=(8,40+e^{-0,003399t})t$	0,82	$U=(568,6t)^{0,5797}$	0,87
10	$U=(21,08+e^{-0,005494t})t$	0,89	$U=(5051t)^{0,5290}$	0,88
11	$U=(16,62+e^{-0,005455t})t$	0,85	$U=(4637t)^{0,5150}$	0,84

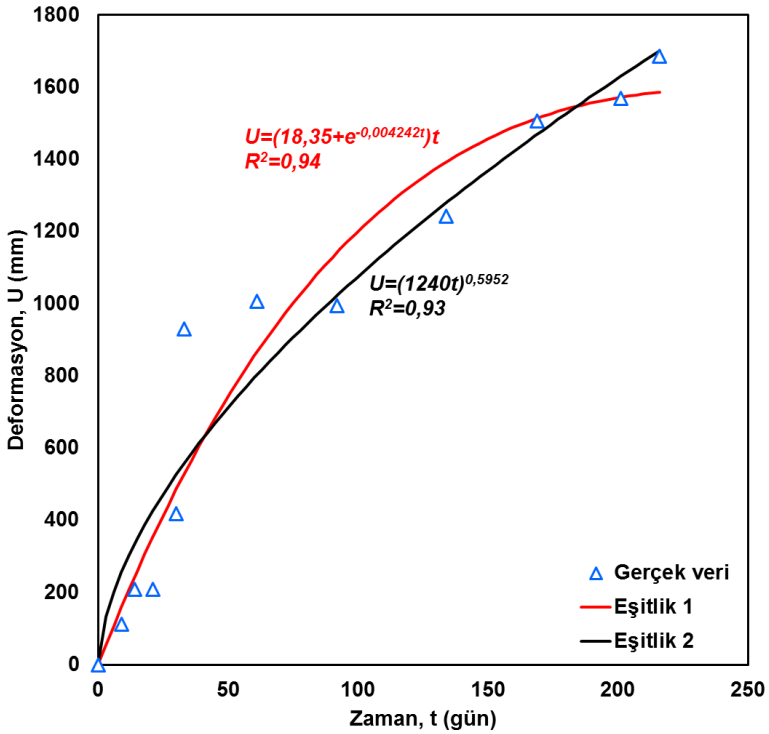

Şekil 5. İstasyon 2'nin Zaman-Deformasyon grafiği
Figure 5. *Time vs. Deformation graph of Station 2*

Çizelge 4'de görülen fonksiyonlarda 216 gün olan nihai ölçüm zamanı yerine konulduğunda Eşitlik 1 ve 2'den Çizelge 5'deki değerler elde edilmiştir. Bu değerlerden de görüleceği üzere her iki eşitlikte de gerçek veriye çok yakın sonuçlara ulaşılmıştır. Bu değerlerin karşılaştırmalı grafikleri oluşturulduğunda

aralarında doğrusal bir bağıntının olduğu belirlenmiş (Şekil 6) ve bu doğrultuda çalışmalar yapılmıştır. Eşitlik 2'deki denklem kullanılarak oluşturulan Eşitlik 2'de bulunan sonuçlar Eşitlik 1'den elde edilen Eşitlik 1'e nazaran daha iyi sonuçlar vermiştir. Arazi deformasyon verileri (adv) ile eşitlik deformasyon verileri (edv) arasındaki bağıntılar Eşitlik 3 ve 4'te verilmiştir. Eşitlik 1 verileri ile gerçek arazi verileri arasındaki doğrusal ilişkiden yola çıkılarak elde edilen regresyon katsayısı 0,88 olurken Eşitlik 2'den elde edilen regresyon katsayısı değeri 0,93 olmuştur. Bu durumda Eşitlik 2'nin gerçeğe daha yakın veriler ürettiği sonucuna varılabilir.

$$adv = 0{,}8152(edv)_1 + 159{,}97 \quad (3)$$

$$adv = 0{,}9324(edv)_2 + 88{,}467 \quad (4)$$

Burada;
adv: Arazi deformasyon verisi (mm),
edv1: Eşitlik 1'den elde edilen deformasyon verisi (mm),
edv2: Eşitlik 2'den elde edilen deformasyon verisi (mm)'dir.

Çizelge 5. Arazide elde edilen deformasyon miktarları ile eşitliklerden elde edilen deformasyon miktarlarının karşılaştırılması

Table 5. *Comparing the amount of deformations obtained from the field and the equations*

İstasyon No	Arazi Verisi *adv* (mm)*	Eşitlik 1 Verisi edv_1 (mm)	Eşitlik 2 Verisi edv_2 (mm)
1	1481	1395	1474
2	1685	1585	1700
3	1581	1561	1651
4	1632	1502	1618
5	1666	1559	1675
6	1598	1456	1573
7	1636	1497	1606
8	868	989	1029
9	989	870	891
10	1669	1389	1563
11	1323	1105	1231

* 216 gün sonunda

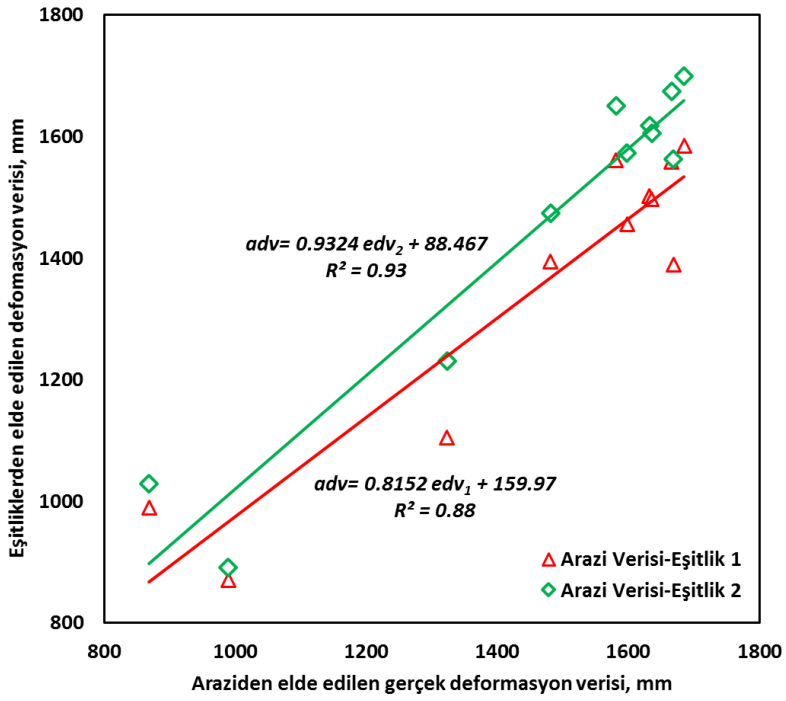

Şekil 6. Arazi deformasyon verileri ile eşitliklerden elde edilen deformasyon verilerinin karşılaştırılması

Figure 6. *Comparing the in-situ data and the data obtained from equations*

SONUÇLAR (CONCLUSIONS)

Bu çalışmada, TKİ-GELİ Eskihisar linyit açık ocağı batı şevlerinde 07.09.2010 tarihinde başlayıp 11.05.2011 tarihinde sona eren ve 216 gün boyunca süren deformasyon ölçümleri gerçekleştirilmiştir. Arazide şev duraylılığı sorunu yaşanabileceği düşünülen noktalara toplam 11 adet ölçüm istasyonu kurulmuş ve deformasyon ölçümleri jeodezik ölçüm metotları kullanılarak elde edilmiştir. Elde edilen veriler değerlendirilerek x, y ve z yönlerindeki deformasyonlar ayrı ayrı belirlenmiş, ardından tüm yönlerdeki deformasyonların bileşkesi alınarak tek bir toplam deformasyon miktarına ulaşılmıştır. Bu işlem yapılırken önce yataydaki deformasyonların bileşkesi alınmış bu bileşke ile düşey deformasyon miktarının bileşkesi alınarak toplam deformasyon miktarı ve yönüne her bir istasyon için ulaşılmıştır.

Bu kapsamda;

- En büyük deformasyon 1685 mm olarak 2 no'lu istasyonda,
- En düşük deformasyon 868 mm olarak 8 no'lu istasyonda gerçekleşmiştir.
- Tüm istasyonlarda hareket doğu yönüne doğru tespit edilmiştir.

Elde edilen deformasyon verilerinin zamana bağlı hareketinin hız ve ivme değerleri incelenmiş ve sonuç olarak sabit hızla da olsa hareketin devamlılık arz ettiği bu hareketin "orta hızlı" şeklinde nitelendirilebilecek bir hareket hızında olduğu belirlenmiştir. Ocakta bu şekilde bir deformasyon hareketliliğinin olması, bu durumun ileride ne şekilde sonuçlanabileceğinin sorgulanmasına yol açmıştır. Öncelikle Özşen ve Özkan (2013) tarafından geliştirilen eşitlik, eldeki veriler üzerinde uygulanarak yüksek korelasyon elde edilmiştir. Ardından bu çalışma kapsamında sonuç değerlerine yakınsamada çok daha iyi sonuçlar veren yeni bir eşitlik geliştirilerek veriler üzerinde uygulanmıştır. İlk eşitliğe nazaran daha yüksek bir korelasyon sağlandığı görülmüş ve her iki eşitlik için de deformasyon verileri elde edilmiştir. Elde edilen matematiksel eşitlikte amaç, bilinen veriler, yani eldeki deformasyonlar kullanılarak elde olmayan deformasyon miktarlarına ulaşmak, bu sayede ileri bir tarihte oluşabilecek deformasyon miktarını tayin edebilmektir. Deformasyon miktarında oluşacak artışların hız

ve ivmesi gibi bazı parametreler göz önüne alınarak kritik hız ve ivme değerlerine yaklaşıldığında bir takım tedbirlerin alınması gerekebilecektir. Bu tedbirler kapsamında oluşan deformasyon hareketinin hızı ve ivmesi gözlem altında tutulmalı ve bu değerler belirtilen sınırların üstüne çıkarsa mutlaka mevcut bölgedeki çalışmalar durdurulmalı ve önlem alınmalıdır. Bu çalışmada ele alınan bölgedeki hız ve ivme değerleri normal değerler içerisinde seyretmektedir. Ancak zaman içerisinde bölgede yapılan çalışmanın yoğunluğu, yapılacak delme-patlatma çalışmaları, bölgede oluşabilecek depremler veya şiddetli yağış gibi bazı parametrelerin değişmesi neticesinde oluşabilecek deformasyon artışları farklı durumlara neden olabilecektir. Şevlerin izlenmesinin sürekli yapılması ve elde edilen sonuçların hemen değerlendirilmesi oluşabilecek kötü durumların önüne geçilmesi açısından önem arz etmektedir. Bu çalışmadaki denklemlerin kısa vadeli sonuçlar için kullanılması uygun olacaktır. Yukarıdaki etkenlerin değişimi ile denklemler de revize edilmeli ve yeni duruma uygun bir şekilde hareket edilmelidir.

TEŞEKKÜR (ACKNOWLEDGEMENTS)

Yazar, bu çalışmanın yapılmasında yardımlarını esirgemeyen TKİ-GELİ Yatağan İşletmesi yönetici, mühendis ve çalışanlarına teşekkür eder.

KAYNAKLAR (REFERENCES)

Altan O., Ayan O.T., Deniz R., Özüer B., Tekin E., "Heyelan Bölgelerinde Zemin Hareketlerinin Jeodezik Yöntemlerle Saptanması ve Bir Uygulama", Türkiye 1. Ulusal Heyelan Sempozyumu, Karadeniz Teknik Üniversitesi, Trabzon, pp. 139-154, 27-29 Kasım 1991.

Cruden DM., Varnes DJ., 1996, "Landslide Types and Processes", Landslides: Investigation and Mitigation Special Report, Transportation Research Board, National Academy of Sciences, pp.36-75, Washington.

Dongming G., Da H., 2016, "A Complex Rock Topple-rock Slide Failure of an Anaclinal Rock Slope in The Wu Gorge, Yangtze River, China", Engineering Geology, Vol. 208, pp.165-180.

Fraštia M., Marčiš M., Kopecký M., Liščák P., Žilka A., 2014, "Complex Geodetic and Photogrammetric Monitoring of the Kraľovany Rock Slide", Journal of Sustainable Mining, Vol.13, no.4, pp.12–16.

Kaizong X., Congxin C., Hua F., Yucong P., Yangyang D., 2016, "Mining-induced Ground Deformation in Tectonic Stress Metal Mines: A Case Study", Engineering Geology, Vol. 210, pp.212-230.

Kennedy BA., Niermeyer KE., Fahm BA., "Slope Monitoring Systems Used in The Prediction of a Major Slope Failure at The Chuquicamata Mine, Chile", Planning Open Pit Mines Symposium, Johannesburg, pp.215-225, 1970.

Kulaksız S., 2012, "Şevlerde Hareket İzleme Teknikleri", Madencilikte Çevre Yönetimi, Afyon, ss. 47-48.

Osasan K.S., Stacey TR., 2014, "Automatic Prediction of Time to Failure of Open Pit Mine Slopes Based on Radar Monitoring and Inverse Velocity Method", International Journal of Mining Science and Technology, Vol. 24, pp. 275-280.

Özgenoğlu A., 2005, "Açık İşletmelerde Şev Stabilitesi Analizi", Maden Mühendisliği Açık Ocak İşletmeciliği El Kitabı, Ankara, ss.337-387.

Özşen H., Özkan İ., 2013, "TKİ-GLİ Ilgın Linyit Açık Ocağı Batı Şevlerinde Oluşan Gerilim Çatlaklarında Oluşan Deformasyonların İzlenmesi ve Zamana Bağlı Matematiksel Modellenmesi", S.Ü. Müh. Bilim ve Tekn. Derg., c.1, s.3, ss. 37-44.

Shengwen Q., Fuzhang Y., Sijing W., Ruichun X., 2006, "Characteristics, Mechanism and Development Tendency of Deformation of Maoping Landslide after Commission of Geheyan Reservoir on The Qingjiang River, Hubei Province, China", Engineering Geology, Vol. 86, pp.37-51.

Ulusay R., Yoleri M., 1990, "TKİ GELİ Yatağan (Muğla) Eskihisar Açık işletmesi Şev Stabilitesi Etüd raporu", MTA Derleme No.8932, 79s., Ankara.

Zhao L., Jin'an W., Lin L., Lixiang W., Robert YL., 2015, "A Case Study Integrating Numerical Simulation and GB-InSAR Monitoring to Analyze Flexural Toppling of an Anti-Dip Slope in Fushun Open Pit, Engineering Geology, Vol. 197, pp. 20-32.

Zvelebil J., Moser M., 2001, "Monitoring Based Time-Prediction of Rock Falls: Three Case-Histories", Physics and Chemistry of the Earth (B), Vol. 26, No. 2, pp. 159-167.

SELÇUK ÜNİVERSİTESİ
MÜHENDİSLİK FAKÜLTESİ

S.Ü. Müh. Bilim ve Tekn. Derg., c.5, s.3, 2017
Selcuk Univ. J. Eng. Sci. Tech., v.5, n.3, 2017
ISSN: 2147-9364 (Electronic)

OPTIMIZATION OF NICKEL EXTRACTION FROM LATERITIC ORE IN HYDROCHLORIC ACID SOLUTION WITH HYDROGEN PEROXIDE BY TAGUCHI METHOD

[1]Ali ARAS, [2]Tevfik AĞAÇAYAK

[1,2]Selcuk University, Department of Mining Engineering, Campus, Selcuklu, Konya, TURKEY
[1]aliaras@selcuk.edu.tr, [2]tevfik@selcuk.edu.tr

(Geliş/Received: 24.02.2017; Kabul/Accepted in Revised Form: 22.03.2017)

ABSTRACT: Taguchi optimization method was used to determine optimum conditions for the extraction of nickel from lateritic ore in hydrochloric acid solution with hydrogen peroxide. Leaching time, stirring speed, temperature, hydrochloric acid concentration and hydrogen peroxide concentration were chosen as parameters. The optimum conditions for dissolution were found as leaching time of 240 min, a temperature of 70°C, hydrochloric acid concentration of 3 M, hydrogen peroxide concentration of 0.1 M and without stirring. The experimental results under optimum leaching conditions, showed that the extraction of nickel from lateritic ore was 90.66%. Analysis of variance (ANOVA) was applied to experimental results. Percentage contributions of each factor for the extraction of nickel were determined.

Key Words: *Leaching, Lateritic ore, Nickel; Hydrochloric acid, Hydrogen peroxide; Taguchi method*

Nikelin Lateritik Cevherden Hidrojen Peroksitli Hidroklorik Asit Çözeltisinde Çözündürülmesinin Taguchi Yöntemiyle Optimizasyonu

ÖZ: Nikelin lateritik cevherden hidrojen peroksitli hidroklorik asit çözeltisinde çözündürülmesinin optimum koşullarını belirlemek için Taguchi optimizasyon yöntemi kullanılmıştır. Deney parametreleri olarak, süre, karıştırma hızı, sıcaklık, hidroklorik asit derişimi ve hidrojen peroksit derişimi seçilmiştir. Çözündürme için optimum koşullar, karıştırma yapılmadan, 240 dakika liç süresi, 70 °C sıcaklık, 3 M hidroklorik asit derişimi ve 0.1 M hidrojen peroksit derişimi olarak bulunmuştur. Optimum koşullarda yapılan deney sonuçları, nikelin lateritik cevherden çözündürülmesinin %90.66 olduğunu göstermiştir. Deney sonuçlarına varyans analizi (ANOVA) uygulanmış ve her faktörün nikel çözündürülmesine olan katkısı belirlenmiştir.

Anahtar Kelimeler: *Liç, Lateritik cevher; Nikel; Hidroklorik asit; Hidrojen peroksit; Taguchi metodu*

INTRODUCTION

Nickel is a widely used metal due to its chemical and physical properties, such as corrosion resistance, alloying, electrical, thermal and catalyst properties. The main use area of nickel is the production of stainless steel and alloys, other uses are electroplating and chemistry. Laterites are oxide ores widely distributed in the equatorial regions. Lateritic nickel deposits occur during laterization, namely, a weathering process of ultramafic rocks containing minerals such as olivine, pyroxene and amphibole (Golightly, 1981). Ni-laterites can be classified in three main groups as oxide, hydrous silicate and clay silicate deposits (Golightly, 1981; Gleeson, *et al.*, 2003; Brand *et al.*, 1998; Sagapoa *et al.*, 2011;

DOI: 10.15317/Scitech.2017.94

Georgiou and Papangelakis, 1998). Nickel laterites constitute an important part of world reserves of nickel. About 70% of the world's nickel reserves occur from laterite deposits, the rest of sulphide deposits (Elias, 2002; Landers *et al*., 2009; Soler *et al*., 2008). However, about 40% of the world's nickel production is provided from lateritic ores (Gleeson, *et al*., 2003; Elias, 2002; Brand *et al*., 1998; Dalvi *et al*., 2004). Nickel production from lateritic ores contains pyrometallurgical and hydrometallurgical processes (Deepatana *et al*., 2006). Generally, pyrometallurgical processes (ferronickel and matte smelting) involve drying, calcining/reduction and electric furnace smelting. However, hydrometallurgical processes can be applied as the Caron process, HPAL (High pressure acid leaching), AL (Atmospheric leaching) and acid heap leaching (Dalvi *et al*., 2004). In the literature, there are several studies related to lateritic nickel leaching in different solutions using high pressure or atmospheric pressure (agitation or heap leaching). The solutions used in these studies can be given as sulphuric acid (Georgiou and Papangelakis, 1998; Agacayak and Zedef, 2012; Luo *et al*., 2010; Stopic *et al*., 2002; Ayanda *et al*., 2011; Rubisov *et al*., 2000; Agatzini-Leonardou and Zafiratos, 2004; McDonald and Whittington, 2008a; Thubakgale *et al*., 2013; Landers *et al*., 2009; Mohammadreza *et al*., 2014), hydrochloric acid (Ayanda *et al*., 2011; Park and Nam, 2008; Agacayak et. al., 2011; Olanipekun, 2000; Wang *et al*. 2012; Guo *et al*., 2015; McDonald and Whittington, 2008b; Li *et al*., 2012), nitric acid (Agacayak and Zedef, 2013; Ayanda *et al*., 2011; Ma *et al*., 2013), ammonia (Zhai *et al*., 2010; Chen *et al*., 2010; Zuniga *et al*., 2010), citric acid, oxalic acid and acetic acid (Sahu *et al*., 2011; Behera *et al*., 2010; Sukla and Panchanadikar, 1993, Kursunoglu and Kaya, 2015). The main aim in leaching studies is to provide metal extraction with high recovery. Therefore, optimization of leaching parameters is very important. Taguchi method is widely used in optimization studies, both leaching studies and other scientific fields (Bese *et al*., 2010; Abali *et al*., 2006; Demir and Donmez, 2008; Babaei-Dehkordi *et al*., 2013; Asl *et al*., 2015; Dogan and Yartasi, 2014; Copur, 2002; Abali *et al*., 2011; Moghaddam *et al*., 2006; Ata *et al*., 2001; Safarzadeh *et al*., 2008; Ilyas *et al*., 2010; Zolfaghari *et al*., 2011). One of the advantages of Taguchi method is to keep costs to a minimum level compared to conventional experimental design methods and closer performance to the desired level. Another advantage is to adapt optimum conditions obtained from laboratory studies to real production conditions (Taguchi, 1987; Demir and Donmez, 2008; Donmez *et al*., 1998; Ata *et al*., 2001; Roy, 1995; Safarzadeh *et al*., 2008).

The dissolution of lateritic nickel ore in hydrochloric acid solution with hydrogen peroxide was investigated. As a result of the literature review, no study was found on the optimization of the dissolution of lateritic nickel ore for this medium. Hence, it was aimed to determine optimum leaching condition of lateritic nickel ore by Taguchi method.

MATERIAL AND METHOD

Lateritic nickel ore sample was taken from the Gördes (Manisa) region of Turkey. The sample used was a typical limonitic laterite ore with high iron content. According to the mineralogic analysis, the sample contains goethite, hematite and quartz. The XRD pattern of the sample was given in Figure 1.

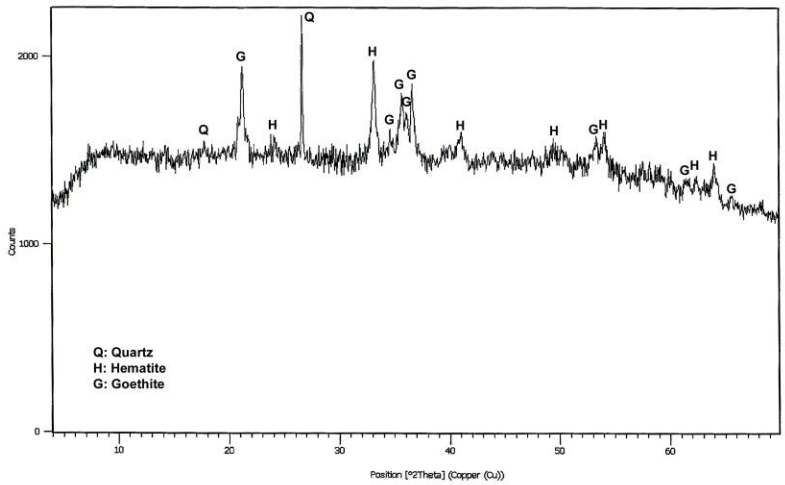

Figure 1. XRD pattern of the sample

First, the sample was ground to –212 μm in order to use in the experiments. Then, the sample was wet sieved to obtain different particle size fractions as –212+150, –150+106, –106+75 and –75+53 μm. Nickel and iron contents were determined with Atomic Absorption Spectrophotometer (AAS). Nickel and iron contents of each size fraction were given in Table 1.

Table 1. Nickel and iron contents of each size fraction

Particle size, μm	Ni content, %	Fe content, %
–212+150	1.05	36.01
–150+106	1.02	37.03
–106+75	1.00	36.40
–75+53	1.01	38.25

Leaching experiments were carried out in a 1 L glass vessel placed in a thermostatically-controlled water bath. For the stirring process, Heidolph brand RZR 2021 model mechanical stirrer equipped with a Teflon-covered propeller was used. For each experiment, 5 g lateritic nickel ore sample with a fraction size of 75x53 μm was used in 500 mL $HCl+H_2O_2$ solution. Taguchi method was used in the design of leaching experiments. Experimental parameters were applied as stirring speed (0–600 rpm), temperature (40–70 °C), HCl concentration (0.5–3.0 M), H_2O_2 concentration (0.1–1 M) and leaching time (30–240 min). At the end of leaching time, 5 mL solution was taken and diluted with distilled water to 100 mL in a volumetric flask. The amount of Ni in the leaching solution was determined using a GBC mark SensAA model flame atomic absorption spectrometer (AAS).

RESULT AND DISCUSSION

Taguchi Method and Optimization Studies

For optimizing a process by using Taguchi method, the design of an experiment involves the following stages: selection of independent process parameters; determination of the number of levels for the process parameters; selection of the suitable orthogonal array and assignment of the process parameters; performing the experiments proper to the orthogonal array; calculation of the performance characteristics; analyzing the data using the performance characteristics; determination of the optimum levels of the process parameters; performing the confirmation experiment using the optimum process parameters (Bese *et al*., 2010; Phadke, 1989; Abali *et al*., 2006). The change in the quality characteristics in reply to a factor presented in the experimental design is the signal of the requested effect. The noise is

the effect of external factors that were not designed in experiments on the outcome. The signal to noise ratio (S/N) shows the sensibility of the quality characteristic to noise factors (Roy, 1995). Usually, three different equations of S/N ratio were used depending on performance characteristics. These are, lower is better, nominal is best and higher is better (Roy, 1995; Atil and Unver, 2000; Zolfaghari *et al*., 2011). The aim of this study was to provide maximum metal extraction, "higher is better" which given in Equation (1) was used,

$$S/N = -10\log_{10}\left[\frac{1}{n}\sum\left(\frac{1}{EoM_i}\right)^2\right] \quad (1)$$

where n is the number of repetitions of the experiments and EoM_i (the extraction of metal) is the result of the experiment. Experimental factors and their levels were given in Table 2. The orthogonal array (OA) experimental design plan (L_{16}) was given in (Table 3). EoM_1 and EoM_2 show the extraction of metal for the first and second leaching test, respectively. As seen from Table 3, the maximum *S/N* value which obtained from test 10 was represented in bold. To investigate the optimum conditions, the analysis of the means (ANOM) statistical method was used. For that reason, the mean of the S/N ratios calculated and the mean of the S/N ratios of factor *I* in level *i,* is given by Equation (2):

Table 2. Experimental factors and their levels

Factor	Description	Level 1	Level 2	Level 3	Level 4
A	Leaching time (min)	30	60	120	240
B	Stirring speed (rpm)	0	200	400	600
C	Temperature (°C)	40	50	60	70
D	Acid concentration (M)	0.5	1	2	3
E	H_2O_2 concentration (M)	0.1	0.3	0.5	1

Table 3. Experimental results and L_{16} (4^5) plan table

Test	Factor					*EoM (%)*		S/N
	A	**B**	**C**	**D**	**E**	***EoM*$_1$**	***EoM*$_2$**	
Test 1	30	0	40	0.5	0.1	24.23	24.80	27.79
Test 2	30	200	50	1	0.3	25.67	26.42	28.31
Test 3	30	400	60	2	0.5	30.93	30.95	29.81
Test 4	30	600	70	3	1	57.04	62.37	35.49
Test 5	60	0	50	2	1	27.96	31.09	29.37
Test 6	60	200	40	3	0.5	26.94	31.21	29.20
Test 7	60	400	70	0.5	0.3	29.23	31.15	29.58
Test 8	60	600	60	1	0.1	30.40	30.93	29.73
Test 9	120	0	60	3	0.3	49.92	51.74	34.12
Test 10	120	200	70	2	0.1	60.97	62.41	**35.80**
Test 11	120	400	40	1	1	28.58	28.56	29.12
Test 12	120	600	50	0.5	0.5	29.33	29.05	29.30
Test 13	240	0	70	1	0.5	48.38	48.50	33.70
Test 14	240	200	60	0.5	1	33.75	33.91	30.59
Test 15	240	400	50	3	0.1	56.44	57.04	35.08
Test 16	240	600	40	2	0.3	32.75	32.45	30.26

For example, $(\mathrm{M})_{\mathrm{Factor}=I}^{\mathrm{Level}=i}$, the mean of the S/N ratio of factor *I* in level *i*, is given by Equation (2):

$$(\mathrm{M})_{\mathrm{Factor}=I}^{\mathrm{Level}=i} = \frac{1}{n_{Ii}} \sum_{j=1}^{n_{Ii}} \left[\left(\frac{S}{N} \right)_{\mathrm{Factor}=I}^{\mathrm{Level}=i} \right]_j \tag{2}$$

In Equation (2), n_{Ii} shows the number of views of factor *I* in the level *i*. $\left(\frac{S}{N}\right)_{\mathrm{Factor}=I}^{\mathrm{Level}=i}$ is the S/N ratio of factor *I* in level *i*, and its sequence of view in Table 3 is the *j*th. Subsequently, the values of the S/N ratio were transferred into Equation (2) and the mean of the S/N ratios of a certain factor in the *i*th level, $(\mathrm{M})_{\mathrm{Factor}=I}^{\mathrm{Level}=i}$, was obtained (Table 4). As seen from Table 4, the bold values show the maximum of the mean of the S/N ratios. Thus, it shows the optimum conditions for Ni extraction from lateritic ore.

Table 4. S/N ratio response table for Ni extraction

Factor/Level	$\left[(\mathrm{S/N})_{Factor}^{Level}\right]_j$				$(\mathrm{M})_{Factor}^{Level}$
	j=1	*j*=2	*j*=3	*j*=4	
A/1	27.79	28.31	29.81	35.49	30.35
A/2	29.37	29.20	29.58	29.73	29.47
A/3	34.12	35.80	29.12	29.30	32.09
A/4	33.70	30.59	35.08	30.26	**32.41**
B/1	27.79	29.37	34.12	33.70	**31.24**
B/2	28.31	29.20	35.80	30.59	30.98
B/3	29.81	29.58	29.12	35.08	30.90
B/4	35.49	29.73	29.30	30.26	31.20
C/1	27.79	29.20	29.12	30.26	29.09
C/2	28.31	29.37	29.30	35.08	30.52
C/3	29.81	29.73	34.12	30.59	31.06
C/4	35.49	29.58	35.80	33.70	**33.65**
D/1	27.79	29.58	29.30	30.59	29.32
D/2	28.31	29.73	29.12	33.70	30.22
D/3	29.81	29.37	35.80	30.26	31.31
D/4	35.49	29.20	34.12	35.08	**33.47**
E/1	27.79	29.73	35.80	35.08	**32.10**
E/2	28.31	29.58	34.12	30.26	30.57
E/3	29.81	29.20	29.30	33.70	30.50
E/4	35.49	29.37	29.12	30.59	31.14

Also, analysis of variance (ANOVA) statistical method was applied to experimental results to investigate the effect of factors on Ni extraction. The percentage contribution of each factor, ρ_F, was given by Equation (3).

$$\rho_{\mathrm{F}} = \frac{SS_{\mathrm{F}} - (DOF_{\mathrm{F}} V_{\mathrm{Er}})}{SS_{\mathrm{T}}} \times 100 \tag{3}$$

In Equation (3), DOF_F is produced by subtracting one from the number of levels. The total sum of squares, the factorial sum of squares and the variance of error are symbolized as SS_T, SS_F and V_{Er}, respectively.

$$SS_{\mathrm{T}} = \sum_{j=1}^{m}\left(\sum_{i=1}^{n}\mathrm{EoM}_i^2\right)_j - mn\left(\overline{\mathrm{EoM}}_T\right)^2 \tag{4}$$

In Equation (4), m and n represents the number of experiments and the number of repetitions, respectively. $\overline{\mathrm{EoM}}_T$ represents the average of total EoM.

$$SS_{\mathrm{F}} = \frac{mn}{L}\sum_{k=l}^{L}\left(\overline{\mathrm{EoM}}_k^F - \overline{\mathrm{EoM}}_T\right)^2 \tag{5}$$

In Equation (5), $\overline{\mathrm{EoM}}_k^F$ is the average value of the experimental results of a certain factor in the kth level. The variance of error, V_{Er}, is given by Equation (6):

$$V_{\mathrm{Er}} = \frac{SS_{\mathrm{T}} - \sum_{F=A}^{E} SS_{\mathrm{F}}}{m(n-1)} \tag{6}$$

Optimization Conditions

For optimization of nickel extraction from lateritic ore, 16 tests were performed according to conditions given in Table 2. By taking into account the number of experimental repetitions and results of metal extraction (EoM), the S/N ratios of each test condition were determined (Table 3). In Table 3, the maximum S/N value was represented in bold. Subsequently, the S/N ratio values were transferred into Equation (2) and the mean of the S/N ratios were given in Table 4. $(\mathrm{M})_{\mathrm{Factor}}^{\mathrm{Level}}$ refers to result of the effect of each level of each factor and the maximum values of these show the optimum conditions for nickel extraction. As a result of this, optimum conditions were given in Table 5. As seen from Table 5, an experiment was carried out to compare the results of test 10 and obtained optimum conditions. Consequently, it was determined that the value of the S/N ratio of optimum conditions was greater than the value of the S/N ratio of test 10. Additionally, the average of EoM rises from 61.69% to 90.66%. Each level of each factor and corresponding the mean of the S/N ratio values which obtained from Table 4 were plotted and shown in Figure 2–6.

Table 5. The optimum condition for Ni extraction

	A	B	C	D	E	EoM_1	EoM_2	S/N
Test 10	120	200	70	2	0.1	60.97	62.41	**35.80**
Optimization condition	240	0	70	3	0.1	89.60	91.71	**39.15**

Table 6. The average of the experimental results of a certain factor in the kth level and the average of total EoM (EoM_T) for Ni extraction

Level	$\overline{\mathrm{EoM}}_K^A$	$\overline{\mathrm{EoM}}_K^B$	$\overline{\mathrm{EoM}}_K^C$	$\overline{\mathrm{EoM}}_K^D$	$\overline{\mathrm{EoM}}_K^E$	$\overline{\mathrm{EoM}}_T$
Level 1	35.30	38.33	28.69	29.43	43.40	37.66
Level 2	29.86	37.66	35.38	33.43	34.92	
Level 3	42.57	36.61	36.57	38.69	34.41	
Level 4	42.90	38.04	50.00	49.09	37.91	

Leaching time

Figure 2 shows the effect of leaching time on the S/N ratio for extraction of nickel from lateritic ore in hydrochloric acid solution with hydrogen peroxide. As seen from Figure 2, it was determined that the optimum leaching time was 240 min. It may be concluded that an increase in time of the presence of ore particles in solution causes to increase the extraction of nickel. Thus, the amount of metal ions dissolved from particle that passes into solution increases with time.

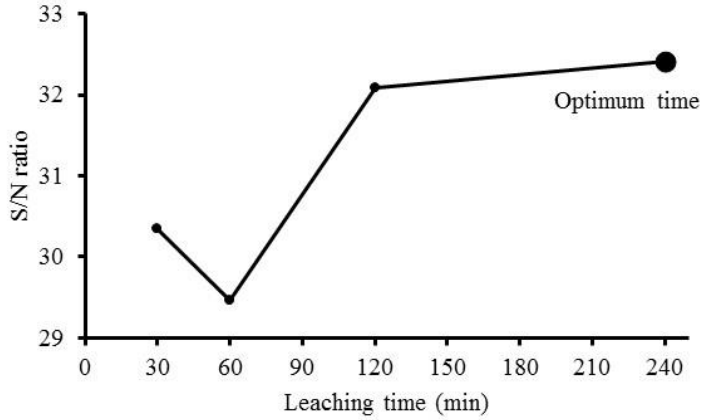

Figure 2. Effect of leaching time on the S/N ratio for extraction of nickel from lateritic ore

Stirring speed

In Figure 3, effect of stirring speed on the S/N ratio for extraction of nickel from lateritic ore in hydrochloric acid solution with hydrogen peroxide was shown. As seen from Figure 3, it was determined that no significant effect of stirring speed on the extraction of nickel. Thus, the optimum condition was provided by no stirring. Although a kinetic investigation was not performed in this study, it may be considered the negligible effect of stirring speed on extraction of nickel from lateritic ore could stem from dissolution mechanism. Georgiou and Papangelakis (1998) expressed that stirring speed had a negligible effect on the rate of nickel dissolution from limonitic laterite.

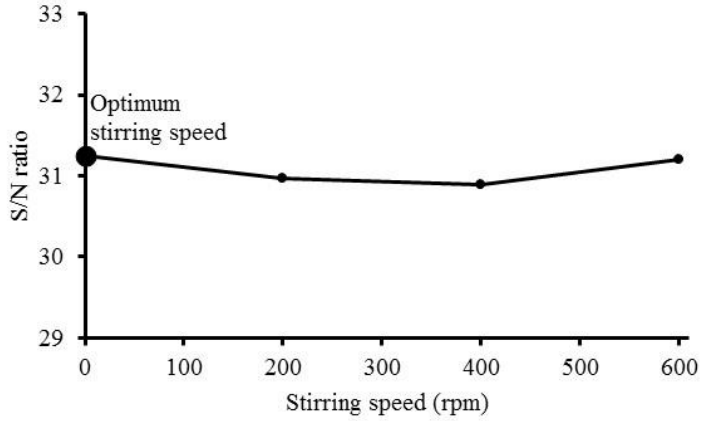

Figure 3. Effect of stirring speed on the S/N ratio for extraction of nickel from lateritic ore

Temperature

The plot of the effect of temperature on the S/N ratio for the extraction of nickel from lateritic ore in hydrochloric acid solution with hydrogen peroxide was shown in Figure 4. As seen from Figure 4, it was determined that the optimum leaching temperature was 70°C. The extraction of nickel increased with an increase in temperature of solution. As known, temperature increases reaction rate and equilibrium constant. However, rapid decomposition of hydrogen peroxide occurs at higher temperatures (Antonijevic *et al*., 1997; Mahajan *et al*., 2007).

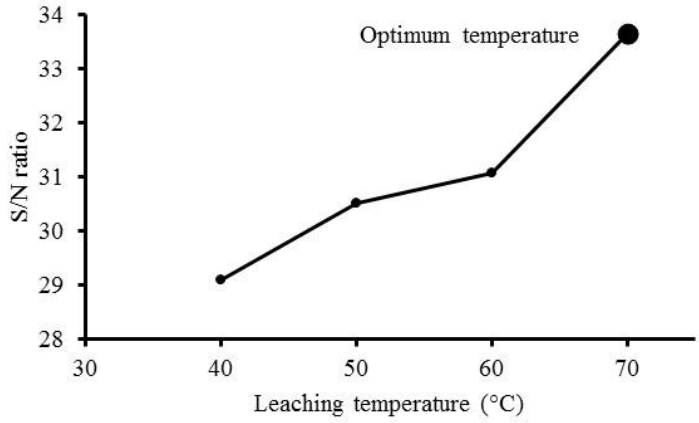

Figure 4. Effect of temperature on the S/N ratio for extraction of nickel from lateritic ore

Acid concentration

Figure 5 shows the effect of acid concentration on the S/N ratio for extraction of nickel from lateritic ore in hydrochloric acid solution with hydrogen peroxide. As seen from Figure 5, it was determined that the optimum hydrochloric acid concentration was 3 M. The results presented in Figure 5 show that, S/N ratio values increase as acid concentration increases. Aydogan (2006) and Antonijevic *et al*. (1997) expressed that hydrogen peroxide shows oxidative action in acidic solutions.

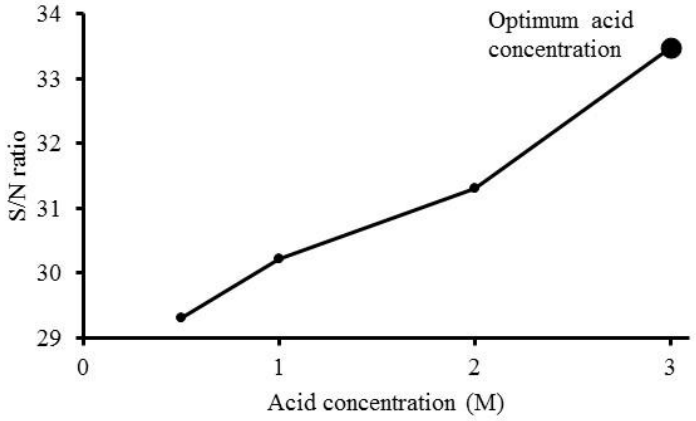

Figure 5. Effect of acid concentration on the S/N ratio for extraction of nickel from lateritic ore

H_2O_2 concentration

The plot of the effect of H_2O_2 concentration on the S/N ratio for extraction of nickel from lateritic ore in hydrochloric acid solution with hydrogen peroxide was shown in Figure 6. As seen from Figure 6, it was determined that the optimum H_2O_2 concentration was 0.1 M. The results presented in Figure 6 show that, S/N ratio values decreases as H_2O_2 concentration increases.

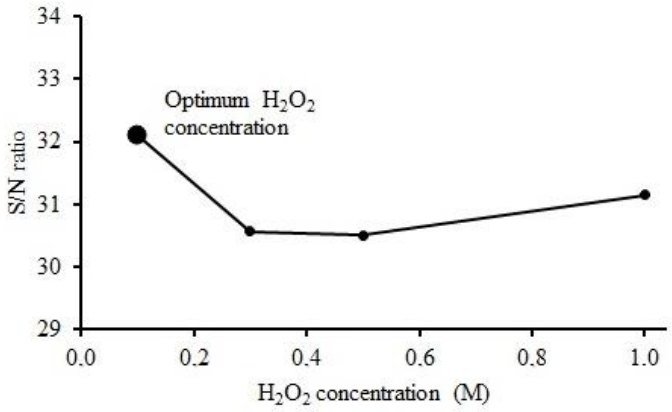

Figure 6. Effect of H_2O_2 concentration on the S/N ratio for extraction of nickel from lateritic ore

Percentage of Contribution

In order to determine the percentage of the contribution of each factor, the average values of the experimental results of a certain factor in the kth level ($\overline{\mathrm{EoM}}_K^{\mathrm{F}}$) were obtained using EoM_i values in Table 3 and given in Table 6. After this, the factorial sum of squares, SS_F, for each factor was calculated. The total sum of squares, SS_T, was determined. After this process, using SS_F and SS_T values, V_{Er} was obtained. Consequently, the percentage contribution of each factor, ρ_F, was determined. All of the obtained values were given in Table 7. As seen from Table 7, the importance order can be seen as; temperature, acid concentration, leaching time, H_2O_2 concentration and stirring speed.

Table 7. Percentage contribution of each factor

Factor	DOF_F	SS_F	ρ_F (%)	SS_T	V_{Er}
Leaching time (min)	3	943.80	18.693	5048.95	1.96
Stirring speed (rpm)	3	13.57	0.269		
Temperature (°C)	3	1912.98	37.889		
Acid concentration (M)	3	1738.65	34.436		
H_2O_2 concentration (M)	3	408.64	8.094		
Error		31.30	0.620		

CONCLUSION

The optimum conditions of extraction of nickel from lateritic ore in hydrochloric acid solution with hydrogen peroxide were determined by Taguchi method. The effects of some parameters (leaching time, stirring speed, temperature, hydrochloric acid concentration and hydrogen peroxide concentration) on extraction of nickel were investigated. The optimum conditions determined by Taguchi method were; leaching time of 240 min, a temperature of 70 °C, hydrochloric acid concentration of 3 M, hydrogen peroxide concentration of 0.1 M and without stirring. As a result of experimental results, it was demonstrated that, extraction of nickel was obtained with a recovery of 90.66% in optimum conditions.

In addition, analysis of variance (ANOVA) was applied to experimental results. Percentage contributions of each factor for extraction of nickel were: temperature (37.889%), acid concentration (34.436%), leaching time (18.693%), H_2O_2 concentration (8.094%) and stirring speed (0.269%). In point of these results, the extraction of nickel is most dependent by temperature.

REFERENCES

Abali, Y., Copur, M., Yavuz, M. 2006, "Determination of The Optimum Conditions for Dissolution of Magnesite with H2SO4 Solutions", Ind. J. of Chem. Technol., Vol. 13, pp. 391–397.

Abali, Y., Bayca, S. U., Arisoy, K., Vaizogullar, A.I., 2011, "Optimization of Dolomite Ore Leaching in Hydrochloric Acid Solutions", Physicochemical Problems of Mineral Processing, Vol. 46, pp. 253–262.

Agacayak, T., Zedef, V., Aydogan, S., 2011, "Leaching of Lateritic Nickel Ores of Karacam (Eskisehir-Turkey) with Hydrochloric Acid", 11th International Multidisciplinary Scientific Geo-Conference&EXPO SGEM, Modern Management of Mine Producing, Geology and Environmental Protection, Albena-Varna/Bulgaria. Vol. 1, pp. 1155–1162, 19-25 June 2011.

Agacayak, T., Zedef, V., 2012, "Dissolution Kinetics of a Lateritic Nickel Ore in Sulphuric Acid Medium", Acta Montanistica Slovaca, Vol. 17 (1), pp. 33–41.

Agacayak, T., Zedef, V., 2013, "Leaching of a Turkish lateritic nickel ore in nitric acid solution", Mine Planning and Equipment Selection, Proceedings of the 22nd MPES Conference, Dresden, Germany.

Agatzini-Leonardou, S., Zafiratos, I. G., 2004, "Beneficiation of a Greek Serpentinic Nickeliferous Ore Part II. Sulfuric Acid Heap and Agitation Leaching", Hydrometallurgy, Vol. 74, pp. 267–275.

Antonijevic, M. M., Dimitrijevic, M., Jankovic, Z., 1997, "Leaching of Pyrite with Hydrogen Peroxide in Sulfuric Acid", Hydrometallurgy, Vol. 46, pp. 71–83.

Asl, M.S., Kakroudi, M. G., Golestani-Fard, F., Nasiri H. 2015, "A Taguchi Approach to The Influence of Hot Pressing Parameters and SiC Content on The Sinterability of ZrB2-Based Composites", International Journal of Refractory Metals and Hard Materials, Vol. 51, pp. 81–90.

Ata, O. N., Colak, S., Ekinci, Z., Çopur, M., 2001, "Determination of The Optimum Conditions for Leaching of Malachite Ore in H2SO4 Solutions", Chemical Engineering & Technology, Vol. 24 (4), pp. 409–413.

Atil, H., Unver, Y., 2000, "A Different Approach of Experimental Design: Taguchi Method", Pakistan Journal of Biological Sciences, Vol. 3 (9), pp. 1538–1540.

Ayanda, O. S., Adekola, F. A., Baba, A. A., Fatoki, O. S., Ximba, B. J., 2011, "Comparative Study of the Kinetics of Dissolution of Laterite in Some Acidic Media", J. of Miner. & Mater. Character. & Eng., Vol. 10 (15), pp. 1457–1472.

Aydogan, S., 2006, "Dissolution Kinetics of Sphalerite with Hydrogen Peroxide in Sulphuric Acid Medium", Chemical Engineering Journal, Vol. 123 (3), pp. 65–70.

Babaei-Dehkordi, A., Moghaddam, J., Mostafaei, A., 2013, "An Optimization Study on The Leaching of Zinc Cathode Melting Furnace Slag in Ammonium Chloride by Taguchi Design and Synthesis of ZnO Nanorods via Precipitation Methods", Materials Research Bulletin, Vol. 48 (10), pp. 4235–4247.

Behera, S. K., Sukla, L. B., Mishra, B. K., 2010, "Leaching of Nickel Laterite Using Fungus Mediated Organic Acid and Synthetic Organic Acid: A Comparative Study", Proceedings of the XI International Seminar on Mineral Processing Technology, pp. 946–954.

Bese, A. V., Borulu, N., Copur, M., Colak, S., Ata, O. N., 2010, "Optimization of Dissolution of Metals from Waelz Sintering Waste (WSW) by Hydrochloric Acid Solutions", Chemical Engineering Journal, Vol. 162 (2), pp. 718–722.

Brand, N. W., Butt, C. R. M., Elias, M., 1998, "Nickel Laterites: Classification and Features", J. of Australian Geo. and Geoph., Vol. 17, pp. 81–88.

Chen, S., Guo, X., Shi, W., Li, D., 2010, "Extraction of Valuable Metals From Low-Grade Nickeliferous Laterite Ore by Reduction Roasting-Ammonia Leaching Method", Journal of Central South University of Technology, Vol. 17 (4), pp. 765–769.

Copur, M., 2002, "An Optimization Study of Dissolution of Zn and Cu in ZnS Concentrate with HNO3 Solutions", Chemical and Biochemical Engineering Quarterly, Vol. 16 (4), pp. 191–197.

Dalvi, A. D., Bacon, W., Osborne, R. C., 2004, "The Past and The Future of Nickel Laterites", PDAC 2004 International Conference Trade Show and Investors Exchange, Toronto, CANADA.

Deepatana, A., Tang, J. A., Valix, M., 2006, "Comparative Study of Chelating Ion Exchange Resins for Metal Recovery from Bioleaching of Nickel Laterite Ores", Minerals Engineering, Vol. 19(2), pp. 1280–1289.

Demir, F., Donmez, B. 2008, "Optimization of The Dissolution of Magnesite in Citric Acid Solutions", International Journal of Mineral Processing, Vol. 87 (1), pp. 60–64.

Dogan, T. H., Yartasi, A., 2014, "Optimization of Dissolution of Ulexite in Phosphate Acid Solutions", Journal of the Chemical Society of Pakistan, Vol. 36 (4), pp. 601–605.

Donmez, B., Celik, C., Colak, S. Yartasi, A., 1998, "The Dissolution Optimization of Copper from Anode Slime in H2SO4 Solutions", Industrial & Engineering Chemistry Research, Vol. 37 (8), pp. 3382–3387.

Elias, M., 2002, "Nickel Laterite Deposits – Geological Overview, Resources and Exploitation, in: Giant Ore Deposits: Characteristics, Genesis and Exploration". Hobart, University of Tasmania, CODES Special Publication, pp. 205–220.

Georgiou, D., Papangelakis, G. V., 1998, "Sulphuric Acid Pressure Leaching of A Limonitic Laterite: Chemistry and Kinetics", Hydrometallurgy, Vol. 49, pp. 23–46.

Gleeson, S. A., Butt, C. R. M., Elias, M., 2003, "Nickel Laterites: A Review". SEG Newsletter, Soc. of Econ. Geo., Vol. 54, pp. 12–18.

Golightly, J. P., 1981, "Nickeliferous Laterite Deposits", Economic Geology Vol. 75 (1), pp. 710–735.

Guo, Q., Qu, J., Han, B., Zhang, P., Song, Y., Qi, T., 2015, "Innovative Technology for Processing Saprolitic Laterite Ores by Hydrochloric Acid Atmospheric Pressure Leaching", Minerals Engineering, Vol. 71, pp. 1–6.

Ilyas, S., Bhatti, H. N., Bhatti, I. A., Sheikh, M. A., Ghauri, M. A., 2010, "Bioleaching of Metal Ions from Low Grade Sulphide Ore: Process Optimization by Using Orthogonal Experimental Array Design", African Journal of Biotechnology, Vol. 9 (19), pp. 2801–2810.

Kursunoglu, S., Kaya, M., 2015, "Dissolution Behavior of Caldag Lateritic Nickel Ore Subjected to a Sequential Organic Acid Leaching Method", Journal of Minerals, Metallurgy, and Materials, Vol. 22 (11), pp. 1131–1140.

Landers, M., Gilkes, R. J., Wells, M. 2009, "Dissolution Kinetics of Dehydroxylated Nickeliferous Goethite from Limonitic Lateritic Nickel Ore", Applied Clay Science, Vol. 42 (3), pp. 615–624.

Li, J., Xiong, D., Chen, H., Wang, R., Liang, Y., 2012, "Physicochemical Factors Affecting Leaching of Laterite Ore in Hydrochloric Acid", Hydrometallurgy, Vol. 129 (130), pp. 14–18.

Luo, W., Feng, Q., Ou, L., Zhang, G., Chen, Y. 2010, "Kinetics of Saprolitic Laterite Leaching by Sulphuric Acid at Atmospheric Pressure", Minerals Engineering, Vol. 23 (6), pp. 458–462.

Ma, B., Wang, C., Yang, W., Yang, B., Zhang, Y., 2013, "Selective Pressure Leaching of Fe (II)-rich Limonitic Laterite Ores from Indonesia Using Nitric Acid", Minerals Engineering, Vol. 45, pp. 151–158.

Mahajan, V., Misra, M., Zhong, K., Fuerstenau, M.C., 2007, "Enhanced Leaching of Copper from Chalcopyrite in Hydrogen Peroxide–Glycol System", Minerals Engineering, Vol. 20, pp. 670–674.

McDonald, R. G., Whittington, B. I. 2008a, "Atmospheric acid leaching of nickel laterites review (Part I). Sulphuric acid technologies", Hydrometallurgy, Vol. 91 (1/4), pp. 35–55.

McDonald, R. G., Whittington, B. I. 2008b, "Atmospheric Acid Leaching of Nickel Laterites Review. Part II. Chloride and Bio-technologies", Hydrometallurgy, Vol. 91, pp. 56–69.

Moghaddam, J., Sarraf-Mamoory, R., Abdollahy, M., Yamini, Y. 2006, "Purification of Zinc Ammoniacal Leaching Solution by Cementation: Determination of Optimum Process Conditions with Experimental Design by Taguchi's Method", Separation and Purification Technology, Vol. 51 (2), pp. 157–164.

Mohammadreza, F., Mohammad, N., Ziaeddin, S. S., 2014, "Nickel Extraction from Low Grade Laterite by Agitation Leaching at Atmospheric Pressure", International Journal of Mining Science and Technology, Vol. 24 (4), pp. 543–548.

Olanipekun, E. O., 2000, "Kinetics of Leaching Laterite", International Journal of Mineral Processing, Vol. 60, pp. 9–14.

Park, K. H., Nam, C. W. 2008, "Status and Prospect of Nickel Resources and Processing", Trending Metals Mater. Eng., Vol. 21, pp. 1–9.

Phadke M. S., 1989, Quality Engineering using Robust Design, Prentice Hall, New Jersey, pp. 61–292.

Roy, R. K., 1995, A Primer on the Taguchi Method, Van Nostrand Reinhold, New York.

Rubisov, D. H., Krowinkel, J. M., Papangelakis, V. G., 2000, "Sulphuric Acid Pressure Leaching of Laterites Universal Kinetics of Nickel Dissolution for Limonites and Limonitic/Saprolitic Blends", Hydrometallurgy, Vol. 58 (1), pp. 1–11.

Safarzadeh, M. S., Moradkhani, D., Ilkhchi, M. O., Golshan, N. H. 2008, "Determination of The Optimum Conditions for The Leaching of Cd–Ni Residues from Electrolytic Zinc Plant Using Statistical Design of Experiments", Separation and Purification Technology, Vol. 58 (3), pp. 367–376.

Sagapoa, C. V., Imai, A., Watanabe, K., 2011, "Laterization Process of Ultramafic Rocks in Siruka, Solomon Islands", Journal of Novel Carbon Resource Sciences, Vol. 3, pp. 32–39.

Sahu, S., Kavuri, N. C., Kundu, M., 2011, "Dissolution Kinetics of Nickel Laterite ore Using Different Secondary Metabolic Acids", Brazilian Journal of Chemical Engineering, Vol. 28 (2), pp. 251–258.

Soler, J. M., Cama, J., Galí, S. Meléndez, W., Ramírez, A., Estanga, J., 2008, "Composition and Dissolution Kinetics of Garnierite from The Loma de Hierro Ni-laterite Deposit, Venezuela", Chemical Geology, Vol. 249 (1/2), pp. 191–202.

Stopic, S., Friedrich, B., Fuchs, R., 2002, "Kinetics of Sulphuric Acid Leaching of the Serbian Nickel Laterite Ore under Atmospheric Pressure", Metalurgica J. of Metall., Vol. 8 (3), pp. 235–244.

Sukla, L. B., Panchanadikar, V., 1993, "Bioleaching of Lateritic Nickel Ore Using A Heterotrophic Micro-Organism", Hydrometallurgy, Vol. 32, pp. 373–379.

Taguchi, G., 1987, System of Experimental Design, Quality Resources, New York.

Thubakgale, C. K., Mbaya, R. K. K., Kabongo, K., 2013, "A Study of Atmospheric Acid Leaching of a South African Nickel Laterite", Minerals Engineering, Vol. 54, pp. 79–81.

Wang, B., Guo, Q., Wei, G., Zhang, P., Qu, J., Qi, T. 2012, "Characterization and Atmospheric Hydrochloric Acid Leaching of A Limonitic Laterite from Indonesia", Hydrometallurgy, Vol. 129–130, pp. 7–13.

Zhai, Y., Mu, W., Liu, Y., Xu, Q. 2010, "A Green Process for Recovering Nickel From Nickeliferous Laterite Ores", Transactions of Nonferrous Metals Society of China, Vol. 20, pp. 65–70.

Zolfaghari, G., Esmaili-Sari, A., Anbia, M., Younesi, H., Amirmahmoodi, S., Ghafari-Nazari, A., 2011, "Taguchi Optimization Approach for Pb(II) and Hg(II) Removal from Aqueous Solutions Using Modified Mesoporous Carbon", Journal of Hazardous Materials, Vol. 192 (3), pp. 1046–1055.

Zuniga, M., Parada, F., Asselin, E., 2010, "Leaching of A Limonitic Laterite in Ammoniacal Solutions with Metallic Iron", Hydrometallurgy, Vol. 104, pp. 260–267.

SELÇUK ÜNİVERSİTESİ
MÜHENDİSLİK FAKÜLTESİ

S.Ü. Müh. Bilim ve Tekn. Derg., c.5, s.3, 2017
Selcuk Univ. J. Eng. Sci. Tech., v.5, n.3, 2017
ISSN: 2147-9364 (Electronic)

DISSOLUTION KINETICS OF NICKEL FROM GÖRDES (MANİSA-TURKEY) LATERITIC ORE BY SULPHURIC ACID LEACHING UNDER EFFECT OF SODIUM FLUORIDE

[1]Tevfik AĞAÇAYAK, [2]Ali ARAS

[1,2]Selcuk University, Department of Mining Engineering, Campus, Selcuklu, Konya, TURKEY
[1]tevfik@selcuk.edu.tr, [2]aliaras@selcuk.edu.tr

(Geliş/Received: 24.02.2017 ; Kabul/Accepted in Revised Form: 22.03.2017)

ABSTRACT: In this study, dissolution kinetics of nickel from Gördes (Manisa-Turkey) lateritic ore by sodium fluoride in sulphuric acid solution was investigated. The effects of stirring speed, sulphuric acid concentration, sodium fluoride concentration and temperature on nickel extraction were examined. To determine the dissolution kinetics of nickel in sulphuric acid medium under effect of sodium fluoride, shrinking core model was applied to dissolution recoveries. As a result of kinetic studies, it was determined that mixed kinetic model was appropriate. The activation energy (E_a) for the dissolution was calculated as 41.24 kJ/mol.

Key Words: *Dissolution kinetics, Lateritic ore, Nickel, Sulphuric acid, Sodium fluoride, Activation energy*

Sodyum Florür Etkisinde Sülfürik Asit Liçi ile Gördes (Manisa-Türkiye) Lateritik Cevherinden Nikelin Çözünme Kinetiği

ÖZ: Bu çalışmada, sodyum florür içeren sülfürik asit çözeltisinde Gördes (Manisa-Türkiye) lateritik cevherinden nikelin çözünme kinetiği araştırılmıştır. Karıştırma hızı, sülfürik asit ve sodyum florür derişimi ve sıcaklığın nikelin çözünmesine olan etkileri incelenmiştir. Sodyum florür etkisinde sülfürik asit ortamında nikelin çözünme kinetiğini belirlemek için elde edilen çözünme verimlerine küçülen çekirdek modeli uygulanmıştır. Kinetik çalışmalar sonucunda karışık modelin uygun olduğu belirlenmiştir. Nikelin çözünmesi için aktivasyon enerjisi 41.24 kJ/mol olarak hesaplanmıştır.

Anahtar Kelimeler: *Çözünme kinetiği, Lateritik cevher, Nikel, Sülfürik asit, Sodyum florür, Aktivasyon enerjisi*

INTRODUCTION

It is known that nickel was used in the production of coins at thousands of years ago. However, the use of nickel in the metal industry is based on two centuries ago. Nickel was discovered and isolated as an element by the Swedish scientist Axel Cronstedt in 1751 (Kamberović et al., 2014; Rezende, 2006).

Owing to its some properties, such as corrosion resistance, alloying, electrical, thermal and catalyst properties, nickel is used as an important metal in producing of stainless steel and super alloys. Laterites are oxide ores widely distributed in the equatorial regions. Lateritic nickel deposits occur during laterization, namely, a weathering process of ultramafic rocks containing minerals such as olivine, pyroxene and amphibole (Golightly, 1981). Ni-laterites can be classified in three main groups as oxide, hydrous silicate and clay silicate deposits (Golightly, 1981; Gleeson, *et al*., 2003; Brand *et al*., 1998; Sagapoa *et al*., 2011; Georgiou and Papangelakis, 1998). It is known that nickel laterites are approximately composed 70 % of the world nickel reserves. However, about 40 % of world's nickel

DOI: 10.15317/Scitech.2017.95

production is provided from lateritic ores (Dalvi *et al*., 2004, Soler *et al*., 2008). The production of nickel from lateritic ores includes pyrometallurgical and hydrometallurgical processes (Deepatana *et al*., 2006). Pyrometallurgical and hydrometallurgical processes are given in Figure 1 for the recovery of nickel and cobalt from the lateritic nickel ores.

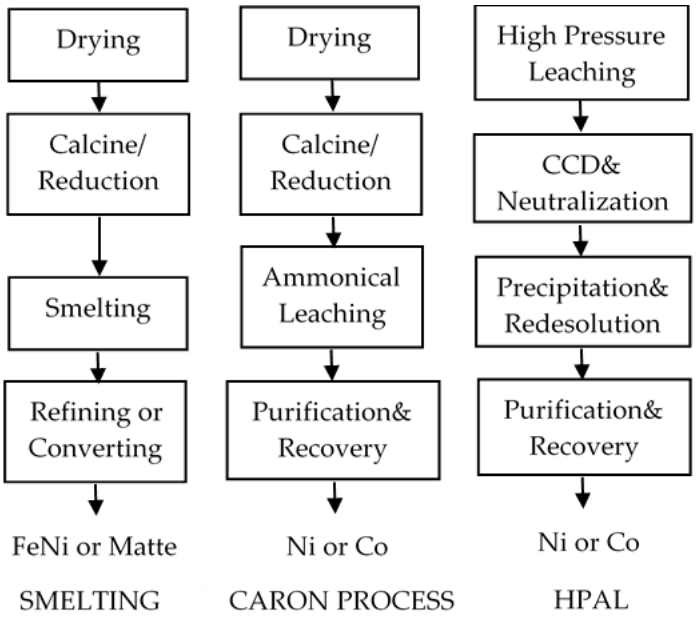

Figure 1. Pyrometallurgical and hydrometallurgical processes for lateritic nickel ore (Dalvi *et al*., 2004).

In the literature, there are several studies related to lateritic nickel leaching in different solutions using high pressure or atmospheric pressure (agitation or heap leaching). The solutions used in these studies can be given as sulphuric acid (Georgiou and Papangelakis, 1998; Agacayak and Zedef, 2012; Luo *et al*., 2010; Stopic *et al*., 2002; Ayanda *et al*., 2011; Rubisov *et al*., 2000; Agatzini-Leonardou and Zafiratos, 2004; McDonald and Whittington, 2008a; Mohammadreza *et al*., 2014), hydrochloric acid (Ayanda *et al*., 2011; Park and Nam, 2008; Agacayak *et al*., 2011; Guo *et al*., 2015; McDonald and Whittington, 2008b; Li *et al*., 2012), nitric acid (Agacayak and Zedef, 2013; Ayanda *et al*., 2011; Ma *et al*., 2013), ammonia (Zhai *et al*., 2010; Chen *et al*., 2010; Zuniga *et al*., 2010), citric acid, oxalic acid and acetic acid (Sahu *et al*., 2011; Behera *et al*., 2010; Sukla and Panchanadikar, 1993; Kursunoglu and Kaya, 2015). In the present work, to investigate the effects of parameters such as stirring speed, sulphuric acid concentration, sodium fluoride concentration and temperature on the leaching of nickel from a limonitic laterite ore and to describe dissolution kinetics of nickel was aimed.

MATERIAL AND METHOD

The lateritic nickel ore used in this study was obtained from Manisa (Gördes) region in Turkey. The sample was ground and wet sieved into three particle size fractions (-150+106, -106+75 and -75+53 μm) for the experiments. Nickel and iron contents of each size fraction were given in Table 1.

Table 1. Nickel and iron contents of each size fraction.

Particle size, μm	Ni %	Fe %
-150+106	1.02	37.03
-106+75	1.00	36.40
-75+53	1.01	38.25

An XRD analysis was carried out to find the mineralogic composition of the laterite ore. The main minerals were determined as goethite, hematite and quartz. XRD pattern of the sample was given in Figure 2.

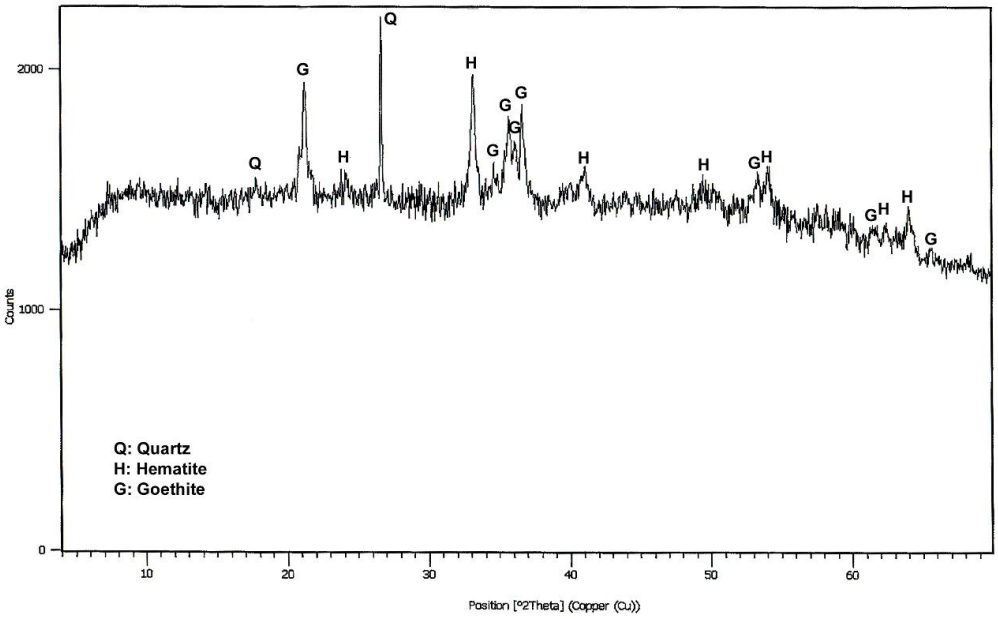

Figure 2. XRD pattern of the sample.

The nickel leaching experiments were conducted in a 1000 mL vessel in a thermostatically-controlled water bath using 5/500 g/mL solid-liquid ratio. Since Ni and Fe contents of each size fraction of the lateritic ore were almost same, -150+106 μm particle size fraction was used in the experiments. The leach solution was stirred by Heidolph brand RZR 2021 model mechanical stirrer with teflon lined impeller. Amount of the nickel in the solution was measured using flame atomic absorption spectrophotometer.

RESULT AND DISCUSSION

Effect of Parameters

The effect of variables such as stirring speed, sulphuric acid concentration, sodium fluoride concentration and leaching temperature on Ni extraction was investigated. The effect of stirring speed on the nickel extraction from lateritic nickel ore was investigated in 0.5 M H_2SO_4+0.3 M NaF solution at 50 °C in the range of 0–600 rpm stirring speed for 180 min. The experimental results were shown in Figure 3a. It was observed that the dissolution increased as the stirring speed increased. Therefore, 600 rpm was selected as optimum stirring speed to investigate the effect of other parameters on dissolution of nickel. To determine effect of the sulphuric acid concentration, leaching experiments were done using different sulphuric acid concentrations under effect of 0.3 M sodium fluoride at 50 °C. The experimental data were presented in Figure 3b. As shown from Figure 3b, nickel extraction increases with increasing leaching time and sulphuric acid concentration. To determine effect of sodium fluoride concentration, leaching experiments were carried out using different sodium fluoride concentrations at 50 °C in 0.5 M H_2SO_4. Figure 3c shows the effect of sodium fluoride concentration on the nickel dissolution. As shown from Figure 3c, nickel extraction increases with increasing sodium fluoride concentration. Thus, it can be concluded that some of nickel in the lateritic ore could be in silicate structure. Harouiya and Oelkers (2004) and Mitra and Rimstidt (2009) reported dissolution of quartz in fluoride solutions. Lateritic nickel ore was leached at different temperatures (40–80 °C). The obtained results were presented in Figure 3d.

The nickel extraction recovery increased for 3 hours of leaching time from 30.89% to 72.63% for 40 °C and 80 °C, respectively.

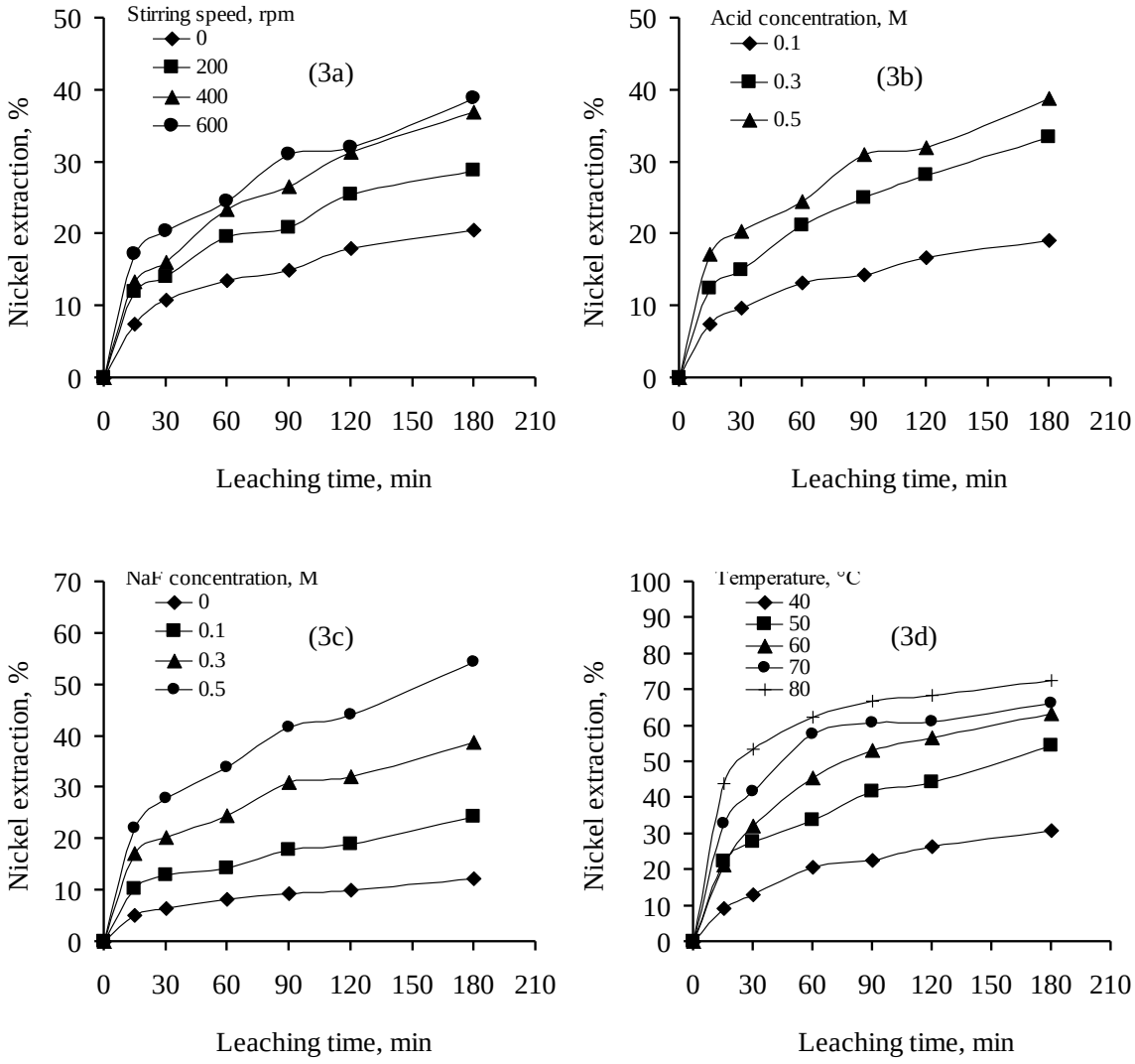

Figure 3. Effects of parameters on the nickel extraction

Kinetic Models and Determination of Activation Energy

The kinetic of dissolution reactions is often described by the shrinking core model. According to the shrinking core model, it is thought that the reaction between solid and fluid reactants takes place on the outer surface of solid (Levenspiel, 1999).

$$aA_{\text{fluid}} + bB_{\text{particle}} \rightarrow \text{Product} \quad (1)$$

Therefore, chemical reaction model, diffusion model and combination of both chemical control and diffusion model (mixed model) were investigated in this work. The dissolution of Ni from the lateritic nickel ore can be explained by a shrinking core model which can be expressed as follows (Habashi 1969; Levenspiel, 1999; Ekmekyapar *et al*., 2003):

if the reaction is controlled by surface reaction,

$$1-(1-\alpha)^{1/3}=k_s t \quad (2)$$

if the reaction is controlled by film diffusion,

$$1-(1-\alpha)^{2/3}=k_f t \quad (3)$$

if the reaction is controlled by diffusion from product layer

$$1-2/3\alpha-(1-\alpha)^{2/3}=k_d t \quad (4)$$

if the reaction is controlled by combination of both chemical and diffusion

$$1-2(1-\alpha)^{1/3}+(1-\alpha)^{2/3}=k_m t \quad (5)$$

where α is the fraction reacted, t is the reaction time, k_s, k_f, k_d and k_m are the rate constants. In this study, shrinking core model was applied to the dissolution recoveries obtained at different temperatures. Plots of the shrinking core model for various temperatures of Ni extraction were given in Figure 4.

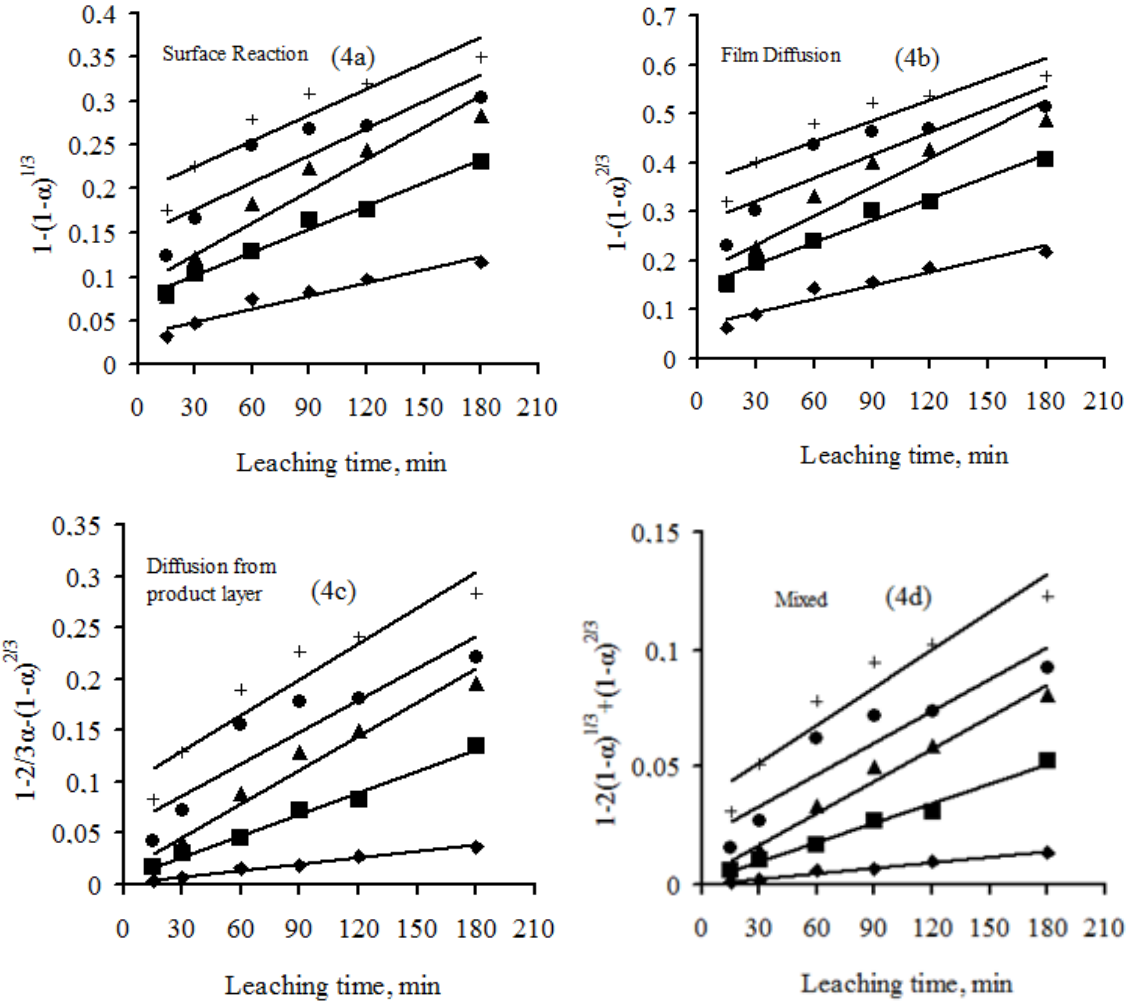

Figure 4. Plots of the shrinking core model vs leaching time for different temperatures.

Apparent rate constants (k) at different temperatures were obtained from the slope of the linear plots in Figure 4 for nickel. The correlation coefficients and apparent rate constants for each temperature were given in Table 2.

Table 2. Values of k_s, k_f, k_d, k_m and correlation coefficients for different temperatures.

Temperature °C	Surface Reaction $1-(1-\alpha)^{1/3}$		Film Diffusion $1-(1-\alpha)^{2/3}$	
	Apparent rate constant (k_s)x10^{-3}	Correlation coefficient, (R^2)	Apparent rate constant (k_s)x10^{-3}	Correlation coefficient, (R^2)
40	0.49521	0.94	0.91549	0.94
50	0.88494	0.99	1.49352	0.98
60	1.21441	0.91	1.97425	0.89
70	1.01943	0.80	1.59097	0.78
80	0.98306	0.86	1.43322	0.84
Temperature °C	**Diffusion from Product Layer $1-2/3\alpha-(1-\alpha)^{2/3}$**		**Mixed Model $1-2(1-\alpha)^{1/3}+(1-\alpha)^{2/3}$**	
	Apparent rate constant (k_s)x10^{-3}	Correlation coefficient, (R^2)	Apparent rate constant (k_s)x10^{-3}	Correlation coefficient, (R^2)
40	0.20633	0.99	0.07493	0.99
50	0.69124	0.99	0.27635	0.99
60	1.08712	0.97	0.45456	0.98
70	1.03451	0.84	0.44789	0.86
80	1.15299	0.90	0.53290	0.92

These results indicate that the dissolution of nickel is combination of both chemical and diffusion controll. The application of the mixed model is shown in Figure 4d. Equation [5] is applied to the data obtained at each temperature to determine the rate constants used in the Arrhenius plot (Figure 5). The activation energy was calculated as 41.24 kJ/mol. The dissolution of nickel from lateritic ore in sulphuric acid solution was reported to be controlled by chemical or diffusion from product layer by different authors. In these studies, activation energies were given as 53.9 kJ/mol (Luo *et al*., 2010), 68.66 kJ/mol (Agacayak and Zedef, 2012), 60.00 kJ/mol (Stopic *et al*., 2002) and 67.53 kJ/mol (Ayanda *et al*., 2011).

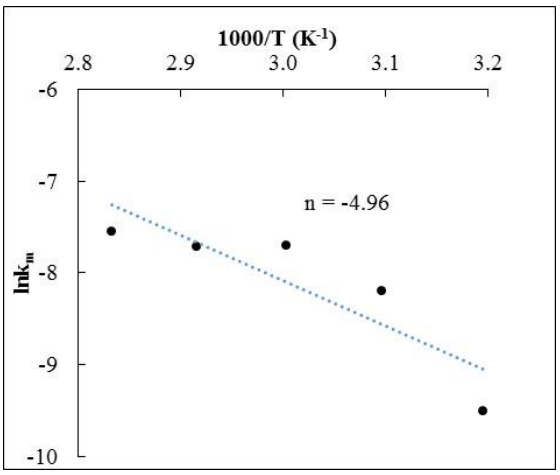

Figure 5. Arrhenius plot of data presented in Fig. 4d.

CONCLUSION

The contents of the lateritic nickel ore and dissolution kinetics results of nickel from the lateritic nickel ore were given as follows: The nickel and iron contents of the ore used in the experiments were determined as 1.02% and 37.03%, respectively. According to XRD results, the main minerals were determined as goethite, hematite and quartz. Dissolution kinetics of nickel from Gördes (Manisa-Turkey) lateritic ore using sodium fluoride in sulphuric acid solution was investigated. Experimental parameters used were stirring speed (0−600 rpm), temperature (40−80 °C), sulphuric acid concentration (0.1−0.5 mol/L), sodium fluoride concentration (0−0.5 mol/L) and particle size (-150+106 μm). It was found that the dissolution rate increased with an increase in the leaching temperature, stirring speed, sulphuric acid and sodium fluoride concentration. In order to determine the dissolution kinetics of Ni, shrinking core model was applied to dissolution recoveries obtained at different temperatures. It was determined that, nickel dissolved in sulphuric acid solution under effect of sodium fluoride from the lateritic nickel ore by combination of both chemical and diffusion control (mixed model). Activation energy (E_a) was calculated for Ni as 41.24 kJ/mol.

REFERENCES

Agacayak, T., Zedef, V., Aydogan, S., 2011, "Leaching of Lateritic Nickel Ores of Karacam (Eskisehir-Turkey) with Hydrochloric Acid", 11th International Multidisciplinary Scientific Geo-Conference&EXPO SGEM, Modern Management of Mine Producing, Geology and Environmental Protection, Albena-Varna/Bulgaria. Vol. 1, pp. 1155–1162, 19-25 June 2011.

Agacayak, T., Zedef, V., 2012, "Dissolution Kinetics of a Lateritic Nickel Ore in Sulphuric Acid Medium", Acta Montanistica Slovaca, Vol. 17 (1), pp. 33–41.

Agacayak, T., Zedef, V., 2013, "Leaching of a Turkish Lateritic Nickel Ore in Nitric Acid Solution", Mine Planning and Equipment Selection, Proceedings of the 22nd MPES Conference, Dresden, Germany, 14 – 19 October 2013.

Agatzini-Leonardou, S., Zafiratos, I. G., 2004, "Beneficiation of a Greek Serpentinic Nickeliferous Ore Part II. Sulfuric Acid Heap and Agitation Leaching", Hydrometallurgy, Vol. 74, pp. 267–275.

Ayanda, O. S., Adekola, F. A., Baba, A. A., Fatoki, O. S., Ximba, B. J., 2011, "Comparative Study of the Kinetics of Dissolution of Laterite in Some Acidic Media", J. of Miner. & Mater. Character. & Eng., Vol. 10 (15), pp. 1457–1472.

Behera, S. K., Sukla, L. B., Mishra, B. K., 2010, "Leaching of Nickel Laterite Using Fungus Mediated Organic Acid and Synthetic Organic Acid: A Comparative Study", Proceedings of the XI International Seminar on Mineral Processing Technology, pp. 946–954.

Brand, N. W., Butt, C. R. M., Elias, M., 1998, "Nickel Laterites: Classification and Features", J. of Australian Geo. and Geoph., Vol. 17, pp. 81–88.

Chen, S., Guo, X., Shi, W., Li, D., 2010, "Extraction of Valuable Metals from Low-Grade Nickeliferous Laterite Ore by Reduction Roasting-Ammonia Leaching Method", Journal of Central South University of Technology, Vol. 17(4), pp. 765−769.

Dalvi, A. D., Bacon, W., Osborne, R. C., 2004, "The Past and The Future of Nickel Laterites", PDAC 2004 International Conference Trade Show and Investors Exchange, Toronto, CANADA.

Deepatana, A., Tang, J. A., Valix, M., 2006, "Comparative Study of Chelating Ion Exchange Resins for Metal Recovery from Bioleaching of Nickel Laterite Ores", Minerals Engineering, Vol. 19 (2), pp. 1280–1289.

Ekmekyapar, A., Oya, R., Kunkul, A., 2003, "Dissolution Kinetics of an Oxidized Copper Ore in Ammonium Chloride Solution", Chemical and Biochemical Engineering Quarterly, Vol. 17 (4), pp. 261–266.

Georgiou, D., Papangelakis, G. V., 1998, "Sulphuric Acid Pressure Leaching of a Limonitic Laterite: Chemistry and Kinetics", Hydrometallurgy, Vol. 49, pp. 23–46.

Gleeson, S. A., Butt, C. R. M., Elias, M., 2003, "Nickel Laterites: A Review. SEG Newsletter", Soc. of Econ. Geo., Vol. 54, pp. 12–18.

Golightly, J. P., 1981, "Nickeliferous Laterite Deposits", Economic Geology, Vol. 75 (1), pp. 710–735.

Guo, Q., Qu, J., Han, B., Zhang, P., Song, Y., Qi, T., 2015, "Innovative Technology for Processing Saprolitic Laterite Ores by Hydrochloric Acid Atmospheric Pressure Leaching", Minerals Engineering, Vol. 71, pp. 1–6.

Habashi, F., 1969, Principles of Extractive Metallurgy, New York: Gordon and Breach.

Harouiya, N., Oelkers, E. H., 2004, "An Experimental Study of The Effect of Aqueous Fluoride on Quartz and Alkali-Feldspar Dissolution Rates", Chemical Geology, Vol: 205, pp.155–167.

Kamberović, Ž., Korać, M., Anđić, Z., Uljarević, J., Mihajlović, A., Vučurović, D., 2014, "Technological and Environmental Aspects of Nickel Production in Serbia" Association of Metallurgical Engineers of Serbia, Vol. 20 (4), pp. 275-284.

Kursunoglu, S., Kaya, M., 2015, "Dissolution Behavior of Caldag Lateritic Nickel Ore Subjected to a Sequential Organic Acid Leaching Method", Journal of Minerals, Metallurgy, and Materials, Vol. 22 (11), pp. 1131–1140.

Levenspiel, O., 1999, Chemical reaction engineering, New York:John Wiley & Sons.

Li, J., Xiong, D., Chen, H., Wang, R., Liang, Y., 2012, "Physicochemical Factors Affecting Leaching of Laterite Ore in Hydrochloric Acid", Hydrometallurgy, Vol. 129 (130), pp. 14–18.

Luo, W., Feng, Q., Ou, L., Zhang, G., Chen, Y., 2010, "Kinetics of Saprolitic Laterite Leaching by Sulphuric Acid at Atmospheric Pressure", Minerals Engineering, Vol. 23 (6), pp. 458–462.

Ma, B., Wang, C., Yang, W., Yang, B., Zhang, Y., 2013, "Selective Pressure Leaching of Fe (II)-rich Limonitic Laterite Ores from Indonesia Using Nitric Acid", Minerals Engineering, Vol. 45, pp. 151–158.

McDonald, R. G., Whittington, B. I., 2008a, "Atmospheric Acid Leaching of Nickel Laterites Review (Part I). Sulphuric Acid Technologies", Hydrometallurgy, Vol. 91 (1/4), pp. 35–55.

McDonald, R. G., Whittington, B. I., 2008b, "Atmospheric Acid Leaching of Nickel Laterites Review, Part II. Chloride and Bio-Technologies", Hydrometallurgy, Vol. 91, pp. 56–69.

Mitra., A., Rimstidt, J. D., 2009, "Solubility and Dissolution Rate of Silica in Acid Fluoride Solutions" Geochimica et Cosmochimica Acta, Vol. 73, pp. 7045–7059.

Mohammadreza, F., Mohammad, N., Ziaeddin, S. S., 2014, "Nickel Extraction From Low Grade Laterite by Agitation Leaching at Atmospheric Pressure", International Journal of Mining Science and Technology, Vol. 24 (4), pp. 543–548.

Park, K. H., Nam, C. W., 2008, "Status and Prospect of Nickel Resources and Processing", Trending Metals Mater. Eng., Vol. 21, pp. 1–9.

Rezende, L., 2006, Chronology of Science, Fact on File, Inc., New York.

Rubisov, D. H., Krowinkel, J. M., Papangelakis, V. G., 2000, "Sulphuric Acid Pressure Leaching of Laterites Universal Kinetics of Nickel Dissolution for Limonites and Limonitic/Saprolitic Blends", Hydrometallurgy, Vol. 58 (1), pp. 1–11.

Sagapoa, C. V., Imai, A., Watanabe, K., 2011, "Laterization Process of Ultramafic Rocks in Siruka, Solomon Islands", Journal of Novel Carbon Resource Sciences, Vol. 3, pp. 32–39.

Sahu, S., Kavuri, N. C., Kundu, M., 2011, "Dissolution Kinetics of Nickel Laterite Ore Using Different Secondary Metabolic Acids", Brazilian Journal of Chemical Engineering, Vol. 28 (2), pp. 251–258.

Soler, J. M., Cama, J., Galí, S. Meléndez, W., Ramírez, A., Estanga, J., 2008, "Composition and Dissolution Kinetics of Garnierite from The Loma De Hierro Ni-Laterite Deposit, Venezuela", Chemical Geology, Vol. 249 (1/2), pp. 191–202.

Stopic, S., Friedrich, B., Fuchs, R., 2002, "Kinetics of Sulphuric Acid Leaching of The Serbian Nickel Laterite Ore Under Atmospheric Pressure", Metalurgica J. of Metall., Vol. 8 (3), pp. 235–244.

Sukla, L. B., Panchanadikar, V., 1993, "Bioleaching of Lateritic Nickel Ore Using A Heterotrophic Micro-Organism", Hydrometallurgy, Vol. 32, pp. 373–379.

Zhai, Y., Mu, W., Liu, Y., Xu, Q., 2010, "A Green Process for Recovering Nickel from Nickeliferous Laterite Ores", Transactions of Nonferrous Metals Society of China, Vol. 20, pp. 65−70.

Zuniga, M., Parada, F., Asselin, E., 2010, "Leaching of A Limonitic Laterite in Ammoniacal Solutions with Metallic Iron", Hydrometallurgy, Vol. 104, pp. 260–267.

SELÇUK ÜNİVERSİTESİ
MÜHENDİSLİK FAKÜLTESİ

S.Ü. Müh. Bilim ve Tekn. Derg., c.5, s.3, 2017
Selcuk Univ. J. Eng. Sci. Tech., v.5, n.3, 2017
ISSN: 2147-9364 (Elektronik)

YERALTI LİNYİT KÖMÜR MADENİNDE TERMAL KONFOR ŞARTLARININ İNCELENMESİ

[1]Ali Ekrem ARITAN, [1]Melek TÜMER

[1]Afyon Kocatepe Üniversitesi, Mühendislik Fakültesi, Maden Mühendisliği Bölümü, AFYONKARAHİSAR
[1] aritan@aku.edu.tr, [1] mlkturmer03@hotmail.com

(Geliş/Received: 06.02.2017; Kabul/Accepted in Revised Form: 28.03.2017)

ÖZ: Yeraltı kömür madenciliğinde termal konfor, iş verimliliğine ve çalışanların sağlığına etki eden önemli bir faktör olmasına rağmen daha az dikkat çekmektedir. Termal konfor, günümüzde yeraltı kömür ocaklarının daha derinlere inmesiyle, artan sıcaklığa bağlı olarak önemini daha da artıracaktır. Bu çalışmada, linyit kömürü üretimi yapan bir yeraltı ocağında termal konfor şartlarına bağlı olarak ocak ortamının çalışanlara zararlı etkileri araştırılmıştır. Yapılan ölçümler sonucunda; çalışma ortamlarının PMV (Predicted Mean Vote) değerleri hesaplanmıştır. Ölçümlerin yürütüldüğü yeraltı ocağında aşırı sıcak ve aşırı soğuk bölgelerin olmadığı görülmüştür. Sonuç olarak termal konforun çalışanların sağlığına zarar vermeyecek düzeyde olması için alınacak tedbirlerden bahsedilmiştir.

Anahtar Kelimeler: *Yeraltı kömür madenciliği, İş sağlığı ve güvenliği, Termal konfor.*

Investigation of Thermal Comfort Conditions in an Underground Lignite Coal Mine

ABSTRACT: Although thermal comfort in underground coal mining, is a major factor affecting the health of the occupants and the work productivity, it attracts less attention. The idea of thermal comfort will increase its significance today as the underground collieries exploit the deeper reserves depending on the temperature also increasing in parallel with the geothermic gradient.

In the present work, the detrimental effect of the temperature of the mine air on the mine workers depending on the thermal comfort conditions in underground collieries was investigated. The factors influencing the thermal load and the climatic conditions in underground working places were discussed. It was seen that the changes in the mine environment caused by these factors adversely affect the mine workers. The precautions to be taken for the maximum comfort level for the occupants were also mentioned. The rules and the standards to be obeyed when taking the measurements for the thermal comfort were additionally given.

Keywords: *Underground coal mining, Occupational health and safety, Thermal comfort.*

GİRİŞ (INTRODUCTION)

Dünyadaki hammadde ve enerji ihtiyacının yükselişi, kömür üretiminin artmasına sebep olmuştur. Günümüzde açık ocak kömür madenciliğine uygun rezerv miktarı azalmıştır. Artan enerji ihtiyacını karşılamak amacıyla yeraltı kömür madenciliği daha fazla önem kazanmıştır. Aynı derinlikte metal madenciliğine oranla, kömür madenciliğinde maruz kalınan sıcaklık daha fazladır (Güyagüler, 1988).

ASHRAE 55 Standardına göre termal çevreden memnun olma durumuna termal konfor denir. Diğer bir ifade ile termal konfor; çalışanların psikolojik, fizyolojik, kültürel ve sosyal durumlarını olumsuz

DOI: 10.15317/Scitech.2017.96

etkilemeyecek ve çalışanları rahatsız etmeyecek şekilde olmalıdır. İşletmede çalışılan ortamda kullanılan soğutucu ve ısıtıcılar, çalışanların sağlığını olumsuz etkilemeyecek şekilde yapılmalıdır. İşyerinde çalışanların bulunduğu ortamların tümü termal konfor şartlarına uygun olmalıdır (İBEASGÖİY, Yön., 2013).

İnsanın, vücudu ve bulunduğu ortamın ısıl dengede olması gerekir. Isıl dengenin sağlanabilmesi için deri nemliliğinin ve çalışanların vücut sıcaklığının değişkenliğinin az olması gerekmektedir (Ekici, 2013).

Yeraltı linyit ocağında çalışanların termal konforlarının değerlendirilebilmesi için bağıl nem, hava hızı, metabolik oran ve giysi yalıtım katsayısı birlikte değerlendirilmelidir. Üretimdeki verimliliğin sağlanması için gerekliliklerden biride termal konfor şartlarının sağlanmasıdır. Termal konfor sağlanmadığı durumlarda, sakatlanmalar, meslek hastalıkları ve iş kazaları artmaktadır (Ergun, 2007; Güyagüler, 2005).

ILO 2011'de belirtildiği gibi yeraltı linyit ocağında termal konfor için tehlike sebepleri; ısı ve nemin aşırı yüksek ve aşırı düşük olduğu durumlar, çalışanların maruz kaldığı yüksek hava hızı, çalışma esnasında giyilen elbiseler ve yapılan işin yüküdür.

Bu çalışmada, bir yeraltı linyit ocağının 9 farklı çalışma bölgesinde ölçümler alınmış ve standartlara göre termal konfor şartları incelenmiştir.

TANIMLAR (DEFINITIONS)

Termal Konfor Şartları (Thermal Comfort Conditions)

Çalışanların bulunduğu ortamda termal konfor şartlarının ifade edilmesi için 6 faktör kullanılmaktadır. Bunlar; hava hızı, nem, hava sıcaklığı, radyant ısı, metabolik oran ve giysi yalıtımıdır. Bu faktörler zamana bağlı olarak değişiklik göstermektedir. Bu sebeple çalışanların ortama uyum sağlamaları gerekeceğinden ölçümlere başlamadan bir saatlik sürenin geçmesi gerekmektedir (İmancı, 2014). Özellikle yeraltı maden ocaklarında termal konforu etkileyen şartlara baktığımızda ısı kaynakları, nem, hava hızı ve kömür ocakları için kendiliğinden yanmanın öne çıktığı görülmektedir.

Yeraltı Maden Ocaklarında Termal Konfor Şartlarını Etkileyen Faktörler (Factors Affecting Thermal Comfort Conditions in Underground Mines)

Isı kaynakları (Heat sources)

Yeraltı linyit kömür ocağındaki ısı yükü, havalandırma sistemi içinde oluşan ısı nakillerinin toplamı olarak tanımlanmaktadır. Isı yükü hesaplanırken linyit ocağının bir bölümü göz önüne alınabilir. İklim şartları ve ısı yüküne sebep olan etkenler; tabaka ve kayaçların hareketi sonucu açığa çıkan ısı, çevre kayaçların ve nakledilen cevherin yaydığı ısı, çalışanların metabolizmasının ve makinelerin yaydığı ısı, patlatmalar esnasında ateşleme yapılırken sebep olan ısı, yeraltı çatlaklarından sızan ısı ve su gelirine bağlı nem artışıdır (Önder ve Saraç, 2003).

Nem (Humidity)

Yeraltı ve yerüstü su kaynakları yeraltı ocakları için önemli tehlikelere sebebiyet vermektedir. Özellikle üretilen maden, kömür ise sorunlar daha büyük olmaktadır. Berkowitz; "Yanma kuru ve nemli kömür ara yüzeylerinde oluşmaktadır. Islanma ile oluşan ısı, ıslanmış yüzey ile doğru orantılıdır ve kömürün nem içeriği kapasitesinin bir fonksiyonudur" ifadesiyle nemin yeraltında yangınlara sebebiyet verdiğini açıkça söylemektedir (Berkowitz, 1979).

Bununla beraber tabii ki ocak içerisindeki havanın fazla nemlenmesi sonucu termal konfor şartları da bozulmaktadır. Çünkü nem miktarının artması ile birlikte ortamda hissedilen sıcaklık artış gösterir.

Hava hızı (Air velocity)

Yeraltı maden ocaklarında havalandırma; doğal ve mekanik havalandırma olmak üzere iki şekilde sağlanır. Maden İşyerlerinde İş Sağlığı ve Güvenliği Yönetmeliği'nde (2013), yeraltı ocaklarında hava hızının 0,5-8,0 m/sn arasında olması gerektiği belirtilmektedir. Burada özellikle bilinmesi gereken husus, ocağın hiçbir yerinde durgun havanın oluşmamasını sağlamaktır. Böylece; zararlı gazların uzaklaştırılması, gerekli hava miktarının temini vb. hususlar dikkate alınarak uygun ocak iklimi sağlanmış ve böylece çalışanlar için; uygun termal konfor ortamı sağlanmış olacaktır (MİİSGY, 2013).

Kömürün kendiliğinden yanması (The spontaneous combustion of coal)

Kömür ocaklarında ocak havasında bulunan oksijeninin bir kısmı kömür yüzeyi tarafından absorbe edilir. Bu oksitlenme olayı sonucu CO, CO2 ve ısı açığa çıkar. Açığa çıkan bu ısının havalandırma akımı ile atılmaması veya ısı üretim hızının havalandırma soğutma hızından yüksek olması durumunda, sıcaklık giderek artacak ve çalışanlar için uygun olmayan termal konfor şartları ortaya çıkar (Saltoğlu, 1983).

MATERYAL VE YÖNTEM (MATERIAL AND METHOD)

Materyal (Material)

Ölçümleri alınan yeraltı ocağı, tam mekanize sistemle kömür üretimi yapılan bir ocaktır. Ocakta çift tamburlu kesici yükleyici ile üretim yapılmaktadır. Galerilerin açılmasında ise galeri açma makinesi kullanılmaktadır. Tahkimat, su atımı, taban taramaları vb. işlemlerde görev alan personel bedenen çalışmaktadır. Ocakta, CH_4 ve CO problemleri bulunmamaktadır (CH_{4ort}=0,06, CO_{ort}=5 ppm). Ocakta üretilen linyit kömürünün ortalama kalorisi 3000-3500 Kcal/kg civarındadır. Kendiliğinden yanma olayı ocak havalandırmasının yeterli olması ve su gelirinin kontrol altında tutulmasından dolayı yapılan sıcaklık ve CO ölçümlerinde kendiliğinden yanma tespit edilmemiştir.

Yöntem (Method)

Termal konfor ölçümleri; özel problar (sıcaklık, nem ve hava hızı) ile donatılmış DELTA OHM WBGT 32.3 termal konfor ölçüm cihazıyla, 08:00-16:00 vardiyası süresince yapılmış ve ortalamaları alınmıştır. Giysi ısıl direnci ve metabolizma oranı çalışma yeri göz önüne alınarak ASHRAE 55 standardına göre kabul edilmiştir (Çizelge 1, Çizelge 2).

Çizelge 1. Çeşitli Giysi Türleri ve Yalıtım Katsayıları (İmancı, 2014; ANSI - ASHRAE 55 - 2010)

Table 1. *Typical garment clo-value*

Kıyafet Yalıtım Katsayısı, Icl (clo*)	Kıyafet Yalıtım Katsayısı, Icl (clo)
Pantolon, kısa kollu gömlek	0,57
Pantolon, uzun kollu gömlek	0,61
Pantolon, uzun kollu gömlek, ceket	0,96
Diz uzunluğunda etek, kısa kollu gömlek	0,54
Ayak bileği uzunluğunda etek, uzun kollu gömlek, ceket	1,1
Etek / Elbise	0,54-1,10
Şort	0,36
Önlük / Tulum	0,72-1,37
Spor Kıyafetleri	0,74

*1 clo = 0.155 m^2K/W

Çizelge 2. Bazı İşler İçin Metabolizma Oranları (ANSI - ASHRAE 55 - 2010)
Table 2. *Metabolic rates of different activities*

Aktivite	Metabolik Oran (W/m²)	Metabolik Oran (met*)
Yürüme	115-220	2,0-3,8
Aşçılık	95-115	1,6-2,0
Ev temizleme	115-200	2,0-3,4
Makine Kullanılarak Yapılan İşler		
Testere ile yapılan işler	105	1,8
Hafif işler (ör. Elektrik end.)	115-140	2,0-2,4
Ağır işler	235	4,0
Ağır yük kaldırma (50 kg)	235	4,0
Kazma, kırma işleri	235-280	4,0-4,8

1 met = 58,2 W/m²

Yeraltı ocağından alınan ölçümler, TS EN 27243, TS EN ISO 7730 standartları ve ASSHRAE 55'den almış olduğumuz verilerle, Fanger modeline göre değerlendirmeye tabi tutulmuştur. Bu modelde, PMV Eşitlik 1'de tanımlanmıştır (Fanger, 1972; TS EN ISO 7730, 2006).

$$PMV = [0{,}303 \times \exp(-0{,}036 \times M) + 0{,}028] \times (M-W) - 3{,}05 \times 10^{-3} \times [5{,}733 - 6{,}99 \times (M-W) - p_a] - 0{,}42 \times [(M-W) - 58{,}15] - 1{,}7 \times 10^{-5} \times M \times (5{,}867 - p_a) - 0{,}0014 \times M\,(34 - t_a) - 3{,}96 \times 10^{-8} \times f_{cl} \times [(t_{cl}+273)^4 - (\bar{tr} + 273)^4] - f_{cl} \times h_c \times (t_{cl} - t_a)$$

Burada, M = metabolik hız (kcal / saat)
A_{Du} = DuBois (vücut yüzey) alanı (m²)
η = mekanik verimlilik
P_a = ortam havasındaki buhar basıncı (mmHg)
t_a = iç ortam hava sıcaklığı (° C)
f_{cl} = giyinmiş gövdenin yüzey alanının, çıplak vücudun yüzey alanına oranı
t_{cl} = giyinmiş vücudun dış yüzeyinin ortalama sıcaklığı (° C)
t_{mrt} = ortalama ışın sıcaklığı (° C)
h_c = konvektif ısı transfer katsayısı (kcal / saat m² ° C).

PMV değerinin yorumlanması Çizelge 3'de verilmiştir. Bu sonuçlara göre; ortamın termal konforunun uygun ya da uygun olmadığından bahsedilebilmektedir (TS EN ISO 7730).

Çizelge 3. Yedi nokta ısıl duyum ölçeği (Fanger, 1967).
Table 3. *Seven-point thermal sensation scale*

PMV	Anlam	Yorum
+3	Aşırı sıcak	Bunaltıcı ve tolere edilemez
+2	Sıcak	Çok sıcak
+1	Hafif sıcak	Tolere edilebilir, sıcak
0	Nötr	Konforlu
-1	Hafif serin	Tolere edilebilir, serin
-2	Serin	Çok serin
-3	Soğuk	Tolere edilemez, soğuk

Ekici'nin 2013'de belirttiği gibi; Fanger metodu aşağıdaki şekilde uygulanmıştır.
1. Hava sıcaklığı, bağıl hava hızı ve bağıl nem değerleri ölçülmüştür.

2. Metabolizma hızı TS EN 27243'den seçilmiştir. Mekanik verim değerleri Fanger'in (1972) verdiği tablodan seçilmiştir.

3. Ortam havasındaki buhar basıncı (p_a); Parsons'un (2005) formülünden hesaplanmıştır (p_a doymuş buhar basıncının bağıl nemle çarpılması ile bulunmaktadır).

4. Kıyafet ısıl direnci değerleri (clo) ASHRAE 55'de bulunan tablolardan seçilmiştir.

5. Kıyafet yüzey sıcaklığı ve hc değeri Fanger'in (1972) oluşturduğu tablodan seçilmiştir.

6. İlk 5 adımda bulunan değerler denklemde yerine konularak PMV değeri elde edilmiştir.

Linyit ocağının termal konfor şartlarının değerlendirilmesinde, ASHRAE 55 standardı temel alınarak oluşturulan, Berkeley Üniversitesi Yapısal Çevre Merkezi tarafından hazırlanan internet arayüzlü termal konfor programı kullanılmıştır.

BULGULAR (RESULTS)

Kömür ocağında, yerinde alınan ölçümler sonucunda hava hızı, çalışma sıcaklığı ve nem değerleri elde edilmiştir. Giysi ısıl direnci ve metabolik oran çalışma yeri göz önüne alınarak ANSI-ASHRAE 55-2010 standardına göre kabul edilmiştir (Çizelge 4).

Çizelge 4. Termal konfor ölçüm ve kabul değerleri
Table 4. *Thermal comfort measurement and acceptance values*

Konum	Hava Hızı (m/sn)	Çalışma Sıcaklığı (ºC)	Nem (%)	Giysi Isıl Direnci Icl (clo)	Metabolik Oran (met)
Desandre 1	1,61	10,4	52	0,96	2,0
Desandre 2	1,79	23,1	91	0,96	2,0
Alt taban yolu 1	0,86	13,5	66	0,96	4,0
Alt taban yolu 2	0,58	25,3	54	0,96	4,0
Alt taban yolu 3	0,79	18,4	72	0,96	4,0
Üst taban yolu 1	0,60	25,0	76	0,96	4,0
Üst taban yolu 2	1,99	24,8	81	0,96	4,0
Kılavuz	1,15	24,2	78	0,96	4,0
Arın	0,57	25,0	87	0,96	4,0

Bu bölgelerin hesaplanan PMV değerlerine ait değerler Çizelge 5'de verilmiştir.

Çizelge 5. PMV değerleri
Table 5. *PMV values*

Bölge	PMV
Desandre 1	-1,71
Desandre 2	0,44
Alt Taban Yolu 1	0,30
Alt Taban Yolu 2	2,41
Alt Taban Yolu 3	1,24
Üst Taban Yolu 1	2,59
Üst Taban Yolu 2	2,07
Kılavuz	2,20
Arın	2,07

9 bölgeye ait termal konfor şartları hesaplanmış ve Şekil 1'de verilmiştir.

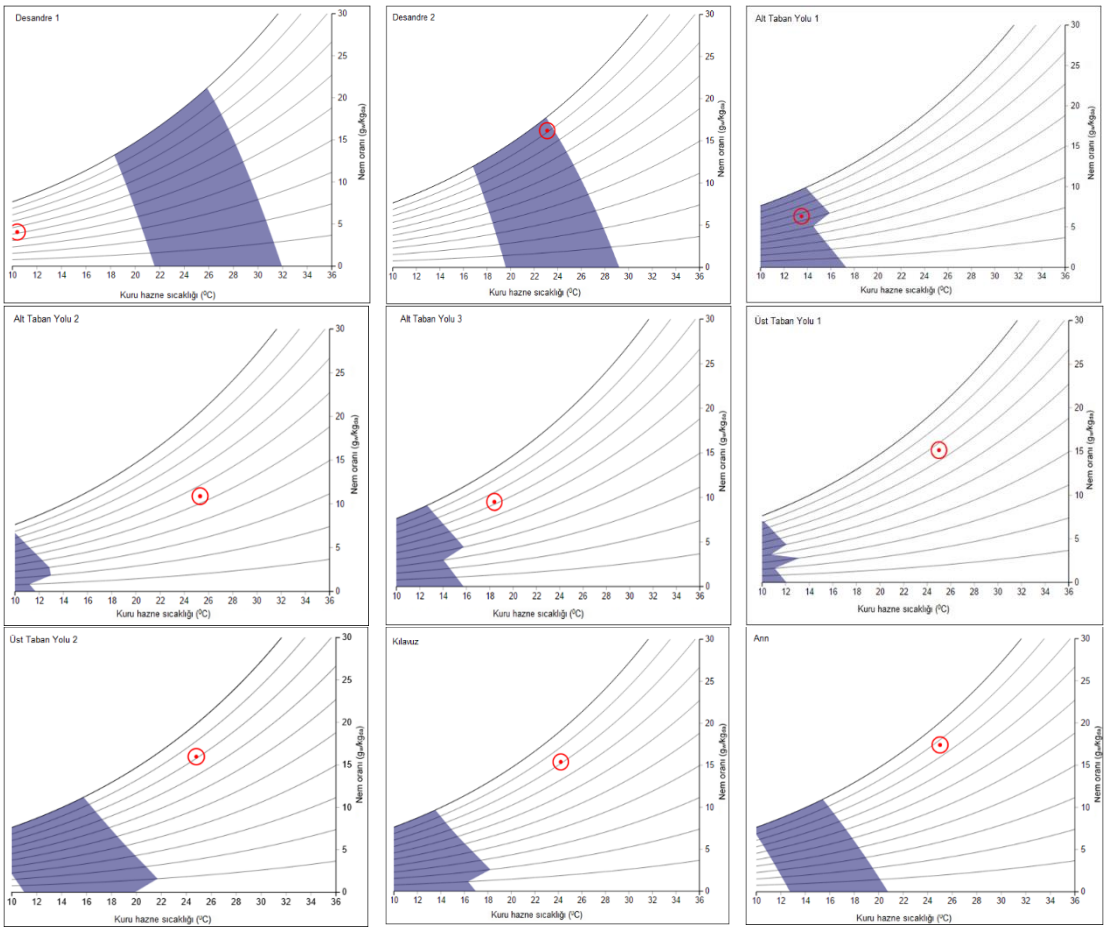

Şekil 1. Linyit ocağındaki termal konfor grafikleri
Figure 1.*Thermal comfort chart in lignite mines*

Bu sonuçlara göre desandre 2 ve alt taban yolu 1 konforlu bölge içerisine girmektedir. Çalışanlar için desandre 1'de tolere edilebilir serin ve alt taban yolu 3'de tolere edilebilir, sıcak ortam vardır. Alt taban yolu 2, üst taban yolu 1-2, kılavuz ve arında ise çok sıcak bir çalışma ortamı bulunmaktadır ki bu da konforsuz bir çalışma ortamıdır.

SONUÇLAR (CONCLUSIONS)

Yeraltı linyit ocağında alınan ölçümler ve yapılan PMV hesaplamaları sonucunda; desandre 1'de alınan verilere bakıldığında ortam sıcaklığının (10,4 ^{0}C) olması PMV değerini eksiye düşürmüştür. Hava hızı ve nem değerlerinin uygun olması ise tolere edilebilir serin bir ortam oluşturmuştur.

Desandre 2'de nem oranının yüksek olmasına rağmen, hava sıcaklığı ve hava hızının termal konfor şartları için uygun aralıkta olması nedeniyle PMV değeri 0,44 bulunmuştur. Bu da Şekil 1'de görüldüğü üzere termal konfor bölgesi içinde kalınmasına olanak sağlamıştır.

Alt taban yolu 1'de ortam sıcaklığının düşük olmasına rağmen diğer şartların uygun olması ve çalışan insan vücudunun serin havayı tolere edebilmesi dolayısıyla PMV 0,30 çıkmış ve termal konfor bölgesi içinde kalınmasını sağlamıştır.

Alt taban yolu 2'de sıcaklığın alt taban yolu 1'den yüksek olması ve hava hızının ise düşük olması ile ortam konforsuz bölgeye girmektedir. Alt taban yolu 2'de oluşan, taban kabarmaları ve kesitin bozulması da etkenlerdendir.

Alt taban yolu 3'de ise, sıcaklığın düşmesi, nemin artması ve alt taban yolu 2'ye göre nispeten hava hızının da artması ile tolere edilebilir serin bir ortam oluşmasına sebep olmuştur. Bu ise konforlu sayılabilecek bir ortamdır.

Üst taban yolu 1'de nem ve sıcaklığın normal değerlerde olmasına rağmen hava hızının düşük olması ortamın termal konfor sınırlarının dışına çıkmasına sebep olmuştur.

Üst taban yolu 2, hava hızı ve sıcaklığın normal ama nemin %80'in üzerine çıkması ile termal konfor şartları sağlanamamaktadır.

Kılavuz galerisinde ise; nemin kritik seviyeye yaklaşması ile Fanger'in vermiş olduğu çizelgede de görüleceği üzere çok sıcak ortam oluşmuştur. Bu da çalışanlar için tolere edilemeyecek seviyede konforsuz bir alan demektir.

Arında beklendiği üzere, çalışan tamburlu kesicinin püskürtmüş olduğu suyun etkisi ile ortamda nem oranı %87'ye çıkmıştır. Sıcaklığın normal bir seviyede olmasına rağmen, hava hızının da yeraltında müsaade edilen en düşük hız olan 0,5 m/sn'ye yaklaşması ile kılavuz galerisinde olduğu gibi çok sıcak bir ortam oluşmuştur.

Bu çalışma bize, sadece sıcaklık değerlerinin ölçülmesinin çalışılan ortamın termal konforuna karar verilmesinde hatalı olacağını göstermiştir. Sıcaklıkla beraber, hava hızı, nem, metabolik oran ve giysi ısıl dirençlerinin de hesaba katılması gerektiğini göstermektedir.

Ocakta termal konfor açısından problemli bölgelerde, nem ve hava hızı sorununun olduğu görülmektedir. Esasında ocak içerisinde hiçbir bölgede yönetmelikte bildirilen 0,5-8,0 m/sn hava hızı aralığının dışına çıkılmamaktadır (MİİSGY, 2013). Buna rağmen alt taban yolu 2, üst taban yolu 1 ve arında hava hızlarının 0,5 m/sn limitine yaklaşmasından dolayı ortamda termal konfordan bahsedilememektedir. Bu bölgelerde ek havalandırma sistemleri (vantüp vb) konularak sorun çözülebileceği düşünülmektedir. Ayrıca çalışanların metabolik oranlarını düşürerek de (iş yükünü azaltmak vb.) sorun aşılabilir.

Nem problemi, su gelirinin fazla olduğu, kılavuz galerisi ve arında kullanılan makinelerin püskürtmüş oldukları suyun havada nem oranını yükseltmesi sonucu oluşmuştur. Bu bölgelerde çalışanlara gerekli olan kişisel koruyucu donanımlar verilerek sorunun aşılabileceği düşünülmektedir.

Ocakta çalışanlar tarafından kullanılan kıyafetlerin giysi ısıl direnci 0,96 clo'dur. Termal konforun sağlanamadığı, sıcak bölgelerde, giysi ısıl direnci 0,61 clo olan iş kıyafetleri tercih edilmelidir.

KAYNAKLAR (REFERENCES)

ASHRAE, ANSI/AHSRAE Standard 55-2010, Thermal Environmental Conditions for Human Occupancy, ASHRAE Publications.

Berkowitz, N., 1979, *An Introduction to Coal Technology*, Academic Press Inc., New York.

Ekici, C., 2013, "PMV Metodu ile Isıl Konfor Ölçümü ve Hesaplanması", *VIII. Ulusal Ölçüm Bilim Kongresi*, Kocaeli, 1-5, 26-28 Eylül 2013.

Ergun, A.R., 2007, *Yeraltı Maden İşletmelerinde Gaz ve Toz Patlamaları ve Önlemler*, İş Sağlığı ve Güvenliği Uzmanlık Tezi, T.C. Çalışma ve Sosyal Güvenlik Bakanlığı İş Sağlığı ve Güvenliği Genel Müdürlüğü, Ankara.

Fanger, P. O., 1967, "Calculation of Thermal Comfort: Introduction of a Basic Comfort Equation", *ASHRAE Transactions*, 73 (2), 1-20.

Fanger, P. O., 1972, *Thermal Comfort: Analysis and Applications in Environmental Engineering*, McGraw-Hill, New York.

Güyagüler, T., "Yeraltı Kömür Ocaklarında Yüksek Sıcaklık ve Rutubet Sorunu", *Türkiye 6. Kömür Kongresi*, Zonguldak, 133-141, 23-27 Mayıs 1988.

Güyagüler, T., 2005, *Occupational Health & Safety*, Orta Doğu Teknik Üniversitesi, Ankara.

ILO, 2011, Safety and Health in Underground Coal Mines, ILO, Cenevre.

İmancı, C., 2014, *Döküm Atölyelerinde Termal Konfor Şartlarının İncelenmesi*, İş Sağlığı ve Güvenliği Uzmanlık Tezi, T.C. Çalışma ve Sosyal Güvenlik Bakanlığı İş Sağlığı ve Güvenliği Genel Müdürlüğü, Ankara.

İşyeri Bina ve Eklentilerinde Alınacak Sağlık ve Güvenlik Önlemlerine İlişkin Yönetmelik, 2013, 28710 Sayılı Resmi Gazete, Ankara.

Maden İşyerlerinde İş Sağlığı ve Güvenliği Yönetmeliği, 2013, 28770 Sayılı Resmi Gazete, Ankara.

Önder, M. ve Saraç, S., 2003, "Yeraltı Ocaklarındaki İklimsel Koşulların Önceden Belirlenmesi", *DEÜ Mühendislik Fakültesi Fen ve Mühendislik Dergisi*, Cilt. 5, 137-146.

Parsons, K. C., 2005, *Human Thermal Environments*, Taylor & Francis, New York.

Saltoğlu, S., 1983, *Madenlerde Havalandırma ve Emniyet İşleri*, İTÜ Maden Fakültesi Ofset Baskı Atölyesi, İstanbul.

TS EN 27243, 2002, Sıcak Ortamlar - WBGT (Yaş - Hazne Küre Sıcaklığı) İndeksine Göre Isının Çalışan Üzerindeki Baskısının Tahmini, Ankara.

TS EN ISO 7730, 2006, Termal Çevrenin Ergonomisi – Analitik Termal Konforun Belirlenmesi ve Yorumlanması PMV ve PPD Endekslerinin Hesaplanması ve Yerel Termal Konfor Kriterleri, Ankara.

Berkeley University. Thermal Comfort Tool. Center for the Built Environment. www.smap.cbe.berkeley.edu/comforttool, ziyaret tarihi: 09 Ocak 2017.

SELÇUK ÜNİVERSİTESİ
MÜHENDİSLİK FAKÜLTESİ

S.Ü. Müh. Bilim ve Tekn. Derg., c.5, s.3, 2017
Selcuk Univ. J. Eng. Sci. Tech., v.5, n.3, 2017
ISSN: 2147-9364 (Elektronik)

ANALITICAL AND ARTIFICIAL NEURAL NETWORK MODELS OF DISCHARGE VALUE PASSING OVER OGEE SPILLWAY

[1]Alpaslan YARAR

[1]Selcuk University, Engineering Faculty, Civil Engineering Department Hydraulics Division, 42031 Konya, Turkey
[1]ayarar@selcuk.edu.tr

(Geliş/Received: 10.02.2017; Kabul/Accepted in Revised Form: 28.03.2017)

ABSTRACT: In this study, analytical and Artificial Neural Network (ANN) models' output of the discharge value, passing over Ogee Spillways, were compared. For this aim, a flume having 7.5 cm width, 15 cm depth and 5 m length, was used in the laboratory. Discharge values above the spillway were measured for different heads. Discharge values were also computed by the formula for the measured heads. An ANN model was set by using the experimental results in order to estimate the discharge value. So, the performance of the ANN model was investigated. As the result, it was seen that ANN model produced very successful output.

Key Words: *Discharge, Ogee spillway, Artificial neural networks*

Ogee Tipi Dolusavakların Üzerinden Geçen Akım Verilerinin Analitik ve Yapay Sinir Ağları Modelleri

ÖZ: Bu çalışmada Ogee tipi bağlamalar üzerinden geçen debilerin analitik ve yapay sinir ağları model sonuçları karşılaştırılmıştır. Bunun için 7.5 cm genişliğinde, 15 cm yüksekliğinde ve 5 m uzunluğunda bir açık kanal düzeneği kullanılmıştır. Kullanılan düzenekte farklı savak yükleri geçmesi durumunda debiler ölçülmüş ve bu debiler formül kullanılarak da hesaplanmıştır. Ayrıca deneyden elde edilen sonuçlar ile yapay sinir ağları modeli kurularak debiler tahmin edilmiş ve modelin performansı araştırılmıştır. Elde edilen sonuçlara göre yapay sinir ağları modeli oldukça tatmin edici sonuçlar vermiştir.

Anahtar Kelimeler: *Akım, Ogee dolusavak, Yapay sinir ağları*

INTRODUCTION

Spillways are used to hold water at a certain level in reservoir besides to store water for different aims, such as energy, irrigation, flood control, etc. Ogee-shaped spillways let excessive water in reservoir pass to downstream. The ideal form of the spillway recommended by The United States Bureau of Reclamation (USBR, 1987) is seen in Fig. 1.

DOI: 10.15317/Scitech.2017.97

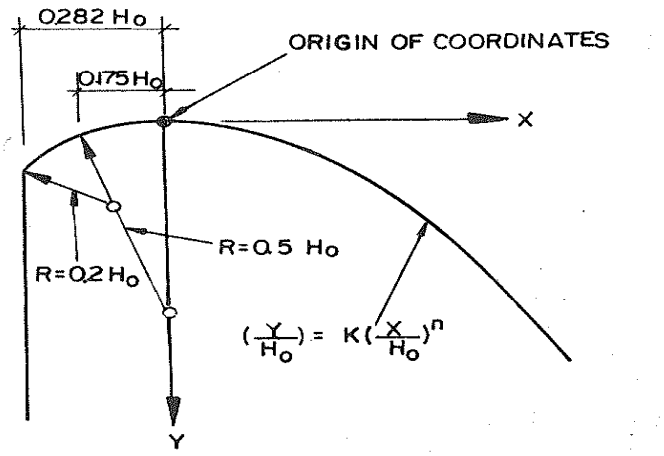

Figure 1. Standard crest profile of an overflow spillway (USBR, 1987)

The downstream of the spillway can be defined by Eq.1.

$$\frac{Y}{H_0} = K\left(\frac{X}{H_0}\right)^n \quad (1)$$

K and n are constant, depend on the upstream inclination and the velocity and H_0 is the design head. The discharge over the spillway can be calculated by Eq.2.

$$Q = CLH^{3/2} \quad (2)$$

Q (m^3/s) is the discharge, C is the discharge coefficient, L (m) is the length of the crest and H (m) is the head over the crest.

Many researchers have studied for numerical and experimental studies on spillways (Savage and Johnson, 2001; Song and Zhou, 1999; Sanchez et. al., 2000). And ANN model have also used for studies on spillways. Azamathulla et. al. (2008), studied for scour depth prediction for ski-jump type of spillways. They also used some traditional methods. Their study showed that the traditional equation-based methods of predicting design scour downstream of a ski-jump bucked could better be replaced by one of the soft computing schemes. Salmasi and Özger (2014), investigated the applicability and accuracy of the neuro-fuzzy approach in estimating the proper values of energy dissipation of skimming flow regime over stepped spillways. They were also developed multi regression equations. They found that neuro-fuzzy model is more successful than regression equations.

In this study, it was aimed that to investigate the capability of ANN model to estimate the discharge value flow over Ogee spillway.

MATERIALS AND METHODS

In this study, an experimental setup containing a simple flume which was made plexiglass and having 7.5 cm width, 15 cm depth and 5 m length, was used in order to calculate discharge passing over ogee-shaped spillway for different heads (Fig. 2). The flume had closed loop water system and the flow to the flume was supplied from constant head water tank and the flow discharge was regulated by a valve. That the transparent flume also enables to see the flow conditions. Flow depth measured with a measurement device holded along the flume to an accuracy of ± 1 mm.

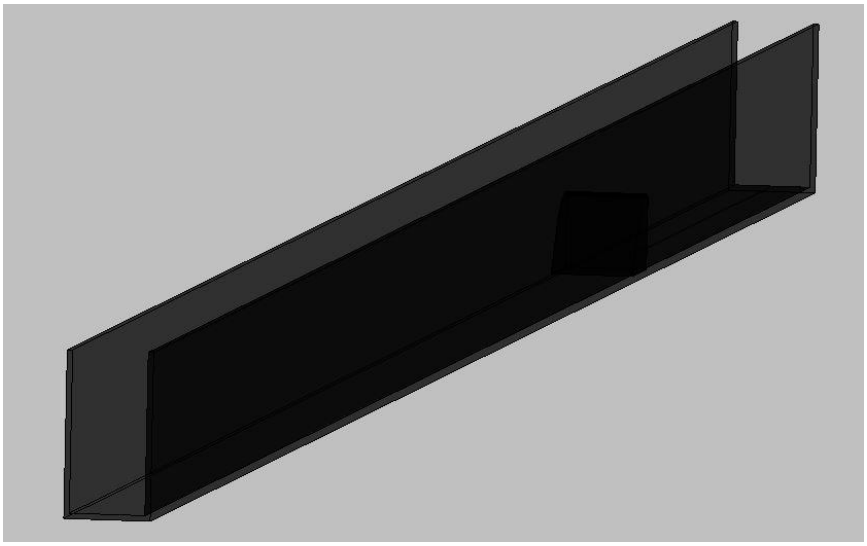

Figure 2. General view of the flume used in the study

A tank, made by smooth plastic which has 63 x 67 x 72 cm dimensions, was used to measure the discharge. An ogee spillway model was modeled by Eq. 1 according to USBR type and manufactured with steel material to use in the experiments (Fig. 3).

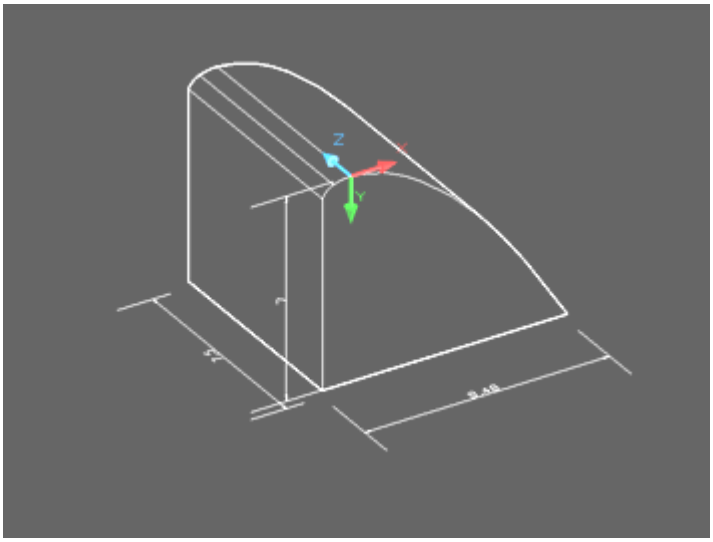

Figure 3. Ogee spillway model

Artificial Neural Networks

The composition of ANN is inspired from biological neural networks. A neuron is one of the basic components of neural networks. It can vary in terms of size and shape, according to its function and mission in neural systems (Dorum et. al., 2010).

The system consisting of three layers, an input layer, an hidden layer and an output layer, named Multi Layer Perceptron (MLP) (Fig.4).

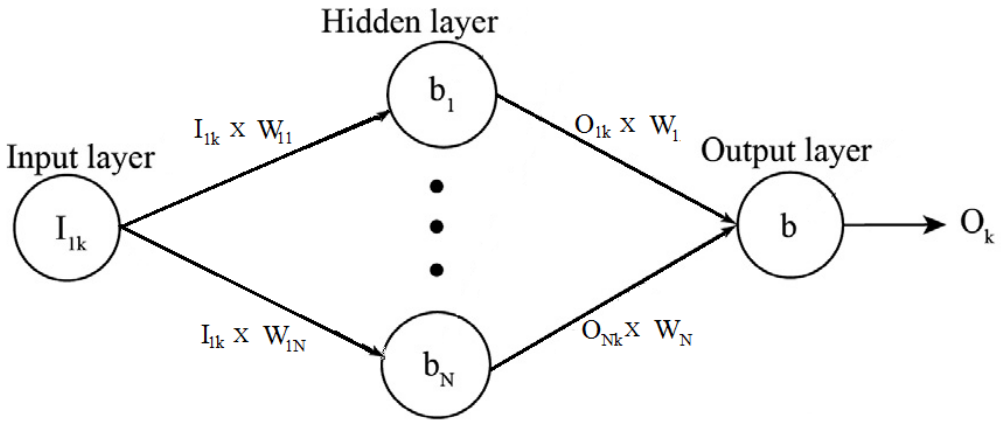

Figure 4. A structure of Multilayer Perceptron

The processing elements in each layer are called neurons or nodes. The input layer contains input parameters. The output layer produces the predictions. The output function of the output layer is a linear function that aggregates the input signals of the output layer. The hidden layers between the input and the output layers deliver signals. The most important part of the hidden layer having a main role in transferring the network inputs to output is an activation function, typically a continuous and bounded nonlinear function such as hyperbolic-tangent-sigmoid (Tansig) or logarithm-sigmoid (Logsig) functions (Cybenko, 1989).

The mathematical expression of a three-layer feedforward ANN for prediction is

$$O_{jk} = f_1\left(b_j + \sum_i W_{ij} I_{ik}\right) \tag{3}$$

$$O_k = b + \sum_i W_j O_{jk} \tag{4}$$

where f_1 is the activation function for the hidden layer, I_{ik} is the ith input for the kth sample point, O_{jk} is the output of jth node of the hidden layer, W_{ij} and W_j are the weights that control the strength of connections between layers and b_j and b are the biases that are used to adjust the mean value for the hidden layer and the output layer, respectively (Chitsazan et. al., 2015).

RESULTS AND DISCUSSION

The flow depths over the spillway were measured for different discharge. The discharges were determined by the tank for each water heads. This process was done with holding time until filling certain volume (Fig. 5).

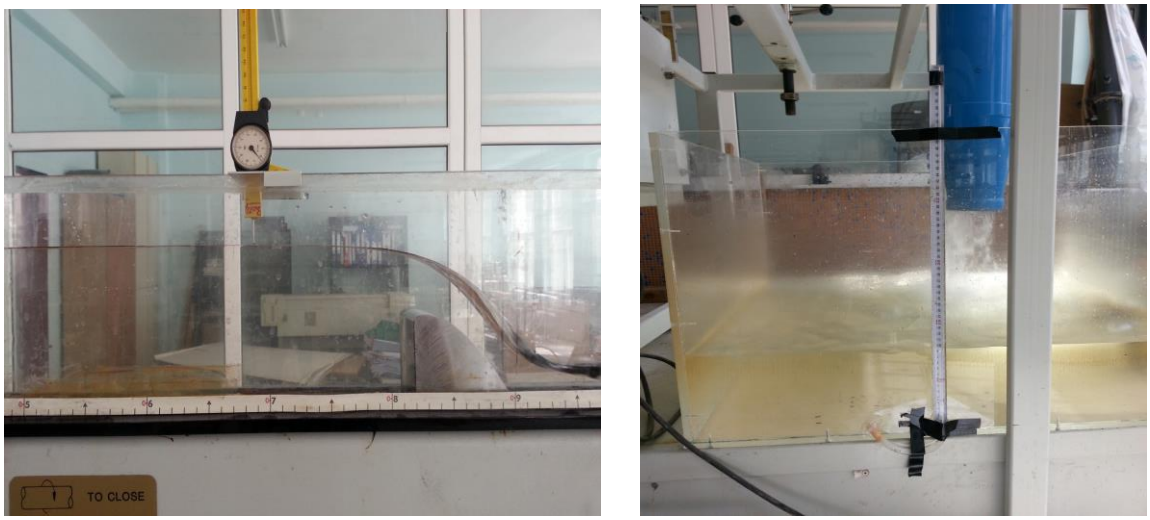

Figure 5. Water depth and discharge measurement points on the experimental set up

Discharge values were also calculated by Eq. 2 using the water heads. Then the discharge values obtained from both experimental and analytical results were compared with each other. Measured water heads and corresponding discharges for both experimental and analytical studies were given in Figure 6 and the relationship between them is also given in Figure 7.

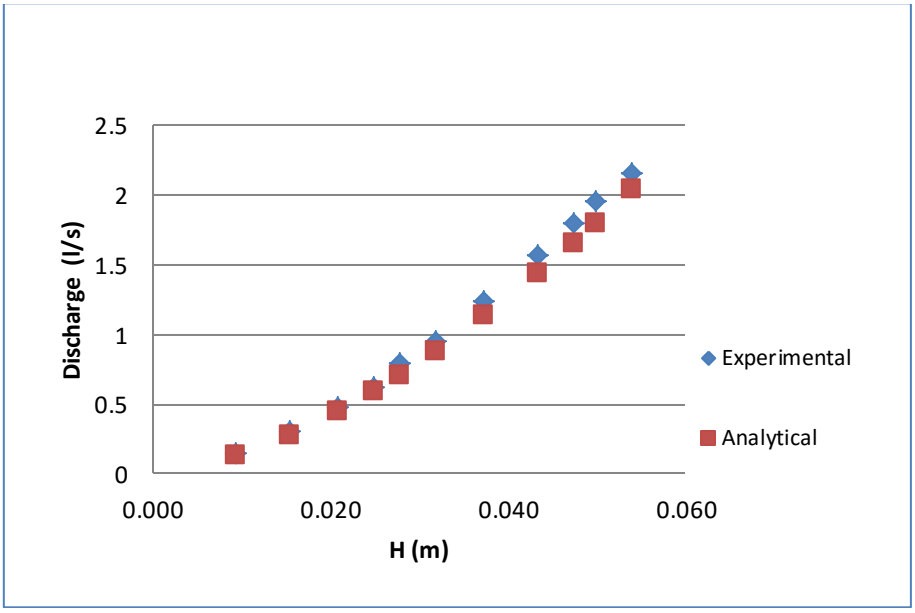

Figure 6. Comparison of the experimental and analytical results

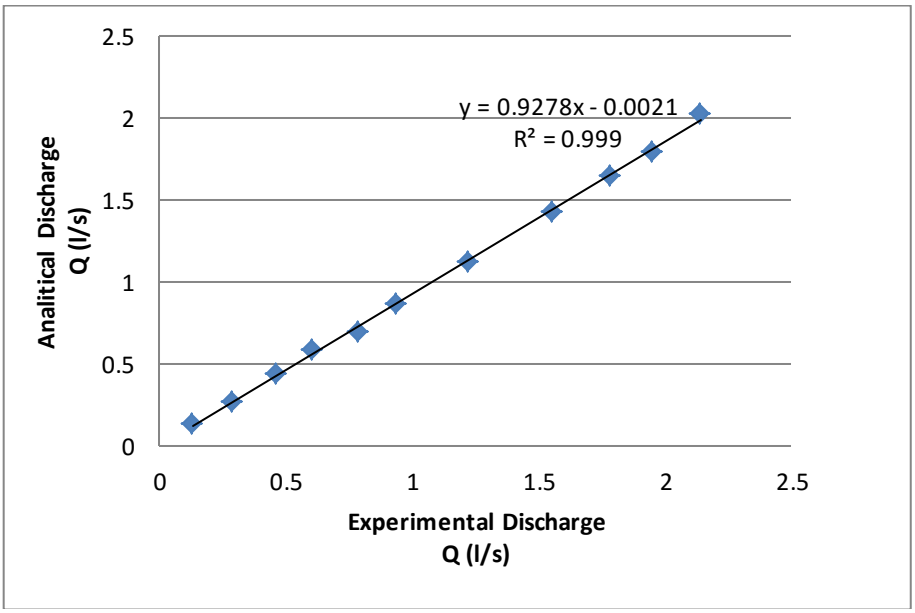

Figure 7. Relationship between the results of experimental and analytical studies

Experimental results were used for ANN modeling. 6 data set of the 11 data set were used for training and remaining 5 data set were used for testing. Feed forward back propagation ANN model and Scaled Conjugate Gradiant (SCG) algorithm were used for modeling. Three layered ANN formed with 1 input layer 1 hidden layer and 1 output layer was used in ANN model. The relationship between ANN results and experimental results is shown in Fig 8.

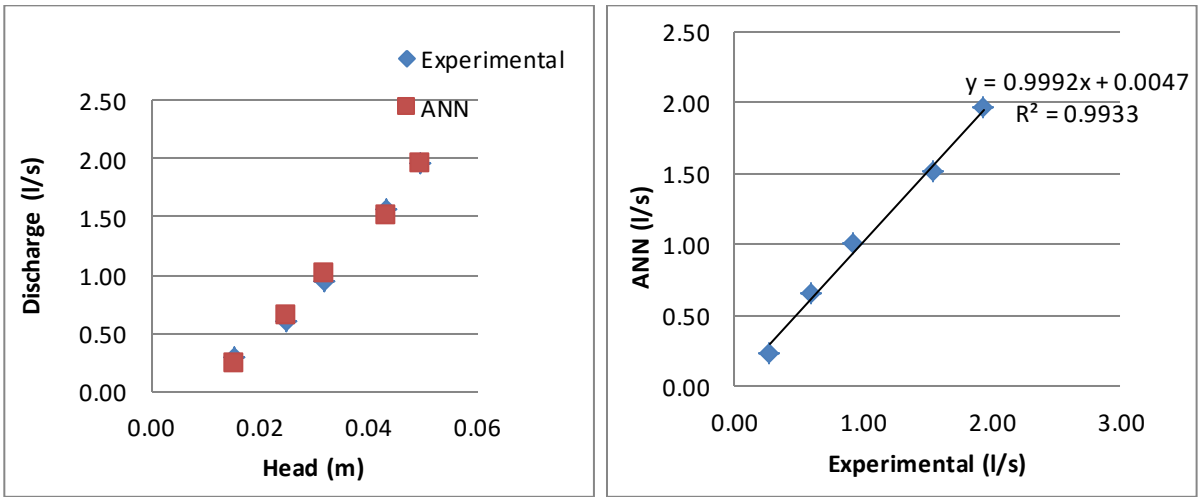

Figure 8. Relationship between the results of experimental and ANN test

CONCLUSIONS

Hydraulic design of a spillway is one of the most studied subject in hydraulic engineering. Properly designed spillways will be able to pass flood flows efficiently and safely to downstream of dams. So, determining the discharges correctly becomes important for the water structures. In recent years, artificial intelligence methods based on learning from examples statistical methods of artificial neural networks have been widely applied in hydraulic structures. In this study, it was aimed to investigate the ANN performance on determining the discharge over the ogee spillways. For this purpose both experimental and analytical studies were done. It was seen that ANN model produced very successful

results. Overall, the studies presented in this paper showed us that ANN model can be an alternative method to determine the discharge value passing over the spillways.

REFERENCES

Azamathulla, H., Md., Deo, M. C., Deolalikar, P. B., 2008, "Alternative Neural Networks to Estimate the Scour Below Spillways", *Advances in Engineering Software,* Vol. 39, pp. 689-698.

Chitsazan, N., Nadiri, A. A., Tsai, F. T. C., 2015, "Prediction and Structural Uncertainty Analyses of Artificial Neural Networks Using Hierarchical Bayesian Model Averaging", *Journal of Hydrology*, Vol. 528, pp. 52–62.

Cybenko, G., 1989, "Approximations by Superpositions of A Sigmoidal Function", *Mathematics of Control, Signals, and Systems,* Vol. 2 (4), pp. 303–314.

Dorum, A., Yarar, A., Sevimli, M. F., Onüçyildiz, M., 2010, "Modelling The Rainfall–Runoff Data of Susurluk Basin", *Expert Systems with Applications,* Vol. 37 (9), pp. 6587–6593.

Salmasi, F., Özger, M., 2014, "Neuro-Fuzzy Approach for Estimating Energy Dissipation in Skimming Flow over Stepped Spillways", *Arabian Journal for Science & Engineering*, Vol. 39, pp. 6099–6108.

Sanchez, J. M., Pomares, J., Dolz, J., "Pressure Field in Skimming Flow over A Stepped Spillway", *In: Proceedings, International Workshop on Hydraulics of Stepped Spillways*, Zurich, Switzerland, 2000.

Savage, B. M., Johnson, M. C., 2001, "Flow over Ogee Spillway: Physical and Numerical Model Case Study", *Journal of Hydraulic Engineering*, ASCE, Vol. 127(8), pp. 640–649.

Song, C., Zhou, F., 1999, "Simulation of Free Surface Flow over Spillway", *Journal of Hydraulic Engineering,* ASCE, Vol. 125(9), pp. 959–967.

USBR, 1987, *Design of Small Dams*, Third Edition, Washington: Water Resources Technical Publication.

SELÇUK ÜNİVERSİTESİ
MÜHENDİSLİK FAKÜLTESİ

S.Ü. Müh. Bilim ve Tekn. Derg., c.5, s.3, 2017
Selcuk Univ. J. Eng. Sci. Tech., v.5, n.3, 2017
ISSN: 2147-9364 (Electronic)

GEOLOGICAL AND GEOMECHANICAL PROPERTIES OF SOME CARBONATE MARBLES AND BASALT STONE FROM MOROCCO

[1]Veysel ZEDEF, [2]Kerim KOÇAK, [3]Najib Mohamed ZAGHLOUL, [4]Adnan DÖYEN, [5]Ali Rıza SÖĞÜT, [6]Hakan ÖZŞEN, [7]Bilgehan KEKEÇ, [8]Ali ARAS, [9]Kemal DOĞAN, [10]Tevfik AĞAÇAYAK

[1,6,7,8,9,10]Selcuk University, Department of Mining Engineering, Campus, Selcuklu, Konya, TURKEY
[2,4,5]Selcuk University, Department of Geology, Campus, Selcuklu, Konya, TURKEY
[3]Abdelmalek Essaadi University, Department of Earth Sciences, Tanger, MOROCCO
[1]vzedef@selcuk.edu.tr, [2]kkocak@selcuk.edu.tr, [3]zaghloul@geologist.com, [4]adoyen@selcuk.edu.tr, [5]arsogut@selcuk.edu.tr, [6]hozsen@selcuk.edu.tr, [7]kekec@selcuk.edu.tr, [8]aliaras@selcuk.edu.tr, [9]kdogan@selcuk.edu.tr, [10]tevfik@selcuk.edu.tr

(Geliş/Received: 02.03.2017; Kabul/Accepted in Revised Form: 28.03.2017)

ABSTRACT: The natural rocks used today as well as in the history for a variety of purposes were a subject of different alteration, weathering and deterioration conditions. These conditions are strictly controlled by environment and nature of rock varieties (marble and stone). This study is a first approach to understand the relation between some geological features and behavior against salt (Na_2SO_4) decay of Moroccan marbles and stones. For this purpose, widely used four dolomitic limestones, two crystalline limestones, one limestone and one basalt sample (total 8) were chosen from Morocco. Extra attention paid to choose locations being a representative of all Moroccan country. The carbonate samples (limestone and dolomite) consist of mainly dolomite and calcite with micritic and sparitic cement. The sole, non-carbonaceous sample is basalt of Khenifra containing mainly plagioclase and pyroxene. In general, both bulk-dry and powder density values of the studied rock samples are homogeneous. The limestone of Bir Jdid has the highest (10.81 %) effective porosity and dry weight loss value (4.61 %). The loss on ignition value of the Khenifra basalt has the lowest value with 1.26 %. The loss on ignition values are also relatively uniform. The obtained data indicate that outdoor uses (especially in coastal areas) of limestones of Bir Jdid and dolomitic limestones of Taza are more risky than the others.

Key Words: *Geomechanical and geological features, Marbles, Stones, Dry-weight loss, Morocco*

Fas'ın Bazı Karbonat Mermerleri ve Bazalt Taşlarının Jeolojik ve Jeomekanik Özellikleri

ÖZ: Hem geçmiş dönemlerde hem de günümüzde çok çeşitli amaçlar için kullanılan doğal taşlar farklı ayrışma, dağılma ve bozunmaya uğramaktadırlar. Bu şartlar çevre ve kayacın türüne (mermer ve taş) sıkı sıkıya bağlıdır. Bu çalışma Fas mermerleri ve taşlarını tuza (Na_2SO_4) karşı dayanımlarını ve bazı jeolojik özelliklerini anlamak için yapılan ilk çalışmadır. Bunun için Fas'tan getirilen çok kullanılan 4 dolomit, 2 kristalize kireçtaşı, 1 kireçtaşı ve bir bazalt (toplam 8 adet) örneği seçilmiştir. Örnekler mümkün mertebe Fas'ın değişik yerlerinden seçilmiştir. Karbonat kayaçları (kireçtaşı ve dolomit) temel olarak dolomit ve kalsit minerallerinden müteşekkil olup çimento mikrit ve sparittir. Karbonatsız tek kayaç olan Khenifra bazaltı esasen plajiyoklas ve piroksen içerir. Genel olarak örneklerin kuru ve öğütülmüş ağırlıkları birbirlerine benzer. Bir Jdid kireçtaşları en yüksek etkili porozite (% 10.81) ve kuru ağırlık kaybına (%4.61) sahiptir. En düşük ateş zayiatı Khenifra bazaltlarındadır (%1.26). Ateş zayiatları genel olarak homojendir. Eldeki veriler Bir Jdid kireçtaşları ve Taza dolomitik kireçtaşlarının dışarda (özellikle sahil bölgelerinde) kullanımlarının diğerlerine göre daha riskli olduğuna işaret etmektedir.

DOI: 10.15317/Scitech.2017.98

Anahtar Kelimeler: *Jeomekanik ve jeolojik özellikler, Mermerler, Taşlar,Kkuru ağırlık kaybı, Fas*

INTRODUCTION

The natural rocks throughout the world have been extensively used for various purposes, for example as building stones, ornamental stones and sculptures. These types of the usage of the natural rocks throughout the history can be seen in places of worships (mosques, churches, synagogues and temples of various civilizations), palaces, fountains, caravanserais and many more. Today, the rocks have been used as building stones, artworks and ornamental stones as in the past. These rocks lose their original look since they affected by natural and artificial reasons. The rocks used in several applications mentioned above, have to be preserved for not only their aesthetic values but for future generations as an important proof from past. To preserve them, enough information has to be provided on rocks' geological, mechanical and chemical properties.

There are many factors that affect weathering-alteration-deterioration conditions of the natural rocks. The natural structure (mineralogical-chemical compositions, petrographic properties and physical resistance) of the rocks, environmental conditions and negative corrosive effect of the salt are the most important of them. Processes that cause alteration- weathering of the rocks have been investigated for long time. The first published data (or to our knowledge) for alteration of rocks belong the year 1895 (Yu and Oguchi, 2010). Important agents affecting the stability of the rocks have been described in detail by Shaffer (1932) and later on by Winkler (1966). These two studies are the milestones of this subject and still find places in reference lists. Extensive works have been published in the last two decades. The factors causing the alteration-weathering and deterioration of the rocks can roughly be divided into three, namely chemical, physical and biological processes (e.g., Blows et al., 2003). In practice almost all type of weathering-alteration processes (chemical, physical and biological) progress altogether within and/or surface of the rocks. Combination of these processes significantly enhances the intensity of decay when compared with the physical or biological agents acting along (e.g., Papida et al., 2000).

Chemical processes start with separation of fresh rocks. During this separation some ions and molecules became free for formation of new minerals (Eden, 1990). Lal Gauri and Bandyopathyay (1999) provided very detailed reaction pathways for especially carbonate rocks. Circulating SO_2, NO_x and CO_x gases within atmosphere and hydrosphere could react with K^+, Ca^+, Na^+, Mg^+, Fe^+ (and so on) found within the rocks and their surface (if any) to form salts. When water phases evacuated from the environment salts start to crystallize to give rise pressure (by volume increase) on the rocks. This pressure causes disintegration of the rocks. The gases mentioned above are directly related to environmental pollution, thus the alteration of rocks is also associated to environmental pollutions. The types of rocks are also an important part of alteration degree and speed (Zedef et al., 2007).

A variety of Moroccan carbonate marbles and stones have been used for several purposes at present as well as in the history. Although there have been many carbonate marble and other building stone sources in Morocco, many of them are under operate, there have been no study (at least to our knowledge) on their physical, chemical, geological and geomechanical properties. This study is a first approach of a research aimed at understanding the nature of the stone materials produced by complex geological processes of Morocco (Because of this, we also displayed a very brief explanation of the geological background of Morocco).

More than 70 % of Morocco is covered by mountains which have been shaped by continental collision. In the geological point of view, Morocco can essentially divided into five parts (also known as tectonic units) from South to North (Stets and Wurster, 1982; Crevello, 1991; Ledo et al., 2011): (I) The Anti-Atlas mountains lies in the South of the country and they can be high up to 2500 m. In this unit, Paleozoic aged formations and Hercinien Orogenesis is dominant, but the rocks were deformed very little. The Anti-Atlas mountains is a part of the northwestern part of African Craton, (II) The High Atlas Mountains raise in the central which has 700 km long from East to West and can be reach up to 4000 m high. This unit has more tectonic deformation when compared to the Anti -Atlases. The unit was formed

during Paleozoic and covered unconformably by slightly folded Mesozoic and Cenozoic formations. (III) The middle Atlas Mountains found in the North of the High Atlas and they include extremely thick Mesozoic aged sedimentary rocks, (IV) The Rif Mountains are located at the far most north of the country along with Atlantic Ocean and Mediterranean costs. Intensively deformed Mesozoic and Cenozoic aged rocks are the main features of the Rif Mountains, and (V) Moroccan Mesata includes plateaus and plains of recent alluviums. The Mesata covers a large area along the cost of Atlantic Ocean, but not considered as tectonic unit (Figure 1). The investigated carbonate marbles and stones are a part of these rock units.

METHODOLOGY

This investigation was limited to 8 locations in which carbonate marbles and basalt stones outcropped (Figure 1). All these rocks have indoor and outdoor applications allover Morocco since they have well developed joint system. Petrographic investigations were carried out on thin sections by using polarizing microscope. The polarizing microscope, in turn, and X-Ray diffractometer (XRD) were used for mineralogical identifications. The XRD analyses were done at the laboratories of Gebze Technology Institute, Izmit, Turkey. All other analyses were undertaken at Selcuk University, Konya, Turkey. The geomechanical tests were applied at least three samples of the rocks studied. The loss on ignition (LOI) was measured on 250 mesh powdered samples at 1000 °C.

The quantification of salt weathering of the samples was measured by assessing the dry weight loss (DWL) of the rocks. There have been many laboratory test proposed for DWL determinations. The most used tests are the American standard test ASTM (C-88, C-128), the Germany standard test DIN (52111) and the Spanish standard test UNE-EN (12370). All these test have three stages: immersion (total), drying and cooling. We followed the Spanish standard test for DWL assessments (except the dimension of the samples since we had some difficulty to provide thick samples, nevertheless the test allow us to compare the rocks against salt effect). In this test 14% Na_2SO_4 solution was used. In the immersion stage, clean and dry rock samples were introduced into a container and covered with the solution at 20 °C for 4 h. In the drying stage, the samples were taken out of the container and settled into the heating cabinet at 60 °C for 16 h. The duration of this cycle is 24 h and the similar procedure was repeated for 15 days (total 15 cycles). The solution was changed every five cycles as the samples lose weight. After 15 days, the tested samples were cleaned with pure water to eliminate salt. The samples were then dried until a constant weight realized. The dry weight loss (DWL %) was calculated at the end of this stage.

Figure 1. Main tectonic units of Morocco (Modified from Crevello, 1991 and Ledo et al., 2011).

The location of the studied samples (1 to 8) are also shown in accordance with Table 1.

RESULT AND DISCUSSION

Specific name (or local name), location and color of the collected samples representing carbonate marbles and basalt stones were displayed in Table 1. The investigated rock types are also shown in Figure 2 and 3. The mineralogical composition, cement characteristics and rock type were also indicated in Table 1. It can be said that the carbonate samples (limestone and dolomite) have micritic and sparitic cement. At most samples (except sample 4 and 5), these two agents found together. Crystalline limestone (marble) of Timahdite (sample 4) and dolomitic limestone of Taza (sample 5) have a cement of sparite. Basalt sample of Khenifra (sample 8) has a volcanic origin and has a glassy matrix. The Khenifra basalt and Volubilis dolomitic limestones have quite large pores (Figure 4 and 5), but limestones of Bir Jdid have more connected pores than all other samples since it has the highest e ffective porosity.

Carbonate samples overwhelmingly made of calcite and dolomite minerals with notable amount of organic matter, iron oxides and extraclasts in some samples, for example sample 4 and sample 5 (Table 1). The glauconite minerals were observed in two samples (sample 1 and sample 4) as intraclasts. On the other hand, dolomitic limestone of Volubilis (sample 2) has plenty of pizoids, while some samples have fossils and stilolites (sample 4 and 7). It is notable that one sample (sample 1) have green algae. The sole, non-carbonaceous sample (sample 8) of this study has mostly pyroxene and plagioclase minerals as well as some olivine and opaque minerals in composition. The XRD examinations also revealed most of these observations. Some of the olivine minerals in this sample were iddingsitised (altered olivine consisting of a mixture of clay minerals, iron oxides and ferrihydrites).

The bulk-dry density, effective porosity, dry weight loss (DWL) and loss on ignition (LOI) values of the studied samples were shown in Table 2. The bulk-dry densities of the samples are between 2.23g/cm^3 and 2.71g/cm^3. Effective porosity values of three samples are very close to zero (sample 3, 4 and 7). The limestone of Bir Jdid (sample 1) has the highest (10.81 %) effective porosity, indicating more connected pores. In addition, this sample has the highest (4.61 %) DWL value. The dolomitic limestones of Taza (Sample 5) and basalt of Khenifra (sample 8) have considerably higher effective porosity values which are 5.25 % and 6.67 % respectively. The highest dry weight loss value belongs to the sample 1 (4.61 %) which represent the limestone of Bir Jdid. The sample 5 has also high DWL while three samples (sample 3, 6 and 7) have DWL value of zero. The Khenifra basalt has the lowest LOI value with 1.26 %. The LOI values are relatively uniform (except sample 3 which has 34 % LOI) for other samples.

Table 1. Specific name, location, color and some mineralogical features of the Moroccan carbonate marbles and basalt stone.

Sample no- specific name- location	Rock type	Color	Cement	Minerals	Remarks
1-Bir Jdid-Sefrou	Limestone	Pale brown	Mainly sparite with less micrite	%92 calcite, %8 dolomite	Opaque minerals and glauconite present, remains of green algae and fossils are observed as extraclasts
2-Volubilis-Taghazout	Dolomitic limestone	Beige	Micrite-dolomicrite Sparite-dolosparite	%60 calcite, %40 dolomite	Plenty of pizoids
3- Rose-Agadır	Crystalline limestone (marble)	Pinkish	Sparite with quarts and feldspar as extraclasts	%94 calcite, %6 extraclasts	
4- Timahdite- Ifrane	Crystalline limestone (marble)	Pink	Sparite	%90 sparite, %8 organic matter and/or iron oxide, %2 extraclasts (mainly glauconite)	Fossils and stylolites are present
5- Taza-Taza	Dolomitic limestone (very porous)	Beige	Sparite	%84 sparite, %13 dolomite, %3 extraclasts	Very porous, idiomorphic and hypidiomorphic dolomite rhombeders are visible
6- Bejaad-Smaala	Dolomitic limestone	Beige-yellow	Micrite, sparrycalcite, dolomite, dolosparite	%55 calcite, %45 dolomite	Fossils, peloidalmicrite and idiomorphic dolomite rhombeders are present
7- Gris-Oued Cherrat	Dolomitic limestone	Grey	Micrite, sparite, dolomicrite, dolosparite	%85 calcite, %15 dolomite	Stilolite and fossils are present
8- Black Khenifra-Meknes	Basalt	Black	Intersertal-phylotacsitic texture	%30 plagioclase, %35 pyroxene, %27 matrix %3 altered matter, %5 olivine and opaque minerals	Some of olivines are iddingsitised

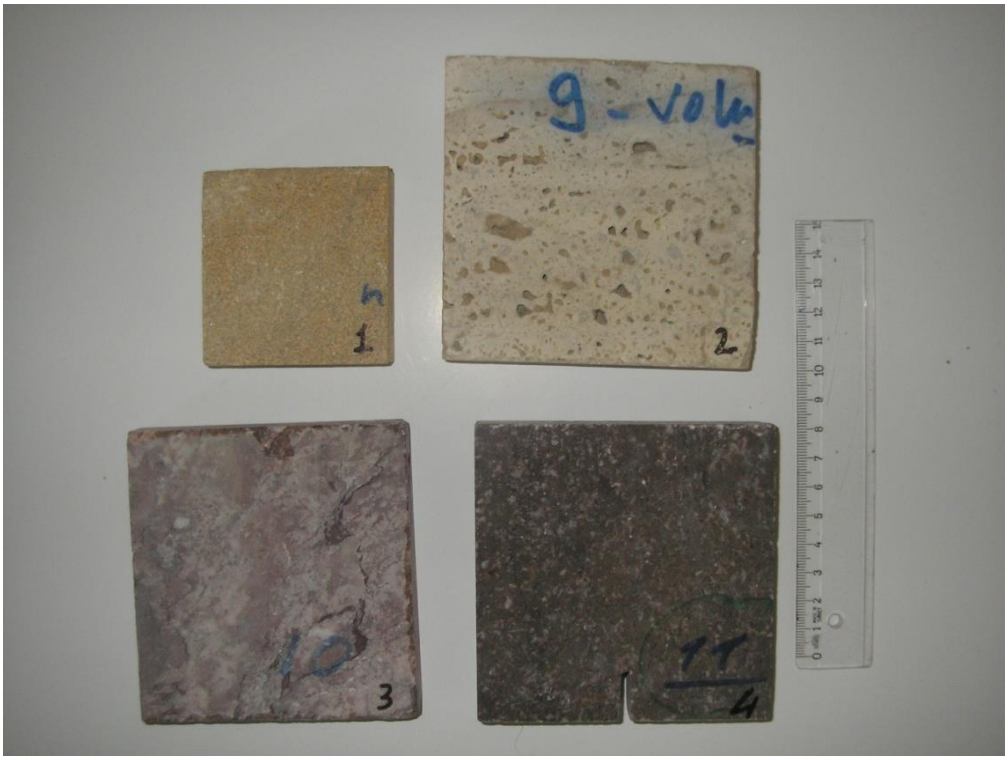

Figure 2. The studied samples of Bir Jdid limestone (1), Volubilis dolomitic limestone (2), Rose marble (Ifrane) (3) and Timahdite marble (4).

Figure 3. The studied samples of dolomitic limestones of Taza (5), Bejaad (6), and Gris (7), and Khenifra basalt (8).

Figure 4. The studied sample of the Volubilis dolomotic limestone. Note that quiet large (up to 5 mm) pores.

Figure 5. The studied sample of Khenifra basalt. The pores relatively more connected than all other samples (except Bir Jdid limestone).

It is clear from the Table 2 that there has been no positive or negative correlation between the bulk-dry densities and powder densities. When excluding sample 8, a slight positive correlation can be seen

between the effective porosities and dry weight loss values of the samples. This is especially true for sample 1 and sample 5. These two samples also have relatively high powder densities. As indicated earlier, the sole non-carbonaceous sample of this study (Khenifra basalt) has a very distinctive effective porosity (6.67 %), dry weight loss (0.99 %) and loss on ignition (1.26 %) values. Note that this sample is also quite different mineralogical composition. This indicates that the effect of salt (in this study Na_2SO_4) on rocks controlled not only by porosity, density and environmental conditions but mineralogical composition is also vital.

Table 2. Density, porosity, dry weight loss and loss on ignition values of the studied carbonate marble and basalt samples.

Sample number	Bulk-dry density (g/cm³)	Effective porosity (%)	Dry weight loss (%)	Loss on ignition (%, 1000°C)
1	2.23	10.81	4.61	41.88
2	2.44	2.36	0.78	44.00
3	2.72	0.18	0	34.00
4	2.72	0.06	0.56	40.35
5	2.51	5.25	3.01	43.36
6	2.62	2.92	0	44.99
7	2.71	0	0	43.19
8	2.58	6.67	0.99	1.26

CONCLUSIONS

The following conclusions can be inferred from this study:

(I) This study is a first approach to understand some geological and geomechanical properties of Moroccan carbonate marbles and basalt stone which are widely used in Morocco.
(II) The studied carbonate marbles and basalt stone have a relatively uniform bulk-dry density values while their effective porosity and dry weight loss values are variable.
(III) The carbonate rocks are mostly made of calcite and dolomite minerals with micritic and sparitic cement. Some rocks also have considerable amount of extraclasts and organic matter as well as fossils.
(IV) The sole, non-carbonaceous sample of Khenifra basalt has very different mineralogical composition than the others. These differences gave rise the different dry weight loss and loss on ignition values of this sample, since it clearly has higher silica and different chemical composition.
(V) Bir Jdid limestone and Taza dolomitic limestone are the most sensitive rocks against salt (Na_2SO_4) decay, therefore the outdoor use of these rocks should be avoided.

ACKNOWLEDGEMENTS

Our thanks go to Dr. M. Salim Öncel for taking XRD graphs and their identification. The marble and stone company of Soreil Marbre Sarl (Rouye de Rabat, Km 5, Tanger, Morocco) provided samples. V. Zedef, A. Döyen and A. R. Söğüt financially supported by the Council of Higher Education (Yüksek Öğretim Kurumu-YÖK) of Turkey during three months visit to Morocco in 2012. The two anonymous referees were also gratefully thanked for their valuable review.

REFERENCES

Blows, J. F., Carey, P.J., Poole, A. B., 2003, "Preliminary Investigations into Caen Stone in The UK; Its Use, Weathering and Comparison with Repair Stone" Building and Environment, Vol. 38, pp.1143 – 1149.

Crevello, P. D., 1991, "High-frequency Carbonate Cycles and Stacking Patterns: Interplay of Orbital Forcing and Subsidence on Lower Jurassic Rift Platforms, High Atlas, Morocco" In Sedimentary Modeling: Computer Simulations and Methods for Improved Parameter Definition (ed. E. V. Franseen, W. L. Watney, C. G. St C. Kendall & W. Ross). Kansas Geological Survey Bulletin no. 233, pp.207-230.

Eden, M. A., 1990, The In-Service Performance of Limestone Building Stones and Their Predominant Mechanisms of Decay, Unpublished M.Sc. dissertation, Queen Mary and West-End College, University of London.

Lal Gauri, K., Bandyopadhyay, J. K., 1999, Carbonate Stone: Chemical Behavior, Durability and Conservation", New York: Wiley.

Ledo, J., Jones, A. G., Siniscalchi, A., Campanya, J., Kıyan, D., Romano, G., Rouai, M., 2011, "Electrical Signature of Modern and Ancient Tectonic Processes in The Crust of The Atlas Mountains of Morocco", Physics of the Earth and Planetary Interiors, Vol. 185, 3–4, pp.82-88.

Papida, S., Murphy, W., May, E., 2000, "Enhancement of Physical Weathering of Building Stones by Microbial Populations", International Biodeterioration & Biodegradation, Vol. 46, 4, pp.305-317.

Schaffer, R.J., 1932, "The Weathering of Natural Building Stones" DSIR, Building Research Special Report, 18, Stationary Office, London. 34 p.

Stets, J., Wurster, P., 1982, "Atlas and Atlantic—Structural Relations" in, Geology of the Northwest Africa Continental Margin, von Rad, U., Hinz, K, Samtheir, M., and Seibold, E., eds.: Springer-Verlag, New York, pp.69-85.

Winkler, E. M., 1966, "Important Agents of Weathering for Building and Monumental Stone" Engineering Geology, Vol .1, pp. 381-400.

Yu, S., Oguchi, C. T., 2010, "Role of Pore Size Distribution in Salt Uptake, Damage, and Predicting Salt Susceptibility of Eight Types of Japanese Building Stones", Engineering Geology, Vol. 115, pp. 226–236.

Zedef, V., Koçak, K., Döyen, A., Özşen, H., Kekeç, B., 2007, "Effect of Salt Crystallization on Stones of Historical Buildings and Monuments, Konya, Central Turkey", Building and Environment, Vol. 42, pp. 1453–1457.